



UNIVERSITAT DE
BARCELONA

Glacial Oscillations and Climate Variability in the NE Greenland

Julia Garcia-Oteyza Cira

ADVERTIMENT. La consulta d'aquesta tesi queda condicionada a l'acceptació de les següents condicions d'ús: La difusió d'aquesta tesi per mitjà del servei TDX (www.tdx.cat) i a través del Dipòsit Digital de la UB (diposit.ub.edu) ha estat autoritzada pels titulars dels drets de propietat intel·lectual únicament per a usos privats emmarcats en activitats d'investigació i docència. No s'autoritza la seva reproducció amb finalitats de lucre ni la seva difusió i posada a disposició des d'un lloc aliè al servei TDX ni al Dipòsit Digital de la UB. No s'autoritza la presentació del seu contingut en una finestra o marc aliè a TDX o al Dipòsit Digital de la UB (framing). Aquesta reserva de drets afecta tant al resum de presentació de la tesi com als seus continguts. En la utilització o cita de parts de la tesi és obligat indicar el nom de la persona autora.

ADVERTENCIA. La consulta de esta tesis queda condicionada a la aceptación de las siguientes condiciones de uso: La difusión de esta tesis por medio del servicio TDR (www.tdx.cat) y a través del Repositorio Digital de la UB (diposit.ub.edu) ha sido autorizada por los titulares de los derechos de propiedad intelectual únicamente para usos privados enmarcados en actividades de investigación y docencia. No se autoriza su reproducción con finalidades de lucro ni su difusión y puesta a disposición desde un sitio ajeno al servicio TDR o al Repositorio Digital de la UB. No se autoriza la presentación de su contenido en una ventana o marco ajeno a TDR o al Repositorio Digital de la UB (framing). Esta reserva de derechos afecta tanto al resumen de presentación de la tesis como a sus contenidos. En la utilización o cita de partes de la tesis es obligado indicar el nombre de la persona autora.

WARNING. On having consulted this thesis you're accepting the following use conditions: Spreading this thesis by the TDX (www.tdx.cat) service and by the UB Digital Repository (diposit.ub.edu) has been authorized by the titular of the intellectual property rights only for private uses placed in investigation and teaching activities. Reproduction with lucrative aims is not authorized nor its spreading and availability from a site foreign to the TDX service or to the UB Digital Repository. Introducing its content in a window or frame foreign to the TDX service or to the UB Digital Repository is not authorized (framing). Those rights affect to the presentation summary of the thesis as well as to its contents. In the using or citation of parts of the thesis it's obliged to indicate the name of the author.

TESI DOCTORAL



UNIVERSITAT DE
BARCELONA

2024

JULIA GARCIA BEYZA CIRIA

GLACIAL OSCILLATIONS
AND CLIMATE VARIABILITY
IN THE NE GREENLAND



Títol tesi:

‘Glacial oscillations and climate variability in the NE Greenland’

Memòria presentada per optar al grau de doctor per la Universitat de Barcelona

Programa Doctorat de Geografia, Planificació Territorial i
Gestió Ambiental

Línia de recerca: Sistemes Naturals i Canvi Global

Facultat de Geografia i Història



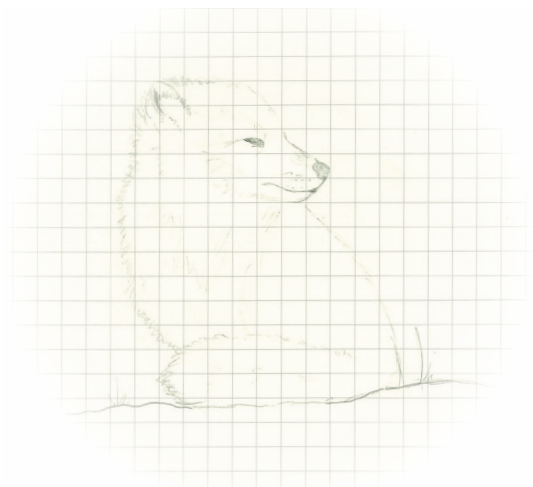
UNIVERSITAT DE BARCELONA

Julia Garcia-Oteyza Ciria

Directors:

Marc Oliva 

Santiago Giralt 



ACKNOWLEDGEMENTS

Si esto va de dar las gracias... querido lector, tome asiento, la lista no es corta... pero aviso, voy con prisas, tengo una tesis que cerrar.

Esta tesis no ha sido un trabajo en solitario, ha sido un trabajo en equipo, no sólo de las personas que han estado por dentro de este documento final, sino que también de todas las que han estado alrededor, porque es imposible separar la tesis de la vida. Por eso, hay muchas personas a las que me gustaría dar las gracias. Habrá muchas otras a las que se me olvidará dárselas, a éstas, les pido perdón y gracias.

Empecé esta tesis sabiendo hablar ya algunos de los idiomas de las rocas, soy geóloga, pero cómo tal, siempre había pintado en mis mapas el Cuaternario como esa área gris en la que hay muchas cosas mezcladas y en general, despertaba poco interés.

Empecé esta tesis sabiendo más bien poco sobre la temática que trata y más bien nada sobre la metodología que aplica. Por eso, lo primero es agradecer a todas las personas que han dado su tiempo y su paciencia a enseñarme todo sobre estos nuevos idiomas para comunicarme con las rocas y los sedimentos.

Por supuesto, en primer lugar, a mis directores:

Gracias a Marc, gracias por todo... pero sobre todo por su energía inagotable, su empuje, por su forma de abordar la ciencia y por su empatía e inteligencia emocional. Sin su orientación y apoyo constante esta tesis habría tardado algunos años más en salir adelante. Es cierto Marc, es mejor trabajar con buenas personas que con personas buenas.

Gracias a Santi, gracias por enseñarme tanto, por las discusiones científicas y por emoción que trae el de repente, entender y encontrarles el sentido a los datos. Es cierto Santi, creo que mi cerebro se ha reestructurado hasta los niveles más insospechados.

A los dos, gracias por creer en mí y en que valía para esto desde el principio.

Gracias a todos los coautores de los artículos que conforman esta tesis. También a todos los que no los firman, pero que han dado su tiempo en revisiones, sugerencias y discusiones de datos o en explicarme detalles importantes.

En especial, gracias a Chema, a quien le debo prácticamente todo lo que puedo llegar a tener de experta en cosmostratigrama. Gracias por tu disponibilidad, paciencia y contagiante pasión. Un especial gracias también a David y a Nuria, por toda la ayuda, enseñanzas y ánimos desde el principio. Gracias a Irene, por todo lo que me ha enseñado en el laboratorio y fuera de él. Gracias también a Vicent, Laetitia y Regis, sin vosotros no habría sobrevivido al peso del laboratorio. Un gran gracias a Dermot. Gracias por todo el conocimiento compartido y gracias por las aventuras canadienses y árticas.

También, gracias a todas las personas geniales con las que he compartido el tiempo en mis estancias y congresos, y que han hecho más llevadero el estar fuera de casa: Jesús, Yohanna, Emma, Hamid, María, Joanna and Tancrede.

Gracias a mis compañeros del grupo ANTALP, en especial a los que han compartido conmigo el proceso de tesis: Marcelo y Josep Ventura.

Gracias también a todos los que han hecho que lo cotidiano no sea aburrido en el

Departamento de Geografía, con los que he compartido *dinars*, café, cerveza, una charla interesante o todo junto. En especial, gracias a Tania, Carolina, Miriam, Edu, Xavi, Filipe, Quim, Jordi, Mariano y Carles.

Gracias a todos los de mi extensa familia dispersa:

A los que ha unido esta aventura, la mayor ganancia de estos años y el mayor gracias va para los miembros de la familia que hemos creado en Barcelona, gracias por las aventuras y desventuras que, compartidas, siempre son mejores. A los que estaban cuando llegué y a los que fueron llegando. No he podido tener más suerte. Gracias por cuidarnos, por los abrazos, las bravas y las cervezas. Vero, Laia, Miquel y Laia (no habrá mejores compañeros de despacho), Damián, Carlos, Josu y Laura: Gracias por vosotros. Gracias en especial a Antonio, por cuidarme, empujarme a que me cuide mejor y por haber intentado entender mis balleneos constantes de estos meses.

Gracias a todas con las que quizás no comparto el día a día, pero sí son una constante en mi vida y sin las nada tendría sentido. Gracias por rescatarme de la tesis todas la veces que lo he necesitado. Chín chín! a mis Troncas... Lucía y Andrea., al PBC... Leyre y Aitana. Y también a las Maris...Adri, Elyan y Cris. Y a mi Val D'Aran... Aran, Cris e Isa.

Um obrigada para a minha família brasileira, sin la que no habría llegado a dar el salto de empezar esta tesis. Obrigada pelo cuidado, apoio constante e pela generosidade. Vocês me ensinaram os abraços apertados. Saudade de um almoço e de um cafezim com vocês.

Lo he dejado para el final, pero es porque no sé ni cómo empezar a agradecer.

Gracias a mi familia materna y, en especial, a mis tías, Sole, Cruz y Pili. Gracias, porque sois las columnas de esta familia y una tremenda inspiración. Gracias por cuidarme siempre. Gracias a mi madre, a la que espero parecerme más de lo que me gustaría reconocer y que me ha enseñado de absolutamente todo. En realidad, esta tesis es suya, ya que el contrato lleva su firma...

Ya llegando al final y sí, menos importante, también debo darle las gracias a esta tesis, que me ha salvado de la vida cuando lo he necesitado.

(Creo) que sólo me queda agradecerme a mí misma, por haber dado el paso (muy meditado) de hacer una tesis y por, a pesar de los obstáculos, haber llegado al final: esta tesis va por mí, y por todas mis compañeras.

Julia



Funding:

NEOGREEN (PID2020-113798GB-C31) and PALEOGREEN (CTM2017-87976-P) projects of the Spanish Ministerio de Economía y Competitividad. Field research was also supported by the research group ANTALP (Antarctic, Arctic, Alpine Environments; 2017-SGR-1102) funded by the Agència de Gestió d'Ajuts Universitaris i de Recerca of the Government of Catalonia.

Julia Garcia-Oteyza was supported by an FPI fellowship (PRE2018-086608) from the Spanish Ministry of Science.



ORIGINAL INCLUDED PAPERS AND AUTHOR CONTRIBUTIONS

LIST OF ORIGINAL INCLUDED PAPERS

The results of this thesis are summarized in the four papers listed below (Papers I-IV). All papers are published (one submitted) in peer-reviewed international journals. Papers I, II, and IV are reproduced with permission from Elsevier Ltd. and John Wiley & Sons Ltd. publishing, respectively (Paper III has been submitted to *Boreas*, date 06-Jan-2024). Along this PhD thesis, research papers are referred using the following Roman numeral.

PAPER I

J. Garcia-Oteyza, M. Oliva, D. Palacios, J.M. Fernández-Fernández, I. Schimmelpfennig, N. Andrés, D. Antoniades, H.H. Christiansen, O. Humlum, L. Léanni, V. Jomelli, J. Ruiz-Fernández, V. Rinterknecht, T.P. Lane, K. Adamson, Georges Aumaître, D. Bourlès, K. Keddadouche. Late Glacial deglaciation of the Zackenberg area, NE Greenland. *Geomorphology*, 401, 2022, 108125, ISSN 0169-555X. <https://doi.org/10.1016/j.geomorph.2022.108125>

Publication chronology: 1st submission: 12th January 2021 Send to journal / 31st March 2021 Rejected / 5th August 2021 Accepted with major revisions / 14th November 2021 Rejected. 2nd submission: 24th November 2021 Send to journal / January 4th 2022 Minor revisions / January 20th 2022 Accepted for publication.

PAPER II

J. Garcia-Oteyza Ciria, M. Oliva, D. Palacios, J. M. Fernández-Fernández, I. Schimmelpfennig, A. Medialdea, M. Fernandes, S. Giralt, V. Jomelli, D. Antoniades & ASTER TEAM (2023). Holocene glacial oscillations in the Tyroler Valley (NE Greenland). *Land Degradation & Development*, 34(9), 2589–2606. <https://doi.org/10.1002/ldr.4633>.

Publication chronology: 1st submission: 28th August 2022 Send to journal / 28th December 2022 Minor revisions / 1st February 2023 Accepted for publication.

PAPER III

J. Garcia-Oteyza, M. Oliva, D. Palacios, J. M. Fernández-Fernández, I. Schimmelpfennig, M. Fernandes, S. Giralt, D. Antoniades, V. Jomelli (2023). A Late Glacial and Holocene chronology of climate-linked landscape evolution in NE Greenland from CRE dating of landforms.(Submitted).

Publication chronology: 1st submission: 6th January 2024 Send to journal (ID: BOR-001-2024) .

PAPER IV

J. Garcia-Oteyza, S. Giralt, S. Pla-Rabes, D. Antoniades, M. Oliva, H. Ghanbari, R. Osorio-Serrano, D. Palacios. A ~5000-year multiproxy record of summer climate in NE Greenland. (2023). Volume 906, 2024, 167713, ISSN 0048-9697, <https://doi.org/10.1016/j.scitotenv.2023.167713>.

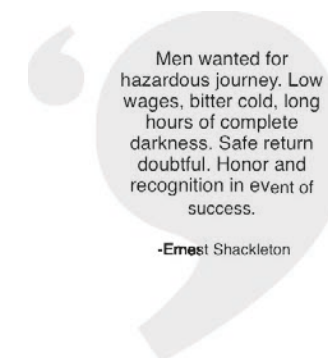
Publication chronology: 1st submission: 3rd July 2023 Sent to journal/ September 13th 2023 Minor revisions/ September 27th 2023 Accepted for publication.

AUTHOR CONTRIBUTIONS

- Garcia-Oteyza Ciria, Julia: JGO
- Oliva, Marc: MO
- Giralt, Santiago: SG
- Antoniades, Dermot: DA
- Palacios, David: DP
- Fernández-Fernández, Jose M^a: JMFF
- Schimmelpfennig, Irene: IS
- Andrés, Nuria: NA
- Christiansen, Hanne: HC
- Humlum, Ole: OH
- Léanni, Laetitia: LL
- Jomelli, Vincent: VJ
- Ruiz-Fernández, Jesús: JRF
- Rinterknecht, Vincent: VR
- Lane, Timothy: TL
- Adamson, Kate: KA
- ASTER Team*: AT
- Fernandes, Marcelo: MF
- Pla-Rabes, Sergi: SPR
- Ghanbari, Hamid: HG
- Osorio-Serrano, Rodrigo: ROS
- Medialdea, Alicia: AM

*The ASTER team is composed of the researchers Georges Aumaître and Karim Keddadouche

Task	Paper I	Paper II	Paper III	Paper IV
Fieldwork	JGO, MO, DP, DA, JRF, VJ, VR, TL, KA	JGO, MO, JRF	JGO, MO, JRF	SG, DA, SPR
Laboratory: sample preparation	JGO, JMFF, LL, TL	JGO, MF, IS, AM	JGO, MF, IS	JGO, SG, SPR, DA, HG
AMS measurements	AT	AT	AT	
Data interpretation	JGO, IS, HC, OH, NA	JGO, IS, AM	JGO, IS	JGO, SG, DA, SPR, MO
Manuscript preparation (main text, figures, tables)	JGO, MO, DP, JMFF, DA	JGO, MO, DP, JMFF, DA	JGO, MO, DP, JMFF, DA	JGO, SG, DA, SPR, MO
Data compilation and mining	JGO, MO, JMFF, NA	JGO, MO, JMFF, DP	JGO, MO, JMFF, DP	JGO, SG, DA, SPR
Statistical analysis	JGO, JMFF, IS, NA	JGO, JMFF, IS	JGO, JMFF, IS	JGO, SG, DA, SPR
GIS & geospstial analysis	JGO, MO, JMFF, NA, DP	JGO, MO, JMFF, DP	JGO, MO, JMFF, DP	
Feedback prior paper submission	All authors	All authors	All authors	All authors



ADDITIONAL CONTRIBUTIONS

SCIENTIFIC ARTICLES ON COMPLEMENTARY RESEARCH TOPICS OF THE PHD THESIS:

1. Antoniades, D., Klanten, Y., Cameron, E., Garcia-Oteyza, J., Oliva, M., and Vincent, F.W. Evidence of summer thermal stratification in extreme northern lakes. *Arctic Science*. <https://doi.org/10.1139/as-2023-0037>.
2. Fernandes, M., Oliva, M., Fernandez-Fernandez, J. M., Vieira, G., Palacios, D., Garcia-Oteyza, J., Ventura, J., Schimmelpfennig, I. & ASTER Team. (2023). Geomorphological record of the glacial to periglacial transition from the Bølling–Allerød to the Holocene in the Central Pyrenees: the Lòcampo cirque in the regional context. *Boreas*. <https://doi.org/10.1111/bor.12633>. ISSN 0300-9483.
3. Oliva, M.; Palacios, D.; Fernández-Fernández, J.M.; Fernandes, M.; Schimmelpfennig, I.; Vieira, G.; Antoniades, D.; Pérez-Alberti, A.; Garcia-Oteyza, J. & ASTER Team (2023). Holocene deglaciation of the northern Fildes Peninsula, King George Island, Antarctica. *Land Degradation & Development*, doi: 10.1002/ldr.4633.
4. Fernandes, M., Oliva, M., Vieira, G., Palacios, D., Fernández-Fernández, J. M., Delmas, M., Garcia Oteyza, J., Schimmelpfennig, I., Ventura, J., Aumaître, G., & Keddadouche, K. (2021). Maximum glacier extent of the Penultimate Glacial Cycle in the Upper Garonne Basin (Pyrenees): new chronological evidence. *Environmental Earth Sciences*, 80(24), 796. <https://doi.org/10.1007/s12665-021-10022-z>.
5. Fernandes, M., Oliva, M., Vieira, G., Palacios, D., Fernández-Fernández, J. M., García-Oteyza, J., Schimmelpfennig, I., Team, A., & Antoniades, D. (2021). Glacial oscillations during the Bølling–Allerød Interstadial–Younger Dryas transition in the Ruda Valley, Central Pyrenees. *Journal of Quaternary Science*, 37(1), 42–58. <https://doi.org/10.1002/jqs.3379>.
6. Fernández-Fernández, J.M.; Oliva, M.; Palacios, D.; Garcia-Oteyza, J.; Navarro, F.; Schimmelpfennig, I.; Léannid, L. & ASTER Team (2021). Ice thinning on nunataks during the Last Glacial Termination in the Antarctic Peninsula according to Cosmic-Ray Exposure dating: evidence and uncertainties. *Quaternary Science Reviews*, 264: 107029.

BOOK CHAPTERS ON COMPLEMENTARY RESEARCH TOPICS OF THE PHD THESIS:

1. Oliva M.; López-Moreno, J.I.; Andrés, N.; Antoniades D.; Bonsoms, J.; Fernández-Fernández J. M.; García-Oteyza J.; García-Sancho, L.; Giralt, S.; González-Herrero, S.; Martín-Díaz, J. & Palacios D. (2023). Las regiones polares. In: Oliva, M.; Barriocanal, C.; Martín-Díaz, J.; López-Moreno, J. & Bonsoms, J. (eds.). *Cambio global. La crisis ecosocial*. Publicacions de la Universitat de Barcelona.
2. Oliva, M.; Gómez-Ortiz, A.; Palacios, D.; Salvador-Franch, F.; Ramos, M.; Sanjosé-Blasco, J.J.; Fernandes, M.; Fernández-Fernández, J.M.; Galindo-Zaldívar, J.; Garcia-Oteyza, J.; González, L.; Hauck, C.; Martín-Díaz, J.; Nofre, J.; Sanz de Galdeano, C. & Tanarro, L.M. (2022). Ancient and present-day periglacial environments in

the Sierra Nevada. In: Zamora, R. & Oliva, M. (eds.). *The landscape of the Sierra Nevada. A unique laboratory of global processes in Spain*. Springer Nature, pp. 115-128.

3. Oliva, M., Gómez-Ortiz, A., Palacios, D., Franch, F. S., Ramos, M., de Sanjosé-Blasco, J. J., Fernandes, M., Fernández-Fernández, J. M., Galindo-Zaldívar, J., García-Oteyza, J., González, L., Hauck, C., Martín-Díaz, J., Nofre, J., de Galdeano, C. S., & Tanarro-García, L. M. (2022). Ancient and Present-Day Periglacial Environments in the Sierra Nevada. In Zamora, Z., & Oliva, M. (eds.), *The Landscape of the Sierra Nevada: A Unique Laboratory of Global Processes in Spain* (pp. 115–128). Springer International Publishing. https://doi.org/10.1007/978-3-030-94219-9_8.

EDITION OF BOOKS:

1. Fernández-Fernández, J.M.; Bonsoms, J.; Garcia-Oteyza, J. & Oliva, M. (2023). Book of abstracts of the 6th European Conference on Permafrost (EUCOP 2018). DOI: 10.52381/EUCOP6.abstracts.
2. Garcia-Oteyza, J. & Oliva, M. (2023). Field guides of the 6th European Conference on Permafrost (EUCOP 2018). DOI: 10.52381/EUCOP6.excursionsbook.1.

SUMMARY

ENGLISH

The remote coastal ice-free areas of Northeast Greenland National Park are considered a unique laboratory to examine the chronology of past cold-climate geomorphological processes and associated climatic conditions. This dissertation endeavors to employ a multidisciplinary approach, leveraging various natural archives and employing complementary techniques. The overarching goal is to enhance our understanding of the glacial history and climate variability within the specified region. Four valley environmental reconstructions are presented here, combining geomorphological mapping and a geochronological dataset of 84 ^{10}Be cosmogenic radionuclide exposure (CRE) dating samples (in some cases complemented with OSL dating and historical data) to reconstruct glacial oscillations. In addition, a multiproxy characterization of lake sediment records is provided, using seven different but complementary paleolimnological methods together with 13 ^{14}C dating, to unravel climate variability of the last millennia, with a focus on local temperature and precipitation regimes. The highest CRE-dated samples indicate that these valleys were fully glaciated before the global Last Glacial Maximum (LGM) at ~80-50 ka. After the LGM, a rapid deglaciation process with massive ice thinning occurred, and most of the currently ice-free areas of the region were deglaciated at the end of Termination-1. The complete sequence of moraine ridges distributed across the slopes surrounding the Zackenberg Valley floor revealed ice thinning between ~13.7 and 11.2 ka, followed by accelerated glacier retreat at ~10-11 ka, when the valley glaciers disconnected from the main ice tongues. Deglaciation of the fjord entrance valleys and terminal valleys occurred during the Early Holocene at ~10-8.5 ka, due to the long-term decrease of precipitation. This long-term recession was interrupted by periods of glacial stillstand/ advance of the valley glaciers that favored the formation of the moraine ridges on the slopes and valley bottoms of the different valleys (as during short periods of cooling, such as the ~11.5 and 9.2 ka events). The prolonged recession exposed the rock slopes and the moraine ridges, favoring rapid paraglacial slope readjustment. The disappearance of the ice has led to the formation of the present landscape through a variety of postglacial processes, mainly periglacial dynamics, glacial-isostatic uplift and redefinition of the coastlines, permafrost aggradation, and nivation processes. As in most areas of NE Greenland, there are no glacial records from the mid-Holocene to the beginning of the Late Holocene (~8.2- 4.2 ka), and therefore no glacial oscillation data were obtained from any of the four valleys. This phase was parallel to low precipitation regimes from ~5.2 to ~3 cal. ka BP in the area. At this time, from ~3 ka BP forward, as conditions became wetter and warmer, new evidence of glacial advances are detected in some valleys (as at ~1.3, ~0.6 and ~0.3 ka BP). The Little Ice Age (LIA) (1300-1850 CE) constitutes the last phase of glacier expansion in Greenland driven by solar minima that favored lower global temperatures. Paleolimnological reconstructions show that the beginning of the LIA was characterized by a marked decrease in air temperatures, followed by a decrease in precipitation, which was lowest at the end of the period. Since the last major LIA advance, the glacier fronts have experienced minor oscillations, as shown by historical images of the 1930s, with glaciers close to LIA moraines. The last 50 years of the Aucella Lake and ZAC1906 Lake records are characterized by abrupt temperature increases, with the highest peaks of the last ~11 cal. ka BP that are associated with anthropogenic global warming. In conclusion, the main findings of this PhD thesis constitute new relevant contributions to understanding climate variability and glacial response in NE Greenland from the last glacial cycle to the present, considering the limitations of using CRE dating in areas where paraglacial dynamics are very active. However, they have also raised new questions and uncertainties that need to be investigated in the future.

PETIT RESUM EN CATALÀ

Les remotes zones costaneres sense gel del Parc Nacional del Nord-est de Groenlàndia es consideren un laboratori únic per a examinar la cronologia dels processos geomorfològics del passat en climes freds i les seves condicions climàtiques associades. Aquesta tesi pretén emprar un enfocament multidisciplinari, aprofitant diversos arxius naturals i emprant tècniques complementàries. L'objectiu global és millorar la nostra comprensió de la història glacial i la variabilitat climàtica en aquesta regió. Aquí es presenten quatre reconstruccions ambientals de valls, combinant cartografia geomorfològica i un conjunt de dades geocronològics de 84 mostres de datació per exposició a radionúclids cosmogènics (en alguns casos complementats amb datació OSL i dades històriques) per a reconstruir les oscil·lacions glacials. A més, s'ofereix una caracterització multiproxy dels registres de sediments lacustres, utilitzant set mètodes paleolimnològics diferents però complementaris juntament amb 13 datacions ^{14}C , per a desentranyar la variabilitat climàtica dels últims mil·lennis, amb especial atenció als règims locals de temperatura i precipitació.

PEQUEÑO RESUMEN CASTELLANO

Las remotas zonas costeras sin hielo del Parque Nacional del Noreste de Groenlandia se consideran un laboratorio único para examinar la cronología de los procesos geomorfológicos del pasado en climas fríos y sus condiciones climáticas asociadas. Esta tesis pretende emplear un enfoque multidisciplinar, aprovechando diversos archivos naturales y empleando técnicas complementarias. El objetivo global es mejorar nuestra comprensión de la historia glacial y la variabilidad climática en esta región. Aquí se presentan cuatro reconstrucciones ambientales de valles, combinando cartografía geomorfológica y un conjunto de datos geocronológicos de 84 muestras de datación por exposición a radionucleidos cosmogénicos (en algunos casos complementados con datación OSL y datos históricos) para reconstruir las oscilaciones glaciares. Además, se ofrece una caracterización multiproxy de los registros de sedimentos lacustres, utilizando siete métodos paleolimnológicos diferentes pero complementarios junto con 13 dataciones ^{14}C , para desentrañar la variabilidad climática de los últimos milenios, con especial atención a los regímenes locales de temperatura y precipitación.

LIST OF ACRONYMS

GrIS	Greenland Ice Sheet
CE	Common Era
ka	kilo annum, thousand years
AO/NAO	Arctic Oscillation/North Atlantic Oscillation
AMOC	Atlantic Meridional Overturning Circulation
GBI	Greenland Blocking Index
LGM	Last Glacial Maximum
MSL	Mean Sea-Level
CRE	Cosmic-Ray Exposure
T-1	Termination-1
OD	Oldest Dryas
YD	Younger Dryas
B-A	Bølling-Allerød
HTM	Holocene Thermal Maximum
PBO	Preboreal Oscillation
RWP	Roman Warm Period
MCA	Medieval Climate Anomaly
DACP	Dark Ages Cold Period
LIA	Little Ice Age
GLOF	Glacial Lake Outburst Flood
NEGIS	Northeast Greenland Ice Stream
OSL	Optically Stimulated Luminescence
GEUS	The Geological Survey of Denmark and Greenland
RQ	Research Questions
AMS	Accelerator Mass Spectrometry
ASTER	Accélérateur pour les Sciences de la Terre, Environnement et Risques
CEREGE	European Centre Research and Teaching in Geosciences De L'envi
CENIEH	Centro Nacional de Investigación sobre la Evolución Humana
XRD	X-Ray Diffraction
CT-Scan	Computed Tomography
XRF	X-Ray Fluorescence
PCA	Principal Component Analysis
RDA	Redundancy Analysis
NH	North Hemisphere

TABLE OF CONTENTS

ACKNOWLEDGEMENTS	
A COSMIC TRIP: WHERE DID THE TIME GO?	
LIST OF ORIGINAL INCLUDED PAPERS AND AUTHOR CONTRIBUTIONS	2
LIST OF ADDITIONAL CONTRIBUTIONS	4
SUMMARY	6
LIST OF ACRONYMS	8
TABLE OF CONTENTS	11
1. INTRODUCTION	12
1.1 RESEARCH BACKGROUND	13
1.1.1 GEOMORPHOLOGICAL RECORDS AND GLACIAL OSCILLATIONS	16
1.1.2 LAKE SEDIMENTARY RECORDS AND CLIMATE VARIABILITY	17
1.1.3 GENERAL PICTURE OF LATE QUATERNARY CLIMATIC AND ENVIRONMENTAL CHANGES IN GREENLAND	17
1.2 STUDY AREA	22
1.2.1 THE GEOMORPHOLOGICAL RECORD AND GLACIAL OSCILLATIONS IN NE GREENLAND AND IN THE STUDY AREA.....	25
1.2.2 THE LAKE SEDIMENTARY RECORD AND CLIMATE VARIABILITY IN NE GREENLAND AND IN THE STUDY AREA	27
1.3 STRUCTURE OF THE THESIS AND OBJECTIVES	28
1.3.1 FRAMEWORK OF THE ARTICLES	29
1.3.2 OBJECTIVES AND RESEARCH QUESTIONS	30
2. METHODS ...	33
2.1 RECONSTRUCTION OF GLACIAL OSCILLATIONS	34
2.1.1 SPACE: GEOMORPHOLOGICAL MAPPING	36
2.1.2 TIME: GEOCHRONOLOGY	37
2.1.2.1 COSMOGENIC RADIONUCLIDE EXPOSURE (CRE) DATING	37
2.1.2.2 OPTICALLY STIMULATED LUMINESCENCE (OSL) DATING	48
2.1.2.3 HISTORICAL DATA	49
2.2 RECONSTRUCTION OF CLIMATE VARIABILITY: PALEOLIMNOLOGY	50
BIBLIOGRAPHY	56
3. RESULTS AND DISCUSSION	72
3.1. LANDSCAPE EVOLUTION OF THE VALLEYS FROM NE GREENLAND	73
3.1.1 PAPER I. LATE GLACIAL DEGLACIATION OF THE ZACKENBERG AREA	73
3.1.2 PAPER II. HOLOCENE GLACIAL OSCILLATIONS IN THE TYROLER VALLEY	95
3.1.3 PAPER III. A LATE GLACIAL AND HOLOCENE CHRONOLOGY OF CLIMATE-LINKED LANDSCAPE EVOLUTION IN NE GREENLAND FROM CRE DATING OF LANDFORMS	115
3.2 LOCAL CLIMATE VARIABILITY IN NE GREENLAND	245
3.2.1 PAPER IV. A ~5000-YEAR MULTIPROXY RECORD OF SUMMER CLIMATE	145
3.2.2 OTHER DATA	159
3.3 LINKING CLIMATE VARIABILITY AND GLACIAL OSCILLATIONS	168
4. CONCLUDING REMARKS AND FUTURE PERSPECTIVES	172

1 INTRODUCTION

OUTLINE

- 1. INTRODUCTION
- 1.1 RESEARCH BACKGROUND
 - 1.1.1 GEOMORPHOLOGICAL RECORDS AND GLACIAL OSCILLATIONS
 - 1.1.2 LAKE SEDIMENTARY RECORDS AND CLIMATE VARIABILITY
 - 1.1.3 GENERAL PICTURE OF LATE QUATERNARY CLIMATIC AND ENVIRONMENTAL CHANGES IN GREENLAND
- 1.2 STUDY AREA
 - 1.2.1 THE GEOMORPHOLOGICAL RECORD AND GLACIAL OSCILLATIONS IN NE GREENLAND AND IN THE STUDY AREA
 - 1.2.2 THE LAKE SEDIMENTARY RECORD AND CLIMATE VARIABILITY IN NE GREENLAND AND IN THE STUDY AREA
- 1.3 STRUCTURE OF THE THESIS AND OBJECTIVES
 - 1.3.1 FRAMEWORK OF THE ARTICLES
 - 1.3.2 OBJECTIVES AND RESEARCH QUESTIONS



1. INTRODUCTION

1.1 RESEARCH BACKGROUND

The significance of the polar regions, the Arctic, the Greenland Ice Sheet (GrIS) and peripheral glaciers is pivotal in the Earth's climate system, as they play a critical role in the environmental and climatic dynamics of our planet. Understanding the events that transpired in these areas beyond the historical instrumental record is essential for gaining deeper insights and comprehending their mechanisms.

In this context, this doctoral thesis puts four environmental reconstructions designed to unveil glacial oscillations and climate variability in Northeast Greenland over the past millennia.

The renowned paleoclimate scientist W. Broecker vividly characterized the climate system as an "angry beast," drawing attention to our precarious engagement, akin to poking it with sticks. This striking metaphor encapsulates the looming prospect of unforeseen challenges that the evolving climate may unveil.

Earth's climate system comprises multiple complex physical, geological, chemical, and biological subsystems interconnected on a wide range of time and spatial scales. In order to grasp the Earth system in its entirety, we need to gain a comprehensive understanding of the intricate subsystems (atmosphere, the hydrosphere, the cryosphere, the lithosphere and the biosphere) that comprise it as how these systems interact and identify linkages between them, both in the present time and in the past (Bradley, 2015).

Inside the linked, complex Earth's intricate climate system puzzle, polar regions (Arctic and Antarctica) are crucial pieces and play a pivotal role in shaping both terrestrial (e.g., glaciers) and marine ecosystems (e.g., sea ice). Changes in these regions do not stay restricted in high latitudes, but have profound effects throughout the planet far beyond the high latitudes, sparked by an intricate cascade of effects globally through complex atmospheric and oceanographic teleconnections (Goosse et al., 2018). The polar regions exhibit local forcings and feedback mechanisms that lead to a warming trend surpassing the global average, a phenomenon known as polar amplification (Cohen et al., 2014). This amplification is evident in historical

Sila - Pronounced [sila] – is the Greenlandic word for weather and climate. But its meaning is deeper. Sila is also the word for "intelligence/consciousness," the all-pervading, live-giving force that manifest in each and every person. Integrates and connects the self with the rhythms of the natural world.
- Nuttall, 1992.

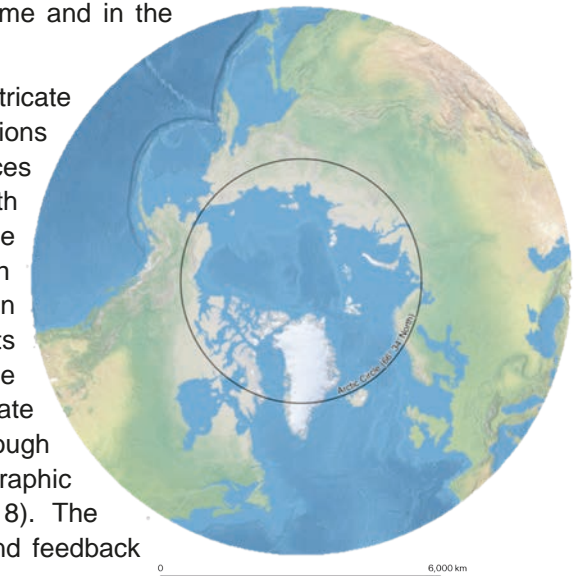


Figure 1. Azimuthal projection from the Geographic North Pole with the Arctic Circle marked by the black line, encompassing all land areas north of latitude 66° N. Source: QGreenland QGIS data package.

periods, but it is also a contemporary reality, currently driving accelerated geocological transformations.

The Arctic region (above the Arctic Circle ($\approx 66^{\circ} 34' N$; Figure 1) is an essential Earth's climate system component, and its ecosystems stand out as some of the most vulnerable areas on our planet, being highly sensitive to environmental disturbances (Anderson et al., 2017; Post et al., 2009; Saros et al., 2019). Both instrumental observations and climate models reveal that the region is undergoing rapid warming - almost four times higher than the global average for the period 1979 to 2021 (Rantanen et al., 2022), and it is expected to experience some of the most intense changes in response to climate warming by the end of the 21st century (Preusser et al., 2008; Saros et al., 2019). According to > 40 years of climatic data, for West Greenland mean June air temperatures from 1994 to 2015 CE increased by 2.2 °C and mean winter precipitation from 1976 to 2012 CE doubled from 21 to 40 mm, while from 2006 to 2015 CE, mean July air temperatures have increased by 1.1 °C (Saros et al., 2019). However, much remains to be understood about the drivers of Arctic amplification, climate variability and the feedback processes between the different environmental and climate components (Lund et al., 2017; Pithan and Mauritsen, 2014; Serreze and Barry, 2011). Arctic climate change shows different spatial and temporal patterns, among which the Arctic Oscillation/North Atlantic Oscillation (AO/NAO) and the Greenland Blocking Index (GBI) are the most prominent (Miller et al., 2010). However, there is a poor understanding of their long-term evolution and fluctuations prior the instrumental records in this key area (Hörhold et al., 2023); therefore, to project climate scenarios accurately it is decisive to contextualize present-day warming within a long-term perspective and thus decipher natural climatic fluctuations from anthropogenic influences.

Within all the interconnected environments or subsystems that exist in the Arctic, one of them can provide an important key to our knowledge of past, present and future global environmental conditions: past and modern glacial landscapes (Nesje and Dahl, 2000). This encompasses the GrIS, ice caps, glacier outlets as well as the deglaciated areas they have left behind its retreat, with a mosaic of landforms and ecosystems.

The GrIS and the still heavily glaciated terrain of the eastern Canadian Arctic comprise the majority of glacier ice in the Northern Hemisphere (Gardner et al., 2013). The GrIS is a mostly land-based ice sheet, the second largest body of ice globally, and the only one in the Northern Hemisphere. It extends over $1.4 \times 10^6 \text{ km}^2$, with a maximum depth of 3.2 km, and a potential sea water equivalent rise of $\sim 7.4 \text{ m}$ (Bamber et al., 2013).

The GrIS is considered a tipping element in Earth's climate (Lenton et al., 2008). This extensive ice sheet has played a major role in the stability of the climate system since the last glacial maximum (LGM; 26–19 ka; (Cohen and Gibbard, 2019)) and is responding fast to present-day climate warming, with major retreats over most of its edges (Vasskog et al., 2015). Similarly, peripheral glaciers in Greenland are also recording an accelerated recession in response to unfavourable climate conditions for glacier stability. Greenland is currently the main source of contribution to sea level rise ($10.8 \pm 0.9 \text{ mm}$ between 1992 and 2018; (IMBIE Team, 2020)) and this contribution may even increase in the forthcoming decades, as the GrIS is currently imbalanced with the present-day climate (King et al.,

2020). The loss of glacial ice is having major implications for Greenlandic ecosystems, and enhancing Arctic amplification effects, ocean currents, surface radiative balance, etc., affecting, thus, the stability of the Earth's climate system (Meredith et al., 2019). Some simulations show that, under CO_2 levels four times higher than preindustrial ones, the GrIS might disappear completely within three thousand years, (Vasskog et al., 2015), rising global mean sea-level (MSL) between 5 and 33 cm by 2100 CE (Aschwanden et al., 2019). Considering these models, the behaviour of the ice-sheets are a primary affair.

Nowadays, despite available instrumental meteorological records can offer a comprehensive understanding of the climate framework for over the last few decades (to one or two centuries, at maximum), it provides a relatively short-term perspective on Earth's climatic history. Furthermore, it encompasses only a limited set of climate variables related to environment processes, resulting in a restricted array of information (Axford et al., 2009; Bradley, 2014; Catalan et al., 2013). The historical data provides a statistical framework for understanding climate over a specific period (at best, a few decades), which is shorter than the time response of ecosystem processes. Consequently, there is a need for long time series observations, which are typically not readily available. Knowledge on the past spatial and temporal patterns of glacial oscillations is needed to frame current GrIS trends, and important for assessing the outputs from numerical ice sheet models, reconstructing the processes that conditioned the deglaciation on timescales beyond the current instrumental records (Smol, 2019) and unveiling the potential contribution of former glaciers to sea-level rise.

Furthermore, a detailed understanding of the short- and long-term temporal and spatial evolution of Greenland climate, mainly related to Greenland blocking (persistent high-pressure system), might help to provide insights describing the North Atlantic Oscillation (NAO) evolution. This major regional pattern of wintertime variability in the Northern Hemisphere has major implications for the weather patterns in many European regions, including the Mediterranean basin (Davini et al., 2012; Hanna et al., 2016). According to some studies, an increasing trend of Greenland blocking in summer and a more variable blocking in winter may led to enhanced early winter NAO variability, mainly at the southern node of this climate mode (Hanna et al., 2015). Therefore, it is of paramount importance to understand the polar climate evolution in order to forecast which could be the potential short- and long-term climate impacts in the Mediterranean and other sensitive areas.

The examination of climate before the instrumental meteorological period relies on climatological reconstructions. Exploring climate-driven natural archives offers a more temporally extended and geographically wide perspectives on climatic variability, providing insights into patterns and factors driving past climate changes as well their impacts, tipping points of the ecosystems, and cascade effects over time and space (Klose et al., 2020); this is needed to augment our understanding of today's shifting climate and the future changes forecasted by climate models. Indirect indicators of past climate and environmental conditions, known as proxies, can be inferred from natural archives through geochemical, physical, geological, and biological measurements. In this sense, modern and former glacial environments, such as NE Greenland, are key areas to improve our knowledge of

past, present, and future global conditions, as they are generally located in remote-sensitive areas far from population centres, where direct human impact can be considered negligible for studying any of the processes implied in global change (Battarbee et al., 2002.; Nesje and Dahl, 2000).

However, not all paleoclimatic records serve as sensitive indicators of abrupt climate changes, and not all offer a temporal continuous record (Bradley 2015). In this sense, the climate reconstructions presented in this PhD thesis primarily focus on two geological, terrestrial sources of proxy data: the geomorphological record, consisting of glacial deposits and features of glacial erosion, and the lake sedimentary records, encompassing the geochemical and biological information preserved in their sediments.

The glacial geomorphological record constitutes a discontinuous and incomplete source of data, representing discrete events in time resulting from the integration of climatic conditions prior to the ice changes. Therefore, the examination of climatic information extracted from lake sediments has helped in contextualizing such episodic information. Hence, these two sources of data complement each other, providing a more comprehensive understanding of the climatic shifts and glacial oscillations under investigation.

1.1.1 GEOMORPHOLOGICAL RECORDS AND GLACIAL OSCILLATIONS

The analysis of the geomorphological record left by retreating glaciers can provide a comprehensive understanding of the landscape evolution and associate climate variability. Besides, these studies also provide insights about the forcings and processes responsible of the development of glacial landforms, as well as subsequent postglacial (periglacial) processes affecting their stability (paraglacial dynamics).

The geological record, especially along the Quaternary period, preserves more or less abundant geomorphic evidence of glacial advances and retreats associated with changes in ice volume, thickness, and length in response to changes in temperature and precipitation (Oerlemans, 2005). Consequently, the distribution of these landforms is indicative of past changes in climate regimes. Dating these glacial remnants will thus supply the chronological framework of glacial histories associated with past climate variability.

The temporal constrains of these past changes will come from direct dating of these glacial records by means of cosmic-ray exposure (CRE) dating. With the introduction of cosmogenic nuclide exposure dating, it is possible to directly constrain the timing of glacial fluctuations by dating polished bedrock, moraines, or erratic boulders left by glaciers (Dunai, 2010). This methodological advancement has reinvigorated the exploration of the glaciation history of the GrIS.

Geomorphologists struggled to establish absolute chronologies on the glacier record until CRE dating was developed (JC and FM, 2001). Until then, the timing of glacial oscillations was relative and approximate, based on local radiocarbon-dated records or on regional/hemispheric records, such as marine sediments and ice cores, losing valuable information on the sensitivity of glaciers to climate changes. The direct dating of glacial sediments with cosmogenic nuclides is a unique and one of the most powerful tools for reconstructing the

timing of past glacier volume changes (Gosse and Klein, 2014). Despite this dating technique has been only available for geomorphologists roughly over the last 35 years, it has become widespread and broadly used in paleoenvironmental studies all across the world, from the poles to the mountain regions, to understand glacial oscillations as well as periglacial dynamics in cold-climate regions of the Earth.

1.1.2 LAKE SEDIMENTARY RECORDS AND CLIMATE VARIABILITY

Proxies generated from lake sediment archives can provide a detailed and holistic view of past climate and environmental changes (Axford et al., 2009). Therefore, lakes serve as essential natural repositories of Earth's history, offering valuable insights into the past environmental and climate evolution through the accumulation of sediment layers. Over time, lakes collect a large array of particles and organisms both from their own internal dynamics and from their surroundings, transforming the extracted sediment cores into rich sources of historical environmental data. Paleolimnology, the multiproxy and high-resolution temporal study of preserved geological records in lakes, primarily relies on sediment coring to unearth this valuable information. Additionally, lake sediments exhibit diverse responses depending on the studied proxy to shifting climates, allowing to characterize with great detail how climate and other forcings have shaped Earth's surface.

To delve into the past and comprehend past dynamics in these aquatic ecosystems, this PhD thesis approach hinges on analyzing changes in sediment characteristics and studying fossil organisms. These proxies aid in reconstructing how lake systems responded to climate shifts (Birks et al., 2012). Given the intricate web of interactions within the ecosystem, a comprehensive understanding of lake behavior and past environmental variations benefits from examining a wide array of proxies (Smol, 2002). In contrast to single-proxy studies, the combination of multiple proxies uncovers more nuanced information and improves paleoenvironmental reconstructions (Bradley, 2015). This PhD thesis adopted a multidisciplinary approach that is accurately explained in the Methods section.

1.1.3 LATE QUATERNARY CLIMATIC AND ENVIRONMENTAL CHANGES IN GREENLAND

To frame the studies on the past changes affecting the GrIS, peripheral ice sheets and glaciers contained in this PhD thesis, it is essential to have a broad understanding of the current state of knowledge.

Over the last decades, ice cores collected from several sites across the GrIS have produced a wealth of information about Late Quaternary climatic and environmental changes (Cook et al., 2022; Rasmussen et al., 2023). However, there are still gaps and limited knowledge on the ice sheet response to climate variability and its sensitivity to temperature/moisture shifts. Here, I present a brief summary about the current knowledge of the GrIS dynamics since the onset of the last deglaciation (Figure 2):

LAST GLACIAL CYCLE

The GrIS, alongside Antarctica, is one of the only ice sheets that survived the last deglaciation during Termination-1 (T-1) (~19–11 ka BP). It persisted through the Last Interglacial period (~130–116 ka BP) despite significantly higher global temperatures, although its Northeast sector was notably reduced (Vasskog et al., 2015). The GrIS expanded considerably during the last glacial cycle (115 – 11.7 ka BP), reaching its peak volume during the LGM (~26.5 – 19 ka BP) (Clark et al., 2009; Vasskog et al., 2015).

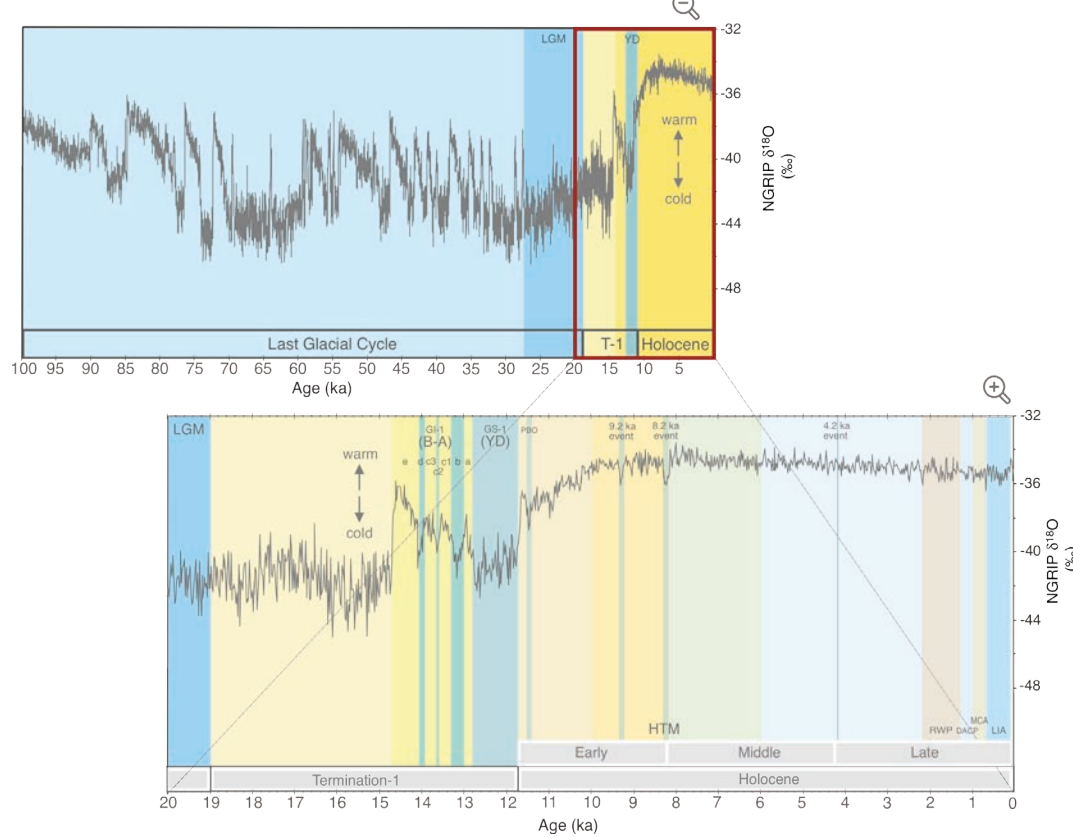


Figure 2. Temperature evolution since the last glacial cycle in the interior of Greenland based on the $\delta^{18}\text{O}$ record of the NGRIP ice core, 5-point running mean. Periods are labelled according to (Rasmussen et al., 2014). Source: own elaboration.

TERMINATION-1 (T-1; ~19–11 KA BP)

Around 20-19 ka BP (Clark et al., 2009), temperatures rose at the onset of T-1 as a result of a gradually increasing of both atmospheric CO_2 concentration (Shakun et al., 2012) and summer insolation in the Northern Hemisphere high latitudes (Clark et al., 2009). The reorganization of the ocean currents, atmospheric pattern changes and climate shifts provoked an enhancement of the temperature rise around 17 ka BP (Kobashi et al., 2017).

This led to a substantial reduction in GrIS volume, causing its margins to retreat, primarily becoming land-based (Funder et al., 2011; Vasskog et al., 2015).

A variety of terrestrial and marine records from Greenland and the North Atlantic region demonstrate the occurrence of abrupt temperature shifts ranging between 5 and 15 °C during T-1 with a marked seasonality (Buizert et al., 2014; Vasskog et al., 2015). These temperature shifts influenced the reorganization of thermohaline circulation in the Southern Ocean, enhancing the ventilation of deep oceanic waters of this hemisphere, and leading to a rapid global CO_2 rise and substantial deglacial environmental and biotic changes in the polar regions (Denton et al., 2010). Palaeoglaciological studies have modeled these oscillations of the GrIS and other peripheral glaciers during T-1 revealing significant spatial changes in response to warm (shrinking) and cold phases (expanding) (Funder et al., 2011; Vasskog et al., 2015). A widely-employed nomenclature for climatic change during T-1 is the sequence of Oldest Dryas, Bølling, Older Dryas, Allerød, and Younger Dryas. T-1 deglaciation was punctuated by two major cooling events affecting the Northern Hemisphere: the Oldest Dryas (OD; ~18.0–14.7 ka BP) and the Younger Dryas (YD; ~12.8–11.5 ka BP), with the Bølling-Allerød warm event (B-A; ~ 14.5 ka BP) in between.

The B-A event is divided into sub-events ‘a’ through ‘e’ named from Björck et al., 1998. To the prominent, very rapid onset of warmth ~14.7 ka BP of the Bølling interstadial followed more than 1/3 of the total deglacial warming (Alley et al., 2010). Bølling warmth was interrupted by the short-lived but prominent Inter-Allerød cold periods otherwise known as Older Dryas (Seierstad et al., 2005).

GrIS began to retreat from the continental shelf by ~16 to 14 ka BP, thus responding in part to the B-A warm event (Vasskog et al., 2015). Oxygen stable isotope data show that climatic conditions generally change from a rather warm climate at the beginning of the Bølling to a much cooler climate at the end of the Allerød, but also that the temperature changes abruptly toward both cooler and warmer conditions several times during this period (Rasmussen et al., 2006). Subsequently the YD cold climate oscillation began with a 200-year-long period of cooling and culminated with a 60-year-long period of abrupt warming, as recorded in Greenland ice cores (Steffensen et al., 2008). Over the GrIS, annual mean temperatures dropped between 5 and 9 °C during the YD, when both summer insolation (65° N) and atmospheric CO_2 were increasing (Buizert et al., 2014). Although temperatures dropped during this cold event, it is noteworthy that there is a particularly pronounced asymmetry in the behaviour of the ice margin during the YD and in some of the GrIS areas there is no evidence for marked ice margin response to the initial cooling. In fact, the GrIS retreat during the YD has been corroborated from the W shelf (Hogan et al., 2016; Oksman et al., 2017) where the ice extending to the outer shelf (Vasskog et al., 2015) and from eastern and southern Greenland (Andrews et al., 2018; Levy et al., 2016) where the ice was situated well inside the fjords mouth (Vasskog et al., 2015). Only on the north coast of Greenland did glaciers apparently advance and retreat at the beginning and end of the YD (Larsen et al., 2016).

HOLOCENE (11.7 KA BP TO PRESENT)

While sediment sequences reconstructing local and regional Holocene climate have been published for various ice-free regions of Greenland, the spatial coverage is still rather poor, and temporal resolution remains coarse, in the realm of the millennia, for many sites.

EARLY HOLOCENE (11.7 TO 8.2 KA BP)

Warmer temperatures during the Early Holocene accelerated deglaciation (Clark et al., 2012; Buizert et al., 2014). GrIS retreat within the modern coastline occurred around 11 to 10 ka BP based on radiocarbon ages (Bennike and Björck, 2002; Vasskog et al., 2015). Following T-1, the Northern Hemisphere experienced the maximum Holocene summer insolation, with temperatures about 2.5°C warmer than present during the Holocene Thermal Maximum (HTM; ~10–6 ka BP) (Axford et al., 2021; Kaufman et al., 2004; Renssen et al., 2009). Indeed, it is estimated that from the late stages of T-1 until the HTM, the GrIS loosed about one third of its areal extent (0.89 million km²; (Leger et al., 2023).

The HTM has been widely documented in Greenland's paleoenvironmental records, with different timing and intensity that is indicative of notable regional variability (Briner et al., 2016a; Buizert et al., 2018; Kjær et al., 2022; Lusas et al., 2017a; Vinther et al., 2008). During the HTM, there was a widespread trend of glacial retreat of the GrIS, mountain glaciers and ice caps, interrupted only by short periods of glacial stabilization in some regions (Young et al., 2020). Glacial response in S and W Greenland during the HTM was more diffuse than in the N and E sectors, where prevailing warmer temperatures led to a strong glacier retreat during the Early Holocene (Briner et al., 2016b). It is estimated that the GrIS receded 65 km inland from 12.7 to 9.8 ka BP in the NE Greenland, corresponding to an average retreat rate of ~22 m yr⁻¹ (Skov et al., 2020).

Across the GrIS, the long-term deglaciation trend was generally interrupted by two cold events: the Preboreal Oscillation (PBO) around 11.5–11.4 ka BP and the 9.2 ka BP event (9.5–9.2 ka BP interval). These abrupt cooling events are well-defined in Greenland ice-core isotope records and appear prominently and synchronously in most of them (Kobashi et al., 2017; Rasmussen et al., 2007; Thomas et al., 2007). Both events likely involved the alteration of the Atlantic Meridional Overturning Circulation (AMOC) driven by freshwater input into the North Atlantic Ocean via rapidly melting ice sheets (Renssen et al., 2009; Thornalley et al., 2018).

MIDDLE HOLOCENE (8.2 TO 4.3 KA BP)

By the mid-Holocene, the GrIS was situated behind its present-day ice limits, while many peripheral glaciers were smaller or completely absent (Solomina et al., 2015). Reduced summer insolation in the Northern Hemisphere, influenced by Earth orbital changes, initiated a gradual cooling trend in Greenland from 8.2 ka BP onwards (Carlson et al., 2014; Larsen et al., 2016; McKay et al., 2018; Reusche et al., 2018; Skov et al., 2020). Over Greenland annual temperatures are estimated to have cooled 3.3 ± 1.1 °C during the 8.2 ka BP event (Kobashi et al., 2007). This century-long event seems to have much in common to the 9.2 ka BP event both in the originating anomalies and their magnitude (Fleitmann et

al., 2008). Although this event is detected in the Greenland ice cores (Thomas et al. 2007) and in some paleorecords around Greenland (Carlson et al., 2021; Young et al. 2013), it lasted less than 150 years (Kobashi et al., 2007). This brevity could have caused to be undetectable by low-temporal resolution records (Fleitmann et al., 2008) and not favor a significant glacier expansion.

Summer temperatures dropped, reaching 1–1.5 °C below present-day temperatures by the end of the mid-Holocene at ~4 ka BP, exhibiting high variability across Greenland (Lasher and Axford, 2019). As a result, glaciers started to re-advance in what is termed the neoglaciation (Porter, 2000). However, due to the time-transgressive nature of the end of the HTM across the island, the onset of glacial advances showed significant regional and local variability. Although the spatial and temporal patterns of the Holocene glacier advances and retreats are still uncertain, this is particularly true for the neoglacial time span starting after ca. 6 ka BP (McKay et al., 2018; Palacios et al., 2020; Porter and Denton, 1967).

The GrIS globally reached its minimum Holocene extent at 7 ka BP, but the retreat of some fronts was delayed until ~4–3 ka BP or even later (Larocca et al., 2020b, 2020a; Larsen et al., 2018; Schweinsberg et al., 2019). Local mountain glaciers and ice caps exhibited a similar response pattern to changing Holocene climate trends. In S Greenland, most glaciers disappeared between ~7.1 and 5.5 ka BP and began recovering from ~3.1 ka BP to 1.3 ka BP onwards (Jomelli et al., 2022; Larocca et al., 2020b). In SW Greenland, some glaciers survived throughout the HTM and started recovering from 4.3 ka BP onwards (Larocca et al., 2020b). In E Greenland, the Renland Ice Cap was smaller than present by 9.5 ka BP and began regrowing at ~4 ka BP (Medford et al., 2021). In NE Greenland, in the area were this thesis focuses, it was only suspected by previous studies that glaciers were smaller than present during the Middle Holocene than during their Late Holocene extension that occurred at ~3 ka BP (Biette et al., 2020b).

LATE HOLOCENE (4.3 KA BP TO PRESENT BP)

Late Holocene climate it is characterized by a general cooling trend (Wanner et al., 2011), with an alternation of warm and cold intervals identified in the Northern Hemisphere; two phases of warmth; the Roman Warm Period (RWP, 1–300 CE, (Ljungqvist, 2010)) and the Medieval Climate Anomaly (MCA, 800–1200 CE; (Lamb, 1965; Stine, 1994)) as well as two cooling episodes, the Dark Ages Cold Period (DACP, 800–300 CE; Ljungqvist, 2010) and the Little Ice Age (LIA, 1300–1850 CE; (Ljungqvist, 2010; Mann and Jones, 2003; Oliva and Ruiz-Fernández, 2018)). The transition from these cold to warm phases has been associated with changes in the mode of the NAO (Darby et al., 2012; Faust et al., 2016; Funder et al., 2011; Jackson et al., 2017; Nesje and Dahl, 2001; Olsen et al., 2012), which describes the main mode of climate variability in the North Atlantic region during winter (Hernández et al., 2020; Wanner et al., 2011). A positive (negative) NAO is broadly associated with increased (reduced) northward advection of Atlantic water by the AMOC and a decrease (increase) in sea ice in the Arctic (Dickson et al., 1996; Thompson and Wallace, 1998).

Despite all this whole picture of GrIS changes related to climate periods and events, important knowledge gaps still exist as to how the GrIS and peripheral glaciers respond to

climate switches, their sensitivity to climate, and spatio-temporal patterns of past glacial oscillations (e.g. Kelly and Lowell, 2009; Vasskog et al., 2015; Larocca et al., 2020a, 2020b), namely:

- What was the glacier response during the YD cold phase?
- Where were the glaciers during the HTM?
- How did the environment readjust to ice-free conditions?

1.2 STUDY AREA

The study areas lie at the ice-free areas around Zackenberg Research Station (74°28' N, 20°34' W), situated in the Wollaston Foreland Peninsula in the SE corner of the Northeast Greenland National Park (Figure 3 and 4).

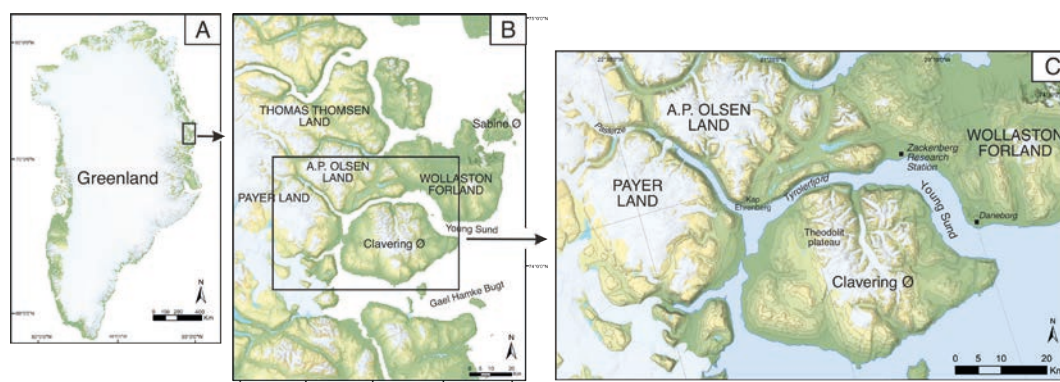


Figure 3: (A) Location of the study area within Greenland. (B) Location of the study area within the region, inside NE Greenland. (C) Regional setting of the study area. Source: own elaboration and Greenland Mineral Resources Portal from GEUS base map.

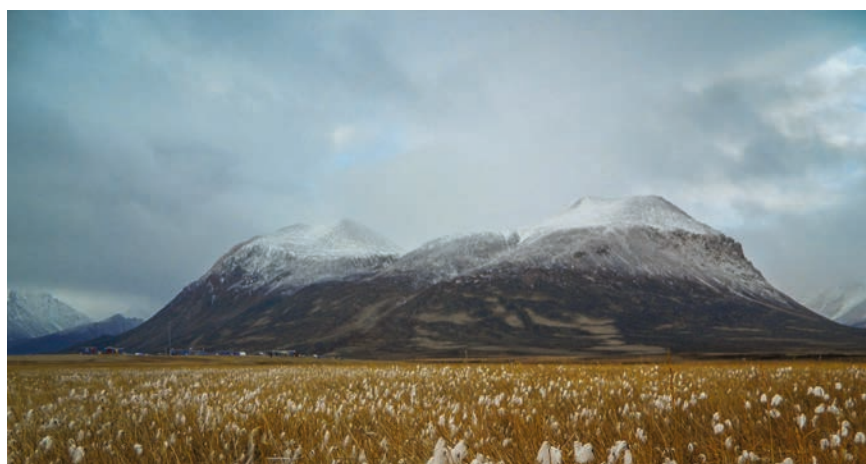


Figure 4. Image of the study area in September 2019, picture taken on the Zackenberg Valley oriented facing W. To the left of the picture, Zackenberg Research Station and The Young Sund fjord beyond; on the middle Zackenberg Mountain (and the Zackenberg peak at 1389 m); To the right, Zackenberg Valley and Store Sodal valley.

It is a very appropriate area for undertaking this PhD research as:

- It is a remote area: defined as those occurring in high latitudes or high-altitude regions, have the advantage of not being heavily overprinted by local anthropogenic processes.
- It is located within the world largest National Park. Contributing to its remoteness and being more isolated from possible anthropogenic intrusions.
- It is affected by the polar amplification and allows to examine the magnitude of glacial and climate oscillations in the High Arctic with regards to other areas.

The coastal ice-free areas around Greenland island are considered as one of the most sensitive ones and much more stable than glaciers and ice sheets. These areas provide excellent proxy data for land-based geological paleoclimatic reconstructions, making possible the study of past GrIS oscillations, since Greenland's local glaciers can respond and record climate changes at sub-millennial timescales (Briner et al., 2016a), faster than inland ice margins (Levy et al., 2014a). Moreover, the NE Greenland region is one of the only of few locations where the margins of the GrIS and local glaciers were located on land (at least partially) by late glacial time (Levy et al., 2016).

Climate and environmental characteristics (permafrost, geomorphology, fauna, flora, etc.) are well known in the area thanks to the existence of long-lasting monitoring programs (e.g. BIOBASIS, GEOBASIS).

Logistically, Zackenberg research station provides excellent support to develop research, being one of the two areas in NE Greenland where research infrastructure is available. This is a key issue in the polar regions and this PhD thesis benefited from the existing facilities.

For all these reasons, the area is considered a unique laboratory where to study the type and chronology of cold-climate geomorphological processes and associated climate conditions in NE Greenland.

THE PHYSICAL ENVIRONMENT

The flat-topped highest summits surrounding the study area rise between 1000 and 1400 meters above sea level. These plateaus are connected to steep hillsides that descend towards the valley floor. The ice-free regions of the valley floor mainly correspond to an outwash plain, with sediments deposited by a fluvial braided system fed by glacial meltwater and other proglacial streams. Some of these areas are periodically affected by glacial lake outburst floods (GLOFs). Rivers drain the broad U-shaped valleys for several kilometers and form large deltas as they reach the fjords.

Exposed bedrock is primarily found at the mountain tops and upper slopes of both valley sides, while the lower parts and valley floors are covered by Late Quaternary sediments (Cable et al., 2018; Gilbert et al., 2017). The studied valleys around the study area contain two distinct bedrock types: metasediments, gneiss, and granite formations of Caledonian Crystalline complexes from the Early Proterozoic with abundant orthogneiss, and Jurassic and Cretaceous mudstones, sandstones, and carbonates sedimentary rocks (Grønnow et al., 2009; Henriksen et al., 2009). Consequently, substantial deposits of Quaternary sediments affected by active hillside processes cover the middle and lower sections of the slopes. The bedrock geology determines the prevailing geomorphological processes in the

ice-free Zackenberg Valley, resulting in distinct landforms and processes on each underlying type of lithology. Erosive and sedimentary glacial landforms are widespread across the valley and have been significantly altered by paraglacial and periglacial dynamics. The whole area is underlain by continuous permafrost (200 to 400 m thick) and a spatially variable active layer (45 to 80 cm thick) (Christiansen et al., 2010, 2008).

The study area exhibits a typical High Arctic polar tundra climate (Kottek et al., 2006). From 1996 to 2015, the mean annual air temperature at Zackenberg Research Station averaged $-9.0\text{ }^{\circ}\text{C}$ (Figure 5), and the mean annual precipitation was 367 mm (Højlund Pedersen, 2017), primarily falling as snow, although occasional rain events may occur in the summer months (Hasholt et al., 2008). The brief summer season plays a pivotal role in the development of the valley's sparse vegetation cover. The extensive lowland areas consist of a moist to dry tundra dominated by shrubs less than 15 cm tall, along with grasslands, fens, and scattered snow patches. The diversity and size of the plants decrease at higher elevations (CAVM Team, 2003). Below 200 meters above sea level, small shrubs, fell fields, and grasses predominate (CAVM Team in 2003), while above 600 meters a.s.l., vegetation becomes exceedingly scarce (Buus-Hinkler et al., 2006; Elberling et al., 2008).

THE HUMAN BACKGROUND

This region has consistently captured significant attention and boasts a rich historical background due to special geographical characteristics. One of the most prominent polynyas defined as recurring opening in the sea ice in an otherwise ice-covered ocean in Northeast Greenland is located between 74° - 75°N latitude and is named 'Sirius Water Polynya' (Pedersen et al., 2010). These areas of open waters are known for bringing an increase in biological productivity. Consequently, the coastal sector in NE Greenland where this polynya is located, stands out as an area with abundant wildlife that was historically used for hunters and fishers. Ice-free waters were rare gateway for sea-going vessels to access the coastal regions (Pedersen et al., 2010), resulting thus in rich prehistoric and historic information. The region has historically been a settlement area for the Inuit for the past 4500 years, pre-dating the arrival of European whalers and explorers to the entire region (Kroon, 2009). Various waves of Inuit populations, including the Independence people I, Greenlandic Dorset, and the Thule Culture, inhabited the favorable northeast coastal environments. According to some authors, the last remnants of this population north of 69°N latitude may have been along the southern shoreline of Clavering Ø ($74^{\circ}15'\text{N}$; (Kroon et al.,

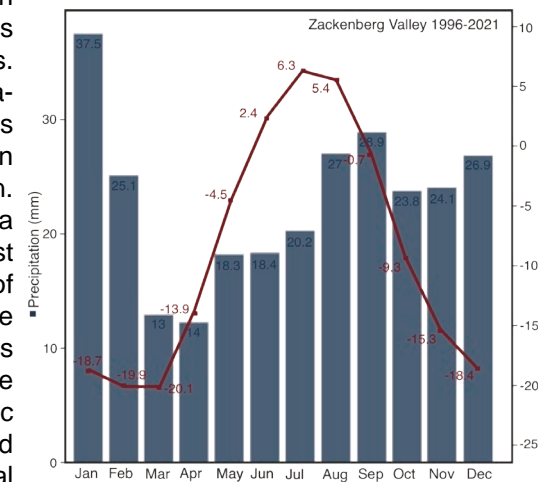


Figure 5. Climatogram for the period between 1996 and 2021 based on temperature and precipitation data from the Zackenberg Research Station (Greenland Ecosystem Monitoring database). Source: own elaboration.

2009; Rule et al., 2005)). In 1923 CE, European explorers encountered a native population in this coastal area for the first and last time (Clavering, 1830). The Greenland whale fishery commenced around 1612 CE (Rule et al., 2005). Consequently, the only available information on the region north of latitude 69°N was derived from whalers' sightings until the comprehensive charting of East Greenland by William Scoresby Jr. in 1822 CE. This marked a pivotal moment, as it not only represented the first scientific observations of the area but also provided the first semblance of accurate information regarding the fjord region of East Greenland (Rule et al., 2005). The NE Greenland region gradually became a site of extensive scientific and non-scientific exploration. In the following years, Norwegian and Danish fishing and hunting endeavors overlapped with the increasingly numerous scientific expeditions from different countries that mapped the area in detail and collected various types of data such as meteorological and glacial conditions, flora and fauna among others (Rule et al., 2005).

1.2.1 THE GEOMORPHOLOGICAL RECORD AND GLACIAL OSCILLATIONS IN NE GREENLAND

Northeast Greenland is the place where the GrIS experienced the largest areal changes since the Last Glacial Maximum. However, the age constraints of the last deglaciation are in some areas sparse (Figure 6). So far, CRE dating has only been used in relatively few



Figure 6. Map assembling cosmogenic-nuclide data from Greenland research works. Red circle marking the study area location of this PhD thesis. Source: ICE-D database project. Published results of this PhD thesis are already displayed in this open repository.

sites in the vast North and Northeast Greenland (Biette et al., 2020b; Håkanson, 2008; Håkansson et al., 2007a; Larsen et al., 2020, 2018; Skov et al., 2020) (Figure 6).

In the Northeast Greenland coastal region, the understanding of the chronology of glacial fluctuations and landscape changes during T-1 and throughout the Holocene remains limited. There is a paucity of studies addressing the timing and the extension of the glacial oscillations in this area (Figure 7). Most of them are at the north and at the south of our

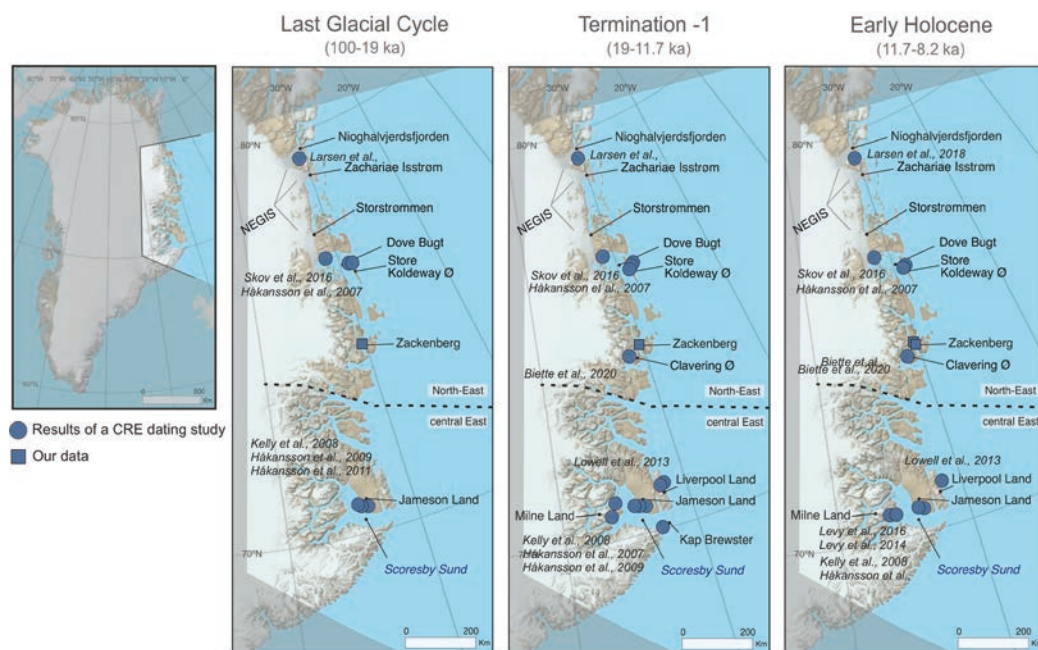


Figure 7. Map of NE Greenland region including the location of exposure ages studies from published glacial CRE chronologies including the results of this PhD thesis divided into the periods from which they have obtained dates (Biette et al., 2020b, 2020a; Håkansson et al., 2009b, 2009a, 2007b, 2007a; Kelly and Lowell, 2008; Larsen et al., 2018; Levy et al., 2016, 2014b; Lowell et al., 2013; Skov et al., 2020). The geographical division (North-East vs. Central-East Greenland) follows that of the Geological Survey of Denmark and Greenland (Dawes and Glendal, 2007). Source: own elaboration and Greenland Mineral Resources Portal from GEUS base map.

Zoom in into our study area within the NE Greenland region, the only previously studied valley of our area, Zackenberg Valley: On the other valleys, the only geo-glacio data available data comes from historical expeditions. Glacial evidence in the Zackenberg area is distributed from mountain plateaus to valley floors and has been described in detail in previous studies (Cable et al., 2018; Christiansen and Humlum, 1993). However, despite the widespread, highly detailed geomorphological mapping of glacial features (moraines, erratic boulders and glacial polished surfaces) from Cable et al., 2018, the chronology of the different glacial phases is not yet constrained. The likely oldest glacial evidence in the area are glacio-lacustrine deposits distributed on the lower slopes, dated by optically stimulated luminescence (OSL) between 84 ± 8 and 114 ± 11 ka, suggesting that during that time part of the Zackenberg Valley was ice-free and probably filled with an ice-dammed lake (Christiansen et al., 2002). Ice-free conditions were also reported from a pronival basin at 600 m in Zackenberg Mountain, where a thermoluminescence date yielded an age

of 66.2 ± 7 ka, thus confirming the absence of glaciers in the upper part of the valley during part of the last glacial cycle (Christiansen, 1994). OSL-dated glaciofluvial deposits indicate that the deglaciation of the lower Zackenberg Valley occurred after 22 ± 3 ka (Christiansen et al., 2002). Based on the distribution of glacial and periglacial landforms, Christiansen and Humlum (1993) proposed a tentative deglaciation chronology and more recently, based on the fjord valley fill, including sedimentary deltaic sequences and OSL ages, Gilbert et al. (2017) suggested that the Zackenberg lowlands may have been ice free as early as 13–11 ka (Christiansen et al. 2002).

1.2.2 THE LAKE SEDIMENTARY RECORD AND CLIMATE VARIABILITY IN NE GREENLAND

The knowledge gap about the local and regional Holocene climate evolution of Northeast Greenland is evident owing to the absence of multi-proxy climate reconstructions. The spatial coverage remains incomplete, and the temporal resolution is usually at millennial-scale, although certain studies have made progress in advancing our understanding in this field (Figure 8)

There have been several studies from the region that have examined paleo-records from lacustrine and continental shelf sediments (Figure 8). The closest lake sediment pollen work is located at the northwestern part of Zackenberg Valley and extends to 9 calibrated (henceforth cal.) ka BP (Bennike et al., 2008). But, the closest work about high-resolution proglacial lake is located ~20 km to the W from Zackenberg Valley (Adamson et al., 2019). However, as happen with geomorphic/chronological records, research has focused on areas to the north (Christiansen, 1998) and the south of our study area (Davies et al., 2022; Klug, 2009; Pados-Dibattista et al., 2022; Schmidt et al., 2011; Wagner et al., 2008). Records from these two regions broadly show a climate evolution with a cold Early Holocene, a warmer Mid-Holocene with a Holocene Thermal Maximum ending at ~5.5 cal. ka BP, and a relatively cold Late Holocene (Axford et al., 2017; H. Cremer et al., 2001; Holger Cremer et al., 2001; Klug and Wagner, 2008; Kolling et al., 2017; Levy et al., 2014b; Lowell et al., 2013; Lusas et al., 2017b; Medford et al., 2021; Wagner et al., 2005, 2000; Wagner and Melles, 2002). According to Klug (2009), coastal lakes show that around 6.2 cal. ka BP, subsurface waters on the Central Northeast Greenland shelf began to cool. After approximately 5.5 cal. ka BP, a distinct cooling phase commenced, accompanied by an increase in sea ice extents (Pados Dibattista et al., 2022), indicating a Neoglacial average cooling of 0.6–0.8°C per thousand years from around 5.5 to 0.5 cal. ka BP. This cooling trend was more pronounced between approximately 4 to 3.5 cal. ka BP and progressively intensified throughout the late Holocene (4.2 cal. ka BP to the present) (Klug, 2009; Klug and Wagner, 2008).

In some cases, paleoceanographic records also indicate greater productivity in the early and middle Holocene compared to the late Holocene (Axford et al., 2017; Pados Dibattista et al., 2022). However, across the entire set of terrestrial and marine records, there is no strong consensus on the timing of the Neoglacial or other events such as the Little Ice Age (LIA). The closest event to our study area was reported as the onset of the Neoglaciation at approximately 3.2–3.5 cal. ka BP, marked by glacial advances (Lusas et al., 2017), a constructed negative temperature anomaly (Medford et al., 2021), and a cooling of subsurface water on the central Northeast Greenland shelf at 3.2 cal. ka BP (Axford et al., 2017). A shift towards more arid conditions was recorded around 2.7 cal. ka BP when the atmospheric circulation over the North Atlantic significantly changed (Pados Dibattista et

al., 2022). The first signs of glacial regrowth appeared initially in high-elevation interior locations around 2.6 cal. ka BP (Wagner et al., 2008a). Diatom analyses suggested that some areas of NE Greenland were seasonally ice-free during much of the Holocene, with perennial ice cover developing only after 1.8 cal. ka BP (Cremer et al., 2001a, 2001b). A gradual change towards colder temperature conditions began after 1.8 cal. ka BP, as observed in other regions (Levy et al., 2014b).

There is no consensus about the timing of the LIA, although most records indicate cold events or glacial advances prior to or around approximately 0.7 cal. ka BP, including at 1.3 cal. ka BP (Lusas et al., 2017) and 1.0–0.8 cal. ka BP (Adamson et al., 2019; Medford et al., 2021), with a subsequent period of ice-marginal retreat around 0.5 cal. ka BP (Adamson et al., 2019; Lusas et al., 2017; Medford et al., 2021).

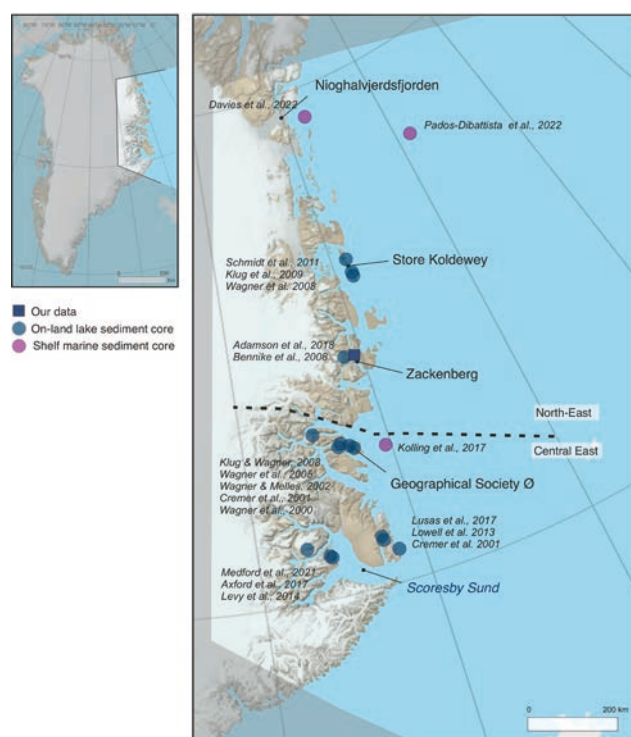


Figure 8. Map of the NE Greenland region including the locations of the previous to this PhD thesis sediment core studies discussed in the text (both marine and lacustrine): (Axford et al., 2017; Holger Cremer et al., 2001; Davies et al., 2022; Klug, 2009; Klug and Wagner, 2008; Kolling et al., 2017; Levy et al., 2014b; Lowell et al., 2013; Lusas et al., 2017b; Medford et al., 2021; Schmidt et al., 2011; Wagner et al., 2008, 2005, 2000; Wagner and Melles, 2002). The geographical division (North-East vs. Central-East Greenland) follows that of the Geological Survey of Denmark and Greenland (Dawes and Glendal, 2007). Source: own elaboration and Greenland Mineral Resources Portal from GEUS base map.

1.3 STRUCTURE OF THE THESIS AND OBJECTIVES

This PhD thesis includes a general introduction and a summarize methodology applied to obtain the main findings that are presented in four research articles that compose the results section, finishing with the general conclusions.

In order to avoid repetition between this PhD thesis and the research articles, the Introduction and Methods sections are a general compilation, and more specific details are accurately described in each of the published articles.

1.3.1 FRAMING THE RESEARCH ARTICLES

As mentioned above, the findings of this PhD thesis are contained inside the four research papers conducted within the designated study area (Figure 9). Three of these papers focus on the reconstruction the glacial oscillations in four valleys with distinct geographical characteristics (Paper I, Paper II, and Paper III). The fourth paper (Paper IV) explores the past climate variability of the area through a multiproxy characterization of lake sediments. In alignment with the content of this fourth paper, additional information from the same area has been incorporated into the study of climate variability, with non-published supplementary results in section 3.2.2 (other data).

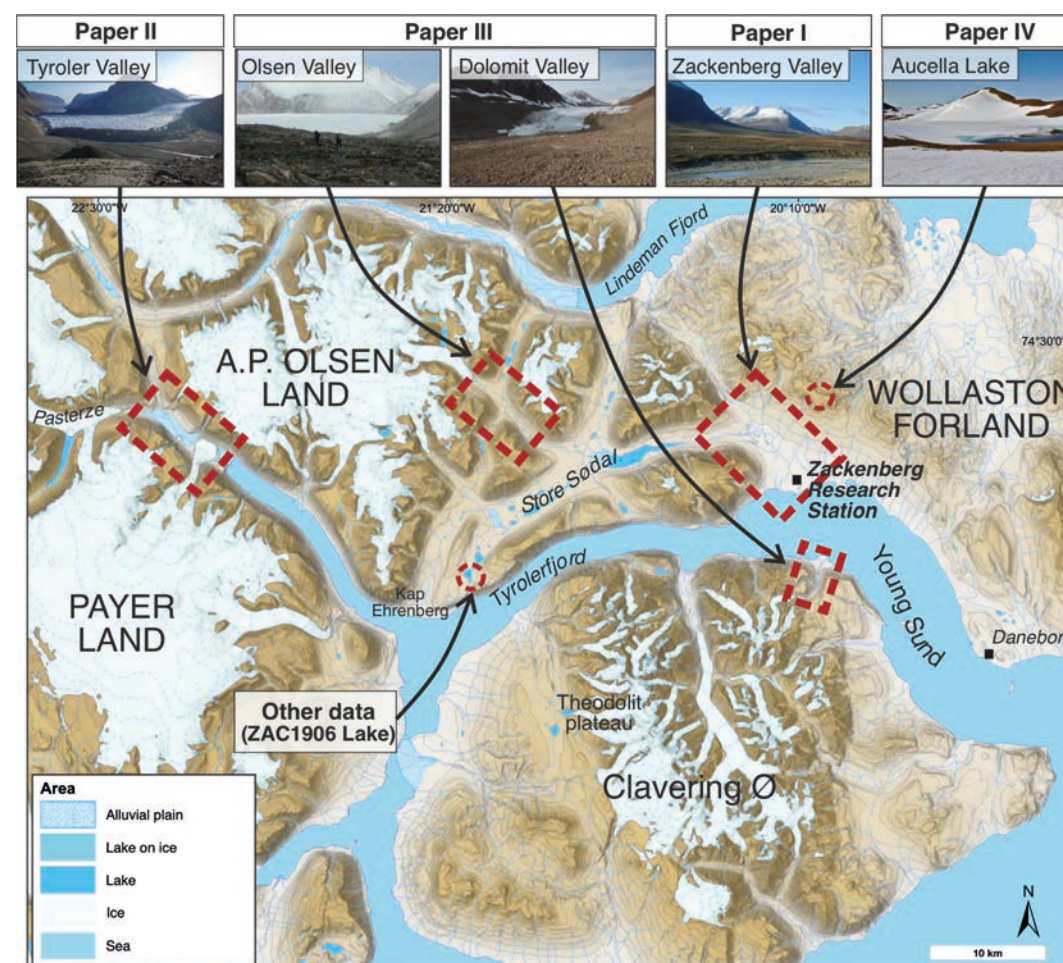


Figure 9. Location of the different valleys and lakes studied, and results included in the published research articles within the study area. Source: own elaboration and Greenland Mineral Resources Portal from Geological Survey of Denmark and Greenland (GEUS) base map.

1.3.2 OBJECTIVES AND RESEARCH QUESTIONS

This PhD thesis gives answer to the following major research questions (RQ):

RQ 1: Which have been the past spatio-temporal patterns of glacial advances /retreats since T-1 and throughout the Holocene in this area? (Paper I, II and III)

- Which landforms have been generated by glacial oscillations in the area?
- When did the GrIS margin start shrinking during the last glacial cycle?
- What were the phases of major glacial advances/stillstands and retreats?
- Can we quantify the magnitude of glacial response during past warm and cold periods and events?

RQ 2: To what extent is CRE dating successfully applied in this area, where post-glacial environmental dynamics are very active? (Paper I, and III)

- What does the chronology inferred from glacial geomorphic features say about the deglaciating process and environmental history of the area?
- Are these geomorphic features representative of the glacial chronology across NE Greenland or have they been intensely reworked by paraglacial processes?

RQ 3: What is the natural climate variability, and which are the climate conditions driving glacial oscillations in this area during the last several millennia? (Paper VI)

- Do lake sediments record a well-preserved climate signal, or do we see other environmental signals in these natural sediment archives?
- The different sensitivity of the proxies employed to reconstruct the lake processes is reflected in their response?
- Are these remote lakes indeed highly sensitive and therefore sentinels of environmental change?

RQ 4: Are the climate and glacial trends detected in the Zackenberg area synchronous with those recorded in other NE Greenland regions and around GrIS? (Paper I, II, III, IV)

- Do climate changes reconstructed from lake sediment records explain glacial responses inferred from the geomorphic record?
- Does the need of multiproxy studies become clear in terms of difference in temporal resolution to understand lake system and glacial oscillations linkages to environment and climate?
- Have remarkable climatic changes occurred during the Holocene which led to important ecosystem changes in terrestrial and aquatic systems?
- What are the relationships between deglaciation chronologies and local/regional and interregional climate variability?

Table 1. Research articles (Papers) that conform this PhD thesis related with the main research questions they answer and the aims of each one.

Article	RQ	Aims of the study
Paper I : 'Late Glacial deglaciation of the Zackenberg area, NE Greenland. Geomorphology.'	RQ1, RQ2, RQ4	<ul style="list-style-type: none"> □ Examine the limits of CRE dating for establishing time constraints in highly dynamic glacial-paraglacial-periglacial environments. □ Create a general framework of how the GrIS and peripheral glaciers respond to climate switches, their sensitivity to climate, and spatio-temporal patterns of past glacial oscillations at the entrance of the fjord area. □ Compare with different paleodata at local, regional and Greenland level.
Paper II : 'Holocene glacial oscillations in the Tyroler Valley (NE Greenland).'	RQ1, RQ4	<ul style="list-style-type: none"> □ Identify the main phases of glacial expansion and associated environmental implications during the Late Holocene creating a deglaciation history of the glacial oscillations , at the end of the fjord area (close to the present-day glacier fronts). □ Identify and differentiate landforms generated by glacial oscillations and by paraglacial processes with the creation of new cartography of the glacial landforms in areas where there are no previous studies. □ Identify the main phases of glacial expansion and retreat , as well as the major postglacial processes reshaping the landscape. □ Compare spatio-temporal patterns of neoglacial fluctuations in the Tyroler Valley with those inferred from other regions across Greenland.
Paper III : 'A Late Glacial and Holocene chronology of climate-linked landscape evolution in NE Greenland from CRE dating of landforms.'	RQ1, RQ2, RQ4	<ul style="list-style-type: none"> □ Identify the main phases of glacial expansion and associated environmental implications during the Late Holocene creating a deglaciation history of the glacial oscillations , in different valleys of the area (near to the present-day glacier fronts). □ Identify and differentiate landforms generated by glacial oscillations and by paraglacial processes with the creation of new cartography of the glacial landforms in areas where there are no previous studies. □ Identify the main phases of glacial expansion and retreat , as well as the major postglacial processes reshaping the landscape. □ Identify the value of CRE dating in an environment of cold-based glaciers and intense paraglacial and periglacial processes accompanying deglaciation and rapid temperature increases. □ Compare spatio-temporal patterns of landscape evolution in these valleys with those detected in other regions across NE Greenland.
Paper IV : 'A ~5000-year multiproxy record of summer climate in NE Greenland.' and Other data	RQ3, RQ4	<ul style="list-style-type: none"> □ Refine our understanding of the timing and patterns of regional environmental and climate variability in NE Greenland. □ Reconstruct climate conditions driving glacial advances/retreats. □ Produce a high-resolution geochemical, biological, and physical reconstruction from a remote lakes.

2 METHODS

OUTLINE

- 2. METHODS
- 2.1 RECONSTRUCTION OF GLACIAL OSCILLATIONS
- 2.1.1 SPACE: GEOMORPHOLOGICAL MAPPING
- 2.1.2 TIME: GEOCHRONOLOGY
- 2.1.2.1 COSMOGENIC RADIONUCLIDE EXPOSURE (CRE) DATING
- 2.1.2.2 OPTICALLY STIMULATED LUMINESCENCE (OSL) DATING
- 2.1.2.3 HISTORICAL DATA
- 2.2 RECONSTRUCTION OF CLIMATE VARIABILITY: PALEOLIMNOLOGY



2.METHODS

While different methodologies employed in the four original papers of this thesis, a consistent approach was followed in all of them. This involved the preparation of the field campaign through a preliminary survey, the collection of samples and data during the fieldwork, the generation of preliminary results via the analysis and treatment of the samples, and ultimately, the presentation of results and their interpretation. Each of the original publications constituted a multiproxy study detailed in Table 1.

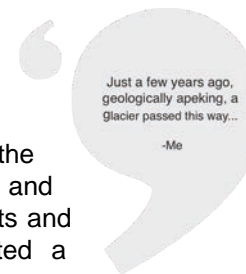


Table 1. Research articles (Papers) that conform this PhD thesis related with the main research questions they answer and the aims of each one.

Record	Method / approach	Paper I	Paper II	Paper III	Paper IV	Other data
Glacial/periglacial landforms	Geomorphological mapping	X	X	X		
	CRE dating	X	X	X		
	OSL dating		X			
	Historical data		X			
Lake sediments	Non-destructive analysis (CT-scan, XRF, hyperspectral imaging)				X	X
	Destructive analysis (¹⁴ C dating, organic matter, XRD, diatoms)				X	X

Papers I, II, and III used the same type of terrestrial records as source of paleoenvironmental information and, despite some differences, a common approach (Figure 1): a combination of mapping glacial and periglacial landforms with CRE dating. On one hand, the landforms shaped and left by the glaciers provided insights into their spatial extent and type of glacial oscillations, while the CRE dating of glacial landforms contributed to the establishment of the glacial chronology.

The strategy of the research commenced with the selection and identification of key valleys for the application of this methodology. Before the fieldwork, the area underwent characterization through existing literature and satellite images, providing preliminary ideas and a sampling strategy for the fieldwork.

Once in the field, we validated the preliminary map based on in-situ observations and collected samples for dating purposes. The samples were sealed, packed, and transported back to Barcelona, where they were processed at the laboratory. Following standard analytical procedures, age calculations, and statistical tests, the final ages datasets were generated. With these two outcomes (geomorphological maps and ages datasets), the chronological framework of the landscape evolution in each studied valley was created.

Additionally, two other dating approaches were used in Paper II: OSL dating of buried sediments and historical data derived from past expeditions in NE Greenland.

Paper IV uses another natural archive, lake sediments, to reconstruct the climatic framework of glacial oscillations in the area. The initial phase of this research involved the

preparation of logistics for fieldwork (Figure 1). Subsequently, during the field campaign, samples and other relevant information are collected. To extract the maximum information from the lake sediment core, we employed both non-destructive and destructive analyses to acquire diverse biological and geological proxies, constrained by time with accelerator mass spectrometry (AMS) ¹⁴C ages dataset.

The fundamental workflow of each methodology employed in this thesis is outlined below. Regarding the structure and length of the following sections, they have a lot to do with the involvement of this PhD author in the different tasks and steps of the applied methodology.

As the geochronological approach (geomorphological mapping and CRE dating of landforms) is used in three of the four research articles and the author of this PhD thesis executed all the steps of the process, this methodology has required more space and time in the tasks execution and will be extensively explained in the following sections. With regard to other methods used in this research, the author has been partially involved in one or more aspects of the workflow, such as field sample collection or given laboratory analyses. On other occasions, experts in these methodologies have conducted the analyses and shared the results for the publications that constituted the core of this PhD thesis.

2.1 RECONSTRUCTION OF SPATIO-TEMPORAL GLACIAL OSCILLATIONS

The reconstruction of glacial oscillations (collected in Papers I, II, and III) has focused on glacial and periglacial records using geomorphological mapping and CRE dating (Table 2). OSL dating and historical data have complemented CRE dating in paper II.

Table 2. Summary of the different types of analysis and methodologies conducted on the glacial and periglacial landforms. Source: own elaboration.

Type of analysis	Method	Principles	Provided information	Laboratory
Geomorphological mapping	Field surveys, satellite images and digital elevation model	Distribution of the glacial and periglacial landforms and its characteristics are indicative of past changes in climate regimes.	Reconstruct the previous glacial extension and the dynamics of the glacier over time.	-
Chronology	CRE dating	Production of terrestrial in situ cosmogenic nuclides. As they build up predictably with time on the rock surface, measuring their concentrations allows the determination of how long a rock surface or sediment has been exposed to cosmic-rays.	Reconstruct the timing of glacial oscillations	Laboratoire National des Nucléides Cosmogéniques of the Centre Européen de Recherche et d'Enseignement des Géosciences de l'Environnement (CEREGE, Aix-en-Provence, France).
	OSL dating	Relies on measuring trapped electrons' release when minerals are exposed to light, helping determine the time elapsed since their last exposure to sunlight or heat.	Quantify the time elapsed since mineral grains were last exposed to sunlight, offering insights into the depositional age of sediments.	National Research Centre on Human Evolution (CENIEH, Burgos, Spain).
	Historical data	Historical pictures and descriptions, used to compare and analyze the evolution of a glacier or landscape.	Provides a spatial and quantitative perspective of changes in the glacier's position.	-

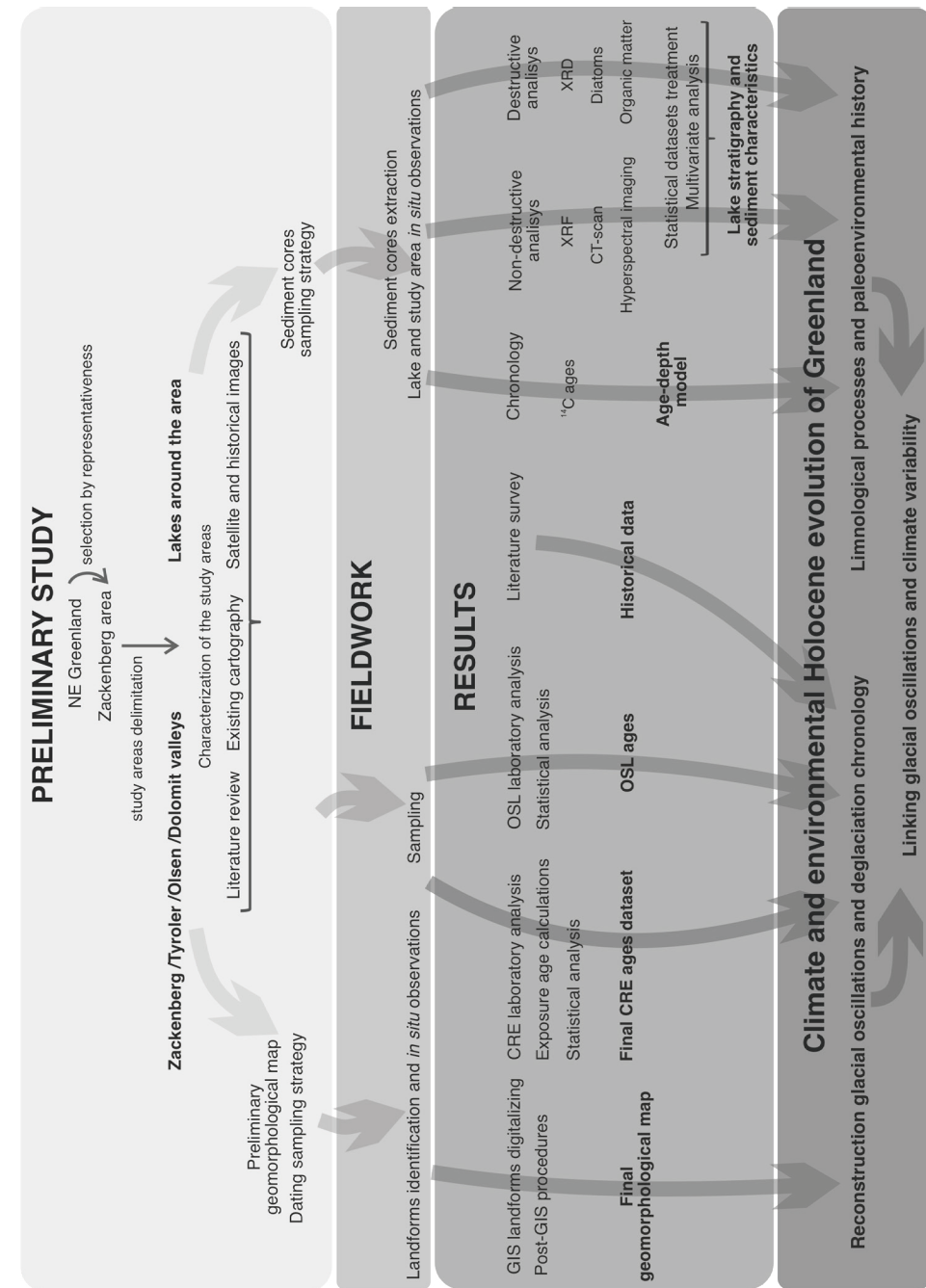


Figure 1. General scheme of the workflow followed in this PhD thesis: Preliminary study; conducting fieldwork; obtention of results; final Holocene climate and environmental reconstructions for Greenland. Source: own elaboration.

2.1.1 SPACE: GEOMORPHOLOGICAL MAPPING

An accurate mapping of geomorphological features is essential, therefore the published geomorphological maps over the deglaciated valleys of the NE Greenland gathered the spatial distribution of major glacial and periglacial landforms to understand the coupling of glacial, periglacial and paraglacial processes in newly exposed terrain. These maps supported the formulation hypotheses about the environmental evolution in the different valleys, including glacial extent during different timescales and periglacial activity as well as landform changes associated with subsequent paraglacial adjustment.

On the one hand, the most common valleys' landforms that offer more information about glacial history are moraine boulders, erratic boulders, and polished surfaces. These are the landforms that have been sampled for CRE dating. Each of these landforms provides different a type of environmental information: Moraine boulders are commonly indicative of periods of the maximum glacier advance or ice stillstands, when the ice-built moraines, with the subsequent moraine stabilization (Davies et al., 2022). Erratic boulders and polished surfaces reveal horizontal and vertical ice retreat changes (Corbett et al., 2011; Fernández-Fernández et al., 2021), and are mostly indicative of the timing of their exposure after a period of glacial shrinking or retreat. All these landforms are widely distributed in all the study areas, although they present different characteristics from one area to another (Figure 2).

On the other hand, periglacial landforms as well as those derived from alluvial and fluvial processes inform about the post-glacial landscape evolution.

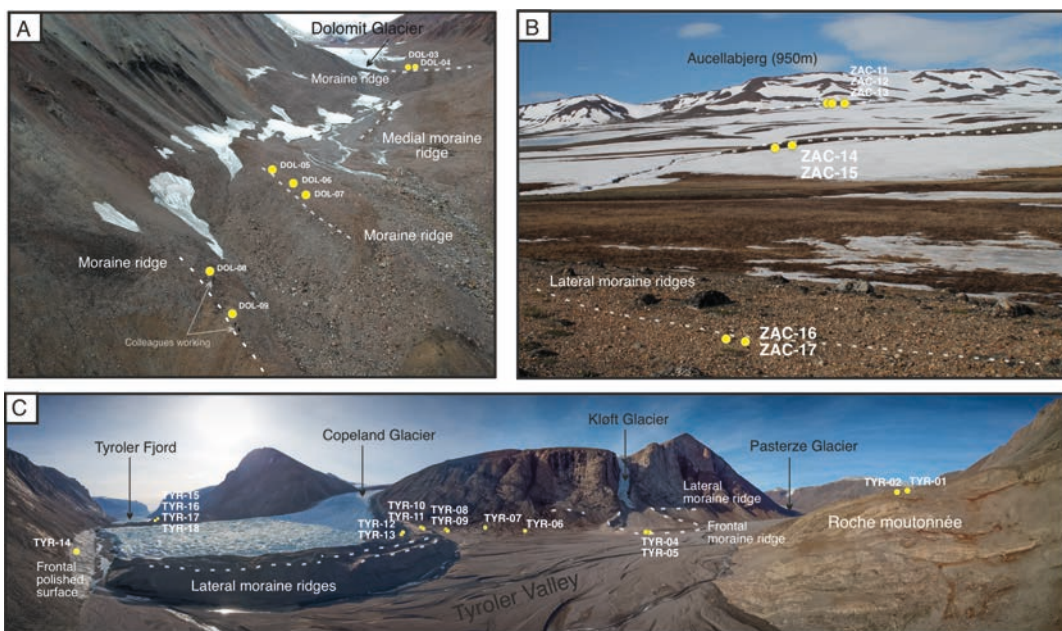


Figure 2: Examples of landforms mapped and sampled for CRE dating (yellow dots) in the different working areas. (A) Upper Dolomit valley near Dolomit glacier ice front with the moraines sampled in this part of the valley. (B) Picture of Aucellabjerg mountain slope with the moraines sampled in the Zackenberg valley area. (C) Panoramic picture of the Tyroler valley with the marked position of all samples collected in this area. Source: own elaboration.

All geomorphological maps included in Papers I, II and III were drawn by outlining the landforms in the ARCMAP 10.8 work environment over precise orthorectified panchromatic satellite images purchased for each study area (detailed in Table 3). The final maps were also supported by the Digital Elevation Model ArcticDEM (2 m spatial resolution) provided by (Porter et al., 2018).

Table 3. Summary details about the geomorphological areas mapped in each study area. Source: own elaboration.

	Study area	Area mapped (Km ²)	Fieldwork	Satellite image
Paper I	Zackenberg Valley	~195	August 2018	2019 WorldView-3 (0.3 m resolution)
Paper II	Tyroler Valley	~42	September 2019	2017 SPOT-6/7 (1.5 m resolution)
Paper III	Olsen Valley	~21	September 2019	2018 WorldView-2 (0.5 m resolution)
	Dolomit Valley	~7	September 2019	2019 WorldView-3 (0.3 m resolution)

2.1.2 TIME: GEOCHRONOLOGY

2.1.2.1 COSMIC-RAY EXPOSURE (CRE) DATING

FROM ROCKS TO DATES

The basic concept of CRE dating is on the fact that the studied isotopes could not exist in minerals before exposure to cosmic radiation or before meteoric nuclides accumulate on the surface. So, the question arises as to how they have been formed and come to appear on the surface of the Earth?

There are two types of cosmogenic isotopes depending on how they were formed: cosmogenic nuclides produced in the Earth's atmosphere; and terrestrial in situ-produced cosmogenic nuclides. Atmospheric (or meteoric) cosmogenic nuclides like ⁷Be, ¹⁰Be, ¹⁴C, and ³⁶Cl are produced when primary cosmic rays (i.e., high-energy cosmic particle originated outside the solar system) hit a given target atom present in the uppermost part of the Earth's atmosphere (Dunai, 2010). Upon entering this layer, these primary cosmic rays initiate a cascade of collisions producing nuclear reactions with the emergence of a multitude of secondary cosmic rays. Such secondary cosmic rays reach the Earth's surface and can even penetrate a few meters of ground rock. They produce in situ cosmogenic nuclides such as rare noble-gas isotopes and radionuclides like ³He, ¹⁰Be, ¹⁴C, ²⁶Al, ³⁶Cl, ⁴¹Ca and ⁵³Mn (Dunai, 2010). When interacting these secondary cosmic rays with atoms at the Earth's surface, they induce nuclear reactions within minerals exposed at the rock's surfaces (Dunai and Lifton, 2014) which remain inside the rock minerals and soils particles until they decay. Because cosmogenic nuclides build up predictably with time (Figure 3), measuring their concentrations allows the determination of how long a rock surface or sediment has been exposed at or near the surface of the Earth (JC and FM, 2001). In other words, when the rocks of the Earth's surface are bombarded by such cosmic radiation, the nuclide clock begins to tick (Figure 3), thus providing dates and rates of Earth-surface processes. The longer a given surface has been exposed to cosmic radiation, the greater is the concentration of cosmogenic radionuclides in the minerals within the rock, so the clock ticks through accumulation.

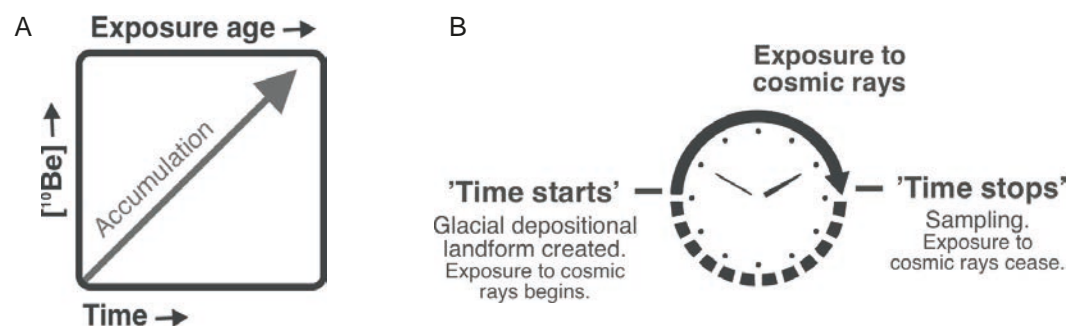


Figure 3. (A) Simplified representation of how nucleide concentration of ^{10}Be accumulates on the surface of the material as time passes and therefore, the exposure of this material to cosmic rays. (B) Simplified principle of how CRE dating works. The nucleide concentration starts to accumulate when the material is no longer protected and is exposed to cosmic rays. This accumulation stops when the material is blocked from the cosmic rays (e.g. when covered or when a sample of that surface is taken). Source: own elaboration.

With the knowledge of these basic principles of cosmogenic in situ radionuclides formation, there are few things to keep in mind when it comes to locate and sample a given rock (Dunai, 2010): (i) The production of cosmogenic nuclides varies depending on the place on Earth where we are and the material we want to date. On the way to Earth, the trajectories of primary cosmic rays' particles are bent by forces exerted by the Sun's magnetic field, and their paths depend upon their angle of entry along the Earth's magnetic field lines. The intensity of this particle flux is greatest at the poles, where the subparallel particle trajectories and Earth's magnetic field lines allow essentially all the charged particles that constitute the cosmic radiation arrive at the Earth's surface (Dunai, 2010). Furthermore, the in situ production of cosmogenic radionuclides at the Earth's surface depends on the total mass of atmosphere in the overlying air column (Stone, 2000), and hence depends on altitude. All these parameters must be considered later when calculating exposure ages (see section subsection 3 for a detailed explanation) and their associated uncertainties. (ii) The choice of the most suitable cosmogenic radionuclide for dating each area depends on the lithology of the materials that will be dated. This is because the production of different isotopes is influenced by the target elements affected by in cosmic rays (Dunai, 2010).

Taking into account all these issues and based on the characteristics of the study area, ^{10}Be was the radionuclide used for dating in this PhD thesis. ^{10}Be forms from O and Si (in a lesser extent) atoms (the main targets for this radionuclide), constituents of quartz (SiO_2) (Dunai, 2010). Quartz is one of the most widespread and common minerals on Earth's surface: it is indeed resistant to weathering, ubiquitous with a simple stoichiometry and has a trigonal structure (Figure 4) that allows confining elements within it (Davies, 2022; Gosse and Phillips, 2001). Quartz-rich lithologies like felsic phaneritic rocks (granites) or high-grade metamorphic rocks (gneiss) are the perfect targets for ^{10}Be expose dating. These lithologies are resistant to weathering and durable, being possible to transport them long distances.

^{10}Be is most widely used to date glacial landforms because its production rate has been well studied and calibrated (Balco et al., 2009; Borchers et al., 2016; Kaplan et al., 2011; Putnam et al., 2010; Small and Fabel, 2015). Also, ^{10}Be has a long half-life (~1.4 My) making it useful for dating samples from covering the entire Quaternary, including historic

time (Schaefer et al. 2009). Added to all this, ^{10}Be has routinely good precision in AMS measurements, a standardized chemistry procedure (Nishiizumi et al., 2007), and the isotope ^9Be is rare in quartz, making it simpler to measure (Granger et al., 2013).

One of the obstacles when dating with ^{10}Be is the presence of atmospheric ^{10}Be in the structure of quartz otherwise called in situ ^{10}Be (Figure 4). The production of atmospheric ^{10}Be is 10^3 times faster than the average in rocks (Gosse and Phillips 2001). This atmospheric beryllium will precipitate and may be absorbed by surface materials. Therefore, a considerable effort in the chemical preparation of these samples should be necessary with sequential chemical dissolutions in order to remove the meteoric ^{10}Be component from the quartz structure (Khol and Nishiizumi 1992).

A total of 84 samples for CRE ^{10}Be dating were sampled from the different study valleys (within Papers I, II and III) from 4 different types of landforms: 56 from moraine boulders,

18 from polished surfaces, 6 from erratic boulders and 2 from slide boulders (Figure 5 and 6). The results of all these samples (Table 4) will be used to constrain the time of the events of the landscape evolution.

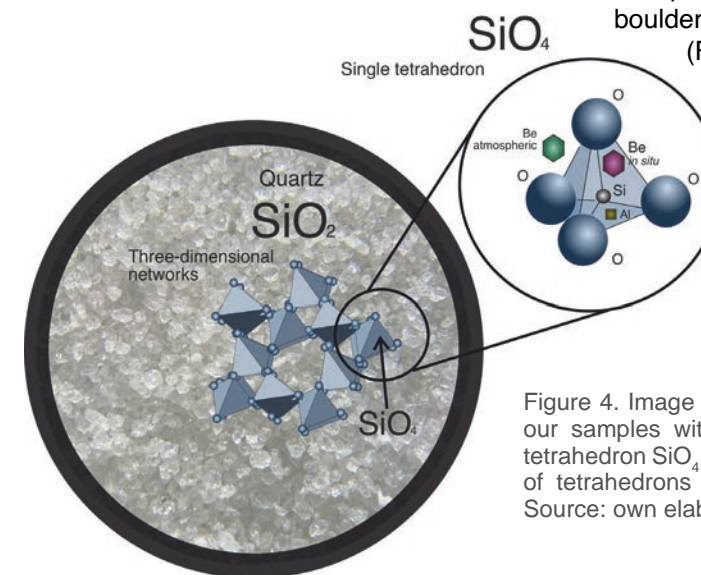


Figure 4. Image of purified quartz grains from one of our samples with the design of an isolated single tetrahedron SiO_4 and the formations of the 3D network of tetrahedrons that form the quartz mineral SiO_2 . Source: own elaboration.

Figure 5. Number and type of samples from the different study areas. Source: own elaboration.

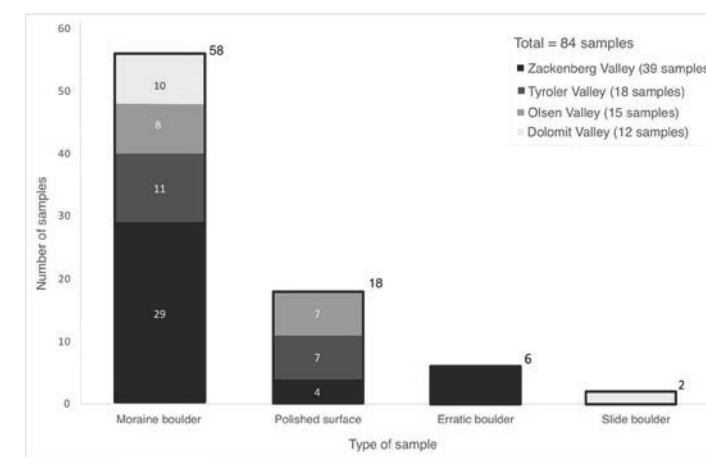


Table 4. Summary with the main characteristics of all the samples collected for ¹⁰Be CRE dating.

Sample ID	Landform	Latitude (DD)	Longitude (DD)	Elevation (m a.s.l.)	Geomorphological setting
Zackenbergl Valley (Paper I)					
ZAC-01	Polished surface	74.5113	-20.6816	132	Zackenbergl Valley bottom_Upstream hummocky terrain
ZAC-03	Erratic boulder	74.5103	-20.6803	137	Zackenbergl Valley bottom_Upstream hummocky terrain
ZAC-05	Erratic boulder	74.5403	-20.6710	201	Zakenbergl/Lindemansdal valley divide
ZAC-06	Erratic boulder	74.5405	-20.6711	201	Zakenbergl/Lindemansdal valley divide
ZAC-07	Polished surface	74.5404	-20.6712	202	Zakenbergl/Lindemansdal valley divide
ZAC-11	Lateral moraine	74.4991	-20.4379	401	Zackenbergl Valley upper W Aucellabjerg slope
ZAC-12	Lateral moraine	74.4991	-20.4379	401	Zackenbergl Valley upper W Aucellabjerg slope
ZAC-13	Lateral moraine	74.4991	-20.4335	403	Zackenbergl Valley upper W Aucellabjerg slope
ZAC-14	Lateral moraine	74.4834	-20.4963	105	Zackenbergl Valley middle W Aucellabjerg slope
ZAC-15	Lateral moraine	74.4834	-20.4990	104	Zackenbergl Valley middle W Aucellabjerg slope
ZAC-16	Lateral moraine	74.4828	-20.5163	64	Zackenbergl Valley lower W Aucellabjerg slope
ZAC-17	Lateral moraine	74.4828	-20.5145	64	Zackenbergl Valley lower W Aucellabjerg slope
ZAC-18	Lateral moraine	74.4755	-20.6414	117	Zackenbergl mountain E lower slope
ZAC-19	Lateral moraine	74.4783	-20.6298	92	Zackenbergl mountain E lower slope
ZAC-20	Lateral moraine	74.4781	-20.6234	80	Zackenbergl mountain E lower slope
ZAC-21	Lateral moraine	74.5281	-20.6862	328	Dombjerg SE upper slope
ZAC-22	Lateral moraine	74.5315	-20.6861	328	Dombjerg SE upper slope
ZAC-23	Lateral moraine	74.5282	-20.6864	331	Dombjerg SE upper slope
ZAC-24	Lateral moraine	74.5262	-20.6929	315	Dombjerg SE middle slope
ZAC-25	Lateral moraine	74.5263	-20.6928	315	Dombjerg SE middle slope
ZAC-26	Lateral moraine	74.5263	-20.6931	317	Dombjerg SE middle slope
ZAC-27	Lateral moraine	74.5236	-20.6965	262	Dombjerg SE lower slope
ZAC-28	Lateral moraine	74.5236	-20.6955	261	Dombjerg SE lower slope
ZAC-29	Lateral moraine	74.5236	-20.6955	262	Dombjerg SE lower slope
ZAC-30	Hummocky moraine	74.4991	-20.6282	96	Zackenbergl Valley bottom_Intermediate moraine ridge
ZAC-31	Hummocky moraine	74.4992	-20.6281	96	Zackenbergl Valley bottom_Intermediate moraine ridge
ZAC-32	Hummocky moraine	74.5002	-20.6266	100	Zackenbergl Valley bottom_Intermediate moraine ridge
Tyroler Valley (Paper II)					
ZAC-33	Hummocky moraine	74.5001	-20.6264	102	Zackenbergl Valley bottom_Intermediate moraine ridge
ZAC-36	Polished surface	74.4942	-20.6325	105	Zackenbergl Valley bottom_Foot rock slope
ZAC-37	Erratic boulder	74.4919	-20.6255	93	Zackenbergl Valley bottom_Foot rock slope
ZAC-38	Erratic boulder	74.4918	-20.6256	92	Zackenbergl Valley bottom_Foot rock slope
ZAC-39	Terminal hummocky moraine	74.4867	-20.5998	74	Zackenbergl Valley bottom_Outermost moraine ridge
ZAC-40	Terminal hummocky moraine	74.4863	-20.5998	76	Zackenbergl Valley bottom_Outermost moraine ridge
B1	Terminal hummocky moraine	74.4848	-20.5849	48	Zackenbergl Valley bottom_Outermost moraine ridge
B2	Terminal hummocky moraine	74.4860	-20.5967	62	Zackenbergl Valley bottom_Outermost moraine ridge
ZAC-01b	Terminal hummocky moraine	74.4869	-20.5797	71	Zackenbergl Valley bottom_Outermost moraine ridge
ZAC-04	Terminal hummocky moraine	74.4842	-20.5944	60	Zackenbergl Valley bottom_Outermost moraine ridge
ZAC-A	Erratic boulder	74.5158	-20.4325	851	Aucellabjerg mountain plateaus
ZAC-C	Erratic boulder	-74.5139	-20.4309	879	Aucellabjerg mountain plateaus
Tyroler Valley (Paper II)					
TYR-01	Polished surface	74.6415	-22.1791	280	Tyroler Upper valley roche moutonnée
TYR-02	Polished surface	74.6372	-22.1815	241	Tyroler Upper valley roche moutonnée
TYR-03	Lateral moraine	74.6336	-22.2080	136	Klöff Glacier external moraine
TYR-04	Lateral moraine	74.6335	-22.2080	134	Klöff Glacier external moraine
TYR-05	Lateral moraine	74.6329	-22.2088	134	Klöff Glacier external moraine
TYR-06	Polished surface	74.6298	-22.2123	135	Tyroler middle valley polished surface
TYR-07	Polished surface	74.6254	-22.2018	153	Tyroler middle valley polished surface
TYR-08	Lateral moraine	74.6232	-22.1987	164	Copeland glacier external moraine
TYR-09	Lateral moraine	74.6231	-22.1987	164	Copeland glacier external moraine
TYR-10	Lateral moraine	74.6234	-22.1913	172	Copeland glacier middle moraine
TYR-11	Lateral moraine	74.6233	-22.1914	170	Copeland glacier middle moraine
TYR-12	Lateral moraine	74.6264	-22.1815	129	Copeland glacier internal moraine
TYR-13	Lateral moraine	74.6264	-22.1813	131	Copeland glacier internal moraine
TYR-14	Polished surface	74.6294	-22.14685	45	Frontal Copeland glacier polished surface
TYR-15	Polished surface	74.6053	-22.1043	150	Tyroler fjord entrance_upper roche moutonnée
TYR-16	Lateral moraine	74.6059	-22.1068	120	Tyroler fjord entrance_moraine
TYR-17	Lateral moraine	74.6059	-22.1070	120	Tyroler fjord entrance_moraine
TYR-18	Polished surface	74.6066	-22.1060	100	Tyroler fjord entrance_lower roche moutonnée

Olsen Valley (Paper III)					
OLS-01	Polished surface	74.53515	-21.196561	389	Lower valley
OLS-02	Polished surface	74.534466	-21.192555	334	Lower valley
OLS-03	Lateral moraine	74.530252	-21.190141	251	Lower valley
OLS-04	Lateral moraine	74.526673	-21.18916	242	Lower valley
OLS-05	Lateral moraine	74.526646	-21.174735	231	Lower valley
OLS-06	Lateral moraine	74.526578	-21.174642	231	Lower valley
OLS-07	Polished surface	74.592999	-21.302957	263	Upper valley
OLS-08	Polished surface	74.592188	-21.301233	263	Upper valley
OLS-09	Polished surface	74.58642	-21.290792	231	Upper valley
OLS-10	Polished surface	74.585605	-21.289947	228	Upper valley
OLS-11	Polished surface	74.575724	-21.28058	293	Upper valley
OLS-12	Lateral moraine	74.566978	-21.261636	183	Middle valley
OLS-13	Lateral moraine	74.566978	-21.261823	183	Middle valley
Dolomit Valley (Paper III)					
DOL-01	Slide boulder	74.380382	-20.615017	336	Middle valley
DOL-02	Slide boulder	74.380576	-20.614789	335	Middle valley
DOL-03	Lateral moraine	74.382262	-20.658827	500	Upper valley
DOL-04	Lateral moraine	74.382227	-20.65788	502	Upper valley
DOL-05	Lateral moraine	74.377432	-20.638129	417	Upper valley
DOL-06	Lateral moraine	74.377492	-20.638035	418	Upper valley
DOL-07	Lateral moraine	74.377384	-20.640582	424	Upper valley
DOL-08	Lateral moraine	74.37714	-20.634161	395	Upper valley
DOL-09	Lateral moraine	74.377078	-20.634958	405	Upper valley
DOL-10	Lateral moraine	74.390437	-20.576733	244	Lower valley
DOL-11	Lateral moraine	74.390499	-20.577294	245	Lower valley
DOL-12	Lateral moraine	74.390598	-20.577354	245	Lower valley



Figure 6. Examples of the main types of samples (Erratic boulders/moraine boulders/polished surfaces) taken in the field at the different study areas (Zackenbergl/Tyroler/Olsen/ Dolomit valleys). Source: own elaboration.

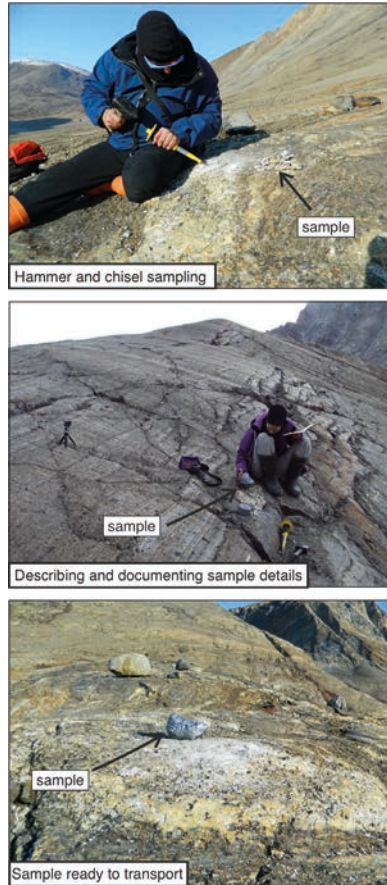


Figure 7. Different moments of fieldwork sampling for CRE dating in the study areas. Source: own elaboration.

All technicalities on sampling and the subsequent treatment of samples are detailed in each of the original publications, together with the physico-chemical treatment protocols followed in the laboratory to measure exposure in situ ¹⁰Be concentrations by AMS.

However, for the sake of facilitating the reading of this PhD thesis, a summary of the general process that all CRE dating samples have followed is presented here:

1. FIELDWORK AND SAMPLING

It consists on the documentation of key field details such as the landform description, precise geographic coordinates, elevation, and measurements, that should be obtained prior the rock sampling. For the CRE samples, approximately 1 kg of the uppermost rock layer (with a thickness of ≤ 5 cm) using hammer and chisel was collected (Figure 7).

2. LABORATORY PROCEDURES

EXTRACTION AND PURIFICATION OF QUARTZ

As impurities at the sample may contain interfering elements and/or meteoric components that disturb or invalidate the later measurements, the first steps of the laboratory procedures focus on obtaining pure quartz.

This step can be divided into physical and chemical separations that aim to separate quartz from the other minerals that compose the rock sample.

Main steps of the physical separation: Crushing/grinding to fragment the rock using a grinder – Sieving - Magnetic separation to isolate the 500 μm fraction, rich in quartz and to separate the paramagnetic minerals like quartz from the magnetic ones.

Main steps of the chemical separation: Carbonates removal - Acid leaching - Atmospheric ¹⁰Be removal.

According to the expected exposure age recorded by the sample, around 20 g of purified quartz, weighted



Figure 8. Pictures of the laboratory physical separations.

after physical preparation and chemical leaching, are necessary to continue with this preparation process.

TOTAL DISSOLUTION OF QUARTZ AND RECOVERY OF TARGETS

The chemical procedure of this phase aims at chemically enrich the ¹⁰Be cosmogenic isotope and separate it from interfering isotopes of other elements. Once we have our target mineral (quartz) separated from the rest of the components of the original sampled rock, the work into an atomic level begins. A ⁹Be carrier is added before the total dissolution to ensure further detection of the ¹⁰Be/⁹Be ratio by the AMS measurements (Dunai, 2010). In this regard, once the purification is completed, ~150 μml of spike spike of an in-house manufactured ⁹Be carrier solution was added to the samples (Merchel et al., 2008). At the end of this process, Be is separated from other elements such as Fe, Mn, Ti and B using anion and cation exchange resin columns and the result will be beryllium oxide (BeO) target.

The main steps of the total dissolution and recovery targets process (Figure 9): Spike adding - Total dissolution - Evaporation - Recovery of the residue - Precipitation - Anion-exchange/cation-exchange chromatography - Oxidation and targets preparation.

CATHODAGE AND MEASUREMENTS ON THE AMS ATER

Finally, the BeO target is mixed with niobium powder at similar proportions into copper cathodes (Figure 9). The measurement of ¹⁰Be/⁹Be ratios on the BeO targets were conducted at the French 5 MV ‘Accélérateur pour les Sciences de la Terre, Environnement et Risques’ (ASTER) facility at European Centre Research And Teaching In Geosciences De L’envi (CEREGE), France, utilizing the identical calibrations and standards in all of them.

The main steps are: Cathodage - ¹⁰Be/⁹Be ratios determination.

3. EXPOSURE AGE CALCULATIONS AND UNCERTAINTIES

Once the AMS measurements have been performed on the samples, several calculations must be made in order to obtain the surface exposure ages. In this sense, there are two major sets of online calculators are available to calculate exposure ages, namely the CRONUS-Earth (Balco et al., 2008; Marrero et al., 2016) and CREp (Martin et al., 2017). The exercise of calculating our ages with one and the other was carried out and returned identical results except for the oldest samples in which different values came out by just 0.3%.

With the main objective of compare our results with other published CRE ages from NE Greenland, after a review of the bibliography of the area, we used the CRONUS-Earth online calculator, version 3.0 (Balco et al., 2008; <https://hess.ess.washington.edu/>) with the following parameters: the calculation incorporated the Arctic-wide sea-level/high-latitude ¹⁰Be production rate (3.96 ± 0.15 atoms g⁻¹ a⁻¹) (Young et al., 2013) and the “Lm” (Lal/Stone) time-dependent scaling model (Lal, 1991; Stone, 2000). Throughout the calculations, a density of 2.7 g cm⁻³ was assumed for all samples, with no adjustments made for erosion or snow shielding. The partial shielding effects of the surrounding topography were factored



Figure 9. Pictures of the different steps in the chemical separation process. Source: own elaboration.

in using the “Topographic Shielding Calculator v.2” (http://stoneage.ice-d.org/math/skyline/skyline_in.html) for all sampling locations.

UNCERTAINTIES:

It is essential to take uncertainties into account when evaluating the accuracy of interpretations derived from CRE measurements. Within CRE dating, these uncertainties arise from three different sources (Dunai, 2010), namely:

Analytical/observational: also known as internal uncertainties. This uncertainty results from the observed and estimated quantities describing a sample and the sampling site, also including all the steps in sample treatment, counting from the sample collection until the AMS measurement. This uncertainty can lead to a 2-6% of error, is mostly random and it affects the precision of the measurement (Gosse and Klein, 2014). This uncertainty is used when comparing samples from a single study area or boulders from the same moraine (Balco, 2008).

Methodological: also named external uncertainties. This source of error is related to methodological parameters as production rates or scaling factors, resulting in a 5-15% error (Dunai, 2010). This source of error is mostly systematic, affecting the accuracy of the calculated ages and all samples equally. In samples from the same area, the concentration of the ^{10}Be will be affected to the same extent by methodological uncertainties. So, when comparing results within one study area, these uncertainties will not be used. The external uncertainty when comparing exposure ages from widely separated locations, or for comparing exposure ages to ages generated by other dating techniques (Balco, 2008).

Geological/natural variations: This error result from the intrinsic geomorphological history of the sample as post-glacial burial, inheritance or shielding history, and can determine the validity of the age, with an error range of 5-15% (Dunai, 2010). Even with a thoughtful sampling strategy to reduce this uncertainty, the limited a priori knowledge of the exposure history of the samples can lead to ages younger than the rest of the dataset (due to possible burial) or ages too old to fit within the dataset owing to inheritance or preexposure.

4. STATISTICAL ANALYSIS, OUTLIERS AND DATASET CONSISTENCY

The interpretation of glacial advance and retreat events temporarily situated thanks to CRE dating and their correlation with other climate proxies relies on the dispersion of the age dataset, which should be evaluated before assigning an age to a rock surface or landform. Consequently, once the ages are computed, the endeavor is to identify outliers using various available tools (Balco, 2011). There is no universally accepted procedure within the cosmogenic community to eliminate outliers. However, once the chemical outliers are discarded from the dataset, and the landform possesses enough samples, the most commonly employed method to identify outliers is based on the statistical chi-squared test, which determines whether scattering is merely a source of uncertainty or if there is another geomorphological process influencing that age (WARD and WILSON, 1978). If the uncertainties are uniformly distributed within the dataset, the mean age provides a more precise estimate of the landform age compared to a single age alone. Conversely, if the scattering is attributed to other processes, it is necessary to exclude outliers to appropriately apply the mean age (Davies, 2022). If the sampled landform lacks enough samples to conduct the statistical analysis. In that case, an interpretive analysis of the possible geomorphological outliers based on the glacial and post-glacial dynamics of the study area

is carried out. These possible outliers have been discussed in the original publications (Paper I, II, and III).

Providing an age to a moraine based on a CRE dataset can involve choosing either the youngest or oldest age. For instance, in regions influenced by cold-based glaciers, age datasets often face issues related to inheritance, leading to skewed older ages. In such situations, opting for the youngest age in the dataset aligns more closely with the real history (Davies, 2022). Conversely, in areas affected by temperate-based glaciers, post-glacial dynamics introduce challenges such as incomplete exposure history due to surface erosion, exhumation, and moraine degradation. This particularly affects ages prior the last glacial cycle, resulting in scattered ages (Davies, 2022). In these cases, resolving the bias toward younger ages involves selecting the oldest age and considering it as the minimum age for the deglaciation (Heyman et al., 2011).

In this sense, Papers I, II and III of this PhD thesis included a detailed interpretation of the validity of the samples, their geomorphological context and the potential surface processes that may have affected their age significance.

5. FINAL CRE AGES DATASET

Once the ages dataset is spruce, with the chemical outliers discarded and the possible geomorphological outliers discussed, the final CRE ages dataset is obtained and ready to be interpreted, compared, and correlated with other climate proxies.

2.1.2.2 OPTICALLY STIMULATED LUMINESCENCE (OSL) DATING

On Paper II, CRE dating was combined with OSL dates, which is a dating technique used to date the last time a mineral grain was deposited and buried; In other words, it quantifies the time since mineral grains were last exposed to sunlight (Small et al., 2017). The technique relies upon the ability of the mineral grains (mostly quartz or K-feldspar) to store energy within the crystal structure and release it when stimulated using light. The technique relies upon the ability of the mineral grains (mostly quartz or K-feldspar) to store energy within the crystal structure and release it when stimulated using light. As sediment is transported, it is exposed to sunlight and resettled of any previous luminescence signal. Once the sediment is deposited and subsequently buried, it is removed from sunlight and exposed to low levels of natural radiation from chemical elements such as U, Th, K, and Rb presents in the surrounding sediment (Davies, 2022). Over time, the mineral grains accumulate a luminescence signal as ionizing radiation excites the electrons, which then become trapped within crystal imperfections (electron traps). When stimulated, the minerals will exhibit luminescence, representing a release of the storage energy. The rate at which electrons are accumulated is termed the “environmental dose rate.”

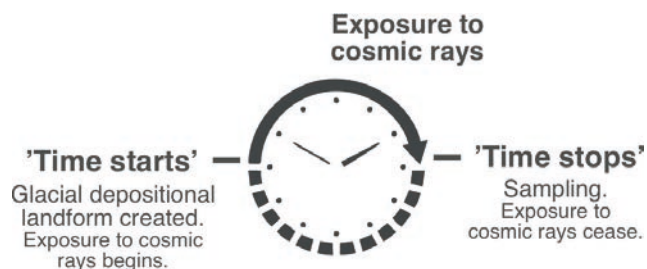


Figure 10. Simplified principle of OSL dating. Source: own elaboration.

The total dose to which the grains were exposed during burial (the “equivalent dose”) can be determined in the laboratory, and divided by the environmental dose rate, to determine the time since deposition (Lian, 2013; Small et al., 2017).



Figure 11. Left: Picture of sampling site for OSL dating on the Tyroler valley field campaign. Detail of sample for OSL dating.

This methodology was a complementary dating method used in Paper II (see original publication for more details) to date perched an alluvial fan associated with a Tyroler Valley ice-dammed palaeolake.

2.1.2.3 HISTORICAL DATA

In the study of the glacial oscillations of the area, two historical scientific expeditions have provided relevant data (used in Paper II) thanks to their great-detail descriptions of the glacial landforms and their graphic documentation:

- 1869-70: The second German North Pole expedition in led by Karl Koldewey (Payer, 1876)
- 1937: Louise A. Boyd Artic expedition (Boyd, 1948) (Figure 12)

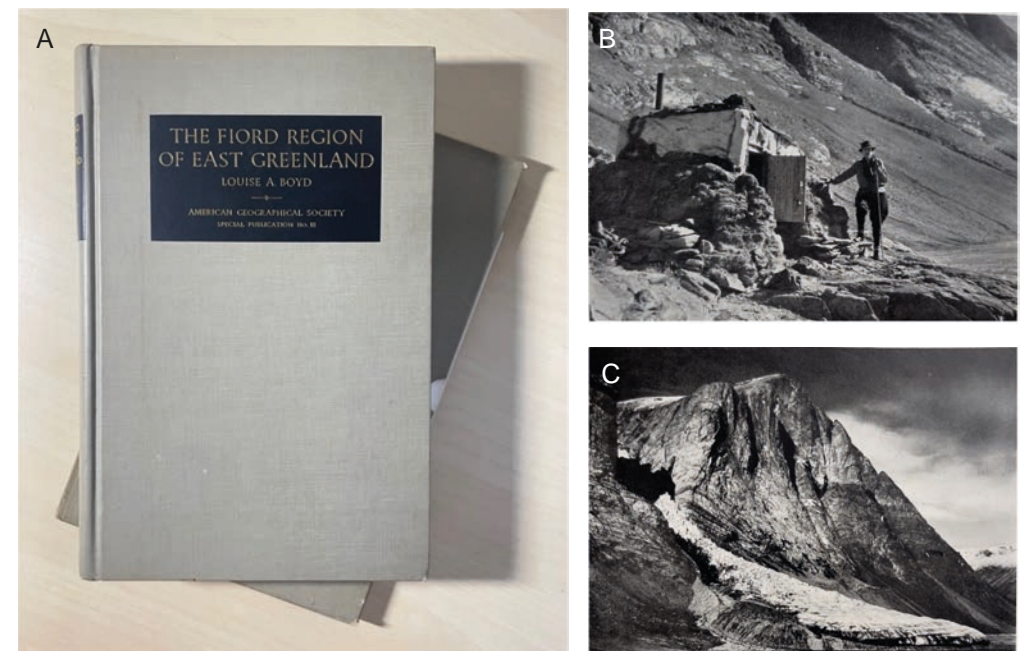


Figure 12. (A) Picture of the Louise A. Boyd books used to extract historical conatined on Paper II. (B) Luise A. Boyd in front of skin-covered hut at the head of the Tyroler Fiord (August 1937), the same hut that serve as refuge in our fieldwork campaign in 2019. (C) Kluft Glacier seen from the southeast, Tyroler Valley. July 30, 1937. Picture from Louise A. Boyd.

2.2 RECONSTRUCTION OF CLIMATE VARIABILITY: PALEOLIMNOLOGY

The reconstruction of climate variability as presented in paper IV as in the other paleolimnology results in this PhD thesis has been carried out using seven different but complementary paleolimnological methodologies in conjunction with ¹⁴C dating. All of these methodologies were applied to lake sediment cores records.

FROM LAKE SEDIMENTS TO DATA

The multidisciplinary approach encompassed chronological, granulometric, biogeochemical, and ecological methods. These methods fall into two categories: non-destructive, where the analysis of recovered material preserves the sediment, and destructive, where information is extracted at the cost of sedimentary material destruction (Figure 13). In multi-proxy investigations, the establishment of a reliable chronology is of paramount importance. AMS ¹⁴C dating is employed to provide this essential chronological context for our sediment records.

In this PhD thesis can be found information from two lakes and their respective sediment cores:

- Aucella Lake (Paper IV) at 911 m a.s.l.; 74° 31'28.80" N, 20° 26'12.47" W.
- ZAC1906 Lake (results at section 3.2.2 of this thesis) at 280 m a.s.l.; 74° 28' 54.54" N, 21° 29' 14.70" W).

Although the same analyzes have not been carried out in each of these records, they shared same general methodology, which is shown below:

1. FIELDWORK AND SAMPLING

Fieldwork was carried out in July 2018 for AUC02 and in summer 2019 for ZAC1906 (Figure 13). In shallow lakes, cores were obtained from the deepest part of the lake by pushing very gentle a 6 cm in diameter transparent liner into the lake bottom sediments until the tube was stopped by the friction of the surrounding sediments. In deep lakes, an UWITEC gravity corer was employed. The corer descended to around 1 m above the lake bottom and was allowed to fall freely. Once the first centimeters of the liner were within the lake sediments, a 5 kg weight was employed as a hammer to push the liner further into the lake sediments. The sediments were retrieved by gently recovering the liner to the lake water surface and immediately sealing both ends with plastic cups. Then, the liner was identified and kept in cold conditions at +4 °C until its study. In the following step, various laboratory analyses were conducted employing a

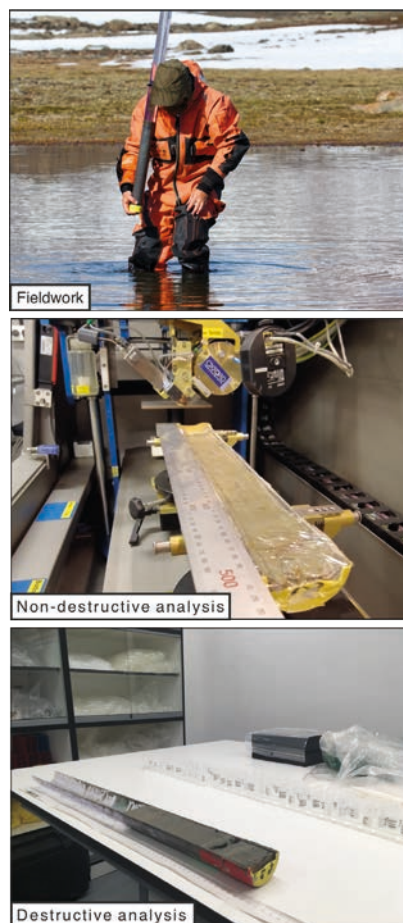


Figure 13. (A) Picture of fieldwork sediment core sampling in the study area (Picture by: Santiago Giralt). (B) Picture of Non-destructive analysis (XRF). (C) Picture of sampling the sediment core for further destructive analysis.separations.

range of analytical techniques and methodologies to yield a diverse set of proxies for the comprehensive analysis of sediment properties. Basic information for all the methodologies used was summarized in Table 4.

2. LABORATORY PROCEDURES

As previously mentioned, the laboratory analysis conducted on sediment cores can be classified into two distinct types based on their impact on the sediment material. The first category, termed "destructive," involves procedures that render the sediment material unusable for subsequent analyses. In contrast, the second category, known as "non-destructive," encompasses analyses that preserve the material, enabling future investigations. Furthermore, the applied methodologies can be further subdivided based on the type of proxy they measure. This can include organic proxies, derived from organic material preserved in the sediment layer, or inorganic proxies, involving elements or substances of non-living origin (Figure 14).

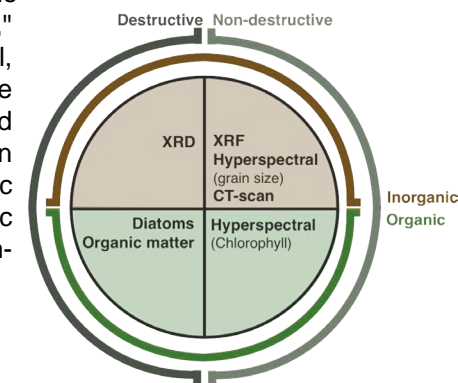


Figure 14: Clasification of analisis based type of proxy they measured and on on their impact on the sediment material. Source: own elaboration.

Destructive analisis:

- Organic proxies: diatoms; organic matter.
- Inorganic proxies: Mineral sediment composition by means of X-Ray Diffraction.

Non-destructive analisis:

- Organic proxies: Chromophyll by hyperspectral imaging.
- Inorganic proxies: X-ray computed tomography (CT-Scan); Elemental chemical sediment composition by X-ray Fluorescence; grain size by hyperspectral imaging.

All of these methodologies are gathered and summarized below (Table 5), indicating the basic principles on which they are based and the information they can provide. As well as the resolution at which they were made and in which laboratory.

All of these methodologies were applied to the Aucella Lake sediment core (AUC02), as outlined in Paper IV (section 3.2.1). In contrast, the ZAC06 sediment core (ZAC1906) underwent only XRF and XRD analyses, in addition to establishing its chronology (section 3.2.2) as Table 6 summarizes.

CHRONOLOGY

For the sediment cores, the chronological framework relied on AMS radiocarbon dates.

On the Aucella Lake sediment core the chronology is based on nine AMS radiocarbon dates. All samples from the chronology were exclusively obtained from moss fragments,

Table 5: Summary of the different types of analysis and methodologies conducted on the sediment core samples. Source: own elaboration.

Type of analysis	Method	Principles	Provided information	Resolution (cm)	Laboratory
Non-destructive	Visu sediment core description	Information about core length, diameter, and any core sections. Layer thickness, layers transitions, color, texture and any distinct features.	Create a comprehensive and informative visual description.	-	Paleolimnology Laboratory at GEO3BCN (Barcelona, Spain).
	X-ray computed tomography (CT-scan)	Records the attenuation of the X-ray directed at the object. X-ray attenuation is dependent on density used to measurements of bulk density.	Identify and better recognize sedimentary structures present on the sediment.	~ 0.05	Computerized 3D X-ray computed tomography Siemens Somatom 64 scanner (CT-scan) at the Institut National de la Recherche Scientifique, Centre Eau Terre Environnement (INRS-ETE) in Quebec City (Canada).
	X-Ray Fluorescence (XRF)	Photoelectric fluorescence of characteristic secondary x-rays from the elements present on the sediment core.	Identify sediment elemental composition, detecting both light and heavy elements.	~ 0.05	ITRAX XRF Core Scanner at the Institut National de la Recherche Scientifique, Centre Eau Terre Environnement (INRS-ETE) in Quebec City (Canada).
	Hyperspectral imaging	Hyperspectral cameras that provide contiguous electromagnetic spectra ranging from visible over near-infrared to shortwave infrared spectral bands, allowing to distinguish between materials with different characteristics of spectral reflectance response curves and characteristics.	Infer high-resolution profiles of mean grain size distribution and total chlorophyll.	~ 0.03	Hyperspectral scanner at the Aquatic Paleocology Laboratory (LPA) in Laval University (Quebec City, Canada), equipped with visible-near infrared (VNIR) and shortwave infrared (SWIR) cameras (SPECIM, Oulu, Finland).
Destructive	Organic matter	It originates from the complex mixture of lipids, carbohydrates, proteins and other organic matter components produced by organisms that have lived in and around the lake.	Measure of: Total Organic Carbon (TOC); Total Nitrogen (TN); $\delta^{13}C$; $\delta^{15}N$; C/N ratio. Provides information to interpretations of both natural and human-induced lake changes.	~ 1.0	Finnigan DELTAplus elemental analyzer-continuous flow-isotope ratio mass spectrometer (EA-CF-IRMS) at the Centres Científics i Tecnològics of the Universitat de Barcelona (CCiTUB) (Spain).
	X-ray diffractometry (XRD)	X-ray generator that bombard the sample with a beam of X-ray. As the atomic planes in the minerals in the sample attain the appropriate critical angle with respect to the incident beam, they will refract the X-rays according to Bragg's Law (each mineral in the sample will produce a unique set of distinctive reflections).	Provide specific information about geochemical and thermal environments at the time of formation.	~ 1.0	Bruker-AXS D5005 X-ray diffractometer at GEO3BCN (Barcelona, Spain).
	Diatoms	Taxonomically diagnostic of populations of organisms (microscopic algae abundant in almost all aquatic habitats) that are sensitive to variations in their external environment. This sensitivity can be recorded as proportional changes in fossil abundances, evolutionary change, or extinction.	Indicate environmental change in the aquatic ecosystems and climate-related processes.	~ 2.0	Counted at 1000x magnification with a light microscope at the CREAM - Centro de Investigación Ecológica y Aplicaciones Forestales (Barcelona, Spain).
Chronology	Radiocarbon dating	Radioactive decay of the ^{14}C isotope that allows to determine the age of a fossil material.	Age control to enable comparisons and correlations on local, regional and global scales. Aimed to obtain a general age control for the studied sequences by dating selected parts.	-	Radiochronology laboratory of the Centre d'études nordiques, Laval University (Quebec City, Canada) and analyzed at the W. M. Keck Carbon Cycle Accelerator Mass Spectrometer Facility (Irvine, United States).

including dating the core's surface to determine the presence or absence of a carbon reservoir effect in the lake.

Dating moss fragments in sediment cores helps avoid the reservoir effect, a phenomenon that can affect the accuracy of radiocarbon dating. The reservoir effect occurs when an organism incorporates carbon from a source that is not in equilibrium with atmospheric ^{14}C . In the case of moss and other aquatic plants, they can take up carbon from the water, which may have a different ^{14}C content than the atmosphere.

In aquatic environments, carbon can be influenced by various factors, such as the input of carbon from older, carbon-depleted sources. This can lead to an inaccurate estimation of

Table 6: Types of analysis, proxies and methods applied to each of the sediment cores gathered in this PhD thesis. Source: own elaboration.

Lake sediment core	Type of analysis	Type of proxy	Method applied (number of samples treated)	
AUC02	Non-destructive	Inorganic	CT-Scan (image)	
			XRF (1674)	
			Grain size-Hyperspectral imaging (4508)	
			XRD (80)	
	Destructive	Organic	Organic matter (80)	
			Chlorophyll-Hyperspectral imaging (4508)	
			Diatoms (40)	
	Chronology (9 AMS radiocarbon ages)			
	ZAC06	Non-destructive	Inorganic	XRF (1575)
				XRD (152)
Chronology (7 AMS radiocarbon ages)				

of the environmental history recorded in the core. This is crucial for reconstructing past environmental changes and events.

The chronology on the AUC02 sediment core was constructed using nine AMS radiocarbon dates. The final age-depth model was constructed Bayesian age-depth modeling in the R package 'rbacon' (Blaauw & Christeny, 2011), with ages calibrated using the IntCal20 calibration curve (Reimer et al., 2020).

The chronology on the ZAC06 sediment core was based on seven AMS radiocarbon dates and in this case, all of them obtained from the sediment.

The final age-depth model was constructed Bayesian age-depth modeling in the R package "clam" (Blaauw 2021) with ages calibrated using the IntCal20 calibration curve (Reimer et al., 2020).

3. STATISTICAL DATASETS TREATMENT AND MULTIVARIATE ANALYSIS

The subsequent step involved the statistical analysis of the datasets, as interpreting and extracting the environmental and climate information from the extensive data generated by the multi-proxy study presents significant challenges. All to end up with the lake sediment stratigraphy constructed and the sediments characteristics defined.

- Stratigraphically constrained cluster analysis for each separate data group:

Independent zonation of different stratigraphical proxies (e.g., sediment geochemistry, diatoms) was achieved through non-hierarchical partitioning. Subsequent comparisons of these various partitionings with the broken-stick model aim to detect the minimal number of

potentially 'significant' zones. Zonation schemes based on different proxies can then be visually compared. Constrained cluster analysis were performed on the data of both lakes

to determine assemblage zones, utilizing squared-chord distance as a measure of dissimilarity.

- Multivariate ordination methods to reduce complexity of the large multi-proxy data set in order to identify underlying system dynamics.

Ordination techniques (e.g., principal components analysis, correspondence analysis) offer valuable summaries of major stratigraphical patterns in a particular paleolimnological variable (e.g., diatoms), especially when the sample scores on significant ordination axes are plotted stratigraphically. This statistical analysis highlights the major patterns of variation and illustrates and summarizes the nature of temporal changes (Bialik et al., 2021).

Principal Component Analysis (PCA) is a multivariate statistical method employed in unconstrained ordination. It utilizes matrix factorization to project high-dimensional data onto a lower-dimensional subspace defined by principal components (Legendre and Birks, 2012). These components capture the maximum variability inherent in the original variables. The interpretation of PCA axes involves synthesizing the local limnological and paleoenvironmental responses to climate-related processes.

For the data from AUC02 sediment core two PCA's were carried out: (i) on the diatom's taxa data. (ii) on the XRF/organic matter data.

For the ZAC06 sediment core data, a PCA was carried out on the XRF dataset.

Redundancy Analysis (RDA) or constrained ordination: statistical technique used in multivariate data analysis. RDA analysis might be employed to examine relationships between environmental variables and biological data in ecological studies. It helps identify patterns and associations in complex datasets, especially when dealing with multiple variables (Van den Wollenberg, 1977).

Both for AUC02 and ZAC06 sediment cores a redundancy analysis was carried out with the XRF dataset (response) and the XRD mineralogical composition (environmental constrain) of the sediments as the constraining matrix (Giralt et al., 2008).

For the data from AUC02 another RDA was carried out: an RDA of the diatom distribution (response) to the geochemistry and organic components (environmental constrain dataset).

4. FINAL DATASETS AND LOCAL / SUPRA-REGIONAL / GREENLAND PROXY CORRELATIONS

Last step is the interpretation of all of the results, linking the different datasets, unveiling limnological processes and reconstructing the paleoenvironmental history. Finally, local to supra regional inferences proxy correlations can be carried out along with the comparison with other independent climate proxies as North Hemisphere (NH) summer insolation or isotope ice core proxies to see which 'predictors' best explained the observed changes in different types of limnological variables.

BIBLIOGRAPHY

In here, the references from the Introduction and the Methods section:

Adamson, K., Lane, T., Carney, M., Bishop, T., & Delaney, C. (2019). High-resolution proglacial lake records of pre-Little Ice Age glacier advance, northeast Greenland. *Boreas*, 48(3), 535–550. <https://doi.org/10.1111/bor.12361>

Alley, R. B., Andrews, J. T., Brigham-Grette, J., Clarke, G. K. C., Cuffey, K. M., Fitzpatrick, J. J., Funder, S., Marshall, S. J., Miller, G. H., Mitrovica, J. X., Muhs, D. R., Otto-Bliesner, B. L., Polyak, L., & White, J. W. C. (2010). History of the Greenland Ice Sheet: paleoclimatic insights. *Quaternary Science Reviews*, 29(15–16), 1728–1756. <https://doi.org/10.1016/j.quascirev.2010.02.007>

Anderson, N. J., Saros, J. E., Bullard, J. E., Cahoon, S. M. P., McGowan, S., Bagshaw, E. A., Barry, C. D., Bindler, R., Burpee, B. T., Carrivick, J. L., Fowler, R. A., Fox, A. D., Fritz, S. C., Giles, M. E., Hamerlik, L., Ingeman-Nielsen, T., Law, A. C., Mernild, S. H., Northington, R. M., ... Yde, A. J. C. (2017). The arctic in the twenty-first century: Changing biogeochemical linkages across a paraglacial landscape of Greenland. *BioScience*, 67(2), 118–133. <https://doi.org/10.1093/biosci/biw158>

Andrews, M. G., Jacobson, A. D., Osburn, M. R., & Flynn, T. M. (2018). Dissolved Carbon Dynamics in Meltwaters From the Russell Glacier, Greenland Ice Sheet. *Journal of Geophysical Research: Biogeosciences*, 123(9), 2922–2940. <https://doi.org/10.1029/2018JG004458>

Aschwanden, A., Fahnestock, M. A., Truffer, M., Brinkerhoff, D. J., Hock, R., Khroulev, C., Mottram, R., & Abbas Khan, S. (2019). Contribution of the Greenland Ice Sheet to sea level over the next millennium. *Science Advances*, 5(6). <https://doi.org/10.1126/sciadv.aav9396>

Axford, Y., Briner, J. P., Cooke, C. A., Francis, D. R., Michelutti, N., Miller, G. H., Smol, J. P., Thomas, E. K., Wilson, C. R., & Wolfe, A. P. (2009). Recent changes in a remote Arctic lake are unique within the past 200,000 years. *Proceedings of the National Academy of Sciences of the United States of America*, 106(44), 18443–18446. <https://doi.org/10.1073/pnas.0907094106>

Axford, Y., De Vernal, A., & Osterberg, E. C. (2021). Past warmth and its impacts during the holocene thermal maximum in greenland. *Annual Review of Earth and Planetary Sciences*, 49, 279–307. <https://doi.org/10.1146/annurev-earth-081420-063858>

Axford, Y., Levy, L. B., Kelly, M. A., Francis, D. R., Hall, B. L., Langdon, P. G., & Lowell, T. V. (2017). Timing and magnitude of early to middle Holocene warming in East Greenland inferred from chironomids. *Boreas*, 46(4), 678–687. <https://doi.org/10.1111/bor.12247>

Balco, G., Stone, J. O., Lifton, N. A., & Dunai, T. J. (2008). A complete and easily accessible means of calculating surface exposure ages or erosion rates from ¹⁰Be and ²⁶Al measurements. *Quaternary Geochronology*, 3(3), 174–195. <https://doi.org/10.1016/j.quageo.2007.12.001>

Bamber, J. L., Griggs, J. A., Hurkmans, R. T. W. L., Dowdeswell, J. A., Gogineni, S. P., Howat, I., Mouginot, J., Paden, J., Palmer, S., Rignot, E., & Steinhage, D. (2013). A new bed elevation dataset for Greenland. *Cryosphere*, 7(2), 499–510. <https://doi.org/10.5194/tc-7-499-2013>

Battarbee, R. W., Catalan, J., John Arvid Grytnes, & Birks, H. J. B. (n.d.). Costs of secondary parasitism in the facultative hyperparasitoid *Pachycrepoideus dubius*: Does host size matter? *Entomologia Experimentalis et Applicata*, 103(3), 239–248. <https://doi.org/10.1023/A>

Bennike, O., & Björck, S. (2002). Chronology of the last recession of the Greenland Ice Sheet. *Journal of Quaternary Science*, 17(3), 211–219. <https://doi.org/10.1002/jqs.670>

Bennike, O., Sørensen, M., Fredskild, B., Jacobsen, B. H., Böcher, J., Amsinck, S. L., Jeppesen, E., Andreasen, C., Christiansen, H. H., & Humlum, O. (2008). Late Quaternary Environmental and Cultural Changes in the Wollaston Forland Region, Northeast Greenland. *Advances in Ecological Research*, 40(07), 45–79. [https://doi.org/10.1016/S0065-2504\(07\)00003-7](https://doi.org/10.1016/S0065-2504(07)00003-7)

Bialik, O. M., Jarochovska, E., & Grossowicz, M. (2021). Ordination analysis in sedimentology, geochemistry and palaeoenvironment—Background, current trends and recommendations. *Depositional Record*, 7(3), 541–563. <https://doi.org/10.1002/dep2.161>

Biette, M., Jomelli, V., Chenet, M., Braucher, R., Rinterknecht, V., & Lane, T. (2020). Mountain glacier fluctuations during the Lateglacial and Holocene on Clavering Island (northeastern Greenland) from ¹⁰Be moraine dating. *Boreas*, 49(4), 873–885. <https://doi.org/10.1111/bor.12460>

Biette, M., Jomelli, V., Chenet, M., Egis, R., & Biette, M. (2020). Mountain glacier fluctuations during the Lateglacial and Holocene on Clavering Island (northeastern Greenland) from ¹⁰ Be moraine dating. <https://doi.org/10.1111/bor.12460>

Birks, H. J. B., Lotter, A., Juggins, S., & Smol, J. P. (2012). Tracking Environmental change using lake sediments- Data Handling and Numerical techniques.

Björck, S., Walker, M. J. C., Cwynar, L. C., Johnsen, S., Knudsen, K. L., Lowe, J. J., & Wohlfarth, B. (1998). An event stratigraphy for the last termination in the North Atlantic region based on the Greenland ice-core record: a proposal by the INTIMATE group. *Journal of Quaternary Science*, 13(4), 283–292. [https://doi.org/10.1002/\(SICI\)1099-1417\(199807/08\)13:4<283::AID-JQS386>3.0.CO;2-A](https://doi.org/10.1002/(SICI)1099-1417(199807/08)13:4<283::AID-JQS386>3.0.CO;2-A)

Blaauw, M., & Christeny, J. A. (2011). Flexible paleoclimate age-depth models using an autoregressive gamma process. *Bayesian Analysis*, 6(3), 457–474. <https://doi.org/10.1214/11-BA618>

Boyd, L. A. (1948). The Coast of Northeast Greenland: With Hydrographic Studies in the Greenland Sea. The Louise A. Boyd Arctic Expeditions of 1937 and 1938 (Issue parte 1). American Geographical Society. <https://books.google.es/books?id=EyYcAAAAMAAJ>

Bradley, R. S. (2014). *Paleoclimatology*, 3rd ed.

Bradley, R. S. (2015). *Paleoclimatology: Reconstructing Climates of the Quaternary Second Edition*. In *Paleoclimatology : reconstructing climates of the Quaternary*. <https://doi.org/10.1029/ea081i050p00613-01>

Briner, J. P., McKay, N. P., Axford, Y., Bennike, O., Bradley, R. S., de Vernal, A., Fisher, D., Francus, P., Fréchet, B., Gajewski, K., Jennings, A., Kaufman, D. S., Miller, G., Rouston, C., & Wagner, B. (2016a). Holocene climate change in Arctic Canada and Greenland. *Quaternary Science Reviews*, 147, 340–364. <https://doi.org/10.1016/j.quascirev.2016.02.010>

Briner, J. P., McKay, N. P., Axford, Y., Bennike, O., Bradley, R. S., de Vernal, A., Fisher, D.,

- Francus, P., Fréchette, B., Gajewski, K., Jennings, A., Kaufman, D. S., Miller, G., Rouston, C., & Wagner, B. (2016b). Holocene climate change in Arctic Canada and Greenland. *Quaternary Science Reviews*, 147, 340–364. <https://doi.org/10.1016/j.quascirev.2016.02.010>
- Buizert, C., Keisling, B. A., Box, J. E., He, F., Carlson, A. E., Sinclair, G., & DeConto, R. M. (2018). Greenland-Wide Seasonal Temperatures During the Last Deglaciation. *Geophysical Research Letters*, 45(4), 1905–1914. <https://doi.org/10.1002/2017GL075601>
- Buizert, Christo, Gkinis, V., Severinghaus, J. P., He, F., Lecavalier, B. S., Kindler, P., Leuenberger, M., Carlson, A. E., Vinther, B., Masson-Delmotte, V., White, J. W. C., Liu, Z., Otto-Bliesner, B., & Brook, E. J. (2014). Greenland temperature response to climate forcing during the last deglaciation. *Science*, 345(6201), 1177–1180. <https://doi.org/10.1126/science.1254961>
- Buus-Hinkler, J., Hansen, B. U., Tamstorf, M. P., & Pedersen, S. B. (2006). Snow-vegetation relations in a High Arctic ecosystem: Inter-annual variability inferred from new monitoring and modeling concepts. *Remote Sensing of Environment*, 105(3), 237–247. <https://doi.org/10.1016/j.rse.2006.06.016>
- Cable, S., Christiansen, H. H., Westergaard-Nielsen, A., Kroon, A., & Elberling, B. (2018). Geomorphological and cryostratigraphical analyses of the Zackenberg Valley, NE Greenland and significance of Holocene alluvial fans. *Geomorphology*, 303, 504–523. <https://doi.org/10.1016/j.geomorph.2017.11.003>
- Carlson, A. E., Winsor, K., Ullman, D. J., Brook, E. J., Rood, D. H., Axford, Y., LeGrande, A. N., Anslow, F. S., & Sinclair, G. (2014). Earliest Holocene south Greenland ice sheet retreat within its late Holocene extent. 5514–5521. <https://doi.org/10.1002/2014GL060800>. Received
- Catalan, J., Pla-Rabés, S., Wolfe, A. P., Smol, J. P., Rühland, K. M., Anderson, N. J., Kopáček, J., Stuchlík, E., Schmidt, R., Koinig, K. A., Camarero, L., Flower, R. J., Heiri, O., Kamenik, C., Korhola, A., Leavitt, P. R., Psenner, R., & Renberg, I. (2013). Global change revealed by palaeolimnological records from remote lakes: A review. *Journal of Paleolimnology*, 49(3), 513–535. <https://doi.org/10.1007/s10933-013-9681-2>
- CAVM Team. (2003). Circumpolar Arctic Vegetation Map. (1:7,500,000 scale), Conservation of Arctic Flora and Fauna (CAFF) Map No. 1. US Fish and Wildlife Service. (Anchorage, AK). Available at <http://www.geobotany.uaf.edu/cavm/> [Verified 1 August 15 July 2015], 2.
- Christiansen, H. H. (1994). Institute of Geography, University of Copenhagen, Osier Voldgade 10, 1350 Copenhagen K, Denmark. 13, 491–496.
- Christiansen, H. H., Etzelmüller, B., Isaksen, K., Juliussen, H., Farbrot, H., Humlum, O., Johansson, M., Ingeman-Nielsen, T., Kristensen, L., Hjort, J., Holmlund, P., Sannel, A. B. K., Sigsgaard, C., Åkerman, H. J., Foged, N., Blikra, L. H., Pernosky, M. A., & Ødegård, R. S. (2010). The thermal state of permafrost in the nordic area during the international polar year 2007-2009. *Permafrost and Periglacial Processes*, 21(2), 156–181. <https://doi.org/10.1002/ppp.687>
- Christiansen, Hanne H., Bennike, O., Böcher, J., Elberling, B., Humlum, O., & Jakobsen, B. H. (2002). Holocene environmental reconstruction from deltaic deposits in Northeast Greenland. *Journal of Quaternary Science*, 17(2), 145–160. <https://doi.org/10.1002/jqs.665>
- Christiansen, Hanne H., & Humlum, O. (1993). Glacial History and Periglacial Landforms of the Zackenberg area, Northeast Greenland: Preliminary results. *Geografisk Tidsskrift-Danish Journal of Geography*, 93(1), 19–29. <https://doi.org/10.1080/00167223.1993.10649332>
- Christiansen, Hanne H., Sigsgaard, C., Humlum, O., Rasch, M., & Hansen, B. U. (2008). Permafrost and Periglacial Geomorphology at Zackenberg. *Advances in Ecological Research*, 40(07), 151–174. [https://doi.org/10.1016/S0065-2504\(07\)00007-4](https://doi.org/10.1016/S0065-2504(07)00007-4)
- Christiansen, Hanne Hvidtfeldt. (1998). Nivation forms and processes in unconsolidated sediments, NE Greenland. *Earth Surface Processes and Landforms*, 23(8), 751–760. [https://doi.org/10.1002/\(SICI\)1096-9837\(199808\)23:8<751::AID-ESP886>3.0.CO;2-A](https://doi.org/10.1002/(SICI)1096-9837(199808)23:8<751::AID-ESP886>3.0.CO;2-A)
- Clark, P. U., Dyke, A. S., Shakun, J. D., Carlson, A. E., Clark, J., Wohlfarth, B., Mitrovica, J. X., Hostetler, S. W., & McCabe, A. M. (2009). The Last Glacial Maximum. *Science*, 325(5941), 710–714. <https://doi.org/10.1126/science.1172873>
- Cohen, J., Screen, J. A., Furtado, J. C., Barlow, M., Whittleston, D., Coumou, D., Francis, J., Dethloff, K., Entekhabi, D., Overland, J., & Jones, J. (2014). Recent Arctic amplification and extreme mid-latitude weather. *Nature Geoscience*, 7(9), 627–637. <https://doi.org/10.1038/ngeo2234>
- Cohen, K. M., & Gibbard, P. L. (2019). Global chronostratigraphical correlation table for the last 2.7 million years, version 2019 QI-500. *Quaternary International*, 500, 20–31. <https://doi.org/10.1016/j.quaint.2019.03.009>
- Cook, E., Abbott, P. M., Pearce, N. J. G., Mojtabavi, S., Svensson, A., Bourne, A. J., Rasmussen, S. O., Seierstad, I. K., Vinther, B. M., Harrison, J., Street, E., Steffensen, J. P., Wilhelms, F., & Davies, S. M. (2022). Volcanism and the Greenland ice cores: A new tephrochronological framework for the last glacial-interglacial transition (LGIT) based on cryptotephra deposits in three ice cores. *Quaternary Science Reviews*, 292, 107596. <https://doi.org/10.1016/j.quascirev.2022.107596>
- Corbett, L. B., Young, N. E., Bierman, P. R., Briner, J. P., Neumann, T. A., Rood, D. H., & Graly, J. A. (2011). Paired bedrock and boulder ¹⁰Be concentrations resulting from early Holocene ice retreat near Jakobshavn Isfjord, western Greenland. *Quaternary Science Reviews*, 30(13–14), 1739–1749. <https://doi.org/10.1016/j.quascirev.2011.04.001>
- Cremer, H., Melles, M., & Wagner, B. (2001). Holocene climate changes reflected in a diatom succession from Basaltsø, east Greenland. *Canadian Journal of Botany*, 79(6), 649–656. <https://doi.org/10.1139/cjb-79-6-649>
- Cremer, Holger, Wagner, B., Melles, M., & Hubberten, H. W. (2001). The postglacial environmental development of Raffles Sø, East Greenland: Inferences from a 10,000 year diatom record. *Journal of Paleolimnology*, 26(1), 67–87. <https://doi.org/10.1023/A:1011179321529>
- Darby, D. A., Ortiz, J. D., Grosch, C. E., & Lund, S. P. (2012). 1,500-year cycle in the Arctic Oscillation identified in Holocene Arctic sea-ice drift. *Nature Geoscience*, 5(12), 897–900. <https://doi.org/10.1038/ngeo1629>
- Davies, B. J. (2022). Cryospheric Geomorphology: Dating Glacial Landforms II: Radiometric Techniques. *Treatise on Geomorphology*, 249–280. <https://doi.org/10.1016/b978-0-12-818234-5.00040-7>
- Davies, J., Mathiasen, A. M., Kristiansen, K., Hansen, K. E., Wacker, L., Alstrup, A. K. O., Munk, O. L., Pearce, C., & Seidenkrantz, M. S. (2022). Linkages between ocean

circulation and the Northeast Greenland Ice Stream in the Early Holocene. *Quaternary Science Reviews*, 286, 107530. <https://doi.org/10.1016/j.quascirev.2022.107530>

Davini, P., Cagnazzo, C., Neale, R., & Tribbia, J. (2012). Coupling between Greenland blocking and the North Atlantic Oscillation pattern. *Geophysical Research Letters*, 39(14), 1–6. <https://doi.org/10.1029/2012GL052315>

Dawes, P. R., & Glendal, E. W. (2007). A glossary for GEUS publications: spelling and usage of troublesome words and names made easy. 59.

Denton, G. H., Anderson, R. F., Toggweiler, J. R., Edwards, R. L., Schaefer, J. M., & Putnam, A. E. (2010). The last glacial termination. *Science*, 328(5986), 1652–1656. <https://doi.org/10.1126/science.1184119>

Dickson, R., Lazier, J., Meincke, J., Rhines, P., & Swift, J. (1996). Long-term coordinated changes in the convective activity of the North Atlantic. *Progress in Oceanography*, 38(3), 241–295. [https://doi.org/10.1016/S0079-6611\(97\)00002-5](https://doi.org/10.1016/S0079-6611(97)00002-5)

Dunai, T. J. (2010). COSMOGENIC NUCLIDES. Principles, Concepts and Applications in the Earth Surface Sciences. In Cambridge University Press.

Dunai, T. J., & Lifton, N. A. (2014). The nuts and bolts of cosmogenic nuclide production. *Elements*, 10(5), 347–350. <https://doi.org/10.2113/gselements.10.5.347>

Elberling, B., Tamstorf, M. P., Sigsgaard, C., Illeris, L., Bay, C., B.H., H., Christensen, T. R., Hansen, E. S., Jakobsen, B. H., & Beyens, L. (2008). Soil and Plant Community-Characteristics and Dynamics at Zackenberg in Meltofte, H. et al. (ed.) (High-Arcti).

Faust, J. C., Fabian, K., Milzer, G., Giraudeau, J., & Knies, J. (2016). Norwegian fjord sediments reveal NAO related winter temperature and precipitation changes of the past 2800 years. *Earth and Planetary Science Letters*, 435, 84–93. <https://doi.org/10.1016/j.epsl.2015.12.003>

Fernández-Fernández, J. M., Oliva, M., Palacios, D., Garcia-Oteyza, J., Navarro, F. J., Schimmelpennig, I., Léanni, L., & Team, A. (2021). Ice thinning on nunataks during the glacial to interglacial transition in the Antarctic Peninsula region according to Cosmic-Ray Exposure dating: Evidence and uncertainties. *Quaternary Science Reviews*, 264. <https://doi.org/10.1016/j.quascirev.2021.107029>

Fleitmann, D., Mudelsee, M., Burns, S. J., Bradley, R. S., Kramers, J., & Matter, A. (2008). Evidence for a widespread climatic anomaly at around 9.2 ka before present. *Paleoceanography*, 23(1), 1–6. <https://doi.org/10.1029/2007PA001519>

Funder, S., Kjeldsen, K. K., Kjær, K. H., & O Cofaigh, C. (2011). The Greenland Ice Sheet During the Past 300,000 Years: A Review. *Developments in Quaternary Science*, 15, 699–713. <https://doi.org/10.1016/B978-0-444-53447-7.00050-7>

Gardner, A. S., Moholdt, G., Cogley, J. G., Wouters, B., Arendt, A. A., Wahr, J., Berthier, E., Hock, R., Pfeffer, W. T., Kaser, G., Ligtenberg, S. R. M., Bolch, T., Sharp, M. J., Hagen, J. O., Van Den Broeke, M. R., & Paul, F. (2013). A reconciled estimate of glacier contributions to sea level rise: 2003 to 2009. *Science*, 340(6134), 852–857. <https://doi.org/10.1126/science.1234532>

Gilbert, G. L., Cable, S., Thiel, C., Christiansen, H. H., & Elberling, B. (2017). Cryostratigraphy, sedimentology, and the late Quaternary evolution of the Zackenberg River delta, northeast Greenland. *Cryosphere*, 11(3), 1265–1282. <https://doi.org/10.5194/tc-11-1265-2017>

Giralt, S., Moreno, A., Bao, R., Sáez, A., Prego, R., Valero-Garcés, B. L., Pueyo, J. J., González-Sampériz, P., & Taberner, C. (2008). A statistical approach to disentangle environmental forcings in a lacustrine record: The Lago Chungará case (Chilean Altiplano). *Journal of Paleolimnology*, 40(1), 195–215. <https://doi.org/10.1007/s10933-007-9151-9>

Goosse, H., Kay, J. E., Armour, K. C., Bodas-Salcedo, A., Chepfer, H., Docquier, D., Jonko, A., Kushner, P. J., Lecomte, O., Massonnet, F., Park, H. S., Pithan, F., Svensson, G., & Vancoppenolle, M. (2018). Quantifying climate feedbacks in polar regions. *Nature Communications*, 9(1). <https://doi.org/10.1038/s41467-018-04173-0>

Gosse, J., & Klein, J. (2014). Encyclopedia of Scientific Dating Methods. *Encyclopedia of Scientific Dating Methods*, 1–23. <https://doi.org/10.1007/978-94-007-6326-5>

Granger, D. E., Lifton, N. A., & Willenbring, J. K. (2013). A cosmic trip: 25 years of cosmogenic nuclides in geology. *Bulletin of the Geological Society of America*, 125(9–10), 1379–1402. <https://doi.org/10.1130/B30774.1>

Grønnow, B., Jensen, J. F., Sørensen, M., Gullov, H. C., Gotfredsen, A. B., & Melgaard, M. (2009). Geographical Report of the GeoArk expeditions to North-East Greenland 2007 and 2008. May.

Håkanson, L. 2008. (2008). Håkanson, Lena 2008.

Håkansson, L., Alexanderson, H., Hjort, C., Möller, P., Briner, J. P., & Possnert, A. A. (2009a). Late Pleistocene glacial history of Jameson Land, central East Greenland, derived from cosmogenic ¹⁰Be and ²⁶Al exposure dating. *Boreas*, 38(2), 244–260. <https://doi.org/10.1111/j.1502-3885.2008.00064.x>

Håkansson, L., Alexanderson, H., Hjort, C., Möller, P., Briner, J. P., & Possnert, A. A. (2009b). Late Pleistocene glacial history of Jameson Land, central East Greenland, derived from cosmogenic ¹⁰Be and ²⁶Al exposure dating. *Boreas*, 38(2), 244–260. <https://doi.org/10.1111/j.1502-3885.2008.00064.x>

Håkansson, L., Briner, J., Alexanderson, H., Aldahan, A., & Possnert, G. (2007). ¹⁰Be ages from central east Greenland constrain the extent of the Greenland ice sheet during the Last Glacial Maximum. *Quaternary Science Reviews*, 26(19–21), 2316–2321. <https://doi.org/10.1016/j.quascirev.2007.08.001>

Håkansson, L., Briner, J. P., Aldahan, A., & Possnert, G. (2011). ¹⁰Be data from meltwater channels suggest that Jameson Land, east Greenland, was ice-covered during the last glacial maximum. *Quaternary Research*, 76(3), 452–459. <https://doi.org/10.1016/j.yqres.2011.06.007>

Håkansson, L., Graf, A., Strasky, S., Ivy-Ochs, S., Kubik, P. W., Hjort, C., & Schlüchter, C. (2007). Cosmogenic ¹⁰Be-ages from the Store Koldewey island, NE Greenland. *Geografiska Annaler, Series A: Physical Geography*, 89(3), 195–202. <https://doi.org/10.1111/j.1468-0459.2007.00318.x>

Hanna, E., Cropper, T. E., Hall, R. J., & Cappelen, J. (2016). Greenland Blocking Index 1851–2015: a regional climate change signal. *International Journal of Climatology*, 36(15), 4847–4861. <https://doi.org/10.1002/joc.4673>

Hanna, E., Cropper, T. E., Jones, P. D., Scaife, A. A., & Allan, R. (2015). Recent seasonal asymmetric changes in the NAO (a marked summer decline and increased winter variability) and associated changes in the AO and Greenland Blocking Index. *International*

- Journal of Climatology, 35(9), 2540–2554. <https://doi.org/10.1002/joc.4157>
- Hasholt, B., Mernild, S. H., Sigsgaard, C., Elberling, B., Petersen, D., Jakobsen, B. H., Hansen, B. U., Hinkler, J., & Søgaard, H. (2008). Hydrology and Transport of Sediment and Solutes at Zackenberg. *Advances in Ecological Research*, 40(07), 197–221. [https://doi.org/10.1016/S0065-2504\(07\)00009-8](https://doi.org/10.1016/S0065-2504(07)00009-8)
- Henriksen, N., Higgins, A. K., Kalsbeek, F., & Pulvertaft, T. C. R. (2009). Greenland from Archaean to Quaternary Descriptive text to the 1995 Geological map of Greenland, 1:2500000. *Geological Survey of Denmark and Greenland Bulletin*, 18, 126.
- Hernández, A., Martín-Puertas, C., Moffa-Sánchez, P., Moreno-Chamarro, E., Ortega, P., Blockley, S., Cobb, K. M., Comas-Bru, L., Giralt, S., Goose, H., Luterbacher, J., Martrat, B., Muscheler, R., Parnell, A., Pla-Rabes, S., Sjolte, J., Scaife, A. A., Swingedouw, D., Wise, E., & Xu, G. (2020). Modes of climate variability: Synthesis and review of proxy-based reconstructions through the Holocene. In *Earth-Science Reviews* (Vol. 209). <https://doi.org/10.1016/j.earscirev.2020.103286>
- Heyman, J., Stroeve, A. P., Harbor, J. M., & Caffee, M. W. (2011). Too young or too old: Evaluating cosmogenic exposure dating based on an analysis of compiled boulder exposure ages. *Earth and Planetary Science Letters*, 302(1–2), 71–80. <https://doi.org/10.1016/j.epsl.2010.11.040>
- Hogan, K. A., Ó Cofaigh, C., Jennings, A. E., Dowdeswell, J. A., & Hiemstra, J. F. (2016). Deglaciation of a major palaeo-ice stream in Disko Trough, West Greenland. *Quaternary Science Reviews*, 147, 5–26. <https://doi.org/10.1016/j.quascirev.2016.01.018>
- Højlund Pedersen, S. (2017). *Scaling-up Climate Change Effects in Greenland* [Aarhus University, Denmark]. www.bios.au.dk/en/
- Hörhold, M., Münch, T., Weißbach, S., Kipfstuhl, S., Freitag, J., Sasgen, I., Lohmann, G., Vinther, B., & Laepple, T. (2023). Modern temperatures in central–north Greenland warmest in past millennium. *Nature*, 613(7944), 503–507. <https://doi.org/10.1038/s41586-022-05517-z>
- IMBIE Team. (2020). Mass balance of the Greenland Ice Sheet from 1992 to 2018. *Nature*, 579(7798), 233–239. <https://doi.org/10.1038/s41586-019-1855-2>
- Jackson, R., Carlson, A. E., Hillaire-Marcel, C., Wacker, L., Vogt, C., & Kucera, M. (2017). Asynchronous instability of the North American-Arctic and Greenland ice sheets during the last deglaciation. *Quaternary Science Reviews*, 164(April), 140–153. <https://doi.org/10.1016/j.quascirev.2017.03.020>
- JC, G., & FM, P. (2001). Terrestrial in situ cosmogenic nuclides: theory and application. *Quaternary Science Reviews*, 20, 1475–1560. http://www.ees.nmt.edu/outside/courses/hyd558/downloads/Set_14b_InSitu/Gosse_Phillips.pdf
- Jomelli, V., Swingedouw, D., Vuille, M., Favier, V., Goehring, B., Shakun, J., Braucher, R., Schimmelpennig, I., Menviel, L., Rabatel, A., Martin, L. C. P., Blard, P.-H., Condom, T., Lupker, M., Christl, M., He, Z., Verfaillie, D., Gorin, A., Aumaître, G., ... Keddadouche, K. (2022). In-phase millennial-scale glacier changes in the tropics and North Atlantic regions during the Holocene. *Nature Communications*, 13(1), 1–12. <https://doi.org/10.1038/s41467-022-28939-9>
- Kaufman, D. S., Ager, T. A., Anderson, N. J., Anderson, P. M., Andrews, J. T., Bartlein, P. J., Brubaker, L. B., Coats, L. L., Cwynar, L. C., Duvall, M. L., Dyke, A. S., Edwards, M. E., Eisner, W. R., Gajewski, K., Geirsdóttir, A., Hu, F. S., Jennings, A. E., Kaplan, M. R., Kerwin, M. W., ... Wolfe, B. B. (2004). Holocene thermal maximum in the western Arctic (0–180°W). *Quaternary Science Reviews*, 23(5–6), 529–560. <https://doi.org/10.1016/j.quascirev.2003.09.007>
- Kelly, M. A., & Lowell, T. V. (2008). Fluctuations of local glaciers in Greenland during latest Pleistocene and Holocene time. *Quaternary Science Reviews*, 28(21–22), 2088–2106. <https://doi.org/10.1016/j.quascirev.2008.12.008>
- King, M. D., Howat, I. M., Candela, S. G., Noh, M. J., Jeong, S., Noël, B. P. Y., van den Broeke, M. R., Wouters, B., & Negrete, A. (2020). Dynamic ice loss from the Greenland Ice Sheet driven by sustained glacier retreat. *Communications Earth and Environment*, 1(1), 1–7. <https://doi.org/10.1038/s43247-020-0001-2>
- Kjær, K. H., Bjørk, A. A., Kjeldsen, K. K., Hansen, E. S., Andresen, C. S., Siggaard-Andersen, M. L., Khan, S. A., Søndergaard, A. S., Colgan, W., Schomacker, A., Woodroffe, S., Funder, S., Rouillard, A., Jensen, J. F., & Larsen, N. K. (2022). Glacier response to the Little Ice Age during the Neoglacial cooling in Greenland. *Earth-Science Reviews*, 227(March). <https://doi.org/10.1016/j.earscirev.2022.103984>
- Klose, A. K., Karle, V., Winkelmann, R., & Donges, J. F. (2020). Emergence of cascading dynamics in interacting tipping elements of ecology and climate. *Royal Society Open Science*, 7(6). <https://doi.org/10.1098/rsos.200599>
- Klug, M., & Wagner, B. (2008). Late Pleistocene and Holocene environmental history of northeastern Geographical Society Ø, East Greenland, inferred from Loon Lake s sediment record. *Leipziger Geowissenschaften*, Leipzig, 1–22. <http://epic.awi.de/20303/1/Klu2008b.pdf>
- Klug, Martin. (2009). *The late Quaternary environmental and climatic history of North-East Greenland, inferred from coastal lakes*. [PhD Thesis. Univ. Köln, 148]. <https://doi.org/DOI:10.23689/figeo-241>.
- Kobashi, T., Menviel, L., Jeltsch-Thömmes, A., Vinther, B. M., Box, J. E., Muscheler, R., Nakaegawa, T., Pfister, P. L., Döring, M., Leuenberger, M., Wanner, H., & Ohmura, A. (2017). Volcanic influence on centennial to millennial Holocene Greenland temperature change. *Scientific Reports*, 7(1), 1–10. <https://doi.org/10.1038/s41598-017-01451-7>
- Kolling, H. M., Stein, R., Fahl, K., Perner, K., & Moros, M. (2017). Short-term variability in late Holocene sea ice cover on the East Greenland Shelf and its driving mechanisms. *Palaeogeography, Palaeoclimatology, Palaeoecology*, 485, 336–350. <https://doi.org/10.1016/j.palaeo.2017.06.024>
- Kottek, M., Grieser, J., Beck, C., Rudolf, B., & Rubel, F. (2006). World map of the Köppen-Geiger climate classification updated. *Meteorologische Zeitschrift*, 15(3), 259–263. <https://doi.org/10.1127/0941-2948/2006/0130>
- Kroon, A., Jakobsen, H., Bj, J., Addingt, L., Brigit, A., & Melgaard, M. (2009). *Ge ogra ph ica l Re por t of t h e Ge oAr k e x pe dit ion s t o N or t h - Ea st Gr e e n la n d*. August 2008.
- Lal, D. (1991). Cosmic ray labeling of erosion surfaces: in situ nuclide production rates and erosion models. *Earth and Planetary Science Letters*. *Earth and Planetary Science Letters*, 104(2–4), 424–439. http://trafficlight.bitdefender.com/info?url=http%3A/www.sciencedirect.com/science/article/pii/0012821X9190220C&language=en_US

- Lamb, H. (1965). THE EARLY MEDIEVAL WARM EPOCH AND ITS SEQUEL. *Palaeogeography, Palaeoclimatology, Palaeoecology*, 1, 13–37.
- Larocca, L. J., Axford, Y., Bjørk, A. A., Lasher, G. E., & Brooks, J. P. (2020). Local glaciers record delayed peak Holocene warmth in south Greenland. *Quaternary Science Reviews*, 241, 106421. <https://doi.org/10.1016/j.quascirev.2020.106421>
- Larocca, L. J., Axford, Y., Woodroffe, S. A., Lasher, G. E., & Gawin, B. (2020). Holocene glacier and ice cap fluctuations in southwest Greenland inferred from two lake records. *Quaternary Science Reviews*, 246, 106529. <https://doi.org/10.1016/j.quascirev.2020.106529>
- Larsen, N. K., Funder, S., Linge, H., Möller, P., Schomacker, A., Fabel, D., Xu, S., & Kjær, K. H. (2016). A Younger Dryas re-advance of local glaciers in north Greenland. *Quaternary Science Reviews*, 147, 47–58. <https://doi.org/10.1016/j.quascirev.2015.10.036>
- Larsen, N. K., Levy, L. B., Carlson, A. E., Buizert, C., Olsen, J., Strunk, A., Bjørk, A. A., & Skov, D. S. (2018). Instability of the Northeast Greenland Ice Stream over the last 45,000 years. *Nature Communications*, 9(1), 3–10. <https://doi.org/10.1038/s41467-018-04312-7>
- Larsen, N. K., Søndergaard, A. S., Levy, L. B., Olsen, J., Strunk, A., Bjørk, A. A., & Skov, D. (2020). Contrasting modes of deglaciation between fjords and inter-fjord areas in eastern North Greenland. *Boreas*, 49(4), 903–917. <https://doi.org/10.1111/bor.12475>
- Lasher, G. E., & Axford, Y. (2019). Medieval warmth confirmed at the Norse Eastern Settlement in Greenland. *Geology*, 47(3). <https://doi.org/10.1130/G45833.1>
- Legendre, P., & Birks, H. J. B. (2012). Clustering and partitioning. *Tracking Environmental Change Using Lake Sediments*, 5(Data handling and numerical techniques.), 1–32.
- Leger, T. P. M., Clark, C. D., Huynh, C., Jones, S., Ely, J. C., Sarah, L., Diemont, C., & Hughes, A. L. C. (2023). A Greenland-wide empirical reconstruction of paleo ice-sheet retreat informed by ice extent markers : PaleoGrIS version 1 . 0. July, 1–97.
- Lenton, T. M., Held, H., Kriegler, E., Hall, J. W., Lucht, W., Rahmstorf, S., & Schellnhuber, H. J. (2008). Tipping elements in the Earth's climate system. *Proceedings of the National Academy of Sciences of the United States of America*, 105(6), 1786–1793. <https://doi.org/10.1073/pnas.0705414105>
- Levy, L. B., Kelly, M. A., Lowell, T. V., Hall, B. L., Hempel, L. A., Honsaker, W. M., Lusas, A. R., Howley, J. A., & Axford, Y. L. (2014a). Holocene fluctuations of Bregne ice cap, Scoresby Sund, east Greenland: A proxy for climate along the Greenland Ice Sheet margin. *Quaternary Science Reviews*, 92, 357–368. <https://doi.org/10.1016/j.quascirev.2013.06.024>
- Levy, L. B., Kelly, M. A., Lowell, T. V., Hall, B. L., Hempel, L. A., Honsaker, W. M., Lusas, A. R., Howley, J. A., & Axford, Y. L. (2014b). Holocene fluctuations of Bregne ice cap, Scoresby Sund, east Greenland: A proxy for climate along the Greenland Ice Sheet margin. *Quaternary Science Reviews*, 92, 357–368. <https://doi.org/10.1016/j.quascirev.2013.06.024>
- Levy, L. B., Kelly, M. A., Lowell, T. V., Hall, B. L., Howley, J. A., & Smith, C. A. (2016). Coeval fluctuations of the Greenland ice sheet and a local glacier, central East Greenland, during late glacial and early Holocene time. *Geophysical Research Letters*, 43(4), 1623–1631. <https://doi.org/10.1002/2015GL067108>
- Ljungqvist, F. C. (2010). A new reconstruction of temperature variability in the extra-tropical northern hemisphere during the last two millennia. *Geografiska Annaler, Series A: Physical Geography*, 92(3), 339–351. <https://doi.org/10.1111/j.1468-0459.2010.00399.x>
- Lowell, T. V., Hall, B. L., Kelly, M. A., Bennike, O., Lusas, A. R., Honsaker, W., Smith, C. A., Levy, L. B., Travis, S., & Denton, G. H. (2013). Late Holocene expansion of Istorvet ice cap, Liverpool Land, east Greenland. *Quaternary Science Reviews*, 63, 128–140. <https://doi.org/10.1016/j.quascirev.2012.11.012>
- Lund, M., Abermann, J., & Skov, K. (2017). Environmental effects of a rare rain event in the high Arctic. *EGU General Assembly Conference Abstracts* 1, 19, Abstract no. 9462.
- Lusas, A. R., Hall, B. L., Lowell, T. V., Kelly, M. A., Bennike, O., Levy, L. B., & Honsaker, W. (2017a). Holocene climate and environmental history of East Greenland inferred from lake sediments. *Journal of Paleolimnology*, 57(4), 321–341. <https://doi.org/10.1007/s10933-017-9951-5>
- Lusas, A. R., Hall, B. L., Lowell, T. V., Kelly, M. A., Bennike, O., Levy, L. B., & Honsaker, W. (2017b). Holocene climate and environmental history of East Greenland inferred from lake sediments. *Journal of Paleolimnology*, 57(4), 321–341. <https://doi.org/10.1007/s10933-017-9951-5>
- Mann, M. E., & Jones, P. D. (2003). Global surface temperatures over the past two millennia. *Geophysical Research Letters*, 30(15), 15–18. <https://doi.org/10.1029/2003GL017814>
- Marrero, S. M., Phillips, F. M., Borchers, B., Lifton, N., Aumer, R., & Balco, G. (2016). Cosmogenic nuclide systematics and the CRONUScalc program. *Quaternary Geochronology*, 31, 160–187. <https://doi.org/10.1016/j.quageo.2015.09.005>
- Martin, L. C. P., Blard, P. H., Balco, G., Lavé, J., Delunel, R., Lifton, N., & Laurent, V. (2017). The CREp program and the ICE-D production rate calibration database: A fully parameterizable and updated online tool to compute cosmic-ray exposure ages. *Quaternary Geochronology*, 38, 25–49. <https://doi.org/10.1016/j.quageo.2016.11.006>
- McKay, N. P., Kaufman, D. S., Routson, C. C., Erb, M. P., & Zander, P. D. (2018). The Onset and Rate of Holocene Neoglacial Cooling in the Arctic. *Geophysical Research Letters*, 45(22), 12,487–12,496. <https://doi.org/10.1029/2018GL079773>
- Medford, A. K., Hall, B. L., Lowell, T. V., Kelly, M. A., Levy, L. B., Wilcox, P. S., & Axford, Y. (2021). Holocene glacial history of Renland Ice Cap, East Greenland, reconstructed from lake sediments. *Quaternary Science Reviews*, 258, 106883. <https://doi.org/10.1016/j.quascirev.2021.106883>
- Merchel, S., Arnold, M., Aumaître, G., Benedetti, L., Bourlès, D. L., Braucher, R., Alfimov, V., Freeman, S. P. H. T., Steier, P., & Wallner, A. (2008). Towards more precise ¹⁰Be and ³⁶Cl data from measurements at the 10-14 level: Influence of sample preparation. *Nuclear Instruments and Methods in Physics Research, Section B: Beam Interactions with Materials and Atoms*, 266(22), 4921–4926. <https://doi.org/10.1016/j.nimb.2008.07.031>
- Meredith, M., Sommerkorn, M., Cassotta, S., Derksen, C., Ekaykin, A., & Hollowed, A. (2019). Polar regions. In *IPCC Special Report on the Ocean and Cryosphere in a Changing Climate*, Edited by H.-O. Pörtner, D.C. Roberts, V. Masson-Delmotte, P. Zhai, M. Tignor, E. Poloczanska, K. Mintenbeck, A. Alegría, M. Nicolai, A. Okem, J. Petzold, B. Rama, and N.M. Weyer, 203–320. [https://doi.org/10.1016/S1366-7017\(01\)00066-6](https://doi.org/10.1016/S1366-7017(01)00066-6)
- Miller, G. H., Alley, R. B., Brigham-Grette, J., Fitzpatrick, J. J., Polyak, L., Serreze, M. C.,

- & White, J. W. C. (2010). Arctic amplification: Can the past constrain the future? *Quaternary Science Reviews*, 29(15–16), 1779–1790. <https://doi.org/10.1016/j.quascirev.2010.02.008>
- Nesje, A., & Dahl, S. O. (2000). Key Issues in Environmental Change Editors. 216.
- Nesje, A., & Dahl, S. O. (2001). The Greenland 8200 cal. yr BP event detected in loss-on-ignition profiles in Norwegian lacustrine sediment sequences. *Journal of Quaternary Science*, 16(2), 155–166. <https://doi.org/10.1002/jqs.567>
- Nishiizumi, K., Imamura, M., Caffee, M. W., Southon, J. R., Finkel, R. C., & McAninch, J. (2007). Absolute calibration of ^{10}Be AMS standards. *Nuclear Instruments and Methods in Physics Research, Section B: Beam Interactions with Materials and Atoms*, 258(2), 403–413. <https://doi.org/10.1016/j.nimb.2007.01.297>
- Oerlemans, J. (2005). Atmospheric science: Extracting a climate signal from 169 glacier records. *Science*, 308(5722), 675–677. <https://doi.org/10.1126/science.1107046>
- Oksman, M., Weckström, K., Miettinen, A., Juggins, S., Divine, D. V., Jackson, R., Telford, R., Korsgaard, N. J., & Kucera, M. (2017). Younger Dryas ice margin retreat triggered by ocean surface warming in central-eastern Baffin Bay. *Nature Communications*, 8(1), 1–8. <https://doi.org/10.1038/s41467-017-01155-6>
- Oliva, M., & Ruiz-Fernández, J. (2018). Late Quaternary environmental dynamics in Lenin Peak area (Pamir Mountains, Kyrgyzstan). *Science of the Total Environment*, 645, 603–614. <https://doi.org/10.1016/j.scitotenv.2018.07.178>
- Olsen, J., Kjær, K. H., Funder, S., Larsen, N. K., & Ludikova, A. (2012). High-Arctic climate conditions for the last 7000 years inferred from multi-proxy analysis of the Bliss Lake record, North Greenland. *Journal of Quaternary Science*, 27(3), 318–327. <https://doi.org/10.1002/jqs.1548>
- Pados-Dibattista, T., Pearce, C., Detlef, H., Bendtsen, J., & Seidenkrantz, M. S. (2022). Holocene palaeoceanography of the Northeast Greenland shelf. *Climate of the Past*, 18(1), 103–127. <https://doi.org/10.5194/cp-18-103-2022>
- Palacios, D., Ruiz-Fernández, J., Oliva, M., Andrés, N., Fernández-Fernández, J. M., Schimmelpennig, I., Leanni, L., & González-Díaz, B. (2020). Timing of formation of neoglacial landforms in the South Shetland Islands (Antarctic Peninsula): Regional and global implications. *Quaternary Science Reviews*, 234. <https://doi.org/10.1016/j.quascirev.2020.106248>
- Payer, J. (1876). Die oesterreichisch-ungarische Nordpol-Expedition in den Jahren 1872-1874 : nebst einer Skizze der zweiten deutschen Nordpol-Expedition 1869-1870, und der Polar-Expedition von 1871. Wien : A. Hoelder, 1876.
- Pedersen, J. B. T., Kaufmann, L. H., Kroon, A., & Jakobsen, B. H. (2010). The Northeast Greenland Sirius Water Polynya dynamics and variability inferred from satellite imagery. *Geografisk Tidsskrift*, 110(2), 131–142. <https://doi.org/10.1080/00167223.2010.10669503>
- Pithan, F., & Mauritsen, T. (2014). Arctic amplification dominated by temperature feedbacks in contemporary climate models. *Nature Geoscience*, 7(3), 181–184. <https://doi.org/10.1038/ngeo2071>
- Porter, C., Morin, P., Howat, I., Noh, M.-J., Bates, B., Peterman, K., Keese, S., Schlenk, M., Gardiner, J., Tomko, K., Willis, M., Kelleher, C., Cloutier, M., Husby, E., Foga, S., Nakamura, H., Platson, M., Wethington Jr., M., Williamson, C., ... Bojesen, M. A.-N. S. F. (2018). ArcticDEM (V1 ed.). Harvard Dataverse. <https://doi.org/doi:10.7910/DVN/OHHUKH>
- Porter, S. C., & Denton, G. H. (1967). Chronology of neoglaciation in the North American Cordillera. In *American Journal of Science* (Vol. 265, Issue 3, pp. 177–210). <https://doi.org/10.2475/ajs.265.3.177>
- Porter, Stephen C. (2000). Onset of neoglaciation in the southern hemisphere. *Journal of Quaternary Science*, 15(4), 395–408. [https://doi.org/10.1002/1099-1417\(200005\)15:4<395::AID-JQS535>3.0.CO;2-H](https://doi.org/10.1002/1099-1417(200005)15:4<395::AID-JQS535>3.0.CO;2-H)
- Post, E., Forchhammer, M. C., Bret-Harte, M. S., Callaghan, T. V., Christensen, T. R., Elberling, B., Fox, A. D., Gilg, O., Hik, D. S., Høye, T. T., Ims, R. A., Jeppesen, E., Klein, D. R., Madsen, J., McGuire, A. D., Rysgaard, S., Schindler, D. E., Stirling, I., Tamstorf, M. P., ... Aastrup, P. (2009). Ecological Dynamics Across the Arctic Associated With Recent Climate Change. *Science*, 325(5946), 1355–1358. <https://doi.org/10.1126/science.1173113>
- Preusser, F., Degering, D., Fuchs, M., Hilgers, A., Kadereit, A., Klasen, N., Krbetschek, M., Richter, D., & Spencer, J. Q. G. (2008). Luminescence dating: basics, methods and applications. *Quaternary Science Journal*, 57(1/2), 95–149. <https://doi.org/10.3285/eg.57.1-2.5>
- Rantanen, M., Karpechko, A. Y., Lipponen, A., Nordling, K., Hyvärinen, O., Ruosteenoja, K., Vihma, T., & Laaksonen, A. (2022). The Arctic has warmed nearly four times faster than the globe since 1979. *Communications Earth and Environment*, 3(1), 1–10. <https://doi.org/10.1038/s43247-022-00498-3>
- Rasmussen, S. O., Vinther, B. M., Clausen, H. B., & Andersen, K. K. (2007). Early Holocene climate oscillations recorded in three Greenland ice cores. *Quaternary Science Reviews*, 26(15–16), 1907–1914. <https://doi.org/10.1016/j.quascirev.2007.06.015>
- Rasmussen, S. Olander, Andersen, K. K., Svensson, A. M., Steffensen, J. P., Vinther, B. M., Clausen, H. B., Siggaard-Andersen, M. L., Johnsen, S. J., Larsen, L. B., Dahl-Jensen, D., Bigler, M., Röthlisberger, R., Fischer, H., Goto-Azuma, K., Hansson, M. E., & Ruth, U. (2006). A new Greenland ice core chronology for the last glacial termination. *Journal of Geophysical Research Atmospheres*, 111(6), 1–16. <https://doi.org/10.1029/2005JD006079>
- Rasmussen, Sune O., Bigler, M., Blockley, S. P., Blunier, T., Buchardt, S. L., Clausen, H. B., Cvijanovic, I., Dahl-Jensen, D., Johnsen, S. J., Fischer, H., Gkinis, V., Guillevic, M., Hoek, W. Z., Lowe, J. J., Pedro, J. B., Popp, T., Seierstad, I. K., Steffensen, J. P., Svensson, A. M., ... Winstrup, M. (2014). A stratigraphic framework for abrupt climatic changes during the Last Glacial period based on three synchronized Greenland ice-core records: Refining and extending the INTIMATE event stratigraphy. *Quaternary Science Reviews*, 106, 14–28. <https://doi.org/10.1016/j.quascirev.2014.09.007>
- Rasmussen, Sune Olander, Dahl-Jensen, D., Fischer, H., Fuhrer, K., Hansen, S. B., Hansson, M., Hvidberg, C. S., Jonsell, U., Kipfstuhl, S., Ruth, U., Schwander, J., Siggaard-Andersen, M. L., Sinnl, G., Steffensen, J. P., Svensson, A. M., & Vinther, B. M. (2023). Ice-core data used for the construction of the Greenland Ice-Core Chronology 2005 and 2021 (GIACC05 and GIACC21). *Earth System Science Data*, 15(8), 3351–3364. <https://doi.org/10.5194/essd-15-3351-2023>
- Reimer, P. J., Austin, W. E. N., Bard, E., Bayliss, A., Blackwell, P. G., Bronk Ramsey, C., Butzin, M., Cheng, H., Edwards, R. L., Friedrich, M., Grootes, P. M., Guilderson, T. P., Hajdas, I., Heaton, T. J., Hogg, A. G., Hughen, K. A., Kromer, B., Manning, S. W.,

- Muscheler, R., ... Talamo, S. (2020). The IntCal20 Northern Hemisphere Radiocarbon Age Calibration Curve (0–55 cal kBP). *Radiocarbon*, 62(4), 725–757. <https://doi.org/10.1017/RDC.2020.41>
- Renssen, H., Seppä, H., Heiri, O., Roche, D. M., Goosse, H., & Fichet, T. (2009). The spatial and temporal complexity of the holocene thermal maximum. *Nature Geoscience*, 2(6), 411–414. <https://doi.org/10.1038/ngeo513>
- Reusche, M. M., Marcott, S. A., Ceperley, E. G., Barth, A. M., Brook, E. J., Mix, A. C., & Caffee, M. W. (2018). Early to Late Holocene Surface Exposure Ages From Two Marine-Terminating Outlet Glaciers in Northwest Greenland. *Geophysical Research Letters*, 45(14), 7028–7039. <https://doi.org/10.1029/2018GL078266>
- Rule, H., Council, B. M., Society, R. G., Affairs, D., Green, N., Park, N., Kyst, B., Aps, N. T., Tobin, K., Ecological, Z., Ecological, Z., Aps, N. T., Sirius, T., Patrol, S., & Patrol, S. S. (2005). Exploration history of northern East Greenland.
- Saros, J. E., Anderson, N. J., Juggins, S., McGowan, S., Yde, J. C., Telling, J., Bullard, J. E., Yallop, M. L., Heathcote, A. J., Burpee, B. T., Fowler, R. A., Barry, C. D., Northington, R. M., Osburn, C. L., Pla-Rabes, S., Mernild, S. H., Whiteford, E. J., Grace Andrews, M., Kerby, J. T., & Post, E. (2019). Arctic climate shifts drive rapid ecosystem responses across the West Greenland landscape. *Environmental Research Letters*, 14(7), 74027. <https://doi.org/10.1088/1748-9326/ab2928>
- Schmidt, S., Wagner, B., Heiri, O., Klug, M., Bennike, O., & Melles, M. (2011). Chironomids as indicators of the Holocene climatic and environmental history of two lakes in Northeast Greenland. *Boreas*, 40(1), 116–130. <https://doi.org/10.1111/j.1502-3885.2010.00173.x>
- Schweinsberg, A. D., Briner, J. P., Licciardi, J. M., Bennike, O., Lifton, N. A., Graham, B. L., Young, N. E., Schaefer, J. M., & Zimmerman, S. H. (2019). Multiple independent records of local glacier variability on Nuussuaq, West Greenland, during the Holocene. *Quaternary Science Reviews*, 215, 253–271. <https://doi.org/10.1016/j.quascirev.2019.05.007>
- Seierstad, I. K., Johnsen, S. J., Vinther, B. M., & Olsen, J. (2005). The duration of the Bølling-Allerød period (Greenland Interstadial 1) in the GRIP ice core. *Annals of Glaciology*, 42(3), 337–344. <https://doi.org/10.3189/172756405781812556>
- Serreze, M. C., & Barry, R. G. (2011). Processes and impacts of Arctic amplification: A research synthesis. *Global and Planetary Change*, 77(1–2), 85–96. <https://doi.org/10.1016/j.gloplacha.2011.03.004>
- Shakun, J. D., Clark, P. U., He, F., Marcott, S. A., Mix, A. C., Liu, Z., Otto-Bliesner, B., Schmittner, A., & Bard, E. (2012). Global warming preceded by increasing carbon dioxide concentrations during the last deglaciation. *Nature*, 484(7392), 49–54. <https://doi.org/10.1038/nature10915>
- Skov, D. S., Andersen, J. L., Olsen, J., Jacobsen, B. H., Knudsen, M. F., Jansen, J. D., Larsen, N. K., & Egholm, D. L. (2020). Constraints from cosmogenic nuclides on the glaciation and erosion history of Dove Bugt, northeast Greenland. *Bulletin of the Geological Society of America*, 132(11–12), 2282–2294. <https://doi.org/10.1130/b35410.1>
- Smol, J. P. (2019). Under the radar: Long-term perspectives on ecological changes in lakes. *Proceedings of the Royal Society B: Biological Sciences*, 286(1906). <https://doi.org/10.1098/rspb.2019.0834>
- Solomina, O. N., Bradley, R. S., Hodgson, D. A., Ivy-Ochs, S., Jomelli, V., Mackintosh, A. N., Nesje, A., Owen, L. A., Wanner, H., Wiles, G. C., & Young, N. E. (2015). Holocene glacier fluctuations. *Quaternary Science Reviews*, 111, 9–34. <https://doi.org/10.1016/j.quascirev.2014.11.018>
- Steffensen, J. P., Andersen, K. K., Bigler, M., Clausen, H. B., Dahl-Jensen, D., Fischer, H., Goto-azuma, K., Hansson, M., Johnsen, S. J., Jouzel, J., Masson-delmotte, V., Popp, T., Rasmussen, S. O., Röthlisberger, R., Ruth, U., Stauffer, B., Sveinbjörnsdóttir, Á. E., Svensson, A., & White, J. W. C. (2008). Happens in Few Years. *Science*, 321(5889), 680–684.
- Stine, S. (1994). Extreme and persistent drought in California and Patagonia during mediaeval time. *Nature*, 369(6481), 546–549. <https://doi.org/10.1038/369546a0>
- Stone, J. O. (2000). Air pressure and cosmogenic isotope production. *Journal of Geophysical Research*, 105(1), 753–759.
- Thomas, E. R., Wolff, E. W., Mulvaney, R., Steffensen, J. P., Johnsen, S. J., Arrowsmith, C., White, J. W. C., Vaughn, B., & Popp, T. (2007). The 8.2 ka event from Greenland ice cores. *Quaternary Science Reviews*, 26(1–2), 70–81. <https://doi.org/10.1016/j.quascirev.2006.07.017>
- Thompson, D. W. J., & Wallace, J. M. (1998). The Arctic oscillation signature in the wintertime geopotential height and temperature fields. *Geophysical Research Letters*, 25(9), 1297–1300. <https://doi.org/10.1029/98GL00950>
- Thornalley, D. J. R., Oppo, D. W., Ortega, P., Robson, J. I., Brierley, C. M., Davis, R., Hall, I. R., Moffa-Sanchez, P., Rose, N. L., Spooner, P. T., Yashayaev, I., & Keigwin, L. D. (2018). Anomalously weak Labrador Sea convection and Atlantic overturning during the past 150 years. *Nature*, 556(7700), 227–230. <https://doi.org/10.1038/s41586-018-0007-4>
- Vasskog, K., Langebroek, P. M., Andrews, J. T., Nilsen, J. E. Ø., & Nesje, A. (2015). The Greenland Ice Sheet during the last glacial cycle: Current ice loss and contribution to sea-level rise from a palaeoclimatic perspective. *Earth-Science Reviews*, 150, 45–67. <https://doi.org/10.1016/j.earscirev.2015.07.006>
- Vinther, B. M., Clausen, H. B., Fisher, D. A., Koerner, R. M., Johnsen, S. J., Andersen, K. K., Dahl-Jensen, D., Rasmussen, S. O., Steffensen, J. P., & Svensson, A. M. (2008). Synchronizing ice cores from the Renland and Agassiz ice caps to the Greenland Ice Core Chronology. *Journal of Geophysical Research Atmospheres*, 113(8), 1–10. <https://doi.org/10.1029/2007JD009143>
- Wagner, B., & Melles, M. (2002). Holocene environmental history of western Ymer, East Greenland, inferred from lake sediments. *Quaternary International*, 89(1), 165–176. [https://doi.org/10.1016/S1040-6182\(01\)00087-8](https://doi.org/10.1016/S1040-6182(01)00087-8)
- Wagner, Bernd, Bennike, O., Bos, J. A. A., Cremer, H., Lotter, A. F., & Melles, M. (2008). A multidisciplinary study of Holocene sediment records from Hjort Sø on Store Koldewey, Northeast Greenland. *Journal of Paleolimnology*, 39(3), 381–398. <https://doi.org/10.1007/s10933-007-9120-3>
- Wagner, Bernd, Heiri, O., & Hoyer, D. (2005). Chironomids as proxies for palaeoenvironmental changes in East Greenland: a Holocene record from Geographical Society Ø. *Zeitschrift Der Deutschen Gesellschaft Für Geowissenschaften*, 156(4), 543–556. <https://doi.org/DOI:10.1127/1860-1804/2005/0156-0543>

Wagner, G., Beer, J., Laj, C., Kissel, C., Masarik, J., Muscheler, R., & Synal, H. A. (2000). Chlorine-36 evidence for the Mono Lake event in the summit GRIP ice core. *Earth and Planetary Science Letters*, 181(1–2), 1–6. [https://doi.org/10.1016/S0012-821X\(00\)00196-5](https://doi.org/10.1016/S0012-821X(00)00196-5)

Wanner, H., Solomina, O., Grosjean, M., Ritz, S. P., & Jetel, M. (2011). Structure and origin of Holocene cold events. *Quaternary Science Reviews*, 30(21–22), 3109–3123. <https://doi.org/10.1016/j.quascirev.2011.07.010>

WARD, G. K., & WILSON, S. R. (1978). Procedures for Comparing and Combining Radiocarbon Age Determinations: a Critique. *Archaeometry*, 20(1), 19–31. <https://doi.org/10.1111/j.1475-4754.1978.tb00208.x>

Young, N. E., Briner, J. P., Miller, G. H., Lesnek, A. J., Crump, S. E., Thomas, E. K., Pendleton, S. L., Cuzzone, J., Lamp, J., Zimmerman, S., Caffee, M., & Schaefer, J. M. (2020). Deglaciation of the Greenland and Laurentide ice sheets interrupted by glacier advance during abrupt coolings. *Quaternary Science Reviews*, 229. <https://doi.org/10.1016/j.quascirev.2019.106091>

Young, N. E., Schaefer, J. M., Briner, J. P., & Goehring, B. M. (2013). A ^{10}Be production-rate calibration for the Arctic. *Journal of Quaternary Science*, 28(5), 515–526. <https://doi.org/10.1002/jqs.2642>

3

RESULTS AND DISCUSSION

OUTLINE

3. RESULTS AND DISCUSSION

3.1. LANDSCAPE EVOLUTION OF THE VALLEYS FROM NE GREENLAND

3.1.1 PAPER I. LATE GLACIAL DEGLACIATION OF THE ZACKENBERG AREA.

3.1.2 PAPER II. HOLOCENE GLACIAL OSCILLATIONS IN THE TYROLER VALLEY

3.1.3 PAPER III. A LATE GLACIAL AND HOLOCENE CHRONOLOGY OF CLIMATE-LINKED LANDSCAPE EVOLUTION IN NE GREENLAND FROM CRE DATING OF LANDFORMS

3.2 LOCAL CLIMATE VARIABILITY IN NE GREENLAND

3.2.1 PAPER IV. A ~5000-YEAR MULTIPROXY RECORD OF SUMMER CLIMATE.

3.2.2 OTHER DATA

3.3 LINKING CLIMATE VARIABILITY AND GLACIAL OSCILLATIONS

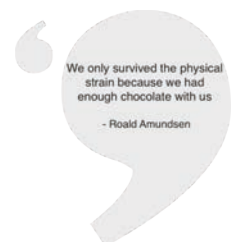


3.1. LANDSCAPE EVOLUTION OF THE VALLEYS FROM NE GREENLAND

3.1.1 PAPER I. LATE GLACIAL DEGLACIATION OF THE ZACKENBERG AREA.

PAPER I

J. Garcia-Oteyza, M. Oliva, D. Palacios, J.M. Fernández-Fernández, I. Schimmelpfennig, N. Andrés, D. Antoniades, H.H. Christiansen, O. Humlum, L. Léanni, V. Jomelli, J. Ruiz-Fernández, V. Rinterknecht, T.P. Lane, K. Adamson, Georges Aumaître, D. Bourlès, K. Keddadouche. Late Glacial deglaciation of the Zackenberg area, NE Greenland. *Geomorphology*, 401, 2022, 108125, ISSN 0169-555X. <https://doi.org/10.1016/j.geomorph.2022.108125>





Late Glacial deglaciation of the Zackenberg area, NE Greenland

J. Garcia-Oteyza^{a,*}, M. Oliva^a, D. Palacios^b, J.M. Fernández-Fernández^{c,b}, I. Schimmelpfennig^d, N. Andrés^b, D. Antoniadis^e, H.H. Christiansen^f, O. Humlum^f, L. Léanni^d, V. Jomelli^d, J. Ruiz-Fernández^g, V. Rinterknecht^d, T.P. Lane^h, K. Adamsonⁱ, ASTER Team:^d

Georges Aumaître, Didier Boulès, Karim Keddadouche

^a Department of Geography, Universitat de Barcelona, Catalonia, Spain

^b Department of Geography, Complutense University of Madrid, Madrid, Spain

^c Centre for Geographical Studies, IGOT, Universidade de Lisboa, Lisbon, Portugal

^d Aix-Marseille Université, CNRS, IRD, INRAE, Coll. France, UM 34 CEREGE, Aix-en-Provence, France

^e Department of Geography & Centre for Northern Studies, Université Laval, Québec, Canada

^f Arctic Geology Department, University Centre in Svalbard, Longyearbyen, Norway

^g Department of Geography, University of Oviedo, Asturias, Spain

^h School of Biological and Environmental Sciences, Liverpool John Moores University, Liverpool, UK

ⁱ Department of Natural Sciences, Manchester Metropolitan University, Manchester, UK

ARTICLE INFO

Article history:

Received 24 November 2021

Received in revised form 19 January 2022

Accepted 20 January 2022

Available online 26 January 2022

Keywords:

NE Greenland

Zackenberg

Deglaciation

Geomorphology

Paraglacial dynamics

Cosmic-ray exposure

ABSTRACT

The Greenland Ice Sheet (GrIS) is a key component of the global climate system. However, our current understanding of the spatio-temporal oscillations and landscape transformation of the GrIS margins since the last glacial cycle is still incomplete. The objective of this work is to study the deglaciation of the Zackenberg Valley (74°N, 20°E), NE Greenland, and the origin of the derived landforms. Based on extensive fieldwork and high-detail geomorphological mapping we identified the different types of landforms, from which those of glacial and paraglacial origin were used to understand the processes driving regional environmental evolution. We applied cosmic-ray exposure (CRE) dating to 32 samples taken from erosive and depositional glacial landforms distributed across the valley. Geomorphological evidence shows that >800-m-thick Late Quaternary glacier filled the valleys and fjords and covered mountain summits. In subsequent phases, as ice thickness decreased, the glacier was limited to the interior of the valley, leaving several lateral moraines. The deglaciation of the Zackenberg Valley that started by ~13.7–12.5 ka also accelerated slope paraglacial processes. Many blocks from lateral moraines were remobilized and fell, reaching the valley floor where they covered the thinning glacier tongue; transforming it into a debris-covered glacier that subsequently melted gradually. By ca. 10.5 ka, the last remnants of glacial ice disappeared from the Zackenberg Valley floor, a chronology of deglaciation that is similar to that observed in other sites across NE Greenland. The results of this work must be considered in similar studies, reinforcing the need to support CRE ages of the different geomorphological phases with paleoclimatic data from other sedimentary records.

© 2022 The Authors. Published by Elsevier B.V. This is an open access article under the CC BY license (<http://creativecommons.org/licenses/by/4.0/>).

1. Introduction

Polar regions are crucial components of the complex global climate system. Changes in these regions are not confined to the high latitudes, but have effects throughout the planet triggered by an intricate set of feedback processes between the atmosphere, ocean, sea ice, ice sheets, and land surfaces (Goosse et al., 2018). The

Greenland Ice Sheet (GrIS) is considered a tipping element in Earth's climate (Lenton et al., 2008) because it has played a major role in the stability of the climate system since the last glacial maximum (LGM; 26–19 ka; Cohen and Gibbard, 2019). This mostly land-based ice sheet is the second largest body of ice globally, and the only ice sheet in the Northern Hemisphere, storing an ice mass with a sea level equivalents of ~7.4 m (Bamber et al., 2013). To predict future sea level rise and other consequences of accelerated GrIS melting, an accurate monitoring of modern ice sheet mass balance as well as a better comprehension of GrIS past dynamics are essential.

Over the last several decades, ice cores obtained from the interior of the GrIS, terrestrial climate records from ice-free areas, and marine sediment records collected from the adjacent sea floor have generated an accurate picture of the Late Quaternary climatic evolution and associated environmental changes (Briner et al., 2016). Together with Antarctica, the GrIS is one of the only ice sheets that survived the last deglaciation during Termination-1 (T-1; ~19–11 ka). The GrIS persisted during the Last Interglacial period (~130–116 ka) when global temperatures were significantly higher than present, although it was particularly reduced in its NE sector (Vasskog et al., 2015). The GrIS significantly expanded during the last glacial cycle (115–11.7 ka), reaching its maximum volume during the LGM (~26.5–19 ka) (Clark et al., 2009; Vasskog et al., 2015). Subsequently, as temperatures increased following the LGM, the GrIS shrank and became mostly land based. However, paleoclimate records reveal abrupt temperature shifts during T-1 (5–15 °C), with strong seasonality (Buizert et al., 2014; Vasskog et al., 2015) that must have driven changes in GrIS volume. Changes in the ice volume stored in Greenland influence freshwater delivery to source areas of North Atlantic deep water formation, and rapid changes may thus affect the stability of the climate system (Broecker, 2018). During T-1, these temperature shifts favoured the reorganisation of the thermohaline circulation in the Southern Ocean that led to rapid global CO₂ rise along with massive deglacial environmental and biotic changes in the polar regions (Denton et al., 2010). A better understanding of GrIS fluctuations within the last glacial cycle and during T-1 can thus provide insights about GrIS response to rapidly changing climate conditions at the present day. However, important knowledge gaps still exist as to how the GrIS and peripheral glaciers respond to climate switches, their sensitivity to climate, and spatio-temporal patterns of past glacial oscillations (e.g. Kelly and Lowell, 2009; Vasskog et al., 2015; Larocca et al., 2020a, 2020b). This is particularly true for areas including the NE Greenland coastal region (in which this research focuses), where the chronology of glacial fluctuations and landscape changes during T-1 are still poorly understood.

The modern ice-free land areas beyond the margin of the GrIS include sources of paleoenvironmental information (glacial records, lake sediments, fens, deltas, etc.) that can be used to reconstruct the evolution of the GrIS and the glaciers at its periphery since deglaciation. This is the case of the Zackenberg Valley, NE Greenland, where the glacial and paraglacial geomorphology is well-known (Christiansen and Humlum, 1993; Christiansen, 1994, 1998; Bennike et al., 2008; Cable et al., 2018), but the chronology of glacial fluctuations and associated paraglacial dynamics is yet to be determined. Here, the reconstruction of glacial history and landscape dynamics is hampered by (i) very active slope processes on the hillsides surrounding the main valley floor (solifluction, debris flows, nivation, etc.); (ii) the intensity of paraglacial processes following deglaciation; (iii) the transformation of the debris-free glacier into a debris-covered glacier during the last stages of glacial retreat and the intense paraglacial readjustment; and (iv), the timing of wastage of debris-covered ice, and how it affected the development of the present-day hummocky terrain (Christiansen and Humlum, 1993; Cable et al., 2018). These processes have all affected the stability of glacial landforms since their deposition and thus represent a challenge to the successful application of cosmic-ray exposure (CRE) dating, which has rarely been applied to glacial landforms in steep valleys and debris-covered glaciers in the (sub)polar regions (e.g. Tanarro et al., 2019; Fernández-Fernández et al., 2020; Charton et al., 2020).

In this study, we combined a detailed geomorphological survey with CRE dating of erosive and depositional landforms left by outlet glaciers in the Zackenberg Valley that calved into Young Sund fjord during the last glacial cycle (Christiansen and Humlum, 1993). Our goals were: (i) to examine the limits of CRE dating for establishing time constraints in highly dynamic glacial-paraglacial-periglacial environments; (ii) to reconstruct the spatio-temporal patterns of glacial culminations and retreats in such a geomorphologically active area; and (iii) to interpret the glacial chronology considering the complex geomorphological

evolution of the valley. To achieve these goals, we specifically addressed the following questions:

- To what extent can CRE dating be successfully applied in this area, where post-glacial erosive and depositional processes are widespread?
- What information do the ages of glacial geomorphic features give about the environmental history of the Zackenberg area? Are they representative of the glacial chronology or have they been intensely reworked by paraglacial processes?
- When did the GrIS margin start shrinking during the last glacial cycle?
- What were the phases of major glacial advances/stillstands and retreats?
- Is there a synchronous pattern of glacial advances/stillstands and retreats during T-1 in NE Greenland and other regions of Greenland?

2. Regional setting

2.1. Study area

This study focuses on the ice-free Zackenberg Valley, situated in the Wollaston Foreland peninsula in the SE corner of the Northeast Greenland National Park, the world largest national park. Our study area encompasses the Zackenberg Valley floor from Young Sund fjord (south) to the mouth of the Store Sødal valley, the Dombjerg mountain (1492 m above sea level, hereafter referred to as a.s.l.) and Lindemandsdal valley (north), as well as the surrounding peaks and slopes descending from Aucellabjerg (985 m a.s.l, east) and Zackenberg (1338 m a.s.l, west) mountains (Fig. 1).

The highest summits surrounding the Zackenberg Valley form relatively horizontal surfaces that are affected by intense periglacial processes. From these high plateaus, steep hillsides descend towards the valley floor on the northern and eastern slope of the Zackenberg mountain and the south-eastern slope of the Dombjerg mountain, with more gentle slopes to the west of the Aucellabjerg mountain. The Zackenberg River drains the 2–3 km wide U-shaped Zackenberg valley fed by snow and glacier meltwater, and forms a large delta where it reaches Young Sund. This flat area has also been affected by glacio-isostatic processes, which have given rise to a sequence of marine terraces largely covered by periglacial slope sediments. The Quaternary marine limit was established at ~40 m, with an intense postglacial crustal rebound during the Early Holocene, and a stabilization of the relative sea level ~3 ka (Christiansen et al., 2002; Pedersen et al., 2011).

The region has a polar tundra climate (Kottek et al., 2006). Between 1996 and 2015, the mean annual air temperature at Zackenberg Research Station was ~9.0 °C and average annual precipitation of 367 mm (Højlund Pedersen, 2017), of which only 10% falls as rain during the summer months from June to September (Hasholt et al., 2008). The short summer season is crucial for the development of the valley's scarce vegetation cover. The large lowland areas include a moist to dry tundra dominated by shrubs <15 cm tall with grasslands, fens and interspersed snow patches, while the variety and size of the plants decrease at higher elevations (CAVM Team, 2003). The whole area is underlain by continuous permafrost (200 to 400 m thick) and a spatially variable active layer (45 to 80 cm thick) (Christiansen et al., 2008, 2010).

The area contains two different bedrock types separated by the Zackenberg and Lindemandsdal valleys that extend along a large N-S fault zone (Escher and Watt, 1976). The western side consists of Caledonian crystalline complexes (Early Proterozoic) with abundant orthogneiss resistant to weathering processes, which provides higher and steeper slopes and rather coarse-grained deposits in the valley bottom. By contrast, the eastern fringe across the slopes of Aucellabjerg is composed of Cretaceous to Jurassic sedimentary rocks (mudstones, sandstones and conglomerates) (Henriksen et al., 2009), which results

* Corresponding author at: Department of Geography, Universitat de Barcelona, Montalegre 6-8, 3r floor, 08001 Barcelona, Spain.
E-mail address: juliagarciaoteyza@ub.edu (J. Garcia-Oteyza).

<https://doi.org/10.1016/j.geomorph.2022.108125>

0169-555X/© 2022 The Authors. Published by Elsevier B.V. This is an open access article under the CC BY license (<http://creativecommons.org/licenses/by/4.0/>).

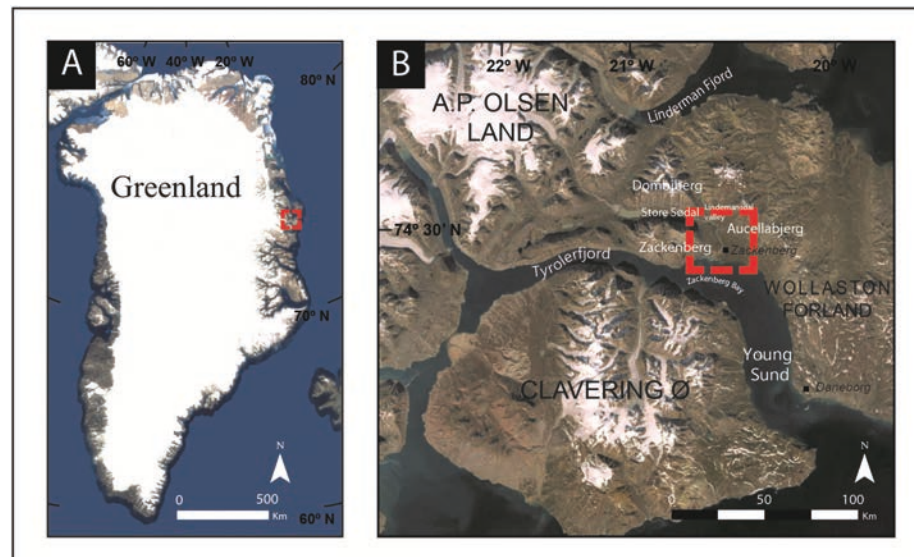


Fig. 1. (A) Location of the study area within Greenland; and (B) detail of the study region.

in a gentler relief with less inclined, long hillslopes with a sediment cover. Exposed bedrock is mostly found at the top of the mountains and upper slopes of both valley sides, whereas the lower parts and the valley floors are covered by Late Quaternary sediments (Gilbert et al., 2017; Cable et al., 2018).

The bedrock geology conditions the geomorphological processes prevailing today in the ice-free Zackenberg Valley, with very different landforms and processes on each side of the valley. Erosive and sedimentary glacial landforms are widespread across the valley and have been intensely transformed by paraglacial and periglacial dynamics. The eastern slopes descending from Zackenberg include a wide range of coarse debris landforms, such as talus cones, proglacial lobes, stone-banked solifluction lobes and blockfields (Cable et al., 2018). The degree of preservation of these landforms is lower on the Aucellabjerg slopes along the eastern flank of the valley, where periglacial dynamics reshape the landscape more intensely through mass-wasting processes, such as solifluction or mudflows. Snow patches here are more abundant due to the local snow drifting, which results in copious meltwater availability during the summer season. The combination of high moisture supply, thin active layer and abundant fine-grained sediments favours widespread downslope mass movements (Cable et al., 2018). In some cases, debris flows and nivation activity also mobilize large amounts of sediment downslope and generate large alluvial fans extending down to the main valley floor.

2.2. The glacial geomorphology and previous chronological knowledge in the Zackenberg area

Glacial evidence in the Zackenberg area is distributed from mountain plateaus to valley floors and has been described in detail in previous studies (Christiansen and Humlum, 1993; Cable et al., 2018). However, despite the widespread, highly detailed geomorphological mapping of glacial features (moraines, erratic boulders and glacial polished surfaces) (Cable et al., 2018), the chronology of the different glacial phases is not yet constrained.

The existence of erratic boulders on the highest parts of Aucellabjerg and the Zackenberg mountains is indicative of a larger GrIS extent in the past, and of the minimum ice thickness during Quaternary glacial periods, when ice extended far onto the shelf (Bennike et al., 2008). In addition, the Zackenberg Valley includes unsorted glacial sediments (till) and several discrete landforms in the form of moraine complexes on the mountain slopes, and in the valley bottom. These landforms indicate phases with larger glaciers than today and other periods of glacial stabilization within the long-term deglaciation trend (Christiansen and Humlum, 1993). In addition, ice-moulded bedrock surfaces between the moraine ridges on the valley bottom also show clear traces of glacial abrasion, including striae in some cases, thus indicating warm/wet-based ice at some point in the past.

The likely oldest glacial evidence in the area are glacio-lacustrine deposits distributed on the lower western slope of Aucellabjerg (Fig. 3), dated by optically stimulated luminescence (OSL) between 84 ± 8 and 114 ± 11 ka, suggesting that during that time part of the Zackenberg Valley was ice-free and probably filled with an ice-dammed lake (Christiansen et al., 2002). Ice-free conditions were also reported from a pronival basin at 600 m in the Favorit Valley at Zackenberg Mountain, where a thermoluminescence date yielded an age of 66.2 ± 7 ka, thus confirming the absence of glaciers in the upper part of the valley during part of the last glacial cycle (Christiansen, 1994). OSL-dated glaciofluvial deposits indicate that the deglaciation of the lower Zackenberg Valley occurred after 22 ± 3 ka (Christiansen et al., 2002). Based on the distribution of glacial and periglacial landforms, Christiansen and Humlum (1993) proposed a tentative deglaciation chronology in several stages: (i) large outlet valley glaciers from the GrIS covering the Zackenberg area until 10–9.5 ka; (ii) inland retreat of glaciers and formation of a terminal moraine at ca. 9 ka; (iii) a period of readvance at ca. 8 ka as indicated by moraine ridges 1.5 km north of this moraine system. More recently, based on the fjord-valley fill, including sedimentary deltaic sequences and OSL ages, Gilbert et al. (2017) suggested that the Zackenberg lowlands may have been ice free as early as 13–11 ka, with the initial formation of the Zackenberg

Delta in the lowest part of the valley taking place at ~10 ka after the major deglaciation of the valley. Christiansen et al. (2002) also reported ^{14}C dates suggesting that the development of the delta continued actively through the Early-Mid Holocene until 6.3 ka. These dates result from radiocarbon dating of organic fragments reflecting a minimum age after first establishment of soils or vegetation (including an unknown lag time behind ice-margin retreat) or fluvio-glacial deposits located downstream from the glacier fronts, which must therefore be younger than the OSL dates.

3. Methodology

We assembled a geomorphological and geochronological approach in order to reconstruct the chronology of glacial oscillations of Zackenberg Valley and their interaction with paraglacial activity during the last stages of the valley's deglaciation. Fieldwork was carried out during late July and early August 2018, when the snow-free landscape allowed the identification of geomorphological features.

3.1. Geomorphological survey and mapping

Before fieldwork, we created a preliminary geomorphological map based on studies of satellite imagery, and adapting the existing cartography conducted by Cable et al. (2018) that identified the main glacial, periglacial, fluvial, and alluvial landforms in the Zackenberg area. Our main target in the geomorphological mapping was the spatial distribution of major glacial and paraglacial landforms, to understand the coupling of glacial, periglacial and paraglacial processes in newly exposed terrain and to optimize the sampling strategy for CRE dating. Considering this, we adapted the previous work with the focus on those

landforms, mapping more precisely the location of the moraine ridges (hummocky and lateral), polished surfaces, and main erratic boulders (Fig. 3). Other landforms (as alluvial fans and fluvial deposits), which had less significance for our study, were simplified and broadly represented. Once in the field, we validated this map based on in situ observations that also allowed us to trace an overall picture of the deglaciation and the importance of paraglacial dynamics shaping the current landscape of the Zackenberg area. The final geomorphological map was drawn by digitizing landforms in the ArcMap 10.4.1 work environment over orthorectified panchromatic satellite WorldView-3 (0.3 m resolution) imagery from 2019. Our observations were also supported on the visual inspection of the shaded relief derived from the Digital Elevation Model (8 m resolution) provided by the GEUS (Geological Survey of Denmark and Greenland) and applied with transparency in our final map (Fig. 3).

3.2. CRE dating and field strategy

Based on the geomorphological map and field evidence, we collected 39 samples for CRE dating using ^{10}Be from sites judged to hold the best potential for glacial and paraglacial reconstruction, considering the complex coupling between deglaciation and paraglacial dynamics. Samples were obtained from depositional and erosional glacial landforms across the Zackenberg area (Fig. 2). They were acquired from three types of glacial surfaces: boulders from well-defined moraine ridges on mountain slopes and the valley floor (29 samples), scattered erratic boulders distributed across the landscape and well-inserted in the ground (6 samples), and exposed bedrock surfaces polished by glacial ice (4 samples) (Fig. 2). Field data and sample characteristics are listed in Table 1.

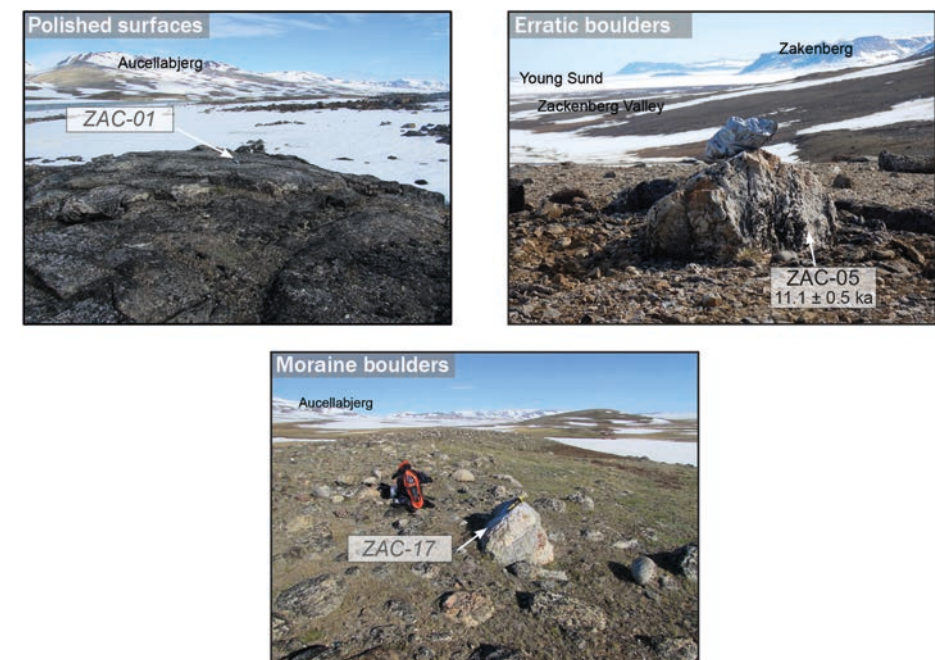


Fig. 2. Different types of glacial landforms sampled in this study: exposed polished bedrock surfaces, erratic boulders and moraine boulders.

Table 1
Sample locations, topographic shielding factor and sample thickness.

Sample ID	Landform	Latitude (DD)	Longitude (DD)	Elevation (m a.s.l.)	Topographic shielding factor (dimensionless)	Thickness (cm)
Valley bottom_Upstream hummocky terrain						
ZAC-01	Polished surface	74.5113	-20.6816	132	0.9911	3
ZAC-03	Erratic boulder	74.5103	-20.6803	137	0.9921	2
Slopes_Zakenberg/Lindemansdal valley divide						
ZAC-05	Erratic boulder	74.5403	-20.6710	201	0.9935	4.5
ZAC-06	Erratic boulder	74.5405	-20.6711	201	0.9928	2.5
ZAC-07	Polished surface	74.5404	-20.6712	202	0.9942	4
Slopes_W slope Aucellabjerg						
Upper slope (first moraine ridge)						
ZAC-11	Lateral moraine	74.4991	-20.4379	401	0.9994	3.5
ZAC-12	Lateral moraine	74.4991	-20.4379	401	0.9994	3
ZAC-13	Lateral moraine	74.4991	-20.4335	403	0.9994	4
Middle slope (fifth moraine ridge)						
ZAC-14	Lateral moraine	74.4834	-20.4963	105	0.9991	2.8
ZAC-15	Lateral moraine	74.4834	-20.4990	104	0.9991	1.5
Lower slope						
ZAC-16	Lateral moraine	74.4828	-20.5163	64	0.9985	4
ZAC-17	Lateral moraine	74.4828	-20.5145	64	0.9928	2.5
Slopes_E slope Zackenberg						
ZAC-18	Lateral moraine	74.4755	-20.6414	117	0.9918	2.5
ZAC-19	Lateral moraine	74.4783	-20.6298	92	0.9937	2.3
ZAC-20	Lateral moraine	74.4781	-20.6234	80	0.9919	2.5
Slopes_SE slope Dombjerg						
Upper slope (second moraine ridge)						
ZAC-21	Lateral moraine	74.5281	-20.6862	328	0.9964	4
ZAC-22	Lateral moraine	74.5315	-20.6861	328	0.9938	3
ZAC-23	Lateral moraine	74.5282	-20.6864	331	0.9945	3
Middle slope (fifth moraine ridge)						
ZAC-24	Lateral moraine	74.5262	-20.6929	315	0.9920	2
ZAC-25	Lateral moraine	74.5263	-20.6928	315	0.9959	2.5
ZAC-26	Lateral moraine	74.5263	-20.6931	317	0.9958	3.5
Lower slope (seventh moraine ridge)						
ZAC-27	Lateral moraine	74.5236	-20.6965	262	0.8828	4
ZAC-28	Lateral moraine	74.5236	-20.6955	261	0.9959	3
ZAC-29	Lateral moraine	74.5236	-20.6955	262	0.9959	2.5
Valley bottom_Intermediate moraine ridge						
ZAC-30	Hummocky moraine	74.4991	-20.6282	96	0.9958	2.5
ZAC-31	Hummocky moraine	74.4992	-20.6281	96	0.9950	3
ZAC-32	Hummocky moraine	74.5002	-20.6266	100	0.9970	3
ZAC-33	Hummocky moraine	74.5001	-20.6264	102	0.9969	3.5
Valley bottom_Foot rock slope						
ZAC-36	Polished surface	74.4942	-20.6325	105	0.9985	2
ZAC-37	Erratic boulder	74.4919	-20.6255	93	0.9950	3
ZAC-38	Erratic boulder	74.4918	-20.6256	92	0.9950	3.5
Valley bottom_Outermost moraine ridge						
ZAC-39	Terminal hummocky moraine	74.4867	-20.5998	74	0.9989	2.5
ZAC-40	Terminal hummocky moraine	74.4863	-20.5998	76	0.9986	3
B1	Terminal hummocky moraine	74.4848	-20.5849	48	0.9841	3
B2	Terminal hummocky moraine	74.4860	-20.5967	62	0.9734	3
ZAC-01b	Terminal hummocky moraine	74.4869	-20.5797	71	0.9963	3
ZAC-04	Terminal hummocky moraine	74.4842	-20.5944	60	0.9703	3
Mountain plateaus. Aucellabjerg.						
ZAC-A	Erratic boulder	74.5158	-20.4325	851	1.0000	2.5
ZAC-C	Erratic boulder	74.5139	-20.4309	879	0.9996	3

Approximately 1 kg of bulk rock was extracted from each sample surface using a hammer and chisel. Samples were taken from a shallow section of the uppermost rock surface (<4 cm), which was mostly flat-topped. We avoided sampling corners, edges, and steep faces (>20°) to ensure optimal reception of the cosmic ray flux. Moraine boulders were

selected for sampling only if they were deeply anchored in the ground to ensure stability and minimize the risk of boulder collapse. Boulders were situated on the moraine crests and protruding such that they were unlikely to have been covered by sediments since their deposition or subject to unusually thick snow cover during the winter season, to

minimize any related effects on nuclide production. The position (latitude, longitude) and elevation of samples were determined using a hand-held GPS (vertical accuracy ±10 m). Topographic shielding from the surrounding horizon was measured in situ with compass and clinometer.

3.3. Laboratory analytical procedures and exposure age calculation

Sample crushing and sieving were carried out in the "Laboratory of Physical Geography" at the Universidad Complutense de Madrid, Spain, to isolate the 0.25–1 mm fraction. Further physical and chemical sample preparation was carried out at the "Laboratoire National des Nucleides Cosmogéniques" (LN₂C) of the Centre Européen de Recherche et d'Enseignement des Géosciences de l'Environnement (CEREGE, Aix-en-Provence, France). First, magnetic grains were discarded using a Frantz LB-2 magnetic separator. Quartz was concentrated in the non-magnetic fraction through repeated acid leaching with a 1:2 mixture of concentrated hydrochloric (HCl) and hexafluorosilicic (H₂SiF₆) acids. Potential contamination by atmospheric ¹⁰Be was removed from the separated quartz by performing 4 rounds of partial dissolution with concentrated hydrofluoric acid (HF). This process also removed the remaining impurities not dissolved in the previous steps.

After adding ~150 µL of a ⁹Be carrier solution to each sample ("spike", concentration: 3025 ± 9 µg g⁻¹; Merchel et al., 2008), the quartz samples were completely dissolved in 48% HF solution (3.6 mL g⁻¹ quartz + 30 mL in excess). The solution was evaporated until dryness on hot plates, and the dry residues were recovered with hydrochloric acid. Following that, beryllium was precipitated to beryllium hydroxide (Be(OH)₂) with ammonia (NH₃) until the supernatant solution pH was 8. Afterward, samples underwent successive separations through anion and cation exchange resin columns to remove first iron and other metals and then boron (Dowex 1 × 8 and 50WX8, respectively) (Merchel and Herpers, 1999). The resulting eluted Be was precipitated to Be(OH)₂ by adding several drops of ammonia, and after being washed and dissolved again in concentrated HNO₃, the solution was evaporated in a quartz crucible, and the residue was oxidized to BeO at 700 °C. Finally, the Be targets were prepared as a 1:1 mixture of niobium (Nb) powder and BeO for Accelerator Mass Spectrometer (AMS) measurements.

The measurements of the ¹⁰Be/⁹Be ratios on the BeO targets were performed at the French 5 MV "Accélérateur pour les Sciences de la Terre, Environnement et Risques" (ASTER) national facility at CEREGE using ion source 2, and ¹⁰Be concentration in the samples was inferred from them. The ¹⁰Be measurements were calibrated against the in-house standard "STD-11", with an assigned ¹⁰Be/⁹Be ratio of (1.191 ± 0.013) × 10⁻¹¹ (Braucher et al., 2015). A ¹⁰Be half-life of (1.387 ± 0.0012) × 10⁶ years was used (Chmieleff et al., 2010; Korschinek et al., 2010). The analytical 1σ uncertainties in the ¹⁰Be/⁹Be ratios include those in AMS counting statistics, the standard ¹⁰Be/⁹Be ratio and an external AMS error of 0.5% (Arnold et al., 2010). The analytical 1σ uncertainties in the inferred ¹⁰Be concentrations include the propagation of the chemical blank correction. Some samples yielded limited ¹⁰Be counting statistics and thus low precisions (~6–8% or more) due to unstable and/or low ⁹Be currents (<1 µA), which can arise either from impurities in the BeO targets or small sizes of the BeO targets. Most samples with low-current AMS ¹⁰Be/⁹Be measurements yielded relatively high uncertainties, and were therefore considered chemical outliers (i.e., ZAC-01, ZAC-16, ZAC-17, ZAC-18, ZAC-22, ZAC-39, and ZAC-40). Such samples were discarded for further exposure age calculations and discussion. For ZAC-C, while bad current values were recorded during the AMS measurement, the sample still provided a good accuracy measurement, and it was therefore retained for the geochronological discussion. All analytical data is shown in Table 2.

Exposure ages were calculated with version 3.0 of the CRONUS-Earth online calculator (Balco et al., 2008; https://hess.ess.washington.edu/). After a bibliographic review of ¹⁰Be-based glacial chronologies in the nearby areas, we applied the same production rates and parameters used in recent publications in order to unify criteria and make our exposure age calculations comparable. Therefore, we used the Arctic-wide sea-level/high-latitude ¹⁰Be production rate (3.96 ± 0.15 atoms g⁻¹ a⁻¹) (Young et al., 2013) and the "Lm" (Lal/Stone) time-dependent scaling model (Lal, 1991; Stone, 2000) (Table 2). For all samples, a 2.7 g cm⁻³ density was assumed, and no corrections of erosion or snow shielding were applied, and thus, exposure ages are reported for zero-erosion and snow-free scenarios. The partial shielding effect of the surrounding topography was corrected for all sampling sites using the "Topographic Shielding Calculator v.2" (http://stoneage.ice-d.org/math/skyline/skyline_in.html). Post-glacial glacio-isostatic rebound (40 m in the last 9.5 kyr; (Christiansen et al., 2002)) was not considered in exposure age calculations, as the resulting age offset represents only ~7% (older) in Greenland (Jones et al., 2019), which does not affect our conclusions.

Exposure ages are given in Table 2 with their internal (only analytical) and external 1σ uncertainties (including production rate uncertainty). In the text and figures, ages are given with their internal uncertainties unless otherwise stated. A chi-squared test (following Ward and Wilson, 1978) considering the analytical uncertainties was applied to different sample populations (e.g. within single moraine ridges, debris-covered glacier deposits, etc.) to identify potential outliers based on statistical criteria. Age outliers (i.e. too old and too young ages; Heyman et al., 2011) may arise from nuclide concentrations inherited from previous exposure periods or post-depositional processes (erosion, exhumation, rock falls etc.). When age outliers were detected, such ages were excluded from the mean age calculations for the corresponding geomorphological units (e.g., moraine ridges). Although these outliers cannot be used for paleoclimate or paleoglacial inferences, they are indicative of the complexity of using CRE dating in these highly dynamic glacial-paraglacial-periglacial environments. The mean ages were calculated arithmetically, and their uncertainties include the standard deviations of the single ages (not excluded) and the squared production rate uncertainties.

4. Results

The distribution of geomorphological landforms across the landscape is indicative of the different phases that occurred during the deglaciation in the Zackenberg Valley (Fig. 3), which are chronologically constrained by ¹⁰Be CRE ages inferred from the glacial record (Table 2).

4.1. Geomorphological setting and sampling strategy

Based on the spatial distribution of glacial, paraglacial and periglacial landforms, we identified three main sectors in the study area:

1. Mountain plateaus

The bedrock is mostly exposed above 400–600 m a.s.l. on the mountain plateaus. Glacio-nival cirques, nivation hollows and perennial snow patches are also found near the mountain tops and upper slopes. The summit surfaces (e.g., Aucellabjerg and Zackenberg mountain plateaus) include geomorphic evidence of past glaciations in the form of large erratic granite boulders distributed across the currently ice-free periglacial landscape. Two of these, well-anchored in the relatively flat area composed of sedimentary rocks of the highest slopes of Aucellabjerg, were sampled for CRE dating (ZAC-A and ZAC-C) in order to infer the onset of glacial thinning. The relatively rounded edges of these boulders (Fig. 4) provide evidence that they were transported for long distances, which diminish the potential of nuclide inheritance.

Table 2
AMS analytical data and calculated exposure ages. ¹⁰Be/⁹Be ratios were inferred from measurements at the ASTER AMS facility. No correction of erosion and snow cover have been made.

¹⁰ Be samples analytical AMS data								
Sample name	Quartz weight (g)	Mass of carrier (⁹ Be mg)	¹⁰ Be/ ⁹ Be (10 ⁻¹⁴)	Blank correction (%)	[¹⁰ Be] (10 ⁴ atoms g ⁻¹ ± 1σ (atoms g ⁻¹))	¹⁰ Be age (ka) ^a	External uncertainty (ka)	Internal uncertainty (ka)
Valley bottom_Upstream hummocky terrain								
Polished surfaces								
ZAC-01**	13.2823	0.46334	3.32 ± 0.398	3.85	7.441 ± 0.931			
Erratic boulder								
ZAC-03	6.7743	0.46373	1.33 ± 0.101	9.60	5.501 ± 0.483	11.7	1.1	1.0
Slopes_Zacken/Lindemansdal valley divide								
Polished surfaces - arithmetic mean age: 10.3 ± 1.3 ka (n = 2) -								
ZAC-05	21.0677	0.46037	3.835 ± 0.162	2.62	5.454 ± 0.239	11.1	0.6	0.5
ZAC-06	20.4927	0.45100	3.297 ± 0.164	3.11	4.698 ± 0.244	9.4	0.6	0.5
Erratic boulder								
ZAC-07	20.1072	0.45227	3.478 ± 0.168	2.94	5.073 ± 0.254	10.2	0.6	0.5
Slopes_W slope Aucellabjerg								
Upper slope (first moraine ridge) - arithmetic mean age: 12.5 ± 1.5 ka (n = 2) -								
ZAC-11*	20.2778	0.45950	10.695 ± 0.344	0.94	16.042 ± 0.522	26.2	1.3	0.9
ZAC-12	20.3521	0.45771	4.859 ± 0.187	2.66	7.108 ± 0.284	11.5	0.6	0.5
ZAC-13	20.8217	0.46119	5.651 ± 0.212	1.77	8.215 ± 0.316	13.4	0.7	0.5
Middle slope (fifth moraine ridge) - arithmetic mean age: 14.1 ± 1.7 ka (n = 2) -								
ZAC-14*	20.1386	0.44912	4.725 ± 0.318	2.79	6.844 ± 0.476	15.1	1.2	1.0
ZAC-15*	21.0148	0.44900	4.45 ± 0.175	2.97	6.165 ± 0.254	13.1	0.7	0.6
Lower slope								
ZAC-16**	17.1192	0.45983	8.554 ± 0.535	1.51	15.122 ± 0.961			
ZAC-17**	21.9894	0.45868	3.959 ± 1.024	3.26	5.338 ± 1.427			
Slopes_E slope Zackenberg - arithmetic mean age: 12.3 ± 0.8 ka (n = 2) -								
ZAC-18**	21.9225	0.46812	2.516 ± 0.269	5.03	3.409 ± 0.387			
ZAC-19	20.3459	0.46509	3.631 ± 0.176	2.74	5.394 ± 0.27	12.1	0.7	0.6
ZAC-20	21.1584	0.46388	3.814 ± 0.191	2.61	5.442 ± 0.282	12.4	0.8	0.6
Slopes_SE slope Dombjerg								
Upper slope (second moraine ridge) - arithmetic mean age: 13.7 ± 1.1 ka (n = 2) -								
ZAC-21	20.0893	0.45018	5.495 ± 0.33	2.40	8.032 ± 0.496	14.2	1.0	0.9
ZAC-22**	11.8193	0.45423	3.852 ± 0.309	3.39	9.558 ± 0.796			
ZAC-23	12.0595	0.45762	3.109 ± 0.141	4.16	7.555 ± 0.366	13.2	0.8	0.4
Middle slope (fifth moraine ridge) - arithmetic mean age: 11.6 ± 0.8 ka (n = 3) -								
ZAC-24	19.3469	0.45777	4.303 ± 0.194	3.01	6.599 ± 0.311	11.6	0.7	0.6
ZAC-25	21.6432	0.45732	4.728 ± 0.358	2.74	6.492 ± 0.508	11.5	1.0	0.9
ZAC-26	16.3057	0.45284	3.685 ± 0.14	3.55	6.596 ± 0.267	11.7	0.6	0.5
Lower slope (seventh moraine ridge) - arithmetic mean age: 11.3 ± 1.1 ka (n = 2) -								
ZAC-27*	5.4422	0.44912	1.326 ± 0.097	9.95	6.583 ± 0.562	14.0	1.3	1.2
ZAC-28	12.2737	0.45299	2.69 ± 0.147	4.86	6.313 ± 0.371	11.8	0.8	0.7
ZAC-29	20.6231	0.45003	4.081 ± 0.191	3.23	5.759 ± 0.282	10.7	0.7	0.5
Valley bottom_Intermediate moraine ridge - arithmetic mean age: 12.6 ± 2.2 ka (n = 3) -								
ZAC-30*	20.321	0.44685	5.327 ± 0.207	1.94	7.675 ± 0.306	17.2	0.9	0.7
ZAC-31	21.9112	0.46113	4.7 ± 0.192	2.73	6.429 ± 0.273	14.4	0.8	0.6
ZAC-32	21.5385	0.46162	4.246 ± 0.236	2.36	5.937 ± 0.34	13.2	0.9	0.8
ZAC-33	20.1907	0.46025	3.13 ± 0.155	3.21	4.615 ± 0.238	10.3	0.6	0.5
Valley bottom_Foot rock slope								
Polished surface								
ZAC-36	20.5615	0.45717	3.396 ± 0.148	2.98	4.895 ± 0.222	10.7	0.6	0.5
Erratic boulders - arithmetic mean age: 10.4 ± 0.7 ka (n = 2) -								
ZAC-37	21.2378	0.45378	3.283 ± 0.163	3.11	4.541 ± 0.235	10.2	0.6	0.5
ZAC-38	21.9112	0.44673	2.902 ± 0.137	4.57	4.675 ± 0.237	10.6	0.7	0.5
Valley bottom_Outmost moraine ridge - arithmetic mean age: 11.2 ± 1.1 ka (n = 4) -								
ZAC-39**	20.414	0.45351	4.316 ± 0.412	2.36	6.256 ± 0.612			
ZAC-40**	20.233	0.45242	3.907 ± 0.535	2.62	5.684 ± 0.799			
B1	18.746	0.4592	3.05 ± 0.145	4.77	4.24 ± 0.202.1	10.2	0.6	0.5
B2	29.7642	0.4443	540.722 ± 0.209	3.86	4.936 ± 0.191	11.8	0.6	0.5
ZAC-01b	11.1618	0.319444	301.219 ± 0.215	7.12	4.787 ± 0.341	11.0	0.9	0.8
ZAC-04	8.396	0.313046	329.095 ± 0.558	16.95	4.948 ± 0.28	11.9	0.8	0.7
Mountain plateaus. Aucellabjerg.								
ZAC-A	20.7965	0.46488	49.537 ± 1.722	0.26	73.805 ± 2.573	78.8	4.1	2.8
ZAC-C	21.5997	0.44942	32.324 ± 1.669	0.41	44.759 ± 2.32	50.3	3.2	2.6

Chemistry blank details ^b			
Blank name	mass of carrier (⁹ Be mg)	¹⁰ Be/ ⁹ Be (10 ⁻¹⁴)	[¹⁰ Be] (10 ⁴ atoms)
BK1	0.44410	13,341.7 ± 0.032	3.96 ± 0.935
BK2	0.46201	10,012.5 ± 0.021	3.09 ± 0.662
BK3	0.4648	45,938.4 ± 0	0.013 ± 10.775
BK4	0.31932	50,940.4 ± 0	0.001 ± 45.679

The outliers are highlighted in italics: samples rejected by the Chi² test or geochronological inconsistent*, and those with low precision AMS measurements**. See methods and results text for more explanation.

^a ¹⁰Be ages assuming a density of 2.7 g cm⁻³ and a zero-erosion scenario.

^b In parallel to the sample treatment, four blanks were prepared: BK1 (processed with samples: ZAC-A, ZAC-C, ZA0-01, ZAC-03, ZAC-12, ZAC-31, ZAC-38, ZAC-14 to ZAC-18 and from ZAC-21 to ZAC-29), BK2 (processed with samples ZAC-05, ZAC-06, ZAC-07, ZAC-11, ZAC-13, ZAC-19, ZAC-20, ZAC-30, ZAC-32, ZAC-33, ZAC-36, ZAC-37, ZAC-39, ZAC-40), BK3 (processed with samples B1 and B2) and BK4 (processed with samples ZAC01 and ZAC04).

2. Mountain slopes

Discontinuous lateral moraine ridges were found on the slopes surrounding the Zackenberg Valley at varying elevations, recording the thickness and geometry of the glacier during past glacial phases (Fig. 3). The limit of the highest remnants of moraine deposits ranges ~200 and 550 m a.s.l. on the western slope of Aucellabjerg (Christiansen and Humlum, 1993), ~200 and 800 m a.s.l. on the southeast slope of Dombjerg, and between ~400 and 200 m a.s.l. on the eastern slope of Zackenberg on the western side of the main valley.

Nine roughly preserved lateral moraines were identified on the western slopes of Aucellabjerg, counting up to twelve discontinuous ridges distributed at elevations between ca. 60 and 400 m a.s.l. Very active periglacial slope processes have dismantled most of the moraine ridges on this slope through widespread nivation activity with debris flows, mudflows and solifluction processes (Cable et al., 2018); remnants of these moraines are found only on mid-low slopes in the form of discontinuous crests. Whereas the moraines at higher elevations are mostly made of fine sediments, the lower, more recent ridges have a greater abundance of large conglomerate and sandstone boulders of these materials. We collected seven samples from orthogneiss moraine boulders distributed across the prevailing sandstone bedrock, from the upper (403 m a.s.l.) to the lowest sector (64 m a.s.l.) of the Aucellabjerg slope (ZAC-11, ZAC-12, ZAC-13, ZAC-14, ZAC-15, ZAC-16, and ZAC-17) to reconstruct past phases representative of stillstand positions of the glacier within its long-term thinning and retreat.

On the eastern slope of Zackenberg, intense frost shattering has favoured rockfall activity, with the development of protalus lobes and talus cones that have dismantled the moraines located at the foot of the rock wall and partially covered the exposed glacially polished bedrock surfaces. Up to four lateral moraines were identified in this area, which descend gradually towards the bottom of Zackenberg Valley (Fig. 3). Three samples were taken from intermediate moraine ridges in this unit, distributed between 80 and 120 m a.s.l. (ZAC-18, ZAC-19, and ZAC-20) (Fig. 3).

In the northern part of the Zackenberg Valley, several orthogneiss boulders are distributed on a heavily weathered rocky sandstone threshold that also constitutes the watershed divide between the Zackenberg and Lindemansdal valleys. Two of these erratic boulders (ZAC-05 and ZAC-06) and the bedrock surface (ZAC-07) were sampled (Fig. 3).

Moraines are specially well-preserved in the northern part of the Zackenberg Valley on the southeast slope of Dombjerg mountain, where eleven fragments of moraine ridges ranging from ~150 to 400 m a.s.l. gradually curve and slope towards the east, particularly the middle and highest ridges (Fig. 3). The intermediate and lower moraine ridges are discontinuous and highly eroded by alluvial processes, with dispersed till across the valley bottom. We collected nine samples from the upper (330 m a.s.l.) to the intermediate moraines (260 m a.s.l.) (ZAC-21 to ZAC-29) (Fig. 3).

3. Valley floor

The base of Zackenberg Valley contains two very different geomorphic settings according to the glacial evidence. The upper part of the valley includes widespread glacial landforms including a well-defined frontal moraine system with internal hummocky terrain derived from thermokarst processes and is the site of several lakes. We collected six samples from the frontal moraine (ZAC-39, ZAC-40, B1, B2, ZAC-01b, and ZAC-04) (Fig. 3) and four more from an internal moraine ridge (ZAC-30 to ZAC-33) that dams two of these lakes. The hummocky terrain only defines a clear frontal ridge occupying the valley floor, but there are no clear recessional moraines composed of transverse moraine ridges, as observed in the field. This area is composed of randomly distributed hummocks, mounds with lakes in between, and is dissected by inactive river channels. On the surface of the hummocky terrain, there are abundant angular to subangular boulders, with the presence of few slightly rounded blocks. Some exposed polished bedrock surfaces are located between the discontinuous lateral moraine remnants in the western side of the valley that have been removed by rock falls from the steep rock walls. These polished surfaces were sampled (ZAC-01 and ZAC-36), as were several erratic boulders distributed on them (ZAC-03, ZAC-37 and ZAC-38) (Fig. 3). The lowest section of the valley extends ca. 3 km inland from the present-day coastline and comprises relatively flat ground moraine areas shaped by glacio-isostatic processes, delta sedimentation and nivation activity (Cable et al., 2018; Christiansen, 1998). Here, several metre-size erratic boulders are scattered across the landscape, partially covered by aeolian, delta and glaciomarine sediments.

4.2. Exposure ages

The samples collected from the three principal geomorphological settings yielded ages ranging from 78.8 ± 2.8 (ZAC-A) to 9.4 ± 0.5 ka (ZAC-06). Here we present the results ordered from the mountain plateaus down to the valley bottoms:

1. Mountain plateaus

Two large erratic boulders of granite found on the highest surfaces of Aucellabjerg (above 800 m a.s.l.) yielded ¹⁰Be exposure ages of 78.8 ± 2.8 (ZAC-A) and 50.3 ± 2.6 ka (ZAC-C), respectively (Fig. 4, Table 2).

2. Mountain slopes

Two boulders sampled from the upper slope (first moraine ridge) (at ~400 m a.s.l.) on the western flank of Aucellabjerg were consistent with each other, with ages of 11.5 ± 0.5 (ZAC-12) and 13.4 ± 0.5 ka (ZAC-13), giving a mean age of 12.5 ± 1.5 ka (n = 2). A third yielding (26.2 ± 0.9 ka; ZAC-11) (Fig. 5A), was identified as a potential outlier according to the chi-squared test and excluded. Two large boulders from the middle slope (fifth moraine ridge) (at ~100 m a.s.l.) returned ages of 15.1 ± 1.0 ka (ZAC-14) and 13.1 ± 0.6 ka (ZAC-15), with an average age of 14.1 ± 1.7 ka (n = 2), (Fig. 5B).

J. García-Oteyza, M. Oliva, D. Palacios et al.

Geomorphology 401 (2022) 108125

J. García-Oteyza, M. Oliva, D. Palacios et al.

Geomorphology 401 (2022) 108125

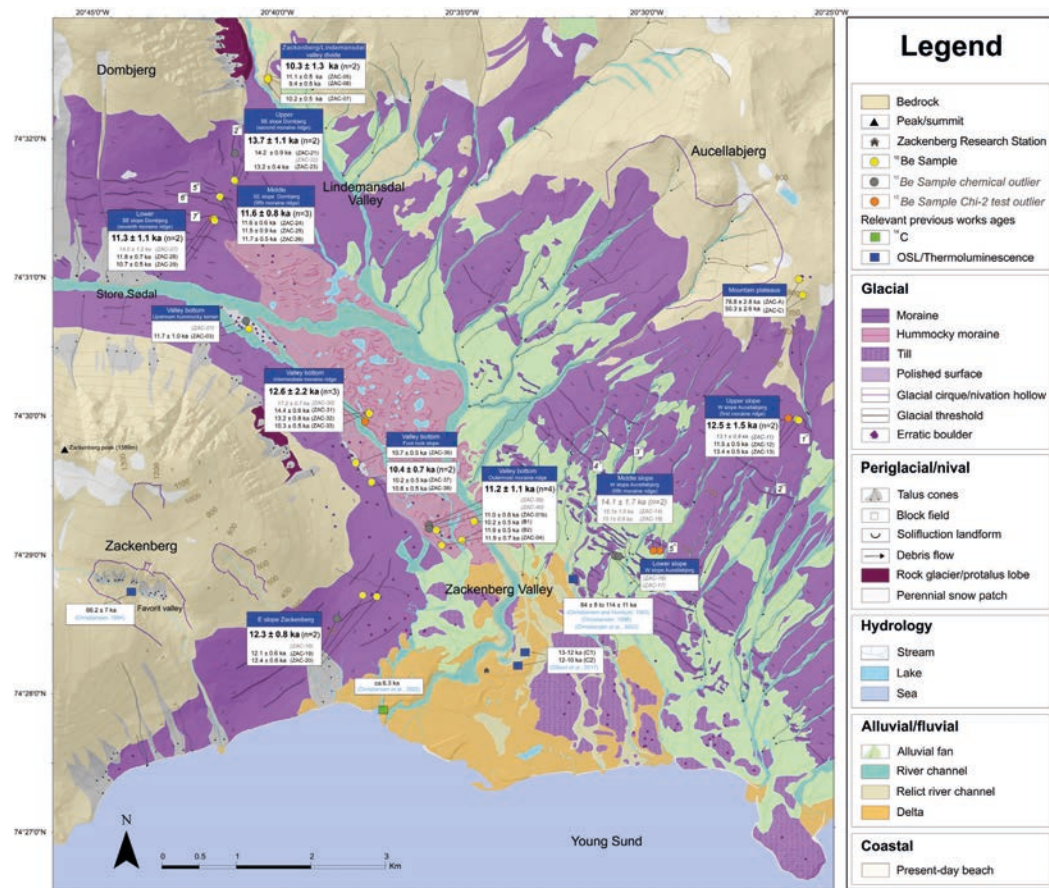


Fig. 3. Geomorphological map (modified from Cable et al., 2018), including the main glacial and periglacial landforms relevant to our study together with the CRE results shown in Tables 1 and 2 as well as the relevant ages from previous works. In the purple areas termed 'moraine', the solid line indicates the crest of individual moraine ridges; the solifluction symbol indicates that this area consists of till affected by postglacial solifluction.



Fig. 5. Dated boulders from different moraine systems surrounding the Zackenberg Valley floor. See Fig. 3 for the location of the samples shown in the photographs.

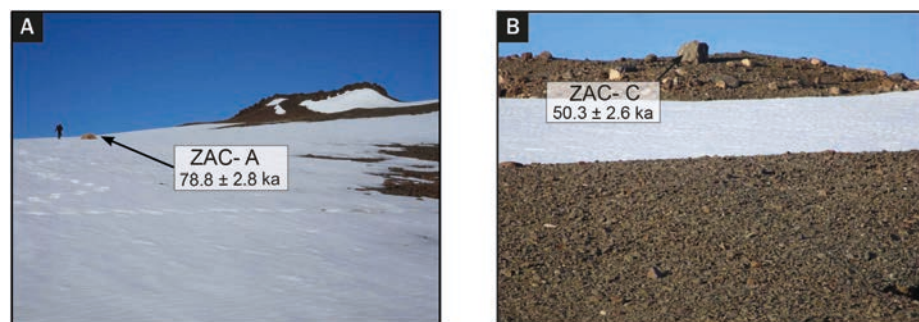


Fig. 4. Glacial erratic boulders deposited during MIS-5a on the Auccellabjerg plateau: samples (A) ZAC-A (length = 2.2 m; height = 1 m); and (B) ZAC-C (length = 3.1 m, height = 1.1 m).

Samples from two boulders located on the lowest moraine ridge (between 80 and 120 m a.s.l.) of the eastern slope of Zackenberg show consistent ages of 12.1 ± 0.6 (ZAC-19) and 12.4 ± 0.6 ka (ZAC-20), with a mean age of 12.3 ± 0.8 ka ($n = 2$) (Fig. 5C).

On the northern fringe of Zackenberg Valley, in the pass dividing the northern and southern sides of the Wollaston Foreland peninsula, the three samples (Fig. 6C), all around 200 m a.s.l. include two erratic boulders that yielded ages of 11.1 ± 0.5 (ZAC-05) and 9.4 ± 0.5 ka (ZAC-06) with a mean age of 10.3 ± 1.3 ka ($n = 2$), and another from polished bedrock that was dated at 10.2 ± 0.5 ka (ZAC-07).

On the south-eastern slope of Dombjerg, three boulders from the upper slope (second moraine ridge) (at ~330 m a.s.l.) that constitutes the largest moraine returned exposure ages of 14.2 ± 0.9 (ZAC-21) and 13.2 ± 0.4 (ZAC-23) with a mean age of 13.7 ± 1.1 ka ($n = 2$) (Fig. 5G). Three samples (ZAC-24, 25, and 26) from the middle slope (fifth moraine ridge) (at ~315 m a.s.l.) were collected in a relatively horizontal area yielded ages of 11.6 ± 0.6 (ZAC-24), 11.5 ± 0.9 (ZAC-25) and 11.7 ± 0.5 ka (ZAC-26) with a mean age of 11.6 ± 0.8 ka ($n = 3$). Finally, on the lower slope (seventh moraine ridge) (at ~260 m a.s.l.), three samples from the most stable area yielded exposure ages of 14.0 ± 1.2 (ZAC-27), 11.8 ± 0.7 ka (ZAC-28) and 10.7 ± 0.5 ka (ZAC-29) with a mean age of 11.3 ± 1.1 ka ($n = 2$). ZAC-27 is statistically inconsistent with the other samples likely due to nuclide inheritance, and therefore considered as a potential outlier and excluded for mean age calculation.

3. Valley bottom

- From the outermost moraine ridge in the central part of the valley (Fig. 3), four samples ranging from 48 to 71 m a.s.l., returned

exposure ages of 10.2 ± 0.5 (B1), 11.8 ± 0.5 (B2), 11.0 ± 0.8 (ZAC-01b), and 11.9 ± 0.7 ka (ZAC-04) with a mean age of 11.2 ± 1.1 ka ($n = 4$).

- From the intermediate ridges of the lake-damming hummocky moraine system (at ~100 m a.s.l.), the four samples gave ages of 17.2 ± 0.7 (ZAC-30), 14.4 ± 0.6 (ZAC-31), 13.2 ± 0.8 (ZAC-32) and 10.3 ± 0.5 ka (ZAC-33) with a mean age of 12.6 ± 2.2 ka ($n = 3$), following exclusion of ZAC-30 as a potential outlier according to the chi-squared test. ZAC-30 was located on the westernmost fringe of the deposit, close to the rock wall (~370 m a.s.l.), and may be a fallen block, explaining its significantly older age. It was thus excluded from mean age calculations.
- From a polished bedrock surface at the foot of the rock slope, we obtained one age of 10.7 ± 0.5 ka (ZAC-36) (Fig. 6A) (at 105 m a.s.l.), while two boulders located on the same surface gave exposure ages of 10.2 ± 0.5 ka (ZAC-37) and 10.6 ± 0.5 ka (ZAC-38), with a mean age of 10.4 ± 0.7 ka ($n = 2$) (at ~90 m a.s.l.).

Upstream from the hummocky terrain, an erratic boulder yielded an exposure age of 11.7 ± 1.0 ka (ZAC-03) (at 137 m a.s.l.) (Fig. 6B).

5. Discussion

We complemented the previous detailed mapping of the glacial and periglacial landforms distributed across the Zackenberg Valley (Cable et al., 2018) with ¹⁰Be CRE ages of samples collected from glacial features of the slopes and valley floor. This approach enabled us to generate a detailed space-time reconstruction of deglaciation in the Zackenberg region.



Fig. 6. Dated polished bedrock surfaces indicative of subaerial exposure following glacial retreat. See Fig. 3 for the location of the samples shown in the photographs.

5.1. General considerations on the chronological process of deglaciation

The 32 ¹⁰Be CRE ages from moraines, erratic boulders and exposed polished bedrock surfaces provide a record of glacial oscillations from ca. 80 ka to the Early Holocene (11.7–8.2 ka). Analysis of the exposure ages and their geomorphological setting also reveals that some of them do not apparently follow a logical sequence.

The western slopes of Aucellabjerg (include abundant fine-grained sediments (mostly silts and sands) with frequent gravels), which enhances the remobilization of surface sediments by solifluction dynamics, affecting the stability of boulders and potentially causing them to roll or move (Balco, 2020). Despite sampling boulders that were well-anchored in the ground and formed part of clearly distinguishable moraine ridges (Fig. 5), it is possible that the very active post-depositional slope processes on Aucellabjerg, or even incomplete exposure due to exhumation, may have resulted in underestimated ages in some cases (Figs. 3 and 9). By contrast, older exposure ages than expected may result from nuclide inheritance or downslope mobilization from (previously exposed) upper parts of a slope. This is the case of samples ZAC-14 and ZAC-15, obtained from a moraine ridge in the middle slope of Aucellabjerg, that do not follow a consistent geochronological pattern, as they are much older than the rest of the highest moraines of the valley, and were thus discarded as outliers. However, once these obvious outliers were removed, there is a consistent geochronological sequence that logically matches the geomorphological observations, and from which the overall deglaciation history of this valley can be reconstructed.

5.2. Coupling CRE ages and geomorphological evidence

The highest samples, collected from the summit plateaus, returned the oldest ages. Granitic erratic boulders situated near the summit plateaus demonstrate that the minimum ice thickness in the Zackenberg Valley during their deposition was >800 m. As local plateaus are not composed of granites, we infer that the ice must have flowed from another source, the nearest of which is adjacent to the current margins of the GrlS, ca. 60 km west of the Zackenberg Valley. According to the ages of the highest samples ZAC-A and ZAC-C, this phase may have occurred sometime between ca. 80–50 ka (MIS 4–3). The occurrence of nuclide inheritance is a well-known issue in deglaciated areas throughout the Arctic (i.e. Greenland: Goehring et al., 2010; Søndergaard et al., 2019; Ceperley et al., 2020; the Canadian Arctic: Bierman et al., 1999; Davis et al., 1999; Briner et al., 2003; Kaplan and Miller, 2003), and should not be ruled out, especially in regions of high relief with gentle topography such as those of the study area, which in turn may determine low ice mobility, low erosion rates and consequently the preservation of an inventory of ¹⁰Be accumulated in previous ice-free periods (see Fernández-Fernández et al., 2021). Future studies should combine multiple nuclides (e.g. ²⁶Al, in-situ ¹⁴C) to explore complex exposure histories and shed light on processes such as exhumation and prior exposures.

However, in NE Greenland, erratic boulders transported tens of km from their source – such as the granitic boulders distributed across Aucellabjerg and the Zackenberg mountains – are not generally affected by nuclide inheritance and have provided CRE ages associated with glacial retreat following the last glacial cycle (Håkansson et al., 2007a; Larsen et al., 2018). This is also valid for moraine boulders that do not usually retain an inheritance signal from past deglacial periods (Levy et al., 2016; Biette et al., 2020a, 2020b), with few exceptions (Håkansson et al., 2009). A thermoluminescence measurement from a pronival basin at 600 m a.s.l. on the western slope of Aucellabjerg returned an age of 66.2 ± 7 ka, which may also indicate that the areas at higher elevations were already ice-free by that time (Christiansen, 1994). It is therefore reasonable to consider a scenario of pre-LGM glaciation in the valley, with most of the Zackenberg Valley ice-filled and only some nunataks protruding above the ice field.

The rest of the CRE ages confirm that the deglaciation of the slopes and valley floor occurred during T-1 (Fig. 7). The lateral moraines on the western slopes of Aucellabjerg suggest an age of deglaciation of 12.5 ± 1.5 ka, which is very similar to the exposure ages obtained from the eastern slope of Zackenberg Mountain (12.3 ± 0.8 ka). These ages overlap with the slightly older average age reported from highest ridges on the south-eastern slope of Dombjerg (13.7 ± 1.1 ka; Fig. 7), suggesting that the formation of the highest moraines in the Zackenberg Valley occurred between 13.7 and 12.5 ka.

Slightly younger ages were found on the northern side of the study area in the pass dividing the northern and southern sides of the Wollaston Foreland peninsula. The boulder from which we obtained the older sample ZAC-05 (11.1 ± 0.5 ka) was more weathered than ZAC-06 (9.4 ± 0.5 ka). The average exposure age of both boulders (10.3 ± 1.3 ka) matched that of nearby polished bedrock (ZAC-07; 10.2 ± 0.5 ka). This indicates the end of the glacial transfluence from Store Sødal towards the north of the peninsula at that time, and thus the separation of the Zackenberg and Lindemansdal as independent glaciers within their respective valley floors, leaving an ice-free pass in between.

The moraine systems on the southeast slope of Dombjerg provided a complete sequence of glacial thinning from 13.7 ± 1.1 to 11.3 ± 1.1 ka (~330–260 m a.s.l.). The higher and middle moraines sloping towards the east suggest that the ice was flowing from Store Sødal, whereas the thinner glacier that generated the lowest moraines was still connected with the Lindemansdal glacier until 10.2 ka. Indeed, the age of formation of these lower ridges fits well with an erratic boulder collected on a bedrock surface located just above the hummocky terrain (11.7 ± 1.0 ka) at the west bank of the river, providing further evidence for glacial retreat at the onset of the Holocene.

The frontal ridge revealed the culmination of the last glacial advance, and included rocks deposited between 11.9 ± 0.7 (ZAC-04) and 10.2 ± 0.5 ka (B1). Average exposure ages indicated that the frontal moraine system was deposited around 11.2 ± 1.1 ka, similar to the lowest moraine system on the southeast slope of Dombjerg (11.3 ± 1.1 ka). This suggests that units formed simultaneously, when the glacier generated a well-defined frontal moraine system extending across the valley floor and encircling the southeast slope of Dombjerg.

As the glacier thinned and retreated, the slopes surrounding the valley floor became ice-free, triggering paraglacial processes (Ballantyne, 2008; Oliva et al., 2019). We hypothesise that the debutting of the steep valley walls delivered large deposits, from lateral moraine boulders in most cases, onto the glacier surface. The terminal section of the glacier, already very thin, gradually transformed into a debris-covered glacier (Fig. 8) following a pattern also observed in other mountain systems (Janke et al., 2015; Anderson et al., 2018; Jones et al., 2019; Kenner, 2019; Mayr and Hagg, 2019). This transformation, from debris-free to debris-covered glacier, reduces ablation and even accelerates glacier flow (Hambrey et al., 2008; Deline et al., 2015; Anderson and Anderson, 2016; Anderson et al., 2018; Mayr and Hagg, 2019). Once the glacier stagnated and began to retreat, ice disintegration favoured the existence of dead ice patches, which can persist for millennia particularly in permafrost environments (Fernández-Fernández et al., 2017). This process can affect the stability of glacial sediments and trigger the readjustment of some boulders, resulting in younger exposure ages (Fernández-Fernández et al., 2020). Other boulders, which would have remained stable for millennia on the glacial surface, were continuously exposed to cosmogenic radiation that resulted in ages pre-dating the stabilization of the deposit (Bibby et al., 2016; Mackay and Marchant, 2016; Amschwand et al., 2020). This may explain the average age of the hummocky terrain samples (12.6 ± 2.2 ka; Fig. 3).

The study of the uncertainties associated with CRE dating in debris-covered glaciers is still incipient with no conclusive evidence, and these uncertainties are highly dependent on local geomorphological settings, as has been observed in mountain environments in the Himalaya (Scherler and Egholm, 2020), central Alaska Range (Dortch et al., 2010) and Iberian Range in Spain (Fernández-Fernández et al., 2017),

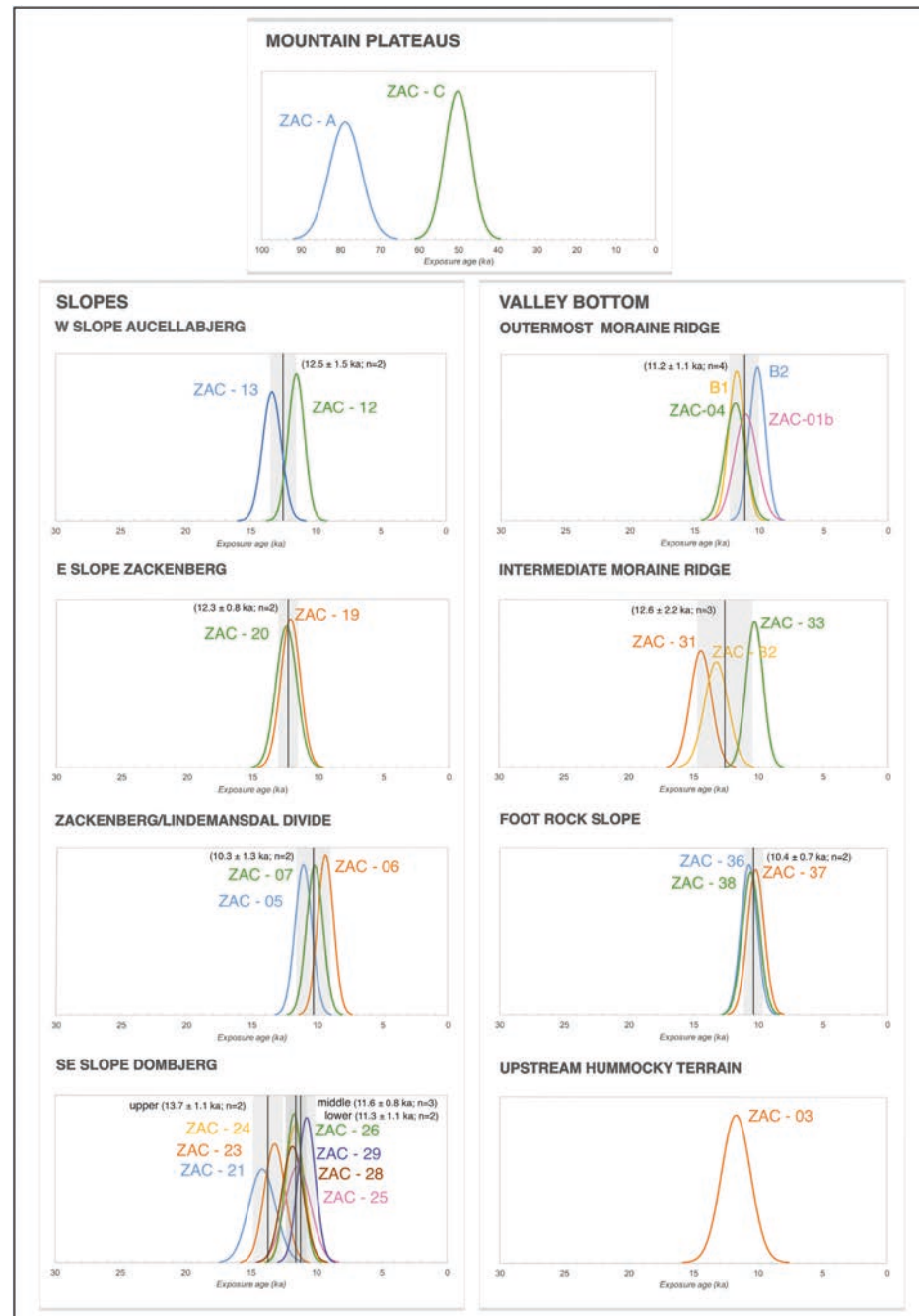


Fig. 7. Probability distribution functions of ¹⁰Be CRE ages (with their internal uncertainties) for the samples from the mountain plateaus, slopes and valley bottom. Black vertical lines indicate the mean ages with full errors.

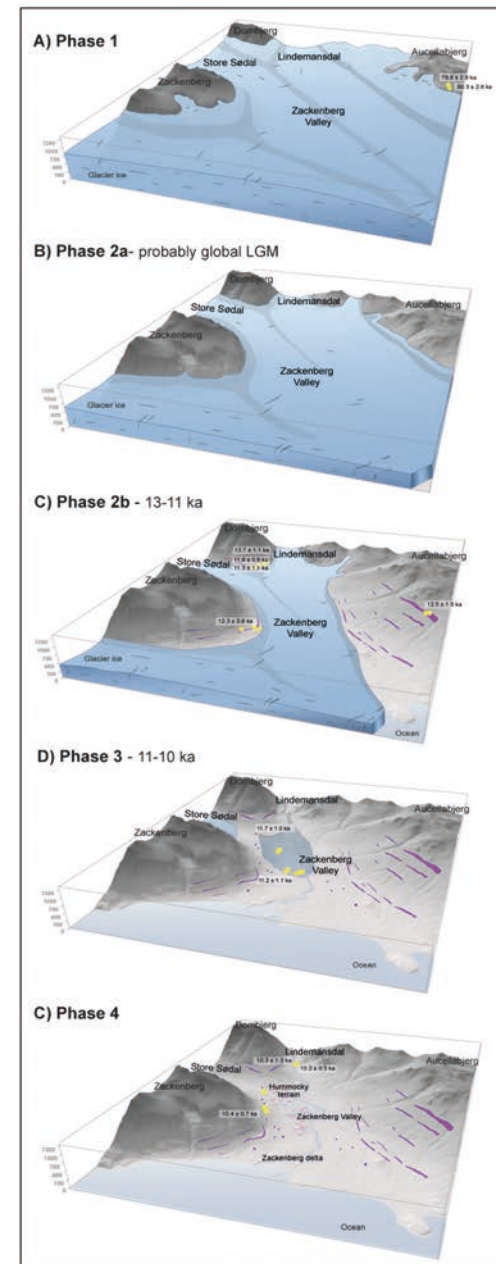


Fig. 8. Idealized reconstruction model for the glacial evolution of Zackenberg Valley (with the base map derived from the current Digital Elevation Model) based on different phases: (1) Near maximum ice extent of the last glacial cycle; (2) Deglaciation of the slopes; 2a- Progressive ice thinning post-LGM; 2b- Formation of moraine systems during the YD; (3) Development of the debris-covered glacier on the Zackenberg Valley floor; and (4) Formation of hummocky terrain.

as well as (sub)polar regions such as in the Kerguelen Archipelago (Charton et al., 2020), Iceland (Tanarro et al., 2021) or in the McMurdo Dry Valleys in Antarctica (Mackay and Marchant, 2016). CRE ages obtained from fossil debris-covered glaciers may not represent the exact time of deglaciation at a specific site, but they may provide wide time-scales ranging between the fall of boulders on the glacier surface and the stabilization after complete melting of the buried ice (Fernández-Fernández et al., 2017). Indeed, ice disappearance may take hundreds or even thousands of years in (almost) static glaciers due to the insulating protection of a thick debris cover (Mackay and Marchant, 2016), and does not necessarily follow a specific spatial pattern, which must be taken into account when interpreting CRE ages from debris-covered glaciers.

Our CRE dates cannot provide further chronological control for climatic changes that led to the formation of the moraines, the withdrawal of the glacier and the stabilization of the hummocky terrain, although the overlapping of the CRE ages within uncertainty ranges suggests that it must have been a rapid process. The application of CRE dating to collapsed debris-covered glaciers must therefore take into account a wide range of possibilities (Charton et al., 2020): (i) fallen boulders from the lateral moraines that may have retained nuclide inheritance (Çiner et al., 2017; Dede et al., 2017) (ii) boulders that overturned during massive melting (Fernández-Fernández et al., 2017); and (iii) boulders that have remained static on the glacier surface and have been continuously exposed to cosmic radiation since their emplacement (Bibby et al., 2016; Mackay and Marchant, 2016; Winkler and Lambiel, 2018; Tanarro et al., 2019; Amschwand et al., 2020; Charton et al., 2020; Fernández-Fernández et al., 2020). Given this diversity of possibilities, it is therefore difficult for a debris-covered glacier to yield rather homogeneous CRE ages after the ice melts. The range of boulder ages within the same geomorphological units must therefore be interpreted in light of the competing processes that control the disintegration of a debris-covered glacier, and its transformation into hummocky terrain. The absence of continuous and clearly aligned ridge crests within the hummocky terrain, together with numerous lakes occupying inter-hummock depressions, supports the interpretation that this hilly terrain formed as a result of stagnation and passive melt-out and not as a consequence of active ice margin retreat (Benn, 1992; Palacios et al., 2021; Rodríguez-Mena et al., 2021; Rodríguez-Mena et al., 2021).

Lastly, the three samples collected from two erratic boulders and a polished surface above the hummocky terrain provided similar results of 10.4 ± 0.7 and 10.7 ± 0.5 ka, respectively. These ages suggest that ice persisted at the foot of the northern slope of Zackenberg almost two more millennia after the valley floor became ice-free (Fig. 3). The most plausible hypothesis is that a slope glacier, fed by the snowdrift and avalanches, persisted at the foot of Zackenberg's shaded northeastern slope at the onset of the Holocene, capable of bedrock erosion on this weathered bedrock. Boulders detached from the rock wall probably slid above the ice mass and accumulated at the base of the slope on the dated exposed polished bedrock when ice had shrunk upslope.

5.3. Deglaciation chronology of the Zackenberg area

Our results provide evidence that the deglaciation of the Zackenberg Valley occurred during the Late Glacial, with the following phases in the environmental evolution of the area:

- Phase 1: Maximum expansion of the glaciers, covering the summits.

Our highest samples indicate that Zackenberg Valley was almost fully filled, likely prior to the LGM of the last glacial cycle at ca. 80–50 ka, and only the highest peaks may have been ice-free (as no erratic boulders have been found across the plateaus) as nunataks that were affected by intense periglacial conditions (Christiansen et al., 2002; Fig. 8A). At that time, the Zackenberg glacier was one of the

J. García-Oteyza, M. Oliva, D. Palacios et al.

Geomorphology 401 (2022) 108125

outlets of the GrIS, and merged with the Tyrolerfjord glacier, another outlet of the GrIS, flowing east towards Young Sund (Christiansen and Humlum, 1993). However, previous research has provided evidence that the GrIS also advanced to the shelf edge during the LGM and probably covered some of the high plateaus in NE Greenland (Håkansson et al., 2007b; Skov et al., 2020). We cannot fully discard that our dated samples may retain some nuclide inheritance, masking a last glacial cycle glacial advance covering most of the Zackenberg Valley.

- Phase 2: Onset of deglaciation of the debris-free glacier.

In NE Greenland, a rapid deglaciation process began after the deglaciation after the global LGM (Clark et al., 2009). The loss of glacier thickness in the Zackenberg Valley occurred parallel to the retreat of the Tyrolerfjord glacier (Fig. 1). As a result, a sequence of recessional moraines formed at different elevations. No robust evidence of LGM or early T-1 moraine deposition has been found, although it is possible that the highest ridges that may have formed during the LGM advance, and the remnants of some moraines were subsequently dismantled due to the very intense slope processes. The long-term recession of the GrIS and surrounding glaciers was interrupted by periods of glacial stillstand/advance of the Zackenberg valley glacier that favoured the formation of the moraine ridges on the slopes surrounding the main valley floor. The highest moraine ridges, dated at 13.7–12.5 ka, may be associated with phases of glacial stabilization during the overall retreat between the Bølling-Allerød (B-A) Interstadial (14.6–12.9 ka; GI-1 Greenland ice cores; Rasmussen et al., 2014) and the early Younger Dryas (YD) stadial (12.9–11.7 ka; GS-1; Rasmussen et al., 2014). The lowest ridges (11.3 ka), deposited concurrently with the outer moraine ridge enclosing the dated hummocky terrain (11.2 ka), formed at the onset of the Holocene (Fig. 9).

- Phase 3: Transformation into a debris-covered glacier.

The glacier stagnated and thinned at this time, triggering the intensification of paraglacial dynamics on the recently deglaciated slopes. The abundant sediment delivery from lateral moraines and recently ice-free rock walls onto the glacier surface favoured its transformation into a debris-covered glacier during the Early Holocene at ca. 11–10 ka.

- Phase 4: Degradation and final collapse of the debris-covered glacier.

As temperatures continued to rise during the Early Holocene, the debris-covered glacier underwent an irregular collapse, and its deposits became a hummocky terrain. The glacier disappeared from the Zackenberg Valley by 10.3 ± 1.3 ka, exposing polished bedrock outcrops and abandoning erratic boulders as the glacier terminus receded up the Store Sødal valley. The valley has not had glacial ice during the last 10 ka as no younger glacial landforms have been identified. As a result of the deglaciation, glacio-isostatic processes exposed a sequence of marine terraces and favoured the incision of the Zackenberg River. A rapid delta progradation began ca. 13–11 ka and continued until 6.3 ka, accompanied by permafrost aggradation (Gilbert et al., 2017; Christiansen et al., 2002).

5.4. Glacial oscillations in NE Greenland since the last glacial cycle

To date, the available glacial reconstructions have focused mostly on the Northeast Greenland Ice Stream (NEGIS), which drains ~12% of the interior GrIS via three marine-terminating outlet glaciers (Larsen et al., 2018), as well as coastal areas of central East Greenland surrounding Scoresby Sund, ~400 km south of Zackenberg (Kelly et al., 2008; Håkansson et al., 2009, 2011; Lowell et al., 2013; Levy et al., 2014, 2016) (Fig. 10). Our ¹⁰Be CRE age dataset, focusing on glacial landforms in the Zackenberg area, expands and strengthens the previous glacial history based on radiocarbon and luminescence dates (Christiansen and Humlum, 1993; Christiansen, 1994, 1998; Christiansen et al., 2002;

Bennike et al., 2008; Gilbert et al., 2017), providing new evidence of the major role that the Late Glacial deglaciation exerted in the environmental evolution of NE Greenland.

Glacial evidence around Greenland shows asynchronous glacial fluctuations of the GrIS and peripheral mountain glaciers during the last glacial cycle and subsequent deglaciation (Kelly and Lowell, 2009; Vasskog et al., 2015). There is a gap of terrestrial empirical evidence of glacial fluctuations prior to the LGM, although available offshore marine records indicate that all GrIS regions underwent significant growth and retreat in millennial-scale phases (Funder and Hansen, 1996; Lecavalier et al., 2014; Vasskog et al., 2015).

To date, it is unclear whether the interfjord plateaus remained ice-free throughout some periods within the last glacial cycle when the fjords were occupied by outlet glaciers (Funder et al., 1994), or on the contrary, were not ice-free at any time until the post-LGM ice thinning (Håkansson et al., 2011). In West Greenland, while some CRE ages of erratic boulders indicated that coastal mountain tops (above ca. 800 m a.s.l.) have been ice free since ca. 130 ka, (and thus were not glaciated during the last glacial cycle; (Roberts et al., 2009; Lane et al., 2014; Roberts et al., 2013), more recent studies suggest that these high-elevation surfaces were ice-free almost ca. 90 ka before the LGM and ice-covered during this period (Strunk et al., 2017). Assuming that the highest dated erratic boulders in the Zackenberg Valley do not retain nuclide inheritance, the maximum glacial expansion of the last glacial cycle would have occurred at ca. 80–50 ka, when most of the valley was inundated by ice but the mountain tops remained ice-free. At this time, the glacier front was probably located ca. 30 km from Zackenberg on the outer shelf (Christiansen and Humlum, 1993), as reported in several other areas across North and central East Greenland (Funder et al., 2011; Lecavalier et al., 2014). An age of 79.1 ± 3.1 ka was reported by Håkansson et al. (2007b) from a moraine boulder in the Store Koldewey island, 250 km north of Zackenberg, although the authors cautioned that it might have been subject to nuclide inheritance. The longest glacial chronology of the last glacial cycle in NE Greenland is from the NEGIS, which was smaller than present between ~41–26 ka, with glacier front at least 20–70 km behind the present ice margin (Larsen et al., 2018).

However, if we assume that nuclide inheritance occurred in the glacial erratic boulders from the Aucellabjerg plateau it is reasonable to suggest that the glacial advance which occurred during the LGM covered most of the Zackenberg Valley. According to the GrIS reconstructions, the ice sheet occupied an area 65% larger than present during the LGM, with margins generally reaching at least the continental shelf (Kelly and Antony, 2009; Funder et al., 2011; Vasskog et al., 2015). This is confirmed in the northeast sector, where NEGIS significantly expanded by 26 ka (Larsen et al., 2018). Evidence for the LGM glacial advance also exists further south near the Scoresby Sund mouth, where ¹⁰Be ages of erratic boulders placed the ice margin into the outer shelf until 17.3 ka, with a thickness of ca. 250 m (Håkansson et al., 2007a). Despite the lack of geomorphic evidence of the LGM glacial advance in Zackenberg Valley, geophysical modeling carried out in the Wollaston Forland region suggested ice between 500 and 1000 m-thick (Fleming and Lambeck, 2004), which was supported by glacial trimlines on the mountain sides indicating that the Zackenberg area was occupied by valley glaciers (Bennike et al., 2008). The highest moraine remnants in the Zackenberg Valley, located at elevations between 500 and 800 m, may thus have formed during this glacial advance (Fig. 10).

Following the LGM, temperatures increased at the onset of T-1 and a more pronounced warming took place ca. 17 ka (Kobashi et al., 2017), resulting in a significant reduction of GrIS volume and retreat of its margins as modelled by palaeoglaciological studies (Funder et al., 2011; Vasskog et al., 2015). It is still unclear whether GrIS deglaciation persisted without interruption well into the Holocene, or if this long-term retreat was interspersed with periods of glacial advance/stabilization that led to phases of moraine formation (Vasskog et al., 2015).

J. García-Oteyza, M. Oliva, D. Palacios et al.

Geomorphology 401 (2022) 108125

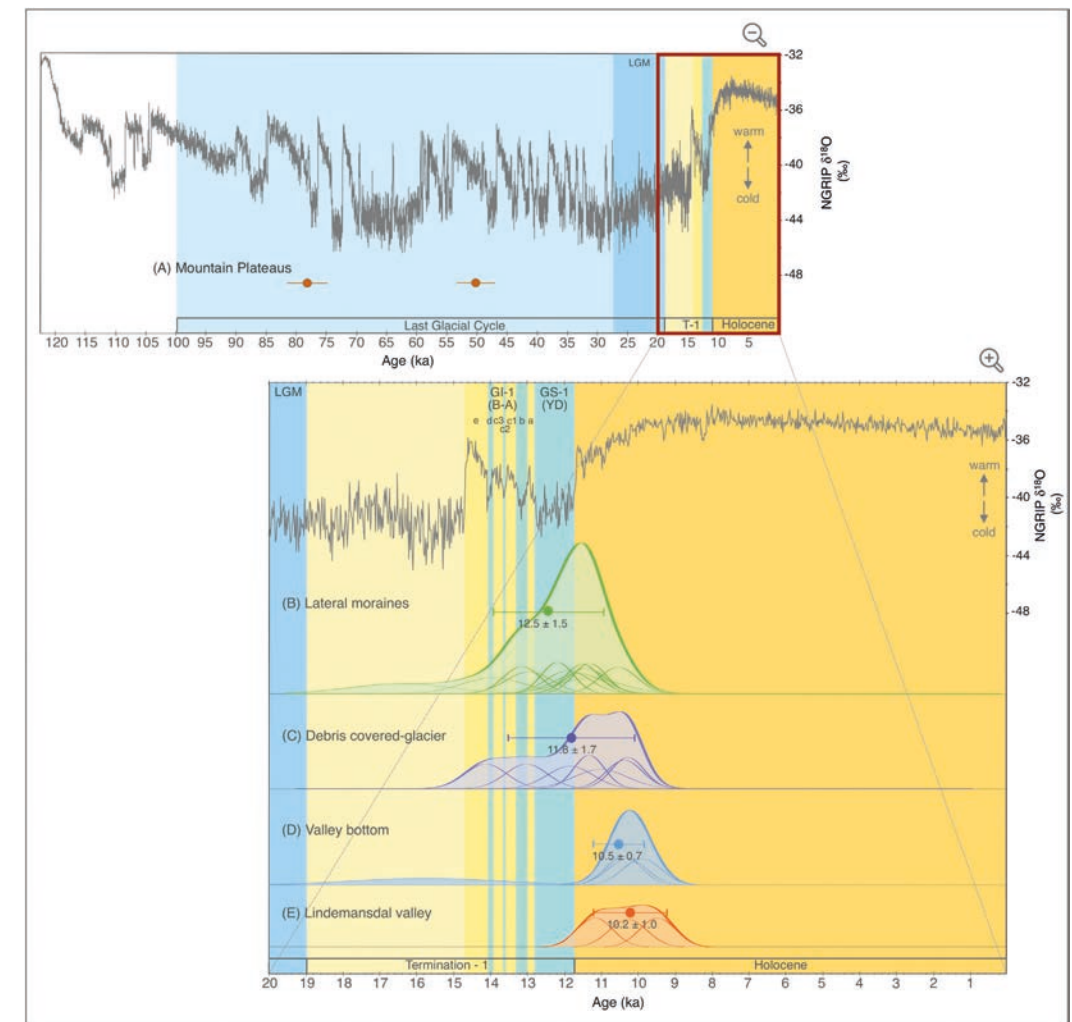


Fig. 9. Probability distribution functions of exposure ages for each group of samples vs. temperature evolution since the last glacial cycle in the interior of Greenland based on the δ¹⁸O record of the NGRIP ice core (GICC05modelext), 5-point running mean. Periods are labelled according to Rasmussen et al. (2014). The proposed deglaciation age of the summits may be associated to the warm period MIS 5a (A). The ages of the lateral moraines are related to the deglaciation of the valley, when the glacier was still debris-free. The ages, partially scattered by paraglacial dynamics, range from 16 to 10 ka (B), and show the most intense deglaciation (peak of the temperature curve) just at the beginning of the Holocene. (C) The ages of the debris-covered glacier show the final phase of the glacier front between 14 and 10 ka. Boulders from the lateral moraines affected by paraglacial processes fell onto the debris-covered glacier, and thus samples retain cosmogenic inheritance, although the peak of the temperature curve may point to the age of its final stabilization at ~10 ka. (D) Ages from the valley bottom confirm an accelerated glacial retreat by ~10 ka, which is also confirmed by the ages from the Lindemansdal valley, where glacial dynamics ended by ~10 ka (E).

Zackenberg data, however, show that the long-term GrIS recession was interrupted by short periods of stillstand or glacial advance. Recent studies have confirmed the occurrence of several glacial oscillations within T-1 across Greenland that led to the development of moraines (Young et al., 2020), confirming previous evidence inferred from marine sediments (Ó Cofaigh et al., 2013). In NE Greenland, few studies have provided CRE ages of deglaciation within T-1. Biette et al. (2020a, 2020b) dated a culmination of moraine formation at 16.2 ka in the

Clavering Island, ca. 30 km south from our study area. This age is significantly older than the sequence of Zackenberg-area moraine ridges that was dated at 13.7–11.2 ka, suggesting a rapid ice thinning of >300 m from the high moraine locations.

Our CRE results highlight the rapid rate of deglaciation during the Late Glacial, although the strong age clustering around 13–11 ka and the associated uncertainty ranges hinders the distinction of whether the deposition of the lowest ridges, and the concurrent outer moraine

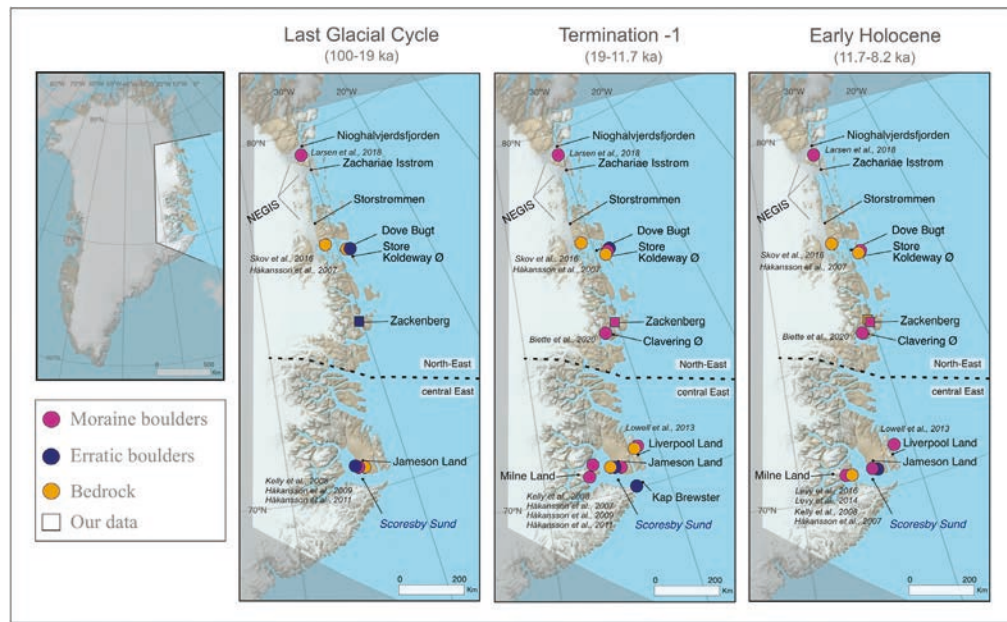


Fig. 10. Map of NE Greenland including the locations discussed in the text, and exposure ages from published glacial ¹⁰Be CRE chronologies (Biette et al., 2020a, 2020b; Håkansson et al., 2007a, 2007b, 2007c, 2009, 2011; Kelly et al., 2008; Larsen et al., 2018; Levy et al., 2014, 2016; Lowell et al., 2013; Skov et al., 2020). The geographical division (North-East vs. Central-East Greenland) follows that of the Geological Survey of Denmark and Greenland (Davies and Glendal, 2007).

J. Garcia-Oteiza, M. Oliva, D. Palacios et al.

Geomorphology 401 (2022) 108125

J. Garcia-Oteiza, M. Oliva, D. Palacios et al.

Geomorphology 401 (2022) 108125

ridge of the valley floor, occurred during the B-A, YD or Early Holocene (Fig. 9). Therefore, we cannot confirm if these moraines correspond to a glacial readvance occurred during the YD, which has rarely been documented in Greenland (Funder et al., 2021). These results coincide with the initial deposition of the Zackenberg Delta at 13–11 ka (Gilbert et al., 2017), confirming that glacial shrinking was parallel to glacio-isostatic uplift and abundant proglacial sedimentation in the lower Zackenberg Valley.

The series of glacial advances/stillstands and retreats that occurred in the Zackenberg area between 13.7 and 11.2 ka is broadly synchronous with glacial records from other sites across NE Greenland indicating that climate conditions favoured glacial shrinking with ephemeral phases of minor glacial advance during the Late Glacial (Fig. 10). A rapid glacial retreat of ~65 km was recorded in Dove Bugt (Fig. 10) between ~13 ka and ~10 ka at a rate of ~22 m yr⁻¹ (Skov et al., 2020). Other ¹⁰Be moraine ages suggest periods of moraine formation during late glacial time: on Store Koldewey island, Håkansson et al. (2007b) reported a post-LGM advance of the GrIS between 14.6 and 11.5 ka, whereas Kelly et al. (2008) described two advances in the Scoresby Sund region at 13.0–11.6 and 11.7–10.6 ka driven by the prevailing cold conditions associated with the YD. On the other hand, Levy et al. (2016) dated glacial advances of the GrIS and of the peripheral Milne Land Ice Cap at 11.4 ka near Scoresby Sund (Fig. 10). Similarly, on neighbouring Clavering Island, local mountain glaciers advanced during the onset of the Holocene at 11.3 and 10.8 ka, respectively (Biette et al., 2020a, 2020b). These heterogeneous ages provide evidence of very active glacial dynamics at the T-1 to Early Holocene transition, with the formation of moraine systems over different timescales.

Deglaciation was accelerated by warmer temperatures during the Early Holocene (Clark et al., 2012; Buizert et al., 2014). CRE dates confirm that the retreat of the NEGIS started at 11.7 ka and accelerated until 9.3 ka (Larsen et al., 2018). In central East Greenland, the Bregne Ice Cap shrunk within its Late Holocene extent by 10.7 ka (Levy et al., 2014). Based on radiocarbon ages, GrIS retreat within the modern coastline occurred between ~11 and 10 ka (Bennike and Björck, 2002; Vasskog et al., 2015), also including NE Greenland (Wagner et al., 2010; Lecavalier et al., 2014). In the Zackenberg area, our data indicates that the valley was mostly deglaciated by ~10.5 ka, although dead ice patches may have survived for millennia under the debris cover, as already observed in mid-latitude mountains (Fernández-Fernández et al., 2017) and subpolar environments (Charton et al., 2020; Fernández-Fernández et al., 2020). Regional glacio-isostatic rebound and rapid relative sea level fall (Christiansen et al., 2002) led to the formation of the current Zackenberg landscape, bringing the rapid incision of the Zackenberg River, high sedimentation rates, rapid delta progradation and permafrost formation (Gilbert et al., 2017). The end of the YD also favoured the readjustment of slopes to the new ice-free setting, with active paraglacial processes that generated a debris-covered glacier and finally resulted in an extensive hummocky terrain. This process is similar to that observed in the Héðinsdalur valley in the Tröllaskagi Peninsula (north Iceland) where a collapsed debris-covered glacier occupied the valley bottom, showing the typical ridge-and-furrow landscape interspersed with thermokarst collapse depressions of various typologies (Fernández-Fernández et al., 2020; Rodríguez-Mena et al., 2021; Palacios et al., 2021).

6. Conclusions

This study provides insights into past changes of the GrIS, introducing new geomorphological and chronological evidence of the deglaciation dynamics at the end of T-1 – when most of the currently ice-free areas in the southern sector of NE Greenland became deglaciated – including the progressive transformation of one of its outlets from a debris-free to a debris-covered glacier during the final stages of deglaciation. Greenland still retains 12% of the planet's debris-covered glaciers, although scientific knowledge of their

evolution is still limited. In fact, this is the first study focused on collapsed debris-covered glaciers in Greenland that has shown the close relationship of their origin with the paraglacial processes that accompany deglaciation.

With a dataset of 32 CRE dates from erratic and moraine boulders, as well as from polished bedrock surfaces, we established the spatio-temporal pattern of deglaciation in the Zackenberg Valley and the impact that paraglacial activity had on the slopes and the valley floor. Glaciers occupied the fjords and surrounding valleys during most part of the last glacial cycle. Ice reached >800 m a.s.l. above the current valley floor during the maximum advance of the last glacial cycle, when only the highest peaks protruded the ice sheet as nunataks. This may have occurred at ca. 80–50 ka, or later, depending on assumptions regarding nuclide inheritance in the highest erratic boulders. In this study, no geomorphic evidence of glacial activity during the LGM was found, although some of the highest, most heavily eroded remnants of moraines existing in the area may correspond to that phase. The complete sequence of moraine ridges distributed across the slopes surrounding the Zackenberg Valley floor revealed ice thinning between ca. 13.7 and 11.2 ka. By 11.3–11.2 ka, the glacier formed the lowest moraines distributed on the slopes and pushed up the terminal moraines crossing the central part of the Zackenberg Valley floor. Concurrently, glacial thinning exposed the rock slopes and the moraine ridges, favouring rapid paraglacial slope readjustment. High rates of debris supply onto the glacier still existing in the valley resulted in the formation of a debris-covered glacier. However, as the glacier retreated and disconnected from the external moraine, a hummocky terrain formed as a consequence of areal deglaciation and the subsequent melting of dead ice masses. Overlapping CRE ages from the outermost moraine ridges of the valley floor and the internal hummocky terrain (ca. 12–11 ka) indicate that this was a very rapid process. Since the Early Holocene (ca. 10.5 ka), no glaciers have been present in the Zackenberg Valley, although ice disappearance has brought the formation of the current landscape due to a wide range of primarily periglacial postglacial processes, in addition to glacio-isostatic uplift and marine terrace and delta formation, permafrost aggradation, and nivation processes largely forming the slopes and the lowland.

Our results demonstrate that CRE dating: (i) needs to be complemented with highly detailed geomorphological mapping; (ii) is a valid method for tracking deglaciation sequences, and; (iii) enables reconstruction of environmental transformations in very active geomorphological settings, including areas that have shifted from debris-free to debris-covered glaciers. However, our results also show that (iv) CRE dating in these areas requires the dating of a large number of samples and landforms; and (v) the uncertainties, considering the problems typically associated with paraglacial processes, remain a challenge for establishing accurate chronologies, as only approximate time ranges can be established for the occurrence of certain events. As such, results need to be supported by other local and regional paleoenvironmental and paleoclimate proxies.

The main phases inferred from our CRE dataset agree with the few existing glacial chronologies from other sites across NE Greenland. However, our results also open new uncertainties that should be addressed in future studies, including the impact of LGM glacial advance on coastal regions and the extent of Holocene glacial fluctuations. A better understanding of the natural pattern of glacial oscillations in NE Greenland during warm and cold phases over the last several millennia would help to better frame the magnitude of current glacial shrinking trends associated with the current warming scenario.

CRedit authorship contribution statement

JG, MO, DP, DA, JRF, VJ, VR, TL and KA conducted field work in Greenland. JG, JMF, LL, and TL prepared the samples at CEREGE. IS led the data interpretation. AT performed AMS measurements. HC and OH contributed to the interpretation of glacial evolution. JG, MO, DP, JMF

J. García-Oteyza, M. Oliva, D. Palacios et al.

and DA prepared the main text, figures and tables assisted by the rest of authors. All authors provided feedback prior to paper submission.

Declaration of competing interest

The authors declare that they have no known competing financial interests or personal relationships that could have appeared to influence the work reported in this paper.

Acknowledgements

This research was funded by the project PALEOGREEN (CTM2017-87976-P) of the Spanish Ministry of Economy and Competitiveness. Field work was also supported by an INTERACT Transnational Access grant (Ref. 730938, GLACIGREEN) and by the Research Group ANTALP (Antarctic, Arctic, Alpine Environments; 2017-SGR-1102), funded by the Government of Catalonia. Julia García-Oteyza was supported by an FPI fellowship from the Spanish Ministry of Science, Innovation and Universities, and Marc Oliva by the Ramón y Cajal Program (RYC-2015-17597). Field work for ZAC-01b and ZAC-04 samples was funded by INTERACT; project DATECH2. The ¹⁰Be measurements were performed at the ASTER AMS national facility (CEREGE, Aix en Provence), which is supported by the INSU/CNRS and the ANR through the “Projets thématiques d'excellence” program for the “Equipements d'excellence” ASTER-CEREGE action and IRD.

Appendix A. Supplementary data

Supplementary data to this article can be found online at <https://doi.org/10.1016/j.geomorph.2022.108125>.

References

- Amschwand, D., Ivy-Ochs, S., Frehner, M., Steinemann, O., Christl, M., Vockenhuber, C., 2020. Deciphering the evolution of the Bleis Marscha rock glacier (Val d'Err, eastern Switzerland) with cosmogenic nuclide exposure dating, aerial image correlation, and finite-element modelling. *Cryosph. Res.* <https://doi.org/10.5194/tc-2020-209> in review.
- Anderson, L.S., Anderson, R.S., 2016. Modeling debris-covered glaciers: response to steady debris deposition. *Cryosphere* 10, 1105–1124. <https://doi.org/10.5194/tc-10-1105-2016>.
- Anderson, L.S., Flowers, G.E., Jarosch, A.H., Ádalgeldisdóttir, G.T., Geirsdóttir, Á., Miller, G.H., Harming, D.J., Thorsteinsson, T., Magnússon, E., Pálsson, F., 2018. Holocene glacier and climate variations in Vestfirðir, Iceland, from the modeling of Drangajökull ice cap. *Quat. Sci. Rev.* 190, 39–56. <https://doi.org/10.1016/j.quascirev.2018.04.024>.
- Arnold, M., Merchel, S., Bourlés, D.L., Braucher, R., Benedetti, L., Finkel, R.C., Aumaitre, G., Gottang, A., Klein, M., 2010. The French accelerator mass spectrometry facility ASTER: Improved performance and developments. 268, pp. 1954–1959. <https://doi.org/10.1016/j.nimb.2010.02.107>.
- Balco, G., 2020. Glacier Change and Paleoclimate Applications of Cosmogenic-Nuclide Exposure Dating, pp. 1–28.
- Balco, G., Stone, J.O., Lifton, N.A., Dunai, T.J., 2008. A complete and easily accessible means of calculating surface exposure ages or erosion rates from ¹⁰Be and ²⁶Al measurements. *Quat. Geochronol.* 3, 174–195. <https://doi.org/10.1016/j.quageo.2007.12.001>.
- Ballantyne, C.K., 2008. After the ice: Holocene geomorphic activity in the Scottish Highlands. *Scott. Geogr. J.* <https://doi.org/10.1080/14702540802300167>.
- Bamber, J.L., Griggs, J.A., Hurlkmans, R.T.W.L., Dowdeswell, J.A., Gogineni, S.P., Howat, I., Mougnot, J., Paden, J., Palmer, S., Rignot, E., Steinhage, D., 2013. A new bed elevation dataset for Greenland. *Cryosphere* 7, 499–510. <https://doi.org/10.5194/tc-7-499-2013>.
- Benn, D.I., 1992. The genesis and significance of ‘hummocky moraine’: evidence from the Isle of Skye, Scotland. *Quat. Sci. Rev.* 11, 781–799. [https://doi.org/10.1016/0277-3791\(92\)90083-K](https://doi.org/10.1016/0277-3791(92)90083-K).
- Bennike, O., Björck, S., 2002. Chronology of the last recession of the Greenland Ice Sheet. *J. Quat. Sci.* 17, 211–219. <https://doi.org/10.1002/jqs.670>.
- Bennike, O., Sørensen, M., Fredskild, B., Jacobsen, B.H., Böcher, J., Amsinck, S.L., Jeppesen, E., Andreasen, C., Christiansen, H.H., Humlum, O., 2008. Late Quaternary Environmental and Cultural changes in the Wollaston Forland Region, Northeast Greenland. *Adv. Ecol. Res.* 40, 45–79.
- Bibby, T., Putkonen, J., Morgan, D., Balco, G., Shuster, D.L., 2016. Million year old ice found under meter thick debris layer in Antarctica. *Geophys. Res. Lett.* 43, 6995–7001. <https://doi.org/10.1002/2016GL069889>.
- Bierman, P.R., Marsella, K.A., Patterson, C., Davis, P.T., Caffee, M., 1999. Mid-Pleistocene cosmogenic minimum-age limits for pre-Wisconsinan glacial surfaces in southwestern Minnesota and southern Baffin Island: a multiple nuclide approach. *Geomorphology* 27, 25–39. [https://doi.org/10.1016/S0169-555X\(98\)00088-9](https://doi.org/10.1016/S0169-555X(98)00088-9).

Geomorphology 401 (2022) 108125

- Biette, M., Jomelli, V., Chenet, M., Braucher, R., Rinterknecht, V., Lane, T., 2020a. Mountain glacier fluctuations during the Lateglacial and Holocene on Clavering Island (northeastern Greenland) from ¹⁰Be moraine dating. *Boreas* 49, 873–885. <https://doi.org/10.1111/bor.12460>.
- Biette, M., Jomelli, V., Chenet, M., Egis, R., Biette, M., 2020. Mountain glacier fluctuations during the Lateglacial and Holocene on Clavering Island (northeastern Greenland) from ¹⁰Be moraine dating. <https://doi.org/10.1111/bor.12460>.
- Braucher, R., Guillou, V., Bourlés, D.L., Arnold, M., Aumaitre, G., Keddadouche, K., Nottoli, E., 2015. Preparation of ASTER in-house ¹⁰Be/⁹Be standard solutions. 361, pp. 335–340.
- Briner, J.P., Miller, G.H., Davis, P.T., Bierman, P.R., Caffee, M., 2003. Last glacial maximum ice sheet dynamics in Arctic Canada inferred from young erratics perched on ancient tors. *Quat. Sci. Rev.* 22, 437–444. [https://doi.org/10.1016/S0277-3791\(03\)00003-9](https://doi.org/10.1016/S0277-3791(03)00003-9).
- Briner, J.P., McKay, N.P., Axford, Y., Bennike, O., Bradley, R.S., de Vernal, A., Fisher, D., Francus, P., Fréchette, B., Gajewski, K., Jennings, A., Kaufman, D.S., Miller, G., Rouston, C., Wagner, B., 2016. Holocene climate change in Arctic Canada and Greenland. *Quat. Sci. Rev.* 147, 340–364. <https://doi.org/10.1016/j.quascirev.2016.02.010>.
- Broecker, W., 2018. CO₂: Earth's climate driver. *Geochim. Perspect.* 7, 111–198. <https://doi.org/10.7185/geochempersp.7.2>.
- Buizert, C., Gkinis, V., Severinghaus, J.P., He, F., Lecavalier, B.S., Kindler, P., Leuenberger, M., Carlson, A.E., Vinther, B., Masson-Delmotte, V., White, J.W.C., Liu, Z., Otto-Bliesner, B., Brook, E.J., 2014. Greenland temperature response to climate forcing during the last deglaciation. *Science* (80-) 345, 1177–1180. <https://doi.org/10.1126/science.1254961>.
- Cable, S., Christiansen, H.H., Westergaard-Nielsen, A., Kroon, A., Elberling, B., 2018. Geomorphological and cryostratigraphical analyses of the Zackenberg Valley, NE Greenland and significance of Holocene alluvial fans. *Geomorphology* 303, 504–523. <https://doi.org/10.1016/j.geomorph.2017.11.003>.
- CAVM Team, 2003. Circumpolar Arctic Vegetation Map. (1:7,500,000 scale), Conservation of Arctic Flora and Fauna (CAFF) Map No. 1. US Fish Wildl. Serv. AK) Available [http://www.Geobot.uaf.edu/cavm/Verified 1 Augus15 July 2015](http://www.Geobot.uaf.edu/cavm/Verified%201%20Aug%2015%202015%20) 2.
- Ceplerley, E., Marcott, S., Reusch, M., Barth, A., Mix, A., Brook, E., Caffee, M., 2020. Widespread early Holocene deglaciation, Washington Land, Northwest Greenland. *Quat. Sci. Rev.* 231, 106181. <https://doi.org/10.1016/j.quascirev.2020.106181>.
- Charton, J., Jomelli, V., Schimmelpfennig, I., Verfaillie, D., Favier, V., Mokadem, F., Gilbert, A., Brun, F., Aumaitre, G., Bourlés, D.L., Keddadouche, K., 2020. A debris-covered glacier at Kerguelen (49°S, 69°E) over the past 15 000 years. *Antarct. Sci.* 13, 1–13. <https://doi.org/10.1017/S0954102020000541>.
- Chmieleff, J., von Blanckenburg, F., Kossert, K., Jakob, D., 2010. Determination of the ¹⁰Be half-life by multicollector ICP-MS and liquid scintillation counting. *Nucl. Instruments Methods Phys. Res. Sect. B Beam Interact. with Mater. Atoms* 268, 192–199. <https://doi.org/10.1016/j.nimb.2009.09.012>.
- Christiansen, H.H., 1994. Thermoluminescence dating of in situ sediments from Zackenberg, Northeast Greenland. *Quat. Sci. Rev.* 13, 491–496. [https://doi.org/10.1016/0277-3791\(94\)90064-7](https://doi.org/10.1016/0277-3791(94)90064-7).
- Christiansen, H.H., 1998. ‘Little Ice Age’ nivation activity in northeast Greenland. 6, pp. 719–728.
- Christiansen, H.H., Humlum, O., 1993. Glacial history and Periglacial Landforms of the Zackenberg area, Northeast Greenland: preliminary results. *Geogr. Tidsskr. J. Geogr.* 93, 19–29. <https://doi.org/10.1080/00167223.1993.10649332>.
- Christiansen, H.H., Bennike, O., Böcher, J., Elberling, B., Humlum, O., Jakobsen, B.H., 2002. Holocene environmental reconstruction from deltaic deposits in Northeast Greenland. *J. Quat. Sci.* 17, 145–160. <https://doi.org/10.1002/jqs.665>.
- Christiansen, H.H., Sigsgaard, C., Humlum, O., Rasch, M., Hansen, B.U., 2008. Permafrost and periglacial geomorphology at Zackenberg. *Adv. Ecol. Res.* 40, 151–174. [https://doi.org/10.1016/S0065-2504\(07\)00007-4](https://doi.org/10.1016/S0065-2504(07)00007-4).
- Christiansen, H.H., Etzelmüller, B., Isaksen, K., Juliussen, H., Farbot, H., Humlum, O., Johansson, M., Ingeman-Nielsen, T., Kristensen, L., Hjort, J., Holmlund, P., Sannel, A.B.K., Sigsgaard, C., Åkerman, H.J., Foged, N., Blikra, L.H., Pernosky, M.A., Ødegård, R.S., 2010. The thermal state of permafrost in the nordic area during the international polar year 2007–2009. *Permafr. Periglac. Process.* 21, 156–181. <https://doi.org/10.1002/ppp.687>.
- Çiner, A., Sarıkaya, M.A., Yıldırım, C., 2017. Misleading old age on a young landform? The dilemma of cosmogenic inheritance in surface exposure dating: Moraines vs. Rock glaciers. *Quat. Geochronol.* 42, 76–88. <https://doi.org/10.1016/j.quageo.2017.07.003>.
- Clark, P.U., Dyke, A.S., Shakun, J.D., Carlson, A.E., Clark, J., Wohlfarth, B., Mitrovica, J.X., Hostetler, S.W., McCabe, A.M., 2009. The Last Glacial Maximum. *Science* (80-) 325, 710–714. <https://doi.org/10.1126/science.1172873>.
- Clark, P.U., Shakun, J.D., Baker, P.A., Bartlein, P.J., Brewer, S., Brook, E., Carlson, A.E., Cheng, H., Kaufman, D.S., Liu, Z., Marchitto, T.M., Mix, A.C., Morrill, C., Otto-Bliesner, B.L., Pahnke, K., Russell, J.M., Whitlock, C., Adkins, J.F., Blois, J.L., Clark, J., Colman, S.M., Curry, W.B., Flower, B.P., He, F., Johnson, T.C., Lynch-Stieglitz, J., Markgraf, V., McManus, J., Mitrovica, J.X., Moreno, P.J., Williams, J.W., 2012. Global climate evolution during the last deglaciation. *Proc. Natl. Acad. Sci. U. S. A.* 109. <https://doi.org/10.1073/pnas.1116619109>.
- Cohen, K., Gibbard, 2020. Global Chronostratigraphical Correlation Table for the Last 2.7 Million Years, Version 2019 Q1-500.
- Davis, P.T., Bierman, P.R., Marsella, K.A., Caffee, M.W., Southon, J.R., 1999. Cosmogenic analysis of glacial terrains in the eastern Canadian Arctic: a test for inherited nucleides and the effectiveness of glacial erosion, pp. 181–188.
- Dawes, P.R., Glendal, E.W., 2007. A glossary for GEUS publications: spelling and usage of troublesome words and names made easy. 59.
- Dede, V., Çiçek, İ., Sarıkaya, M.A., Çiner, A., Uncu, L., 2017. First cosmogenic geochronology from the Lesser Caucasus/Late Pleistocene glaciation and rock glacier development in the Karçal Valley, NE Turkey. *Quat. Sci. Rev.* 164, 54–67. <https://doi.org/10.1016/j.quascirev.2017.03.025>.

J. García-Oteyza, M. Oliva, D. Palacios et al.

- Deline, P., Akçar, N., Ivy-Ochs, S., Kubik, P.W., 2015. Repeated Holocene rock avalanches onto the Brenva Glacier, Mont Blanc massif, Italy: a chronology. *Quat. Sci. Rev.* 126, 186–200. <https://doi.org/10.1016/j.quascirev.2015.09.004>.
- Denton, G.H., Anderson, R.F., Toggweiler, J.R., Edwards, R.L., Schaefer, J.M., Putnam, A.E., 2010. The last Glacial termination. *Science* (80-) 328, 1652–1656. <https://doi.org/10.1126/science.1184119>.
- Dortch, J.M., Owen, L.A., Caffee, M.W., Brease, P., 2010. Late Quaternary glaciation and equilibrium line altitude variations of the McKinley River region, Central Alaska Range. *Boreas* 39, 233–246. <https://doi.org/10.1111/j.1502-3885.2009.00121.x>.
- Escher, A., Watt, W.S., 1976. *Geology of Greenland*.
- Fernández-Fernández, J.M., Palacios, D., García-Ruiz, J.M., Andrés, N., Schimmelpfennig, I., Gómez-Villar, A., Santos-González, J., Álvarez-Martínez, J., Arnáez, J., Úbeda, J., Léanni, L., Aumaitre, G., Bourlés, D., Keddadouche, K., 2017. Chronological and geomorphological investigation of fossil debris-covered glaciers in relation to deglaciation processes: a case study in the Sierra de La Demanda, northern Spain. *Quat. Sci. Rev.* 170, 232–249. <https://doi.org/10.1016/j.quascirev.2017.06.034>.
- Fernández-Fernández, J.M., Palacios, D., Andrés, N., Schimmelpfennig, I., Tamarit, L.M., Brynjólfsson, S., López-Acevedo, F.J., Sæmundsson, B., Team, A.S.T.E.R., 2020. Constraints on the timing of debris-covered and rock glaciers: an exploratory case study in the Hólar area, northern Iceland. *Geomorphology* 361, 107196. <https://doi.org/10.1016/j.geomorph.2020.107196>.
- Fernández-Fernández, J.M., Oliva, M., Palacios, D., García-Oteyza, J., Navarro, F.J., Schimmelpfennig, I., Léanni, L., Team, A., 2021. Ice thinning on nunataks during the glacial to interglacial transition in the Antarctic Peninsula region according to Cosmic-Ray Exposure dating: Evidence and uncertainties. *Quat. Sci. Rev.* 264, 107029. <https://doi.org/10.1016/j.quascirev.2021.107029>.
- Fleming, K., Lambeck, K., 2004. Constraints on the Greenland Ice Sheet since the last Glacial Maximum from sea-level observations and glacial-rebound models. *Quat. Sci. Rev.* 23, 1053–1077. <https://doi.org/10.1016/j.quascirev.2003.11.001>.
- Funder, S., Hansen, L., 1996. The Greenland ice sheet - a model for its culmination and decay during and after the last glacial maximum, pp. 137–152.
- Funder, S., Hjort, C., Landvik, J.Y., 1994. The last glacial cycles in East Greenland, an overview. *Boreas* 23, 283–293. <https://doi.org/10.1111/j.1502-3885.1994.tb00601.x>.
- Funder, S., Kjeldsen, K.K.K.K., Kjar, K.H.K.H., O'Coaigh, C., 2011. The Greenland Ice Sheet during the past 300,000 years: a review. *Dev. Quat. Sci.* 15, 699–713. <https://doi.org/10.1016/B978-0-444-53447-7.00050-7>.
- Funder, S., Sørensen, A.H.L., Larsen, N.K., Björk, A.A., Briner, J.P., Olsen, J., Schomacker, A., Levy, L.B., Kjar, K.H., 2021. Younger Dryas ice margin retreat in Greenland: new evidence from southwestern Greenland, pp. 587–601.
- Gilbert, G.L., Cable, S., Thiel, C., Christiansen, H.H., Elberling, B., 2017. Cryostratigraphy, sedimentology, and the late Quaternary evolution of the Zackenberg River delta, Northeast Greenland. *Cryosphere* 11, 1265–1282. <https://doi.org/10.5194/tc-11-1265-2017>.
- Goehring, B.M., Kelly, M.A., Schaefer, J.M., Finkel, R.C., Lowell, T.V., 2010. Dating of raised marine and lacustrine deposits in East Greenland using beryllium-10 depth profiles and implications for estimates of subglacial erosion. *J. Quat. Sci.* 25, 865–874. <https://doi.org/10.1002/jqs.1380>.
- Goosse, H., Kay, J.E., Armour, K.C., Bodas-Salcedo, A., Chepfer, H., Docquier, D., Jonko, A., Kushner, P.J., Lemont, O., Massonnet, F., Park, H.S., Pithan, F., Svensson, G., Vancoppenolle, M., 2018. Quantifying climate feedbacks in polar regions. *Nat. Commun.* 9, 3–10. <https://doi.org/10.1038/s41467-018-04312-7>.
- Häkansson, L., Briner, J.P., Alexanderson, H., Aldahan, A., Possnert, G., 2007a. ¹⁰Be ages from central East Greenland constrain the extent of the Greenland ice sheet during the last Glacial Maximum. *Quat. Sci. Rev.* 26, 2316–2321. <https://doi.org/10.1016/j.quascirev.2007.08.001>.
- Häkansson, L., Graf, A., Straský, S., Ivy-Ochs, S., Kubik, P.W., Hjort, C., Schlüchter, C., 2007b. Cosmogenic ¹⁰Be-ages from the Store Koldewey island, NE Greenland. *Geogr. Ann. Ser. A Phys. Geogr.* 89, 195–202. <https://doi.org/10.1111/j.1468-0459.2007.00318.x>.
- Häkansson, L., Graf, A., Straský, S., Ivy-Ochs, S., Kubik, P.W., Hjort, C., Schlüchter, C., 2007c. Cosmogenic ¹⁰Be-ages from the Store Koldewey island, NE Greenland. *Geogr. Ann. Ser. A Phys. Geogr.* 89, 195–202. <https://doi.org/10.1111/j.1468-0459.2007.00318.x>.
- Häkansson, L., Alexanderson, H., Hjort, C., Möller, P., Briner, J.P., Possnert, A.A., 2009. Late Pleistocene glacial history of Jameson Land, central East Greenland, derived from cosmogenic ¹⁰Be and ²⁶Al exposure dating. *Boreas* 38, 244–260. <https://doi.org/10.1111/j.1502-3885.2008.00064.x>.
- Häkansson, L., Briner, J.P., Aldahan, A., Possnert, G., 2011. ¹⁰Be data from meltwater channels suggest that Jameson Land, East Greenland, was ice-covered during the last glacial maximum. *Quat. Res.* 76, 452–459. <https://doi.org/10.1016/j.yqres.2011.06.007>.
- Hambrey, M.J., Quincey, D.J., Glasser, N.F., Reynolds, J.M., Richardson, S.J., Clemmens, S., 2008. Sedimentological, geomorphological and dynamic context of debris-mantled glaciers, Mount Everest (Sagarmatha) region, Nepal. *Quat. Sci. Rev.* 27, 2361–2389. <https://doi.org/10.1016/j.quascirev.2008.08.010>.
- Hasholt, B., Mernild, S.H., Sigsgaard, C., Elberling, B., Petersen, D., Jakobsen, B.H., Hansen, B.J., Hinkler, J., Søgaard, H., 2008. Hydrology and Transport of Sediment and Solutes at Zackenberg. *Adv. Ecol. Res.* 40, 197–221. [https://doi.org/10.1016/S0065-2504\(07\)00009-8](https://doi.org/10.1016/S0065-2504(07)00009-8).
- Henriksen, N., Higgins, A.K., Kalsbeek, F., Pulvertaft, T.C.R., 2009. Greenland from Archaean to Quaternary Descriptive text to the 1995 Geological map of Greenland, 1:2500000. *Geol. Surv. Denmark Greenl. Bull.* 18, 126.
- Heyman, J., Stroeven, A.P., Harbor, J.M., Caffee, M.W., 2011. Too young or too old: evaluating cosmogenic exposure dating based on an analysis of compiled boulder exposure ages. *Earth Planet. Sci. Lett.* 302, 71–80. <https://doi.org/10.1016/j.epsl.2010.11.040>.
- Højlund Pedersen, S., 2017. Scaling-up Climate Change Effects in Greenland. Aarhus University, Denmark.

- Janke, J.R., Bellisario, A.C., Ferrando, F.A., 2015. Classification of debris-covered glaciers and rock glaciers in the Andes of Central Chile. *Geomorphology* 241, 98–121. <https://doi.org/10.1016/j.geomorph.2015.03.034>.
- Jones, R.S., Whitehouse, P.L., Bentley, M.J., Small, D., Dalton, A.S., 2019. Impact of glacial isostatic adjustment on cosmogenic surface-exposure dating. *Quat. Sci. Rev.* 212, 206–212. <https://doi.org/10.1016/j.quascirev.2019.03.012>.
- Kaplan, M., Miller, G., 2003. Early Holocene deleveling and deglaciation of the Cumberland Sound region, Baffin Island, Arctic Canada. *Geol. Soc. Am. Bull.* - GEOL SOC AMER BULL 115, 445–462. [https://doi.org/10.1130/0016-7606\(2003\)115<0445:EHDADO>2.0.CO;2](https://doi.org/10.1130/0016-7606(2003)115<0445:EHDADO>2.0.CO;2).
- Kelly, M.A., Antony, J.L., 2009. The dimensions of the Greenland Ice Sheet since the Last Glacial Maximum. *PAGES News* 17, 60.
- Kelly, M.A., Lowell, T.V., 2009. Fluctuations of local glaciers in Greenland during latest Pleistocene and Holocene time. *Quat. Sci. Rev.* 28, 2088–2106. <https://doi.org/10.1016/j.quascirev.2008.12.008>.
- Kelly, M.A., Lowell, T.V., Hall, B.L., Schaefer, J.M., Finkel, R.C., Goehring, B.M., Alley, R.B., Denton, G.H., 2008. A ¹⁰Be chronology of glacial and Holocene mountain glaciation in the Scoresby Sund region, East Greenland: implications for seasonality during lateglacial time. *Quat. Sci. Rev.* 27, 2273–2282. <https://doi.org/10.1016/j.quascirev.2008.08.004>.
- Kenner, R., 2019. Geomorphological analysis on the interaction of Alpine glaciers and rock glaciers since the Little Ice Age. *L. Degrad. Dev.* 30, 580–591. <https://doi.org/10.1002/ldr.3238>.
- Kobashi, T., Menviel, L., Jeltsch-Thömmes, A., Vinther, B.M., Box, J.E., Muscheler, R., Nakaegawa, T., Pfister, P.L., Döring, M., Leuenberger, M., Wanner, H., Ohmura, A., 2017. Volcanic influence on centennial to millennial Holocene Greenland temperature change. *Sci. Rep.* 7. <https://doi.org/10.1038/s41598-017-01451-7>.
- Korschinek, G., Bergmaier, A., Faestermann, T., Gerstmann, U.C., Knie, K., Rugel, G., Wallner, A., Dillmann, I., Dollinger, G., von Gostomski, C.L., Kossert, K., Maiti, M., Poutivestev, M., Remmert, A., 2010. A new value for the half-life of ¹⁰Be by heavy-ion elastic recoil detection and liquid scintillation counting. *Nucl. Instruments Methods Phys. Res. Sect. B Beam Interact. with Mater. Atoms* 268, 187–191. <https://doi.org/10.1016/j.nimb.2009.09.020>.
- Kottek, M., Grieser, J., Beck, C., Rudolf, B., Rubel, F., 2006. World map of the Köppen-Geiger climate classification updated. *Meteorol. Zeitschrift* 15, 259–263. <https://doi.org/10.1127/0941-2948.2006.0130>.
- Lal, D., 1991. Cosmic ray labeling of erosion surfaces: in situ nuclide production rates and erosion models: Earth and Planetary Science letters. *Earth Planet. Sci. Lett.* 104, 424–439.
- Lane, T.P., Roberts, D.H., Rea, B.R., Cofaigh, C.O., Vieli, A., Rodés, A., 2014. Controls upon the last Glacial maximum deglaciation of the northern Uppmannag ice stream system, West Greenland. *Quat. Sci. Rev.* 92, 324–344.
- Larocca, L.J., Axford, Y., Björk, A.A., Lasher, G.E., Brooks, J.P., 2020a. Local glaciers record delayed peak Holocene warmth in South Greenland. *Quat. Sci. Rev.* 241, 106421. <https://doi.org/10.1016/j.quascirev.2020.106421>.
- Larocca, L.J., Axford, Y., Woodroffe, S.A., Lasher, G.E., Gawin, B., 2020b. Holocene glacier and ice cap fluctuations in Southwest Greenland inferred from two lake records. *Quat. Sci. Rev.* 246, 106529. <https://doi.org/10.1016/j.quascirev.2020.106529>.
- Larsen, N.K., Levy, L.B., Carlson, A.E., Buizert, C., Olsen, J., Strunk, A., Björk, A.A., Skov, D.S., 2018. Instability of the Northeast Greenland Ice Stream over the last 45,000 years. *Nat. Commun.* 9, 3–10. <https://doi.org/10.1038/s41467-018-04312-7>.
- Lecavalier, B.S., Milne, G.A., Simpson, M.J.R., Wake, L., Huybrechts, P., Tarasov, L., Kjeldsen, K.K., Funder, S., Long, A.J., Woodroffe, S., Dyke, A.S., Larsen, N.K., 2014. A model of Greenland ice sheet deglaciation constrained by observations of relative sea level and ice extent. *Quat. Sci. Rev.* 102, 54–84. <https://doi.org/10.1016/j.quascirev.2014.07.018>.
- Lenton, T.M., Held, H., Kriegler, E., Hall, J.W., Lucht, W., Rahmstorf, S., Schellnhuber, H.J., 2008. Tipping elements in the Earth's climate system. *Proc. Natl. Acad. Sci. U. S. A.* <https://doi.org/10.1073/pnas.0705414105>.

J. García-Oteyza, M. Oliva, D. Palacios et al.

Geomorphology 401 (2022) 108125

- Oliva, M., Mercier, D., Ruiz-Fernández, J., McColl, S., 2019. Paraglacial processes in recently deglaciated environments. *L. Degrad. Dev.* 1–6. <https://doi.org/10.1002/ldr.3283>.
- Palacios, D., Rodríguez-Mena, M., Fernández-Fernández, J.M., Schimmelpfennig, I., Tanarro, L.M., Zamorano, J.J., Andrés, N., Úbeda, J., Sæmundsson, Þ., Brynjólfsson, S., Oliva, M., Team, A.S.T.E.R., 2021. Reversible glacial-periglacial transition in response to climate changes and paraglacial dynamics: a case study from Héðinsdalsjökull (northern Iceland). *Geomorphology* 388. <https://doi.org/10.1016/j.geomorph.2021.107787>.
- Pedersen, J.B.T., Kroon, A., Jakobsen, B.H., 2011. Holocene sea-level reconstruction in the Young Sound region, Northeast Greenland. *J. Quat. Sci.* 26, 219–226. <https://doi.org/10.1002/jqs.1449>.
- Rasmussen, S.O., Bigler, M., Blockley, S.P., Blunier, T., Buchardt, S.L., Clausen, H.B., Cvijanovic, I., Dahl-Jensen, D., Johnsen, S.J., Fischer, H., Gkinis, V., Guillevic, M., Hoek, W.Z., Lowe, J.J., Pedro, J.B., Popp, T., Seierstad, I.K., Steffensen, J.P., Svensson, A.M., Vallelonga, P., Vinther, B.M., Walker, M.J.C., Wheatley, J.J., Winstrup, M., 2014. A stratigraphic framework for abrupt climatic changes during the last Glacial period based on three synchronized Greenland ice-core records: refining and extending the INTIMATE event stratigraphy. *Quat. Sci. Rev.* 106, 14–28. <https://doi.org/10.1016/j.quascirev.2014.09.007>.
- Roberts, D.H., Long, A.J., Schnabel, C., Davies, B.J., Xu, S., Simpson, M.J.R., Huybrechts, P., 2009. Ice sheet extent and early deglacial history of the southwestern sector of the Greenland Ice Sheet. *Quat. Sci. Rev.* 28, 2760–2773. <https://doi.org/10.1016/j.quascirev.2009.07.002>.
- Roberts, D.H., Rea, B.R., Lane, T.P., Schnabel, C., Rodés, A., 2013. New constraints on Greenland ice sheet dynamics during the last glacial cycle: evidence from the Uummannaq ice stream system. *J. Geophys. Res. Earth Surf.* 118 (2), 519–541.
- Rodríguez-Mena, M., Fernández-Fernández, J.M., Tanarro, L.M., Zamorano, J.J., Palacios, D., 2021. Héðinsdalsjökull, northern Iceland: geomorphology recording the recent complex evolution of a glacier. *J. Maps* 17, 301–313. <https://doi.org/10.1080/17445647.2021.1920056>.
- Scherler, D., Egholm, D.L., 2020. Production and Transport of Supraglacial Debris: Insights from Cosmogenic ¹⁰be and Numerical Modeling, Chhota Shigri Glacier, Indian Himalaya. *J. Geophys. Res. Earth Surf.* 125, 3. <https://doi.org/10.1029/2020JF005586>.
- Skov, D.S., Andersen, J.L., Olsen, J., Jacobsen, B.H., Knudsen, M.F., Jansen, J.D., Larsen, N.K., Egholm, D.L., 2020. Constraints from cosmogenic nuclides on the glaciation and erosion history of dove Bugt, Northeast Greenland. *Bull. Geol. Soc. Am.* 132, 2282–2294. <https://doi.org/10.1130/b35410.1>.
- Søndergaard, A.S., Larsen, N.K., Olsen, J., Strunk, A., Woodroffe, S., 2019. Glacial history of the Greenland Ice Sheet and a local ice cap in Qaanaaq, Northwest Greenland. *J. Quat. Sci.* 34, 536–547. <https://doi.org/10.1002/jqs.3139>.
- Stone, J.O., 2000. Isotope production T, T. *J. Geophys. Res.* 105, 753–759.
- Strunk, A., Knudsen, M.F., Egholm, D.L., Jansen, J.D., Levy, L.B., Jacobsen, B.H., Larsen, N.K., 2017. One million years of glaciation and denudation history in West Greenland. *Nat. Commun.* 8, 1–8. <https://doi.org/10.1038/ncomms14199>.
- Tanarro, L.M., Palacios, D., Andrés, N., Fernández-Fernández, J.M., Zamorano, J.J., Sæmundsson, Þ., Brynjólfsson, S., 2019. Unchanged surface morphology in debris-covered glaciers and rock glaciers in Tröllaskagi peninsula (northern Iceland). *Sci. Total Environ.* 648, 218–235. <https://doi.org/10.1016/j.scitotenv.2018.07.460>.
- Tanarro, L.M., Palacios, D., Fernández-Fernández, J.M., Andrés, N., Oliva, M., Rodríguez-Mena, M., Schimmelpfennig, I., Brynjólfsson, S., Zamorano, J.J., Úbeda, J., Aumaitre, G., Bourlés, D., Keddadouche, K., Sæmundsson Þorsteinn, 2021. Origins of the divergent evolution of mountain glaciers during deglaciation: Hofsdalur cirques, Northern Iceland. *Quat. Sci. Rev.* 273. <https://doi.org/10.1016/j.quascirev.2021.107248>.
- Vasskog, K., Langebroek, P.M., Andrews, J.T., Nilsen, J.E.Ø., Nesje, A., 2015. The Greenland Ice Sheet during the last glacial cycle: current ice loss and contribution to sea-level rise from a palaeoclimatic perspective. *Earth-Science Rev.* 150, 45–67. <https://doi.org/10.1016/j.earscirev.2015.07.006>.
- Wagner, B., Bennike, O., Cremer, H., Klug, M., 2010. Paleontological and sedimentological investigations of a sediment profile from northeast Greenland. *PANGAEA* <https://doi.org/10.1594/PANGAEA.759229>.
- Ward, G.K., Wilson, S.R., 1978. Procedures for comparing and Combining Radiocarbon Age Determinations: a Critique. *Archaeometry* 20, 19–31. <https://doi.org/10.1111/j.1475-4754.1978.tb00208.x>.
- Winkler, S., Lambiel, C., 2018. Age constraints of rock glaciers in the Southern Alps/New Zealand – exploring their palaeoclimatic potential. *The Holocene* 28, 778–790. <https://doi.org/10.1177/0959683618756802>.
- Young, N.E., Schaefer, J.M., Briner, J.P., Goehring, B.M., 2013. A ¹⁰Be production-rate calibration for the Arctic. *J. Quat. Sci.* 28, 515–526. <https://doi.org/10.1002/jqs.2642>.
- Young, E., Briner, J.P., Miller, G.H., Lesnek, A.J., Crump, S.E., Thomas, E.K., Pendleton, S.L., Cuzzone, J., Lamp, J., Zimmerman, S., Caffee, M., Schaefer, J.M., 2020. Deglaciation of the Greenland and Laurentide ice sheets interrupted by glacier advance during abrupt coolings. 229. <https://doi.org/10.1016/j.quascirev.2019.106091>.

3.1.2 PAPER II. HOLOCENE GLACIAL OSCILLATIONS IN THE TYROLER VALLEY

PAPER II

J. García-Oteyza Ciria, M. Oliva, D. Palacios, J. M. Fernández-Fernández, I. Schimmelpfennig, A. Medialdea, M. Fernandes, S. Giralt, V. Jomelli, D. Antoniadis & ASTER TEAM (2023). Holocene glacial oscillations in the Tyroler Valley (NE Greenland). *Land Degradation & Development*, 34(9), 2589–2606. <https://doi.org/10.1002/ldr.4633>.

Received: 28 August 2022 | Revised: 28 December 2022 | Accepted: 1 February 2023

DOI: 10.1002/ldr.4633

RESEARCH ARTICLE

WILEY

Holocene glacial oscillations in the Tyroler Valley (NE Greenland)

Julia Garcia-Oteyza Ciria¹  | Marc Oliva¹  | David Palacios²  |
 José M. Fernández-Fernández² | Irene Schimmelpfennig³ | Alicia Medialdea⁴ |
 Marcelo Fernandes⁵ | Santiago Giralt⁶ | Vincent Jomelli³ | Dermot Antoniades⁷ |
 ASTER TEAM^{3,8}

¹Department of Geography, Universitat de Barcelona, Barcelona, Spain²Department of Geography, Universidad Complutense de Madrid, Madrid, Spain³Aix-Marseille Université, CNRS, IRD, INRAE, Coll. France, UM 34 CEREGE, Aix-en-Provence, France⁴National Research Centre on Human Evolution (CENIEH), Burgos, Spain⁵Centre for Geographical Studies, IGOT, Universidade de Lisboa, Lisbon, Portugal⁶Geosciences Barcelona (GEO3BCN-CSIC), Barcelona, Spain⁷Department of Geography & Centre for Northern Studies, Université Laval, Quebec, Québec, Canada⁸Consortium: Georges Aumaitre, Karim Keddadouche

Correspondence

Julia Garcia-Oteyza Ciria, Department of Geography, Universitat de Barcelona, Montalegre 6-8, 3r floor, Barcelona 08001, Spain.
 Email: juliagarciaoteyza@ub.edu

Funding information

Agència de Gestió d'Ajuts Universitaris i de Recerca of the Government of Catalonia; research group ANTALP (Antarctic, Arctic, Alpine Environments; 2017-SGR-1102); Spanish Ministerio de Economía y Competitividad; Spanish Ministry of Science, Innovation and Universities

Abstract

Although the spatiotemporal oscillations of the Greenland Ice Sheet (GrIS) during the last millennia have played a prominent role in global environmental changes, its glacial response to the natural variability still needs to be better constrained. Here, we focused on the reconstruction of the glacial behavior and deglaciation process along the Tyroler Valley (74° N, 22° E), within the Northeast Greenland National Park. This NW-SE valley connects with the GrIS via the Pasterze Glacier and divides two ice caps (A.P. Olsen Land and Payer Land), this last one feeding two piedmont glaciers (Copeland and Kløft glaciers). For this study, we combined the interpretation of the spatial pattern of geomorphological features and the chronological framework defined by a new dataset of 15 ¹⁰Be cosmic-ray exposure (CRE) ages from glacially polished bedrock surfaces and moraine boulders together with one optically stimulated luminescence (OSL) age of a glaciolacustrine deposit. CRE ages indicate that the deglaciation of the lowest parts of the valley and the exposure of the highest slopes took place during the Early Holocene, at ca. 10–8.5 ka (ka = thousand year [BP]). Furthermore, this ice thinning also favored the disconnection of the valley tributary glaciers. Samples from the moraines of the two tributary glaciers indicate that the deglaciation was not continuous, but it was interrupted by at least three phases of glacial advance during the Neoglacial cooling (before ca. 5.9 ka), and the Little Ice Age

(LIA, 0.6, and 0.3 ka). The larger piedmont glacier (Copeland Glacier) occupied the valley floor during these major advances, damming the river and allowing the formation of a proglacial glacial lake upvalley, as confirmed by the OSL date of lacustrine sediments that yielded an age of 0.53 ± 0.06 ka. In short, our study provides new evidence of the relative stability of GrIS and the regional ice caps in the area, in which glacial fronts have been rather stable since their advances during the Neoglacial and the LIA.

KEYWORDS

cosmic-ray exposure dating, glacial oscillations, Greenland, Holocene, little ice age, Tyroler Valley

1 | INTRODUCTION

Spatio-temporal oscillations of the Greenland Ice Sheet (GrIS) have played a prominent role in global environmental changes since the last glacial cycle. At present, the GrIS is a mostly land-based ice mass that stores water equivalent to a ca. 7.2–7.4 m sea level rise (Aschwanden et al. 2019; Bamber et al. 2013), and it is the only Northern Hemisphere ice sheet to have persisted during the last deglacial period. Fluctuations of the ice stored in the GrIS, as well as in the surrounding ice caps and mountain glaciers, promote a large-scale redistributions of oceanic and atmospheric circulation patterns, sea-level changes, redefinition of coastlines, shifts in land cover and ecosystems, and variations in greenhouse gas concentrations (Oliva et al. 2021).

A wide range of terrestrial and marine records from Greenland and the North Atlantic region have shown evidence of abrupt temperature shifts during Termination-1 (T-1; ca. 19–11 ka) that ranged from 5 to 15°C and also featured strong seasonality (Buizert et al. 2014; Vasskog et al. 2015). Such oscillations of the GrIS and other peripheral glaciers during T-1 have been modeled in palaeoglaciological studies (Funder et al. 2011; Vasskog et al. 2015) and have been largely documented based on geomorphological and geochronological data, including the NE sector of Greenland (Biette et al. 2020; Håkansson et al., 2007, 2009, 2011; Kelly et al., 2008; Larsen et al., 2018; Lowell et al., 2013; Skov et al., 2020).

Following T-1, the Northern Hemisphere reached the maximum Holocene insolation in summer (Ressen et al., 2009) and temperatures ca. 2.5°C warmer than present (Axford et al., 2021; Kaufman et al. 2004) were recorded during the Holocene Thermal Maximum (HTM; ca. 10–6 ka; Rensen et al., 2009, 2012). The HTM has been documented in a wide range of paleoenvironmental records in Greenland (Briner et al., 2016; Buizert et al., 2018; Kjær et al., 2022; Vinther et al., 2008; Lusas et al., 2017). Glacier fronts across the GrIS responded to this warm event by receding tens of kilometres within present-day margins during the Early and Mid-Holocene (Kelly et al., 2008). For NE Greenland, most studies suggest an intense deglaciation during late T-1 and the Early Holocene, and since then glaciers have recorded minor advances or retreats depending on the prevailing climate conditions (Adamson et al., 2019; Biette et al., 2020; Garcia-Oteyza et al., 2022).

A cooling trend with relatively high climatic variability occurred in the High Arctic region following the HTM. Although the spatial and temporal patterns of the Holocene glacier advances and retreats are still uncertain, this is particularly true for the Neoglacial time span (starting after ca. 6 ka; Porter & Denton, 1967; McKay et al., 2018; Palacios et al., 2020). The Little Ice Age (LIA; ca. 1300–1850 CE; Grove, 2001) was the last period with documented widespread glacial expansion in NE Greenland (Kjær et al. 2022), as demonstrated by the direct dating of glacial records by means of cosmic-ray exposure (CRE) dating (Biette et al. 2020; Garcia-Oteyza et al. 2022; Jomelli et al. 2022) or even by historical pictures provided by early travellers or hunters that show glaciers larger than those of the present during the late 19th and early 20th centuries in this region (Boyd 1948; Payer 1876).

The deglaciation process at the edges of the Payer Land and A.P. Olsen Land ice caps (NE Greenland) where this research focuses is still poorly understood. Previous research has demonstrated that the major deglaciation took place at the end of T-1 (Garcia-Oteyza et al. 2022). However, knowledge of glacial oscillations during the Holocene is sparser, as studies only report the final deglaciation of the lowest parts of the valleys at ca. 10.5 ka (i.e., Zackenberg; Garcia-Oteyza et al., 2022) with two periods of moraine formation at ca. 11.3 and 10.8 ka and minor Holocene glacial advances at ca. 3.3, 1.2, and 0.4 ka (Clavering Island; Biette et al. 2020; Jomelli et al. 2022).

The objective of this study was to chronologically constrain glacial oscillations in the Tyroler Valley during the Holocene, with a particular focus on the Neoglacial period, to shed light on the prevailing climate regime and environmental response in the region, where this knowledge is still lacking. To this end, we had the following specific objectives:

- To identify landforms generated by glacial oscillations in the Tyroler Valley since the Early Holocene.
- To identify the main phases of glacial expansion and associated environmental implications during the Late Holocene.
- To compare spatio-temporal patterns of neoglacial fluctuations in the Tyroler Valley with those inferred from other regions across Greenland.

This is an open access article under the terms of the [Creative Commons Attribution-NonCommercial-NoDerivs](https://creativecommons.org/licenses/by-nc-nd/4.0/) License, which permits use and distribution in any medium, provided the original work is properly cited, the use is non-commercial and no modifications or adaptations are made.

© 2023 The Authors. *Land Degradation & Development* published by John Wiley & Sons Ltd.

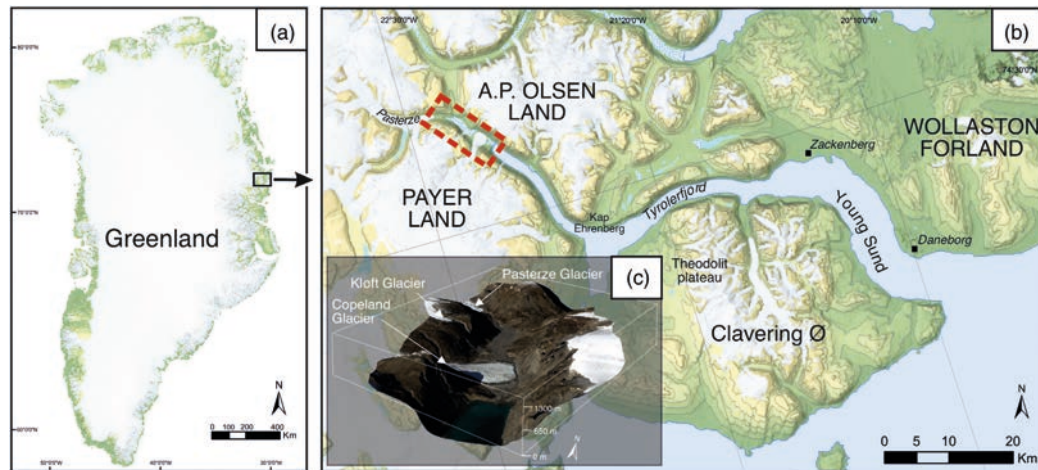


FIGURE 1 (a) Location of the study area within Greenland; (b) regional setting of the Tyroler Valley, with (c) a 3D representation of the study area. [Colour figure can be viewed at [wileyonlinelibrary.com](https://onlinelibrary.wiley.com)]

2 | REGIONAL SETTING

The Tyroler Valley (74° 39' N, 22° 15' W), constitutes an ice-free area forming the unsubmerged continuation of Tyroler Fjord, situated in NE Greenland, within the Northeast Greenland National Park (Figure 1a). The fjord encircles the NW fringe of Clavering Island and extends inland to the NW between Payer Land and A.P. Olsen Land ice caps. The only human infrastructure in the Tyroler Valley is a hunting hut at the entrance of the valley, which is located ca. 50 km north-west of the Zackenberg Research Station (Figure 1b).

The study area encompasses ca. 10 km NW-SE long and an average width of 1 km, from the mouth of the Tyroler Fjord until the front of the Pasterze Glacier, which drains from the GrIS. Two tributary piedmont glaciers (Kluft and Copeland) descend along the NW slopes of the valley from the Payer Land ice cap and spread across the Tyroler Valley floor, occasionally interrupting the drainage of the river during glacial advances (Figure 1c). The surrounding flat-topped summits rise on either side to between 1000 and 1300 m above sea level (hereafter referred to as sl) and connect with steep hillsides descending into the valley. The ice-free areas of the valley floor mainly correspond to an outwash plain, with sediments deposited by a fluvial braided system fed by the Pasterze Glacier meltwater as well as by other proglacial streams. The high sediment load transported by the river has created a delta in contact with the Tyroler Fjord (Figure 1c).

Quaternary sediments cover the valley floor and the lower parts of the hillsides and metamorphic bedrock (Proterozoic orthogneiss and migmatitic sedimentary rocks) is mostly exposed on the upper sections of the slopes (Henriksen & Higgins, 2008). The deglaciated area in Tyroler Valley is underlain by continuous permafrost, probably 200–400 m thick, as observed in nearby Zackenberg Valley (Christiansen et al., 2008; Christoffersen et al., 2008; Hansen et al., 2008).

The study area is characterized by a typical High Arctic polar tundra climate (Kottek et al., 2006). The mean annual air temperature (MAAT) is -9.0°C at the nearby Zackenberg Research Station, with mean monthly values ranging between -19.8°C in February and 6.3°C in July (1996–2015 series; Pedersen, 2017). Mean annual precipitation is 367 mm (Pedersen, 2017) that mostly falls as snow, although rain events may occur during the summer months (Hasholt et al., 2008). The fjord remains covered by land-fast sea ice during approximately 9 months per year (Boone et al. 2017). These cold-climate conditions, highly influenced by the East Greenland Current, determine the existence of a High Arctic tundra, with vegetation dominated by dwarf shrub heaths (decreasing in variety and size with elevation), and fell fields on the lower slopes (CAVM Team, 2003).

3 | METHODOLOGY

In this study, we combined geomorphological and geochronological approaches – CRE ^{10}Be and optically stimulated luminescence (OSL) dating, together with historical pictures – to unveil the spatial and temporal patterns of glacial oscillations in the valley. Field work took place in early September 2019, when the snow-free landscape allowed clear identification of geomorphological features as well as the subsequent collection of samples for dating.

3.1 | Geomorphological mapping

Prior to field work, to define the sampling strategy, we created a preliminary geomorphological map based on satellite images with a focus on the main glacial landforms as moraines and polished surfaces. This

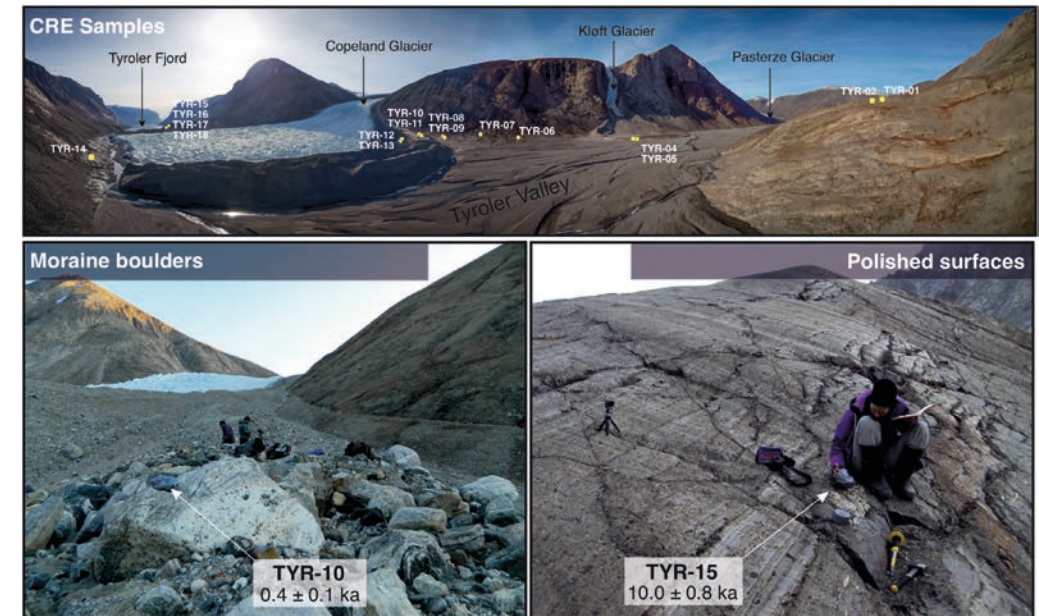


FIGURE 2 Location of all CRE samples and examples of the different types of glacial features sampled in this study. [Colour figure can be viewed at [wileyonlinelibrary.com](https://onlinelibrary.wiley.com)]

map was validated based on in-situ observations and included newly observed landforms. The final geomorphological map was drawn by outlining the landforms in the ARCMAP 10.8 work environment over an orthorectified panchromatic satellite SPOT-6/7 (1.5 m resolution) image from 08-19-2017 and the digital surface model ArcticDEM (2 m spatial resolution) provided by Porter et al. (2018).

3.2 | Sample collection

Considering the geomorphological map and field observations, we collected 18 samples for ^{10}Be CRE dating from two types of glacial features (Figure 2): moraine boulders (11 samples) and polished bedrock surfaces (7 samples). For each sample, we took approximately 1 kg of the rock's most surficial layer (≤ 5 cm thick) using a hammer and chisel and recorded the main field data: geomorphological unit, geographical coordinates, elevation, and the measurements for the subsequent geometric correction of the topographic shielding by the surrounding relief. Field data and sample attributes are listed in Table 1.

In addition, we also collected two samples for OSL dating from an alluvial fan deposit upstream of the Copeland Glacier front (Figure 3). Samples were collected from the upper, middle, and lower parts of this 20-m thick sedimentary deposit composed of fine gravels and coarse sands. To avoid sunlight exposure when collecting the samples, we used a light-proof (opaque) core tube of dark PVC (4 cm diameter).

3.3 | CRE laboratory analytical procedures and age calculation

Sample crushing and sieving (0.25–1 mm fraction) were carried out at the Laboratory of Physical Geography of the Universidad Complutense de Madrid, Spain. Further physical and chemical procedures were conducted at the Laboratoire National des Nucleides Cosmogéniques (LN₂C) of the Centre Européen de Recherche et d'Enseignement des Géosciences de l'Environnement (CEREGE, Aix-en-Provence, France).

Laboratory procedures followed the same protocol and guidelines of our previous work in the area as described in Garcia-Oteyza et al. (2022). A small change in the procedure was made before performing the magnetic separation, with a first leaching of a mixture of hydrochloric (HCl), hexafluorosilicic (H_2SiF_6) and hydrofluoric (HF) acids, in order to facilitate the quartz isolation process and to start the physical separation of quartz/non-quartz minerals with a more concentrated sample. The measurement of the $^{10}\text{Be}/^9\text{Be}$ ratios on the BeO targets were performed at the French 5 MV 'Accélérateur pour les Sciences de la Terre, Environnement et Risques' (ASTER) the facility at CEREGE, using the same calibrations and standards previously described in Garcia-Oteyza et al. (2022). Some samples yielded relatively high uncertainties (TYR-02, TYR-06) due to low current values, and one provided a non-valid measurement (TYR-03) and were thus considered chemical outliers and discarded

TABLE 1 Sample locations, topographic shielding factor, and sample thickness.

Sample ID	Landform	Latitude (dd)	Longitude (dd)	Elevation (m asl)	Topographic shielding factor (dimensionless)	Thickness (cm)
<i>Upper valley roche moutonnée</i>						
TYR-01	Polished surface	74.6415	-22.1791	280	0.9938	2
TYR-02	Polished surface	74.6372	-22.1815	241	-	4
<i>Kløft Glacier external moraine</i>						
TYR-03	Lateral moraine	74.6336	-22.2080	136	-	4
TYR-04	Lateral moraine	74.6335	-22.2080	134	0.9807	4
TYR-05	Lateral moraine	74.6329	-22.2088	134	0.9807	4
<i>Middle valley polished surface</i>						
TYR-06	Polished surface	74.6298	-22.2123	135	-	3.8
TYR-07	Polished surface	74.6254	-22.2018	153	0.9872	2.5
<i>Copeland Glacier</i>						
<i>External moraine</i>						
TYR-08	Lateral moraine	74.6232	-22.1987	164	0.9873	3
TYR-09	Lateral moraine	74.6231	-22.1987	164	0.9873	3.2
<i>Middle moraine</i>						
TYR-10	Lateral moraine	74.6234	-22.1913	172	0.9871	3.4
TYR-11	Lateral moraine	74.6233	-22.1914	170	0.9871	3.5
<i>Internal moraine</i>						
TYR-12	Lateral moraine	74.6264	-22.1815	129	0.9699	3.5
TYR-13	Lateral moraine	74.6264	-22.1813	131	0.9699	2.7
<i>Frontal Copeland polished surface</i>						
TYR-14	Polished surface	74.6294	-22.14685	45	0.9754	2.0
<i>Fjord entrance_upper roche moutonnée</i>						
TYR-15	Polished surface	74.6053	-22.1043	150	0.9890	5.0
<i>Fjord entrance moraine</i>						
TYR-16	Lateral moraine	74.6059	-22.1068	120	0.9813	5
TYR-17	Lateral moraine	74.6059	-22.1070	120	0.9813	3.5
<i>Fjord entrance_lower roche moutonnée</i>						
TYR-18	Polished surface	74.6066	-22.1060	100	0.9779	5

Note: Highlighted in italics: samples with a non-valid AMS measurement, considered chemical outliers and discarded for exposure age calculations and discussion.

for further exposure age calculations and discussion. All analytical data are shown in Table 2.

Exposure ages were calculated with the CRONUS-Earth online calculator, version 3.0 (Balco et al., 2008; <https://hess.ess.washington.edu/>), with the Arctic-wide sea-level/high-latitude ^{10}Be production rate ($3.96 \pm 0.15 \text{ atoms g}^{-1} \text{ yr}^{-1}$) (Young et al. 2013) and the "Lm" (Lal/Stone) time-dependent scaling model (Lal 1991; Stone 2000). For all samples, a 2.7 g cm^{-3} density was assumed, and no corrections of erosion or snow shielding were applied and the partial shielding effect of the surrounding topography was corrected for all sampling sites using the Topographic Shielding Calculator

version 2 (http://stoneage.ice-d.org/math/skyline/skyline_in.html) (Table 2).

3.4 | OSL laboratory analytical procedures

The two collected samples for OSL dating were treated at the luminescence laboratory of the National Research Centre on Human Evolution (CENIEH, Burgos, Spain), under controlled light conditions to extract quartz grains of 90–250 μm size. These were used for OSL measurements to estimate the burial dose. Luminescence

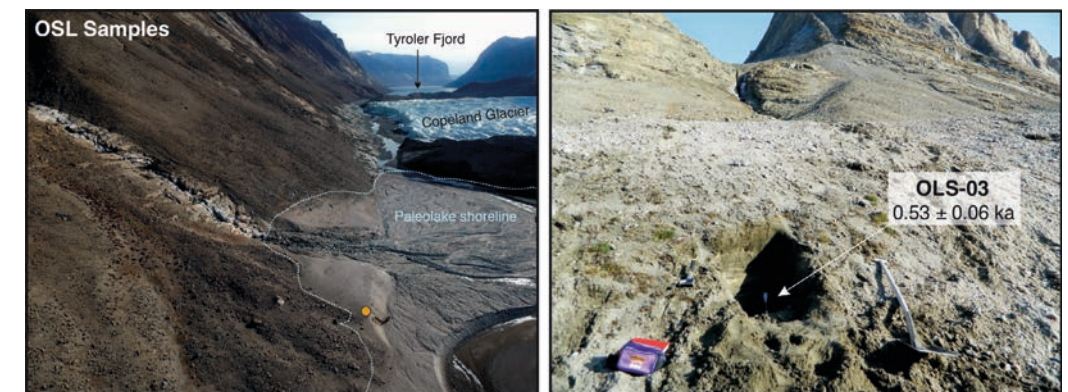


FIGURE 3 Location and picture of the OSL sample site. [Colour figure can be viewed at wileyonlinelibrary.com]

measurements were carried out in a Risø OSL/TL reader (TL-DA 20) equipped with a built-in beta source.

The radionuclide activities measured by high-resolution gamma spectrometry (Table 3) at the Radioisotopes Unit of the University of Sevilla were used to calculate the annual dose rate by applying conversion factors from (Guérin et al., 2011). The contribution from cosmic rays was calculated according to Prescott and Hutton (1994) and attenuation caused by water content was taken into account. Total annual dose rates were determined using 'DRAC' (dose rate and age calculator, Durcan et al., 2015) and are summarized in Table 4.

The luminescence signal from sample TYROSL-2 was dim and the poor signal-to-noise ratio did not allow the estimation of an equivalent dose. In contrast, quartz multi-grain aliquots of sample TYROSL-3 showed a well-defined luminescence signal, and despite showing a slow decay, the dose recovery test indicated that a given dose could be recovered within 1-sigma. The dose distribution derived from the measurement of 48 aliquots was normally distributed (Figure 4). The population of the dose was reduced by excluding outliers (values outside 1.5-times the interquartile range) from the estimation of the equivalent dose which was done applying the central age model (CAM; Galbraith et al. 1999). The estimated burial dose and derived age are summarized in Table 4.

3.5 | Historical data

The Tyroler Fjord area is the site of an extensive scientific and non-scientific exploration history framed within the first European expeditions in NE Greenland carried out during the 19th and first half of the 20th centuries (Rule et al. 2005). The texts and pictures provided in those early surveys included descriptions of the landforms and processes in the region. Two expeditions in particular described in detail the features in the Tyroler Valley, particularly the glaciers: The Second German North Pole expedition of 1869–70 led by Karl Koldewey (Payer 1876) and the Louise A. Boyd's Arctic expedition of 1937

(Boyd 1948). The comparison of the data in these documents with the present-day glacier fronts allowed us to establish the magnitude of ice recession since the end of the LIA.

4 | RESULTS

4.1 | Geomorphological setting

The Tyroler Valley is a U-shaped glacial valley that is mostly deglaciated, but is also occupied by one large piedmont glacier (Copeland Glacier) that covers a large portion of the lower valley floor. The valley is surrounded by several ice caps on its NE (A.P. Olsen Land) and SW (Payer Land) fringes, and connects with the GrIS via the Pasterze Glacier at the western end of the valley (Figure 5). Current glaciers display a clear asymmetry between the opposite slopes of the valley, with well-developed ice tongues forming piedmont glaciers on NE slopes fed by the ice sheet that caps the Payer Land, and much shorter or almost non-existent tongues on the steep NW slopes descending from the A.P. Olsen Land ice cap. The Copeland Glacier (Figure 5) is currently the only glacier reaching the valley bottom, where it has generated a complex moraine system with several ridges surrounding the margins and with its front at present being ca. 100 m away from the opposite hillside (left slope) of the valley. This tongue descends from the Payer Land Ice Cap through a steep and narrow valley for ca. 5 km, and it is on average 700 m wide. Field work allowed the identification of a wide range of Tyroler Valley geomorphological landforms.

The terminal lobe of the piedmont glacier (ca. $2 \times 1.5 \text{ km}$ and 3.5 km^2) is surrounded on both sides by similarly shaped moraine complexes with their outer flanks standing 30 to 50 m above the outwash plain and with a maximum slope of 35° . The lobe's front consists of a 15 m (on average) high ice cliff with a calving base washed out by the river. The Kløft Glacier (Figure 5) echoes its larger neighbor in source and distance from it but does not reach the valley bottom at

TABLE 2 AMS analytical data and calculated exposure ages.

Sample name	Quartz weight (g)	Mass of carrier (⁹ Be mg)	¹⁰ Be/ ⁹ Be (10 ⁻¹⁴)	Blank correction (%)	[¹⁰ Be] (10 ⁴ atoms g ⁻¹ ± 1σ (atoms g ⁻¹))	¹⁰ Be age (ka) ^a	Internal uncertainty (ka)	External uncertainty (ka)
<i>Upper valley roche moutonnée</i>								
TYR-01	43.6794	0.44135	7.805 ± 0.402	2.91	5.116 ± 0.273	9.2	0.6	0.5
<i>Kløft Glacier external moraine—Arithmetic mean age: 0.3 ± 0.2 ka (n = 2)</i>								
TYR-04	33.0422	0.44259	0.371 ± 0.044	62.51	0.125 ± 0.049	0.3	0.1	0.1
TYR-05	32.0741	0.44307	0.375 ± 0.077	60.30	0.138 ± 0.08	0.3	0.2	0.2
<i>Middle valley polished surface</i>								
TYR-07	37.1995	0.15035	5.553 ± 0.216	3.51	4.537 ± 0.178	9.3	0.4	0.5
<i>Copeland Glacier</i>								
<i>External moraine</i>								
TYR-08	40.6263	0.45290	1.034 ± 0.06	21.92	0.602 ± 0.05	1.3	0.1	0.1
TYR-09	38.4679	0.45284	8.537 ± 0.266	2.66	6.537 ± 0.211	13.8	0.4	0.7
<i>Middle moraine—Arithmetic mean age: 0.6 ± 0.2 ka (n = 2)</i>								
TYR-10	40.2721	0.44740	0.486 ± 0.056	46.17	0.194 ± 0.052	0.4	0.1	0.1
TYR-11	35.7175	0.44368	0.656 ± 0.063	34.46	0.357 ± 0.062	0.7	0.1	0.1
<i>Internal moraine—Arithmetic mean age: 0.3 ± 0.2 ka (n = 2)</i>								
TYR-12	35.7226	0.44861	0.366 ± 0.035	62.58	0.115 ± 0.04	0.3	0.1	0.1
TYR-13	36.1246	0.44927	0.318 ± 0.038	71.97	0.074 ± 0.041	0.2	0.1	0.1
<i>Frontal Copeland polished surface</i>								
TYR-14	30.7325	0.44870	3.144 ± 0.117	7.28	2.844 ± 0.119	5.9	0.2	0.3
<i>Fjord entrance_upper roche moutonnée</i>								
TYR-15	14.9181	0.44915	2.728 ± 0.195	8.38	5.029 ± 0.398	10.0	0.8	0.9
<i>Fjord entrance moraine</i>								
TYR-16	22.7161	0.45045	3.156 ± 0.12	6.23	3.921 ± 0.164	8.3	0.3	0.5
TYR-17	40.5580	0.44973	49.44 ± 1.535	0.46	36.464 ± 1.138	77.4	2.5	3.8
<i>Fjord entrance_lower roche moutonnée</i>								
TYR-18	31.2899	0.45021	4.245 ± 0.155	4.64	3.892 ± 0.152	8.4	0.3	0.5
Chemistry blank details^b								
Blank name	Mass of carrier (⁹ Be mg)	¹⁰ Be/ ⁹ Be (10 ⁻¹⁴)	[¹⁰ Be] (10 ⁴ atoms)					
BK1	0.45088	0.222 ± 0.04	6.703 ± 1.219					
BK2	0.44576	0.23 ± 0.032	6.862 ± 0.964					
BK3	0.45242	0.196 ± 0.028	5.921 ± 0.832					

Note: ¹⁰Be/⁹Be ratios were inferred from measurements at the ASTER AMS facility. No correction of erosion and snow cover have been made.

^a¹⁰Be ages assuming a density of 2.7 g cm⁻³ and a zero-erosion scenario.

^bIn parallel to the sample treatment, four blanks were prepared: BK1 (processed with samples TYR-01, TYR-05, TYR-06, TYR-10, and TYR-11), BK2

TABLE 3 Radionuclide activity concentration.

Sample	Lab (US) code	Depth (m)	Moisture (%)	⁴⁰ K (Bq/kg ⁻¹)	²³² Th (Bq/kg ⁻¹)	²³⁸ U (Bq/kg ⁻¹)
TYROSL-2	4198	0.4	20	613 ± 25	27.4 ± 1.1	12.3 ± 0.5
TYROSL-3	4199	0.7	20	519 ± 23	33.5 ± 1.3	22.3 ± 1.3

Note: Also shows the depth used to calculate the contribution of cosmic rays to the total dose rate and the moisture. A 5% error have been added to the moisture values.

TABLE 4 Summary of total dose rates for the two samples, estimated burial dose and corresponding age of sample TYR-3 for which OSL measurements were possible.

Sample	Dose rate (Gy/ka)	Burial dose (Gy)	Age (ka)
TYROSL-2	2.44 ± 0.11	X ± X	X ± X
TYROSL-3	2.42 ± 0.11	1.3 ± 0.1	0.53 ± 0.06

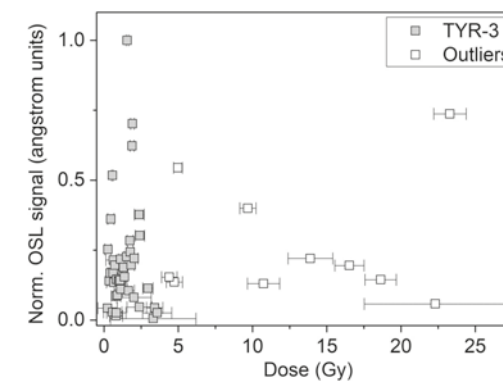


FIGURE 4 Dose distribution derived from the OSL measurement of sample TYR-3. Open icons indicate the identified outliers excluded from the age estimation. The normalized natural OSL signal is plotted as a function of the measured dose and corresponding uncertainty for each individual aliquot.

present. It also descends from the plateau through a deep, narrow gorge that is ca. 1 km long, and is 100 m wide on average. At present, the glacier front remains hanging at the lower-middle part of the slope at ca. 600 m from the external moraine system mapped and ca. 300 m from the internal moraine system.

Finally, at the head of the valley, the Pasterze Glacier flows between steep slopes and there is a frontal moraine 200 m from the current glacier terminus. A large proglacial outwash plain, reshaped by the braided fluvial system, extends from the terminus of the Pasterze Glacier to the external moraines created by the Copeland and Kløft glaciers (Figure 5). In some places along the margins of this plain, glacio-lacustrine sequences of fine-grained sediments have accumulated due to the damming of the valley by the advance of glaciers descending from the slopes.

A wide range of glacial, periglacial, and alluvial landforms is also found on the slopes surrounding the valley floor, with two main domains. Slopes above ~400 m a.s.l. have exposed bedrock and are affected by very intense periglacial conditions (i.e., with the presence of permafrost and frost heave): This setting includes flat-topped summits (at ca. 1000 m asl), mostly covered by ice caps and their outlet tongues. These plateaus connect with the Tyrolean Valley through steep slopes (30° on average), where hanging valleys and scarps can be found. On slopes below ~400 m asl, erosive and depositional glacial landforms are widespread, including glacially polished bedrock surfaces, lateral moraine systems and erratic boulders. In some cases, these glacial features are partially covered by debris slopes, talus cones, and alluvial fans, particularly on the lower sections of the slopes.

The existence of polished bedrock surfaces at between 40 and 300 m above the valley floor is indicative of the ice thickness reached by the glacier in the past. In past glacial phases, the area must have been occupied by a single glacial tongue formed by the coalescence of the Pasterze Glacier and other tributaries descending from both the Payer Land and A.P. Olsen Land ice caps. Next to the fjord, at the lowest part of the valley, there is a roche moutonnée (ca. 150 m high) that was sampled for CRE dating to establish the onset of deglaciation of the Tyrolean Valley. In this sector, we collected four samples: one from the highest exposed bedrock surfaces ca. 150 m a.s.l. (TYR-15), another from the lower part of the bedrock ca. 100 m a.s.l. (TYR-18), and two from scattered moraine boulders in the middle part of the slope ca. 120 m a.s.l. (TYR-16 and TYR-17). This moraine located at the entrance of the valley from the fjord represents the most distal remnants of a lateral moraine stretching along the valley's slopes, with no signs of reworking on its right hillside (Figure 5).

We also took two samples from a roche moutonnée located on the left valley side, upstream of the Copeland Glacier, to reconstruct the glacier's past recession and thinning: one near the culmination of the bedrock surface (TYR-1) and the other ca. 40 m lower (TYR-2). On the other side of the valley, between Copeland and Kløft glaciers, two polished and striated gneiss surfaces at the foot of the slope were targeted (TYR-6 and TYR-7) to determine the time of individualization of these two glaciers.

The valley also includes geomorphic evidence of potentially recent glacial oscillations near the termini of the Copeland and Kløft glaciers. The former created a complex moraine system, with two main polygenic lateral moraines on the southern side and up to five ridges on the northern margin of the glacier, where we focused the sampling strategy: (i) Two samples were taken from the most external ridge (TYR-8 and TYR-9), which shows stable slopes as suggested by

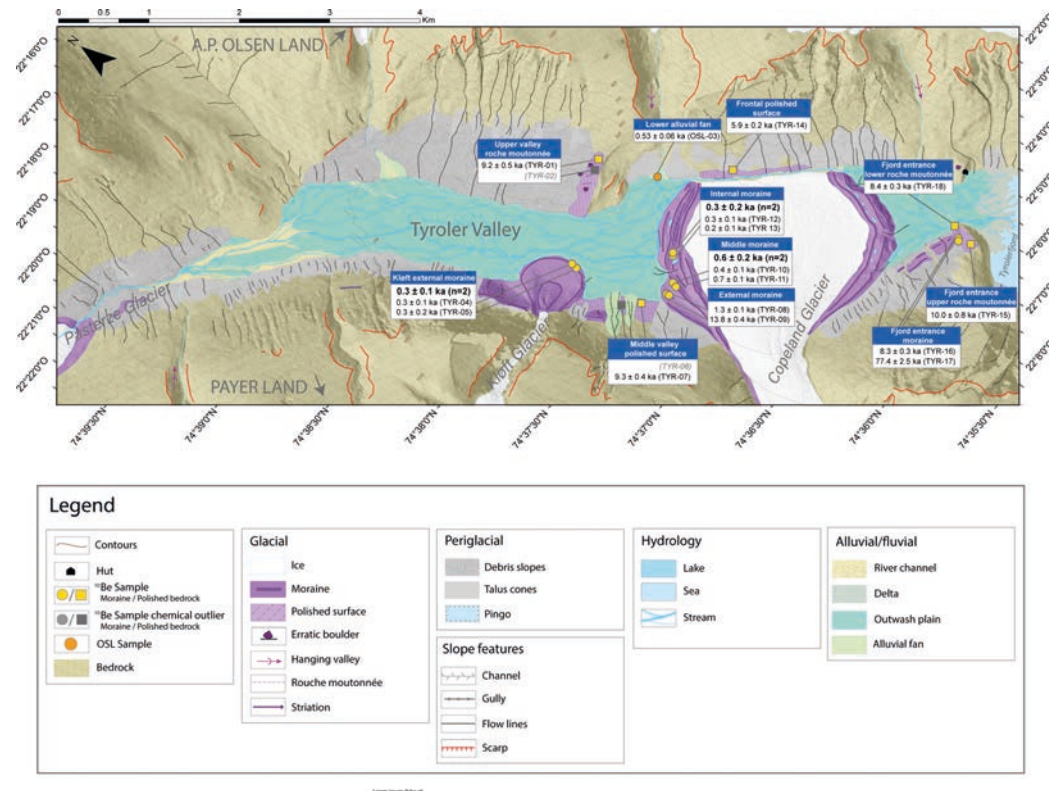


FIGURE 5 Geomorphological map including the main landforms together with the CRE and OSL results. [Colour figure can be viewed at wileyonlinelibrary.com]

the presence of mosses; (ii) Two more samples (TYR-10 and TYR-11) were taken from the middle and more voluminous unvegetated ridge; and (iii) two further samples (TYR-12 and TYR-13) were obtained from an internal moraine crest. The two moraine ridges next to the glacier were ice-cored features and were thus not sampled to avoid unexpected ages associated with ongoing stabilization as the inner ice core melts. These lateral moraines do not extend over the frontal part of the glacier, which is very close to the opposite slope. The existence of polished and striated bedrock devoid of unconsolidated sediments on the lower part of the slope (from the riverbed level to 50 m above it) in front of the Copeland Glacier terminus reveals the occurrence of past periods of glacial expansion. One sample (TYR-14) was obtained from this polished surface. Past phases of glacier expansion favored the formation and evolution of glacier-dammed lakes. River drainage must have been blocked in the past due to the expansion of the Copeland Glacier across to the opposite valley slope, causing the formation of a proglacial lake extending over much of the present-day outwash plain fed by the meltwater stream from the Pasterze Glacier and other tributaries. This lake's level would have fluctuated depending on the

glacier volume blocking the valley. Its last maximum advance favored the development of its maximum paleo-shoreline level of ca. 151 m above the present-day valley bottom. This paleo-shoreline is widely continuous along the valley and is defined by horizontal layers of fine-grained silt and clay-sized sediments, although in some areas it has been eroded or disturbed by streams and mass wasting processes. Indeed, lateral streams formed alluvial fans upon contact with the hypothesized paleolake that must have been frozen several months per year. This is the case of the alluvial fan formed by the stream draining the Olsen Land ice cap on the NW edge of the Copeland Glacier (Figure 3) that is composed of two terraces of fine-grained sediments (mostly sands and small gravels). Two samples were taken for OSL dating of the middle (TYROSL -02) and lower (TYROSL -03) parts of the deposit.

The two moraine systems of the Kløft Glacier extend across the valley floor, with the external moraines being of greater size than the inner ones and showing evidence of the piedmont character of the glacier when they were formed. We collected three samples from the external frontal moraine arch to establish the phase of its maximum

expansion (TYR-3, TYR-4, and TYR-5). The inner arched moraine complex is located at the foot of the slope, with a 5-m high frontal moraine arch; inside, the area is filled with fine-grained sediments deposited by an active alluvial fan from the meltwater stream of the Kløft Glacier.

4.2 | Geochronological data

The location and the chronological data of the samples are presented in Figure 5. CRE results show evidence of the occurrence of past periods during the Holocene with larger glacial systems than today. The lower area of the Tyroler Valley was deglaciated during the Early Holocene, as indicated by samples from the highest surfaces of the roche moutonnée aged 10.0 ± 0.8 ka (TYR-15) and the lower surface at 8.4 ± 0.3 ka (TYR-18). Two boulders of the moraine constrained between these surfaces yielded exposure ages of 8.3 ± 0.3 ka (TYR-16) and 77.4 ± 2.5 ka (TYR-17) respectively. The sample collected from the roche moutonnée located in the middle part of the valley yielded an exposure age of 9.2 ± 0.6 ka (TYR-01), and of the two samples taken from polished surfaces between the Kløft and Copeland glaciers, only one returned a valid age of 9.3 ± 0.4 ka (TYR-07).

The sample obtained from the polished surface on the slope opposite the Copeland Glacier returned an exposure age of 5.9 ± 0.2 ka (TYR-14). In general, more recent ages were obtained from boulders of the Copeland Glacier moraine system: (i) two boulders from the external moraine ridge returned ages of 1.3 ± 0.1 ka (TYR-08) and 13.8 ± 0.4 ka (TYR-09); (ii) two boulders from the middle moraine ridge yielded ages of 0.4 ± 0.1 ka (TYR-10) and 0.7 ± 0.1 ka (TYR-11) with a mean age of 0.6 ± 0.2 ka; and (iii) two moraine boulders of the inner ridge reported ages of 0.3 ± 0.1 ka (TYR-12) and 0.2 ± 0.1 ka (TYR-13), with a mean age of 0.3 ± 0.2 ka (Figure 5).

The samples collected from the external moraines of the Kløft Glacier were aged 0.3 ± 0.1 ka (TYR-04) and 0.3 ± 0.2 ka (TYR-05), with a mean of 0.3 ± 0.2 ka. Finally, the only available OSL age estimated from the samples taken from the glacio-lacustrine deposit on the left side of the valley gave an age of 0.53 ± 0.06 ka (TYROSL -03).

5 | DISCUSSION

The combined interpretation of the spatial pattern of geomorphological features and the chronological framework defined by CRE and OSL ages enabled the reconstruction of the spatio-temporal glacial oscillations in the Tyroler Valley.

5.1 | Considerations on the geochronology dataset prior to interpretation

Some CRE ages must be interpreted with caution as, apparently, they do not follow the expected chronostratigraphical sequence. TYR-09

(13.8 ± 0.4 ka), collected from the external lateral moraine ridge of the Copeland Glacier, had a much older exposure age than the other boulder of the same moraine system (TYR-10). Although this moraine ridge seemed geomorphologically stable, the CRE age may indicate nuclide inheritance in this boulder, probably associated with insufficient reworking given the proximity of the moraine to the upper sections of exposed bedrock that supply debris to the glacier. TYR-17 (77.4 ± 2.5 ka), from a moraine boulder at the valley entrance, also returned a much older exposure age than expected relative to the ages obtained in the valley. The moraine's age as constrained by two samples of the exposed bedrock surface from the upper and lower parts of the roche moutonnée (TYR-15, 10.0 ± 0.8 ka; TYR-18, 8.4 ± 0.3 ka) fits reasonably well with the other sample collected from this landform (TYR-16; 8.3 ± 0.3 ka). The moraine ridge was defined by dispersed boulders forming a line on a relatively horizontal step of the exposed bedrock; while the subrounded morphology of the TYR-17 boulder suggests that it was efficiently reworked during englacial transport, its CRE age indicated that the boulder retained an inheritance signal from past deglacial phases. The horizontal plateau surfaces of the ice caps must favor the existence of cold-based glaciers with reduced erosion capacity, which may also help explain the occurrence of nuclide concentrations inherited from previous exposure phases. As such, these two samples were not considered when establishing the geomorphological evolution in this valley, which thus includes 13 ¹⁰Be CRE samples of Holocene age ranging from 10.0 ± 0.8 (TYR-15) to 0.2 ± 0.1 ka (TYR-13) (Figure 6).

5.2 | Deglaciation chronology

The oldest moraine (TYR-16) as well as the glacially polished surfaces distributed across the valley were of Early-Middle Holocene age. The remaining ages, from moraine boulder samples, were of Late Holocene age (Figure 7). Based on the geomorphological and geochronological evidence, we identify three major glacial phases in Tyroler Valley during the Holocene:

1. Glacial occupation of the valley

The presence of glacially polished surfaces from ca. 300 m above the valley floor demonstrates that the area was heavily glaciated during the last glacial cycle (Figure 7). The entire valley was probably filled by ice to the mountain tops, similar to what occurred in neighbouring valleys tens of km beyond the current glacier fronts where ice thicknesses reached ca. 800 m asl (Garcia-Oteyza et al., 2022). The expansion of the GrIS as well as of the surrounding ice caps during the last glacial cycle has been already documented in several regions of NE Greenland. Prior to the Last Glacial Maximum (LGM), between 115–75 ka glacier fronts reached the inner shelf (Funder et al., 2011; Lecavalier et al. 2014). The Tyroler Valley must therefore have been occupied by one large glacial system fed by several tributaries descending from the GrIS, as well as from the Payer Land and A.P. Olsen Land ice caps, which were connected at that time.

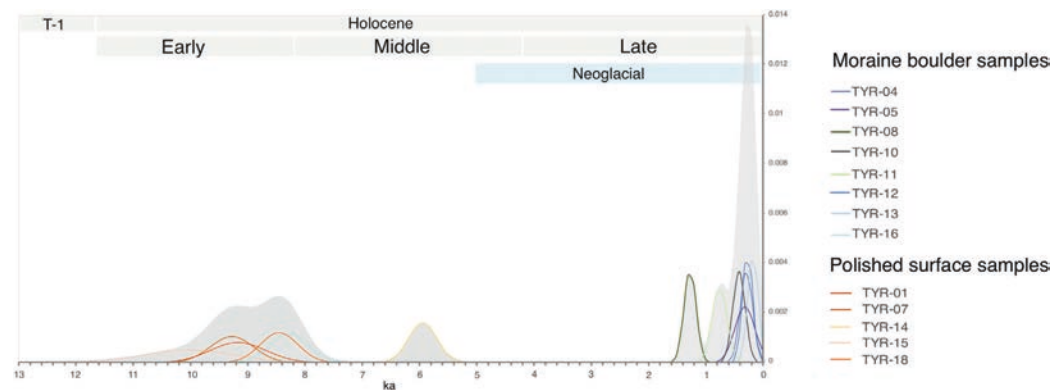


FIGURE 6 Probability distribution functions of ¹⁰Be ages with (with external uncertainties) for all the samples of our final accepted age dataset (TYR-09 and TYR-17 were not considered). [Colour figure can be viewed at wileyonlinelibrary.com]

2. Glacial recession and individualization of ice masses

As temperatures rose more than 20°C in central Greenland during T-1 (Buizert et al. 2018), the glaciers present in Tyroler Valley receded and thinned significantly. As a result, some tributaries disconnected from the main ice stream extending over much of the Tyroler Fjord, as occurred in Zackenberg Valley at 11–10 ka (Garcia-Oteyza et al., 2022) and on the Theodolit plateau (Clavering Island) after ca. 10 ka (Biette et al., 2020). The lowlands of the Tyroler Valley also became ice-free at ca. 10–8.5 ka as suggested by the polished surfaces at the entrance of the valley (10.0 ± 0.8–8.4 ± 0.3 ka) as well as upstream from the Copeland Glacier (9.2 ± 0.5 ka). Indeed, sample TYR-07 indicates that ice thinning favored the disconnection of the Copeland and Kløft glaciers, which occurred at 9.3 ± 0.4 ka. The Early Holocene deglaciation was not continuous, and long-term glacial shrinking was interrupted by at least one period of minor glacier advance or standstill as indicated by the formation of valley side moraines, and by the remnants of moraines of the same phase identified at the upper part of the roche moutonnée (8.3 ± 0.3 ka) (Figure 7). The thinning glaciers progressively exposed the upper slopes of the valley, where paraglacial dynamics started to operate, and shrinking glaciers were supplied with sediments that accumulated on the lower mountain slopes, forming alluvial fans, talus cones, and debris slopes. Since ca. 9–8.5 ka, only two (piedmont) glaciers persisted on the NE side of the valley (Kløft and Copeland), expanding or retreating in response to prevailing climate conditions.

3. Neoglacial and LIA advances

No geomorphic evidence of glacial activity is preserved from the Middle Holocene, between ca. 8 and 6 ka. The only CRE age obtained from the polished bedrock located on the opposite slope of the Copeland Glacier front indicated that a Holocene glacial advance was followed by a retreat at 5.9 ± 0.2 ka. Further CRE ages are needed to

confirm that this glacial advance corresponded to the onset of the neoglacial in the region. Any glacial advances during the last millennia must have been of reduced scope, as suggested by the moraine systems generated by the Copeland and Kløft glaciers that extend between ca. 700 and 100 m from present-day fronts. Whereas the most external moraine of the Copeland Glacier suggests a phase of glacial expansion during the Dark Ages Cold Period (DACP; ca. AD 400–765; Helama et al., 2017) at ca. 1.3 ka – as also reported by Biette et al. (2020) in the neighboring Clavering Island –, the rest of the multiple moraine ridges of these piedmont glaciers reported ages spanning different phases of the LIA, with two major glacial advances at ca. 0.6 ka and 0.3 ka. During these major advances Copeland Glacier occupied the valley floor, damming the river and causing the formation of a proglacial glacial lake, as confirmed by the accumulation of the fine-grained sediments of the alluvial fan aged 0.53 ± 0.06 ka (Figure 7). Glacial retreat after the last LIA advance at ca. 0.3 ka must have favored the drainage of the paleolake. Since that time, glacier fronts fluctuated within limits defined by the dated internal moraines. This pattern of pulses of retreat and advance resulting from post-LIA climatic shifts also been reported in other (sub)Arctic small debris-free glaciers (Fernández-Fernández et al. 2017).

The comparison of the current situation in the valley with pictures from historical expeditions (Figure 8) shows evidence of the glacier retreat in the valley since 1869 CE, when glaciers were much more extensive (Payer 1876). Descriptions and sketches of the valley entrance show an ice barrier close to the fjord and five glacier tributaries descending from the plateaus and feeding the main valley glacier (two glacial tributaries from the A.P Olsen Land, Kløft, Copeland and Pasterze glacial tongues). Pictures taken in 1937 CE during the expedition led by Louise A. Boyd (Boyd 1948) show the position of the Copeland Glacier front, tens of metres beyond its current front. Moreover, the river has washed away the frontal moraine that existed in these pictures (Figure 8). However,

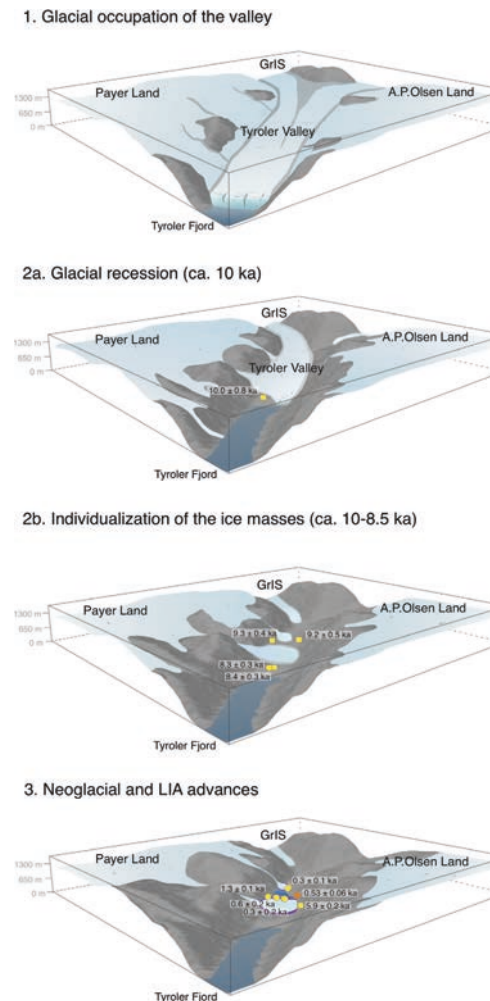


FIGURE 7 Idealized reconstruction model for the glacial evolution of Tyroler Valley and the proposed glacial phases. Base map obtained from the current Digital Elevation Model (Porter et al. 2018). [Colour figure can be viewed at wileyonlinelibrary.com]

the most considerable change is found in the Kløft Glacier, which reached the bottom of the valley in 1937 CE, forming a terminal lobe surrounded by the outermost moraine (Figure 8). Indeed, Google Earth Pro satellite images ranging from 1984 until 2015 (Google Earth Pro 7.3.4.8642 (1984–2015), 74°37'31.99"N, 22°10'03.48"W, elevation 70 m, LANDSAT/COPERNICUS, [Online]. Available at <https://www.google.com/earth/>) show that the front of the Kløft Glacier still formed a lobe in the valley floor inside the inner moraines until ca. 2010, when it began to recede upslope.

5.3 | Glacial oscillations in NE Greenland since termination 1

Holocene climate variability and glacial evolution of Greenland shows complex and diverse spatio-temporal patterns (Briner et al., 2016; Young et al. 2020). Following the temperature evolution reconstructed from the NGRIP 1 and 2 ice cores (Walker et al., 2018), we identify the following phases regarding the glacial evolution in the Tyroler Valley:

5.3.1 | Early Holocene (11.7 to 8.2 ka; Greenlandian)

The maximum Holocene summer insolation in the Northern Hemisphere during the Early Holocene led to the highest summer temperatures (Buizert et al., 2018), initiating the HTM (Renssen et al., 2009). The timing and intensity of the HTM in Greenland show high regional variability, promoting a widespread trend of glacial retreat of both the GrIS and mountain glaciers and ice caps (Axford et al. 2021), only interrupted by short periods of glacial stabilization in some regions (Young et al., 2020). Glacial response in S and W Greenland during the HTM was more diffuse than in the N and E sectors of the island, where the prevailing warmer temperatures promoted a strong glacier retreat during the Early Holocene (Briner et al. 2016).

In summary, broadly across Greenland, the GrIS had already retreated behind present-day boundaries by 10–9 ka and the retreat continued, except during the 8.2 ka cold event (Carlson et al., 2014; Larsen et al., 2015; Reusche et al., 2018; Skov et al. 2020). The valley lowlands of our study area became ice-free and the different tributaries disconnected from the main glacier at ca. 10–8.5 ka, which correlated with the GrIS long-term glacial shrinking during the HTM. One of our samples also shows the interruption of this trend, reporting a minor glacial advance or stillstand with moraine formation at ca. 8.3 ka, which might be associated with the cold peak that occurred at 8.2 ka (Figure 9).

5.3.2 | Middle Holocene (8.2 to 4.3 ka; Northgrippian)

Orbital-induced reduced summer insolation in the Northern Hemisphere promoted a gradual cooling trend in Greenland from 8.2 ka onwards (McKay et al. 2018). Superimposed on this long-term trend, changes in the strength of the Atlantic Meridional Overturning Circulation and other regional forcing mechanisms affected glacial dynamics: ice masses of the North Atlantic region generally retreated significantly during the mid-Holocene and re-advanced in the late Holocene (Jomelli et al. 2022). Summer temperatures fell until 1–1.5 °C below present-day temperatures by the end of the mid-Holocene, albeit with a high degree of variability across Greenland (Lasher and Axford 2019). Consequently, glaciers began to re-advance in what has been called the neoglaciation (Porter 2000). However, as the end

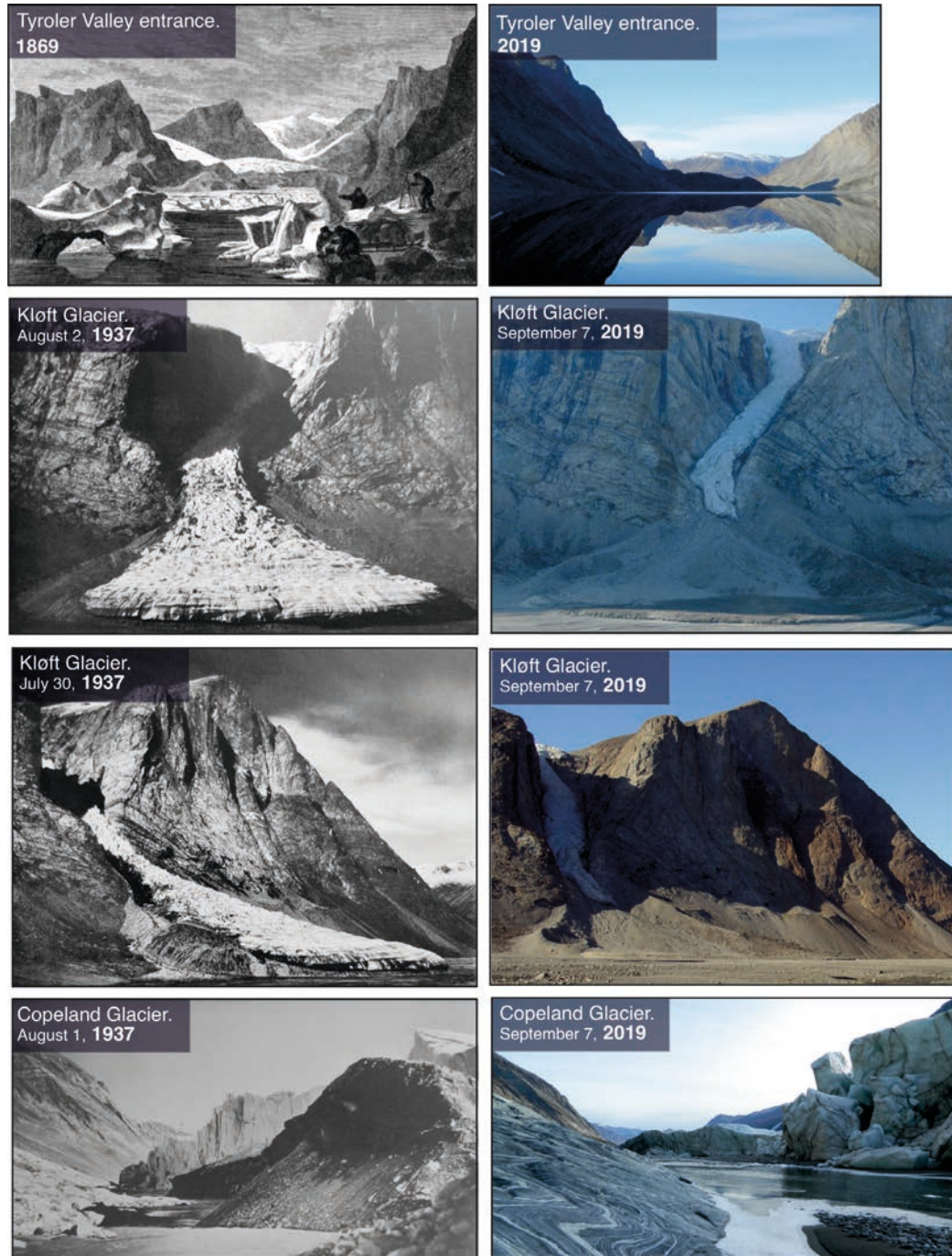


FIGURE 8 Sketch and photographs from historical expeditions (Boyd 1948; Payer 1876) that visited the area compared with modern pictures

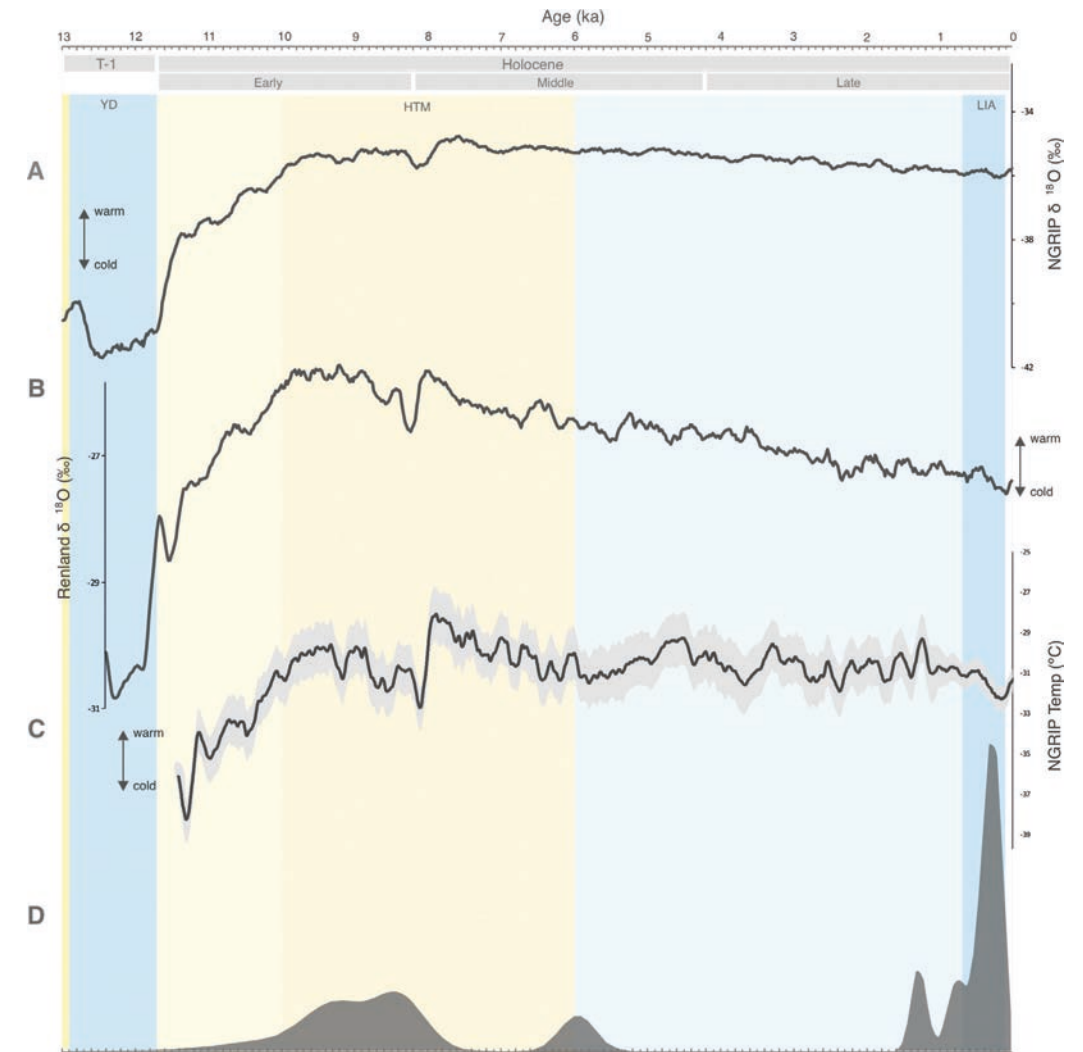


FIGURE 9 (a) $\delta^{18}\text{O}$ record of the NGRIP ice core smoothed with 15 interval moving average (GICC05modelext, 5-point running mean; Rasmussen et al. (2006). (b) $\delta^{18}\text{O}$ record of the ice core from Renland Ice Cap in eastern Greenland with 10 interval moving average (GICC05 timescale) (Vinther et al. 2008). (c) NGRIP ice core reconstructed temperature from argon and nitrogen isotopes (^{15}N - ^{40}Ar), with 2σ error bands (gray shading) and 150 interval moving average (Kobashi et al. 2017). (d) Probability distribution functions of our final dataset of exposure ages. [Colour figure can be viewed at wileyonlinelibrary.com]

of the HTM was time-transgressive across the island, the beginnings of glacial advances show great regional, even local, variability.

The GrlS reached its global minimum Holocene extent at 7 ka, but the retreat of some of its fronts was delayed until 4–3 ka, or even later (Larocca et al., 2020a,b; Larsen et al., 2018; Schweinsberg et al., 2019). Local mountain glaciers and ice caps recorded a similar response pattern to the GrlS to changing Holocene climate trends. In

S Greenland most of the glaciers disappeared between 7.1 and 5.5 ka and began to recover from 3.1 ka to 1.3 ka onwards (Larocca et al., 2020a; Jomelli et al. 2022). In SW Greenland, some glaciers survived throughout the HTM and began to recover from 4.3 ka onwards (Larocca et al., 2020b). In E Greenland, the Renland Ice Cap was smaller than present by 9.5 ka and began to recover at 4 ka (Medford et al., 2021).

In NE Greenland, the Tyroler Valley lacks extensive geomorphic evidence of glacial activity for the Middle Holocene, as was also reported in other studies in the region (Biette et al. 2022). We only detected a phase of glacial advance prior to ca. 5.9 ka that may be associated with the onset of neoglaciation in the area (Figure 9). Since that time, and until ca. 1.3 ka, climate conditions must not have been conducive to periods of major glacial expansion in the valley. It should be noted, however, that the proximity of the glacier front to the opposite hillside hinders the preservation of glacial landforms that may have been deposited during that phase.

5.3.3 | Late Holocene (4.3 ka to present; Meghalayan)

The most widespread neoglaciation advances in Greenland can be grouped into three main periods: at 2.5–1.7 ka, 1.2–0.9 ka, and 1250–1900 CE (Kjær et al., 2022), albeit with a significant regional variability. In W Greenland, glaciers advanced and exceeded their present-day limits at 3.7, 2.8, 1.5 ka, and during the LIA at 1400 and 1700 CE (Schweinsberg et al., 2019). In Inglefield Land, NW Greenland, glaciers remained behind current boundaries from 5.8 ka until the beginning of the LIA at 1450 CE (Søndergaard et al., 2020). The northern GrlS margin also showed a relative stability during the Late Holocene, with only two neoglaciation advances of similar magnitude detected at 2.8 ka and 1650 CE (Reusche et al., 2018). In E Greenland, the Renland Ice Cap exceeded the present limits by 3.3 ka, 1.3 ka, and 1 ka, advancing similarly during the LIA (Medford et al., 2021), and the Bregne Ice Cap in Scoresby Sund recorded the maximum glacial expansion during the LIA at ca. 0.74 ka (Levy et al., 2014).

In NE Greenland, glacial advances were dated in Clavering Island at ca. 3 ka, 1.2 ka, and 0.5 ka based on CRE on moraine boulders (Biette et al. 2020). The analysis of proglacial lake sediments near the Zackenberg Valley (Figure 1) revealed the occurrence of three neoglaciation advances over the last two millennia (Adamson et al., 2019): one occurred at 1.3–1.2 ka during the Dark Ages Cold Period, a second advance took place at ca. 0.8 ka during the Medieval Climate Anomaly, and the last one was associated with the onset of the LIA that showed a smaller advance than the previous ones and peaked at 1250–1400 CE (Adamson et al., 2019). Our records from the Tyroler Valley also showed three main glacial advances for the Late Holocene at ca. 1.3, 0.6 and 0.3 ka, broadly synchronous with previous glacial chronologies as well as with ice core temperature reconstructions in Greenland (Figure 9).

6 | CONCLUSIONS

This study introduces new geomorphological and geochronological data of glacial oscillations in Tyroler Valley, NE Greenland, during the Holocene. Scientific knowledge about the response of glaciers to changing temperature and moisture regimes in Greenland during the present-day interglacial is still incipient. As in other areas in NE Greenland, CRE ages indicate that the deglaciation of the lowest parts of the valley, as well as the exposure of the highest slopes, took place

during the Early Holocene, at ca. 10–8.5 ka. Our data reveal that the GrlS and surrounding ice caps in the area only expanded during neoglaciation advances and the LIA. Prior to this historical phase, the Copeland Glacier recorded two periods of glacial growth before ca. 5.9 ka and at ca. 1.3 ka. Subsequently, both the Copeland and Kløft glaciers expanded during the LIA forming moraines ca. 100–700 m from present-day glacier fronts. Two periods of moraine formation were detected in Copeland Glacier at ca. 0.6 and 0.3 ka, while only one at ca. 0.3 ka was detected for the Kløft Glacier. The expansion of the Copeland Glacier during the LIA dammed Tyroler Valley and caused the formation of a large proglacial lake, as confirmed by glaciolacustrine sediments OSL dated ca. 0.53 ka. Since the last major LIA advance, glacial fronts have oscillated as demonstrated by historical images but have remained relatively close to the LIA moraines.

In summary, our data expands and strengthens the chronology of Holocene glacial oscillations in Greenland, in particular its NE sector where no previous studies have precisely constrained neoglaciation oscillations. Future studies should elucidate whether the chronology of glacial culminations and retreats in the Tyroler Valley over the Mid-Late Holocene represents a local response to prevailing climate conditions or formed part of a more general pattern that occurred across the High Arctic region.

ACKNOWLEDGMENTS

This study was funded by the NEOGREEN (PID2020-113798GB-C31) and PALEOGREEN (CTM2017-87976-P) projects of the Spanish Ministerio de Economía y Competitividad. Field research was also supported by the research group ANTALP (Antarctic, Arctic, Alpine Environments; 2017-SGR-1102) funded by the Agència de Gestió d'Ajuts Universitaris i de Recerca of the Government of Catalonia. Julia Garcia-Oteyza was supported by an FPI fellowship from the Spanish Ministry of Science, Innovation and Universities, and Marcelo Fernandes by a PhD fellowship of the Fundação para a Ciência e Tecnologia of Portugal (UIDB/00295/2020). The ¹⁰Be measurements were performed at the ASTER AMS national facility (CEREGE, Aix-en-Provence), which is supported by the INSU/CNRS and the ANR through the “Projets thématiques d'excellence” programme for the “Equipements d'excellence” ASTER-CEREGE action and IRD. We are also grateful to Jesús Ruiz and Zackenberg Research Station for field support.

DATA AVAILABILITY STATEMENT

All data used in this study are available upon request from the authors.

ORCID

Julia Garcia-Oteyza Ciria  <https://orcid.org/0000-0002-0187-2922>

Marc Oliva  <https://orcid.org/0000-0001-6521-6388>

David Palacios  <https://orcid.org/0000-0002-8289-0398>

REFERENCES

Adamson, K., Lane, T., Carney, M., Bishop, T., & Delaney, C. (2019). High-resolution proglacial lake records of pre-Little Ice Age glacier advance, Northeast Greenland. *Boreas*, 48(3), 535–550. <https://doi.org/10.1111/bor.12361>

Aschwanden, A., Fahnestock, M. A., Truffer, M., Brinkerhoff, D. J., Hock, R., Khroulev, C., Mottram, R., & Abbas Khan, S. (2019). Contribution of the Greenland Ice Sheet to sea level over the next millennium. *Science Advances*, 5(6), eaav9396. <https://doi.org/10.1126/sciadv.aav9396>

Axford, Y., De Vernal, A., & Osterberg, E. C. (2021). Past warmth and its impacts during the Holocene thermal maximum in Greenland. *Annual Review of Earth and Planetary Sciences*, 49, 279–307. <https://doi.org/10.1146/annurev-earth-081420-063858>

Balco, G., Stone, J. O., Lifton, N. A., & Dunai, T. J. (2008). A complete and easily accessible means of calculating surface exposure ages or erosion rates from ¹⁰Be and ²⁶Al measurements. *Quaternary Geochronology*, 3(3), 174–195. <https://doi.org/10.1016/j.quageo.2007.12.001>

Bamber, J. L., Griggs, J. A., Hurkmans, R. T. W. L., Dowdeswell, J. A., Gogineni, S. P., Howat, I., Mouginot, J., Paden, J., Palmer, S., Rignot, E., & Steinhage, D. (2013). A new bed elevation dataset for Greenland. *The Cryosphere*, 7(2), 499–510. <https://doi.org/10.5194/tc-7-499-2013>

Biette, M., Jomelli, V., Chenet, M., Braucher, R., Menviel, L., Swingedouw, D., Rinterknecht, V., & ASTERTeam. (2022). Evidence of the largest Late Holocene mountain glacier extent in southern and southeastern Greenland during the middle Neoglacial from 10Be moraine dating. *Boreas*, 51, 61–77. <https://doi.org/10.1111/bor.12555> ISSN 0300-9483.

Biette, M., Jomelli, V., Chenet, M., Braucher, R., Rinterknecht, V., Lane, T., & Aster Team. (2020). Mountain glacier fluctuations during the Lateglacial and Holocene on Clavering Island (northeastern Greenland) from ¹⁰Be moraine dating. *Boreas*, 49, 873–885. <https://doi.org/10.1111/bor.12460>

Boone, W., Rysgaard, S., Kirillov, S., Dmitrenko, I., Bendtsen, J., Mortensen, J., Meire, L., Petrushevich, V., & Barber, D. G. (2017). Circulation and fjord-shelf exchange during the ice-covered period in Young Sound-Tyrolerfjord, Northeast Greenland (74° N). *Estuarine, Coastal and Shelf Science*, 194, 205–216. <https://doi.org/10.1016/j.ecs.2017.06.021>

Boyd, L. A. (1948). *The coast of Northeast Greenland: With hydrographic studies in the Greenland Sea. The Louise A. Boyd Arctic expeditions of 1937 and 1938*. American Geographical Society.

Briner, J. P., McKay, N. P., Axford, Y., Bennike, O., Bradley, R. S., Vernal, A. D., Fisher, D., Francus, P., Fréchet, B., Gajewski, K., Jennings, A., Kaufman, D. S., Miller, G., Rouston, C., & Wagner, B. (2016). Holocene climate change in Arctic Canada and Greenland. *Quaternary Science Reviews*, 147, 340e364. <https://doi.org/10.1016/j.quascirev.2016.02.010>

Buizert, C., Gkinis, V., Severinghaus, J. P., He, F., Lecavalier, B. S., Kindler, P., Leuenberger, M., Carlson, A. E., Vinther, B., Masson-Delmotte, V., White, J. W. C., Liu, Z., Otto-Bliesner, B., & Brook, E. J. (2014). Greenland temperature response to climate forcing during the last deglaciation. *Science*, 345(6201), 1177–1180. <https://doi.org/10.1126/science.1254961>

Buizert, C., Keisling, B. A., Box, J. E., He, F., Carlson, A. E., Sinclair, G., & DeConto, R. M. (2018). Greenland-wide seasonal temperatures during the last deglaciation. *Geophysical Research Letters*, 45(4), 1905–1914. <https://doi.org/10.1002/2017GL075601>

Carlson, A. E., Winsor, K., Ullman, D. J., Brook, E. J., Rood, D. H., Axford, Y., LeGrande, A. N., Anslow, F. S., & Sinclair, G. (2014). Earliest Holocene south Greenland ice sheet retreat within its late Holocene extent. *Geophysical Research Letters*, 41, 5514–5521. <https://doi.org/10.1002/2014GL060800>

CAVM Team. (2003). Circumpolar Arctic Vegetation Map. (1:7,500,000 scale). Conservation of Arctic Flora and Fauna (CAFF) Map No. 1. US Fish Wildl. Serv. AK. <https://www.Geobot.uaf.edu/cavm/> [Verified 1 August 15 July 2015] 2.

Christiansen, H. H., Sigsgaard, C., Humlum, O., Rasch, M., & Hansen, B. U. (2008). Permafrost and periglacial geomorphology at Zackenberg.

Advances in Ecological Research, 40, 151–174. ISSN 0065-2504, ISBN 9780123736659. [https://doi.org/10.1016/S00652504\(07\)00007-4](https://doi.org/10.1016/S00652504(07)00007-4), <https://www.sciencedirect.com/science/article/pii/S0065250407000074>

Christoffersen, K. S., Amsinck, S. L., Landkildehus, F., Lauridsen, T. L., & Jeppesen, E. (2008). Lake flora and fauna in relation to ice-melt, water temperature and chemistry at Zackenberg. *Advances in Ecological Research*, 40, 371–389. ISSN 0065-2504, ISBN 9780123736659. [https://doi.org/10.1016/S00652504\(07\)00016-5](https://doi.org/10.1016/S00652504(07)00016-5)

Durcan, J. A., King, G. E., & Duller, G. A. T. (2015). DRAC: Dose rate and age calculator for trapped charge dating. *Quaternary Geochronology*, 28 (January 2013), 54–61. <https://doi.org/10.1016/j.quageo.2015.03.012>

Fernández-Fernández, J. M., Andrés, N., Sæmundsson, P., Brynjólfsson, S., & Palacios, D. (2017). High sensitivity of North Iceland (Tröllaskagi) debris-free glaciers to climatic change from the ‘little ice age’ to the present. *Holocene*, 27(8), 1187–1200. <https://doi.org/10.1177/0959683616683262>

Funder, S., Kjeldsen, K. K., Kjær, K. H., & Cofaigh, C. O. (2011). The Greenland ice sheet during the past 300,000 years: A review. *Developments in Quaternary Science*, 15, 699–713. <https://doi.org/10.1016/j.quascirev.2011.07.022>

Galbraith, R. F., Roberts, R. G., Laslett, G. M., Yoshida, H., & Olley, J. M. (1999). Optical dating of single and multiple grains of quartz from Jimmum rock shelter, northern Australia: Part I, experimental design and statistical models. *Archaeometry*, 41(2), 339–364. <https://doi.org/10.1111/j.1475-4754.1999.tb00987.x>

García-Oteyza, J., Oliva, M., Palacios, D., Fernández-Fernández, J. M., Schimmelpfennig, I., Andrés, N., Antoniadou, D., Christiansen, H. H., Humlum, O., Léanni, L., Jomelli, V., Ruiz-Fernández, J., Rinterknecht, V., Lane, T. P., Adamson, K., Aumaitre, G., Bourlès, D., & Keddadouche, K. (2022). Late glacial deglaciation of the Zackenberg area, NE Greenland. *Geomorphology*, 401, 108125. <https://doi.org/10.1016/j.geomorph.2022.108125>

Grove, J. M. (2001). The Initiation of the ‘Little Ice Age’ in Regions Round the North Atlantic. *Climatic Change*, 48, 53–82. <https://doi.org/10.1023/A:1005662822136>

Guérin, G., Mercier, N., & Adamiec, G. (2011). Dose-Rate Conversion Factors: Update Dose-Rate Conversion Factors: Update. *Ancient TL*, 29(1), 5–8.

Håkansson, L., Alexanderson, H., Hjort, C., Möller, P., Briner, J. P., & Possnert, A. A. (2009). Late Pleistocene glacial history of Jameson Land, Central East Greenland, derived from cosmogenic ¹⁰Be and ²⁶Al exposure dating. *Boreas*, 38(2), 244–260. <http://dx.doi.org/10.1111/j.1502-3885.2008.00064.x>

Håkansson, L., Briner, J. P., Aldahan, A., & Possnert, G. (2011). 10Be data from meltwater channels suggest that Jameson Land, East Greenland, was ice-covered during the last glacial maximum. *Quaternary Research*, 76(3), 452–459. <https://doi.org/10.1016/j.yqres.2011.06.007>

Håkansson, L., Graf, A., Strasky, S., Ivy-Ochs, S., Kubik, P. W., Hjort, C., & Schlüchter, C. (2007). Cosmogenic ¹⁰Be-ages from the store Koldewey Island, NE Greenland. *Geografiska Annaler, Series A: Physical Geography*, 89(3), 195–202. <http://www.jstor.org/stable/4621510>

Hansen, B. U., Sigsgaard, C., Rasmussen, L., Cappelen, J., Hinkler, J., Mernild, S. H., Petersen, D., Tamstorf, M. P., Rasch, M., & Hasholt, B. (2008). Present-day climate at Zackenberg. *Advances in Ecological Research*, 40, 111–149. ISSN 0065-2504, ISBN 9780123736659. [https://doi.org/10.1016/S0065-2504\(07\)00006-2](https://doi.org/10.1016/S0065-2504(07)00006-2), <https://www.sciencedirect.com/science/article/pii/S0065250407000062>

Hasholt, B., Mernild, S. H., Sigsgaard, C., Elberling, B., Petersen, D., Jakobsen, B. H., Hansen, B. U., Hinkler, J., & Sogaard, H. (2008). Hydrology and transport of sediment and solutes at Zackenberg. *Advances in Ecological Research*, 40, 197–221. Academic Press ISSN 0065-2504. ISBN 9780123736659. <https://doi.org/10.1016/>

- S00652504(07)00009-8. <https://www.sciencedirect.com/science/article/pii/S0065250407000098>
- Helama, S., Jones, P. D., & Briffa, K. R. (2017). Dark Ages cold period: A literature review and directions for future research. *Holocene*, 27, 1600–1606. <https://doi.org/10.1177/0959683617693898>
- Henriksen, N., & Higgins, A. (2009). Descriptive text to Geological map of Greenland, 1:500 000, Dove Bugt, Sheet 10. *Geological Survey of Denmark and Greenland Map Series*, 4, 1–32. <https://doi.org/10.34194/geusm.v4.4581>
- Jomelli, V., Swingedouw, D., Vuille, M., Favier, V., Goehring, B., Shakun, J., Braucher, R., Schimmelpfennig, I., Menviel, L., Rabatel, A., Martin, L. C. P., Blard, P. H., Condom, T., Lupker, M., Christl, M., He, Z., Verfaillie, D., Gorin, A., Aumaitre, G., ... Keddadouche, K. (2022). In-phase millennial-scale glacier changes in the tropics and North Atlantic regions during the Holocene. *Nature Communications*, 13(1), 1–12. <https://doi.org/10.1038/s41467-022-28939-9>
- Kaufman, D. S., Ager, T. A., Anderson, N. J., Anderson, P. M., Andrews, J. T., Bartlein, P. J., Brubaker, L. B., Coats, L. L., Cwynar, L. C., Duvall, M. L., Dyke, A. S., Edwards, M. E., Eisner, W. R., Gajewski, K., Geirsdóttir, A., Hu, F. S., Jennings, A. E., Kaplan, M. R., Kerwin, M. W., ... Wolfe, B. B. (2004). Holocene thermal maximum in the Western Arctic (0–180° W). *Quaternary Science Reviews*, 23(5–6), 529–560. <https://doi.org/10.1016/j.quascirev.2003.09.007>
- Kelly, M. A., Lowell, T. V., Hall, B. L., Schaefer, J. M., Finkel, R. C., Goehring, B. M., Alley, R. B., & Denton, G. H. (2008). A 10Be chronology of Lateglacial and Holocene Mountain glaciation in the Scoresby Sund region, East Greenland: Implications for seasonality during Lateglacial time. *Quaternary Science Reviews*, 27(25–26), 2273–2282. <https://doi.org/10.1016/j.quascirev.2008.08.004>
- Kjær, K. H., Björk, A. A., Kjeldsen, K. K., Hansen, E. S., Andresen, C. S., Siggaard-Andersen, M. L., Khan, S. A., Søndergaard, A. S., Colgan, W., Schomacker, A., Woodroffe, S., Funder, S., Rouillard, A., Jensen, J. F., & Larsen, N. K. (2022). Glacier response to the little ice age during the neoglacial cooling in Greenland. *Earth-Science Reviews*, 227(March). <https://doi.org/10.1016/j.earscirev.2022.103984>
- Kobashi, T., Menviel, L., Jeltsch-Thömmes, A., Vinther, B. M., Box, J. E., Muscheler, R., Nakaegawa, T., Pfister, P. L., Döring, M., Leuenberger, M., Wanner, H., & Ohmura, A. (2017). Volcanic influence on centennial to millennial Holocene Greenland temperature change. *Scientific Reports*, 7(1), 1441. <https://doi.org/10.1038/s41598-017-01451-7>
- Lal, D. (1991). Cosmic ray labeling of erosion surfaces: In situ nuclide production rates and erosion models. *Earth and Planetary Science Letters*, 104(2–4), 424–439. [https://doi.org/10.1016/0012-821X\(91\)90220-C](https://doi.org/10.1016/0012-821X(91)90220-C)
- Larocca, L. J., Axford, Y., Björk, A. A., Lasher, G. E., & Brooks, J. P. (2020a). Local glaciers record delayed peak Holocene warmth in South Greenland. *Quaternary Science Reviews*, 241, 106421. <https://doi.org/10.1016/j.quascirev.2020.106421>
- Larocca, L. J., Axford, Y., Woodroffe, S. A., Lasher, G. E., & Gawin, B. (2020b). Holocene glacier and ice cap fluctuations in southwest Greenland inferred from two lake records. *Quaternary Science Reviews*, 246, 106529. <https://doi.org/10.1016/j.quascirev.2020.106529>
- Larsen, N. K., Kjær, K. H., Lecavalier, B., Björk, A. A., Colding, S., Huybrechts, P., ... Olsen, J. (2015). The response of the southern Greenland ice sheet to the Holocene thermal maximum. *Geology*, 43(4), 291–294.
- Larsen, N. K., Levy, L. B., Carlson, A. E., Buizert, C., Olsen, J., Strunk, A., Björk, A. A., & Skov, D. S. (2018). Instability of the Northeast Greenland ice stream over the last 45,000 years. *Nature Communications*, 9(1), 1–8. <https://doi.org/10.1038/s41467-018-04312-7>
- Lasher, G. E., & Axford, Y. (2019). Medieval warmth confirmed at the Norse Eastern Settlement in Greenland. *Geology*. <https://doi.org/10.1130/g45833.1>
- Lecavalier, B. S., Milne, G. A., Simpson, M. J. R., Wake, L., Huybrechts, P., Tarasov, L., Kjeldsen, K. K., Funder, S., Long, A. J., Woodroffe, S.,

- Dyke, A. S., & Larsen, N. K. (2014). A model of Greenland ice sheet deglaciation constrained by observations of relative sea level and ice extent. *Quaternary Science Reviews*, 102, 54–84. <https://doi.org/10.1016/j.quascirev.2014.07.018>
- Levy, L. B., Kelly, M. A., Lowell, T. V., Hall, B. L., Hempel, L. A., Honsaker, W. M., ... Axford, Y. L. (2014). Holocene fluctuations of Bregne ice cap, Scoresby Sund, east Greenland: A proxy for climate along the Greenland Ice Sheet margin. *Quaternary Science Reviews*, 92, 357–368. <https://doi.org/10.1016/j.quascirev.2013.06.024>
- Lowell, T. V., Hall, B. L., Kelly, M. A., Bennike, O., Lusas, A. R., Honsaker, W., Smith, C. A., Levy, L. B., Travis, S., & Denton, G. H. (2013). Late Holocene expansion of Istorvetlce Cap, Liverpool Land, East Greenland. *Quaternary Science Reviews*, 63, 128–140. <https://doi.org/10.1016/j.quascirev.2012.11.012>
- Lusas, A. R., Hall, B. L., Lowell, T. V., Kelly, M. A., Bennike, O., Levy, L. B., & Honsaker, W. (2017). Holocene climate and environmental history of East Greenland inferred from lake sediments. *Journal of Paleolimnology*, 57(4), 321–341. <https://doi.org/10.1007/s10933-017-9951-5>
- McKay, N. P., Kaufman, D. S., Routson, C. C., Erb, M. P., & Zander, P. D. (2018). The onset and rate of Holocene neoglacial cooling in the Arctic. *Geophysical Research Letters*, 45, 12,487–12,496. <https://doi.org/10.1029/2018GL079773>
- Medford, A. K., Hall, B. L., Lowell, T. V., Kelly, M. A., Levy, L. B., Wilcox, P. S., & Axford, Y. (2021). Holocene glacial history of Renland Ice Cap, East Greenland, reconstructed from lake sediments. *Quaternary Science Reviews*, 258, 106883. <https://doi.org/10.1016/j.quascirev.2021.106883>
- Oliva, M., Fernandes, M., Palacios, D., Fernández-Fernández, J. M., Schimmelpfennig, I., Antoniadis, D., Aumaitre, G., Bourlès, D., & Keddadouche, K. (2021). Rapid deglaciation during the Bølling-Allerød interstadial in the Central Pyrenees and associated glacial and periglacial landforms. *Geomorphology*, 385, 107735. <https://doi.org/10.1016/j.geomorph.2021.107735>
- Palacios, D., Stokes, C. R., Phillips, F. M., Clague, J. J., Alcalá-Reygosa, J., Andrés, N., Angel, I., Blard, P. H., Briner, J. P., Hall, B. L., Dahms, D., Hein, A. S., Jomelli, V., Mark, B. G., Martini, M. A., Moreno, P., Riedel, J., Sagredo, E., Stansell, N. D., ... Ward, D. J. (2020). The deglaciation of the Americas during the last glacial termination. *Earth-Science Reviews*, 203(February), 103113. <https://doi.org/10.1016/j.earscirev.2020.103113>
- Payer, J. (1876). *Die Oesterreichisch-Ungarische Nordpol-Expedition in Den Jahren 1872–1874: Nebst Einer Skizze Der Zweiten Deutschen Nordpol-Expedition 1869–1870, Und Der Polar-Expedition von 1871* (p. 1876). A. Hoelder.
- Pedersen, S. H. (2017). *Scaling-up climate change effects in Greenland*. Aarhus University.
- Porter, C., Morin, P., Howat, I., Noh, M.-J., Bates, B., Peterman, K., Keeseey, S., Schlenk, M., Gardiner, J., Tomko, K., Willis, M., Kelleher, C., Cloutier, M., Husby, E., Foga, S., Nakamura, H., Platson, M., Michael Wethington, C. W., Jr., Bauer, G., ... Mikkel A4-National Science Foundation A4-National Science Foundation Bojesen. (2018). ArcticDEM.
- Porter, S. C. (2000). Onset of neoglaciation in the Southern Hemisphere. *Journal of Quaternary Science*, 15(4), 395–408. [https://doi.org/10.1002/1099-1417\(200005\)15:4%3C395::AID-JQS535%3E3.0.CO;2-H](https://doi.org/10.1002/1099-1417(200005)15:4%3C395::AID-JQS535%3E3.0.CO;2-H)
- Porter, S. C., & Denton, G. H. (1967). Chronology of neoglaciation in the North American Cordillera. *American Journal of Science*, 265(3), 177–210.
- Prescott, J. R., & Hutton, J. T. (1994). Cosmic ray contributions to dose rates for luminescence and ESR dating: Large depths and long-term time variations. *Radiation Measurements*, 23(2–3), 497–500. ISSN 1350-4487. [https://doi.org/10.1016/13504487\(94\)90086-8](https://doi.org/10.1016/13504487(94)90086-8) <https://www.sciencedirect.com/science/article/pii/S1350448794900868>
- Renssen, H., Seppä, H., Crosta, X., Goosse, H., & Roche, D. (2012). Global characterization of the Holocene thermal maximum. *Quaternary Science Reviews*, 48, 7–19.

- Renssen, H., Seppä, H., Heiri, O., Roche, D. M., Goosse, H., & Fichefet, T. (2009). The spatial and temporal complexity of the Holocene thermal maximum. *Nature Geoscience*, 2(6), 411–414. <https://doi.org/10.1038/ngeo513>
- Reusche, M. M., Marcott, S. A., Ceperley, E. G., Barth, A. M., Brook, E. J., Mix, A. C., & Caffee, M. W. (2018). Early to late Holocene surface exposure ages from two marine-terminating outlet glaciers in north-west Greenland. *Geophysical Research Letters*, 45(14), 7028–7039. <https://doi.org/10.1029/2018GL078266>
- Rule, Home. (2005). British Mountaineering Council, Royal Geographical Society, Domestic Affairs, North-east Green, National Park, Blosseville Kyst, Nanu Travel Aps, Kap Tobin, Zackenberg Ecological, Zackenberg Ecological, Nuna Travel Aps, The Sirius, Sledge Patrol, and Sirius Sledge Patrol. 2005. "Exploration History of Northern East Greenland."
- Søndergaard, A. S., Larsen, N. K., Steinemann, O., Olsen, J., Funder, S., Egholm, D. L., & Kjær, K. H. (2020). Glacial history of Ingfield Land, north Greenland from combined in situ 10 Be and 14 C exposure dating. *Climate of the Past*, 16(5), 1999–2015. <https://doi.org/10.5194/cp-16-1999-2020>
- Schweinsberg, A. D., Briner, J. P., Licciardi, J. M., Bennike, O., Lifton, N. A., Graham, B. L., ... Zimmerman, S. H. (2019). Multiple independent records of local glacier variability on Nuussuaq, West Greenland, during the Holocene. *Quaternary Science Reviews*, 215, 253–271. <https://doi.org/10.1016/j.quascirev.2019.05.007>
- Skov, D. S., Andersen, J. L., Olsen, J., Jacobsen, B. H., Knudsen, M. F., Jansen, J. D., Larsen, N. K., & Egholm, D. L. (2020). Constraints from cosmogenic nuclides on the glaciation and erosion history of Dove Bugt, Northeast Greenland. *Bulletin of the Geological Society of America*, 132(11–12), 2282–2294. <https://doi.org/10.1130/B35410.1>
- Stone, J. O. (2000). Air pressure and cosmogenic isotope production. *Journal of Geophysical Research*, 105(1), 753–759. <https://doi.org/10.1029/2000JB900181>
- Vasskog, K., Langebroek, P. M., Andrews, J. T., Nilsen, J. E. Ø., & Nesje, A. (2015). The Greenland ice sheet during the last glacial cycle: Current ice loss and contribution to sea-level rise from a Palaeoclimatic

- perspective. *Earth-Science Reviews*, 150, 45–67. <https://doi.org/10.1016/j.earscirev.2015.07.006>
- Vinther, B. M., Clausen, H. B., Fisher, D. A., Koerner, R. M., Johnsen, S. J., Andersen, K. K., Dahl-Jensen, D., Rasmussen, S. O., Steffensen, J. P., & Svensson, A. M. (2008). Synchronizing ice cores from the Renland and Agassiz ice caps to the Greenland ice core chronology. *Journal of Geophysical Research Atmospheres*, 113(8), 1–10. <https://doi.org/10.5194/gp-4-47-2008>
- Walker, M., Head, M. J., Berkelhammer, M., Björck, S., Cheng, H., Cwynar, L., Fisher, D., Gkinis, V., Long, A., Lowe, J., Newnham, R., Rasmussen, A. O., & Weiss, H. (2018). Formal ratification of the subdivision of the Holocene Series/Epoch (Quaternary System/Period): Two new Global Boundary Stratotype Sections and Points (GSSPs) and three new stages/subseries. *Episodes*, 41(4), 1–11. <https://doi.org/10.18814/epiugs/2018/018016>
- Young, N. E., Briner, J. P., Miller, G. H., Lesnek, A. J., Crump, S. E., Thomas, E. K., Pendleton, S. L., Cuzzone, J., Lamp, J., Zimmerman, S., Caffee, M., & Schaefer, J. M. (2020). Deglaciation of the Greenland and Laurentide ice sheets interrupted by glacier advance during abrupt Coolings. *Quaternary Science Reviews*, 229, 106091. <https://doi.org/10.1016/j.quascirev.2019.106091>
- Young, N. E., Schaefer, J. M., Briner, J. P., & Goehring, B. M. (2013). A 10Be production-rate calibration for the Arctic. *Journal of Quaternary Science*, 28(5), 515–526. <https://doi.org/10.1002/jqs.2642>

How to cite this article: Garcia-Oteyza Ciria, J., Oliva, M., Palacios, D., M. Fernández-Fernández, J., Schimmelpfennig, I., Medialdea, A., Fernandes, M., Giralt, S., Jomelli, V., Antoniadis, D., & ASTER TEAM (2023). Holocene glacial oscillations in the Tyrolean Valley (NE Greenland). *Land Degradation & Development*, 1–18. <https://doi.org/10.1002/ldr.4633>

3.1.3 PAPER III. A LATE GLACIAL AND HOLOCENE CHRONOLOGY OF CLIMATE-LINKED LANDSCAPE EVOLUTION IN NE GREENLAND FROM CRE DATING OF LANDFORMS

PAPER III

J. Garcia-Oteyza, M. Oliva, D. Palacios, J. M. Fernández-Fernández, I. Schimmelpfennig, M. Fernandes, S. Giralt, D. Antoniades, V. Jomelli (2023). A Late Glacial and Holocene chronology of climate-linked landscape evolution in NE Greenland from CRE dating of landforms.(Submitted).



A Late Glacial and Holocene chronology of climate-linked landscape evolution in NE Greenland from CRE dating of landforms.

Journal:	<i>Boreas</i>
Manuscript ID:	BOR-001-2024
Wiley - Manuscript type:	Original Article
Date Submitted by the Author:	06-Jan-2024
Complete List of Authors:	Garcia-Oteyza, Julia; University of Barcelona Faculty of Geography and History, Department of Geography Oliva, Marc; University of Barcelona, Geography Palacios, David; Complutense University of Madrid, Geography Fernández-Fernández, José; Complutense University of Madrid, Geography Schimmelpfennig, Irene; CEREGE, France Fernandes, Marcelo; University of Lisbon Institute of Geography and Spatial Planning Giralt, Santiago; GEO3BCN-CSIC Antoniades, Dermot; Université Laval, Geography Jomelli, Vincent; CEREGE; Aix-Marseille Université
Keywords:	CRE dating, Glacial landforms, landscape evolution, paraglacial dynamics

SCHOLARONE™
Manuscripts

ABSTRACT

The Greenland Ice Sheet is highly sensitive to climate change, leading to significant retreats along its edges, including peripheral mountain glaciers. This rapid ice loss contributes to rising sea levels and impacts the Earth's climate stability. Understanding the extent of recent glacier retreat is crucial in order to determine if it is unprecedented or within ranges of natural variability. Paleoenvironmental studies aim to identify past glacial phases and landscape changes using advanced dating methods such as cosmic ray exposure (CRE) dating. In Northeast Greenland, CRE dating has helped establish the timing of glacial oscillations, yet a comprehensive understanding of glacial fluctuations during specific periods still needs to be developed. This study aims to chronologically constrain the landscape evolution of two NE Greenland valleys from the Young Sund - Tyrolerfjord area (74°N, 20-25°E) from the onset of deglaciation and throughout the Holocene to better understand glacial and post-glacial changes. The chronological framework relies on 27 ¹⁰Be cosmic-ray exposure ages that constrain our interpretation of the geomorphological features from both valleys. Inconsistencies were observed in age sequences, highlighting potential bias associated with nuclide inheritance and post-glacial dynamics. Despite limitations, CRE results confirm the general pattern observed in NE Greenland: (i) massive deglaciation and disconnection of glaciers from the main glacial systems during the Late Glacial and Early Holocene with a rapid but not homogeneous deglaciation within the range

from ~14.3 to 11.9 ka; (ii) no evidence of glacial activity during the mid-Holocene, probably associated with the withdrawn position of the ice masses fronts; and (iii) glacier expansion during the Late Holocene, with a Little Ice Age advance as the last significant period of glacial regrowth.

Key words: CRE dating, Glacial landforms, landscape evolution, paraglacial dynamics.

1. INTRODUCTION

The Greenland Ice Sheet (GrIS), a tipping component of Earth's climate system (Lenton et al., 2008), is responding rapidly to present-day climate warming, with major retreats along most of its margins (Vasskog et al., 2015). Similarly, peripheral glaciers in Greenland are recording accelerated recession in response to unfavorable climate conditions for glacier stability. Greenland melting is currently the main contributor to sea level rise (10.8 ± 0.9 mm between 1992 and 2018; IMBIE Team 2020); this contribution may further increase in the coming decades as the GrIS is in imbalance with the current climate (King et al., 2020). The loss of glacial ice has major implications for Arctic amplification, including ocean currents, surface radiative balance, etc, that affect the stability of Earth's climate system (Meredith et al., 2019).

Paleoenvironmental studies focus on identifying different phases of glacial retreat and advances, together with landscape evolution and the environmental implications of glacial oscillations. To that end, recent advances in absolute dating have refined the chronologies of past glacial dynamics, with particular success in the use of cosmic ray exposure (CRE) dating of glacial landforms (Balco, 2019; Gosse and Klein, 2014). In NE Greenland, the focus of this study, CRE dating has been increasingly used over the last several years to frame the timing of glacial oscillations through its application to erosive and accumulation glacial records (Biette et al. 2020; Garcia-Oteyza et al. 2022; Garcia-Oteyza et al. 2023a; Håkansson et al. 2007a, 2009, 2011; Kelly and Lowell 2008; Larsen et al. 2018; Levy et al. 2014, 2016; Lowell et al. 2013; Skov et al. 2020). Despite this, the chronology of glacial fluctuations and landscape evolution across NE Greenland is still poorly understood and few studies have provided CRE ages for temporal and spatial deglaciation patterns during Termination-1 (T-1; ~19-20 to 11.7 ka) and the Early Holocene (~11.7 to 8.2 ka), when most of the currently ice-free areas became deglaciated (Håkansson et al. 2007b, 2009, 2011; Kelly et al. 2008; Larsen et al. 2018; Skov et al. 2020; Garcia-Oteyza et al. 2022). Since that time, glaciers have recorded only minor advances and retreats depending on the prevailing climate conditions, with the Little Ice Age (LIA; ~0.6–0.2 ka BP) being the last period with a documented widespread glacial expansion in NE Greenland (Biette, et al. 2020; Garcia-Oteyza et al. 2023a; Jomelli et al. 2022).

The application of CRE dating in NE Greenland is strongly constrained by the occurrence of nuclide inheritance and postglacial environmental dynamics. The existence of cold-based glaciers in many parts of Greenland lead to the preservation and co-existence of the glacial record from several glaciations and deglaciations. Hence, this often impedes robust dating of the glacial record from the last glacial cycle and subsequent deglaciation (Skov et al., 2020). In addition, some studies have also highlighted the impact of postglacial dynamics on the conservation of the glacial signal and the interpretation of the geomorphological significance of the dated samples (Garcia-Oteyza et al., 2022). Therefore,

special care needs to be taken when taking CRE dating samples and interpreting landscape evolution based on their results.

The objective of this study is to chronologically constrain the landscape evolution of two valleys from the Young Sund - Tyrolerfjord area, from the Late Glacial and throughout the Holocene, to shed light on glacial responses to climate variability in the region and to assess the environmental transformation following deglaciation. To this end, we had the following specific objectives:

- To identify and differentiate landforms generated by glacial oscillations and by paraglacial processes.
- To identify the millennium main phases of glacial expansion and retreat, as well as the major postglacial environmental processes reshaping the glacial landscape.
- To compare spatio-temporal patterns of landscape evolution in these valleys with those detected in other regions across NE Greenland.
- To identify the value of CRE dating in an environment of cold-based glaciers and intense paraglacial and periglacial processes accompanying deglaciation and rapid temperature increases.

2. REGIONAL SETTING

This study focuses on two deglaciated U-shaped valleys located in the Northeast Greenland National Park: Olsen Valley, in the interior of the Wollaston Forland Peninsula, and Dolomit Valley, on the northern coast of Clavering Island (Figure 1).

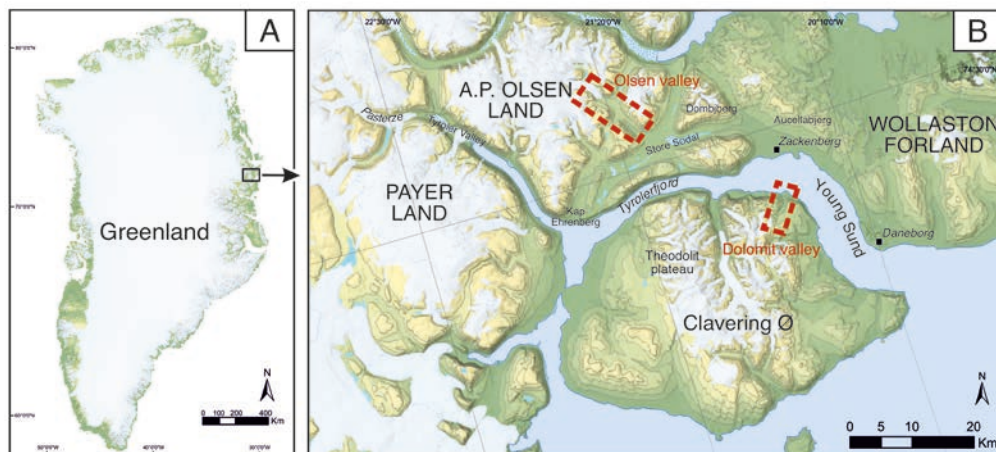


Figure 1. (A) Location of the study area within Greenland; and (B) detail of the study region with the study areas.

The Olsen Valley extends over ~10 km NW-SE from the shoreline of the Store Sødal Lake to the front of the Southeast Outlet Glacier (SEOG) of the A. P. Olsen Land Ice Cap. This is a predominantly cold-based ice cap (Behm et al., 2020), with its front located ~35 km inland

from the Zackenberg Research Station (Figure 1). Two deglaciated tributary valleys descending from the NE and SW sides merge with the main valley floor at the middle part of the Olsen Valley. The surrounding flat-topped summits around the Olsen Valley rise on either side to elevations between 800 and 1200 m above sea level (hereafter referred to as a.s.l.) and connect with steep hillsides (up to 20-35°) descending into the valley. Quaternary sediments cover the valley floor and the slopes, while metamorphic rocks (relatively homogeneous Paleoproterozoic orthogneiss) are exposed on the upper slope sections (Koch & Haller, 1971). A braided river system fed by SEOG meltwater and other streams descending from the surrounding mountains occupies the valley floor and flows into the Store Sødal Lake. The Olsen Valley and the river that flows 38 km to the Zackenberg delta is repeatedly affected by glacial lake outburst floods (GLOFs). These extreme events originate at the ice-dammed lake impounded by the SEOG that dams an adjacent ice-free side valley; here, water accumulates and forms a lake, which is regularly drained over a quasi-annual cycle monitored since the first known GLOF in 2005 (Behm et al., 2020). These events have a strong influence on environmental dynamics at the catchment scale (Kroon et al., 2017), with occasional megaflood characteristics (Behm et al., 2020).

The Dolomit Valley stretches ~5 km NE-SW between the coast at the Young Sound fjord and the Dolomit Glacier front. The valley includes only one tributary in its upper part that is still partially occupied by a small alpine glacier descending from the mountain plateaus distributed at elevations of 1000-1200 m a.s.l. The hillsides descending from these flat-topped summits are moderately sloped (15-25°). A braided river with a high sediment load flows along the valley floor, and has created a delta in contact with the Young Sound fjord (Kroon et al., 2017). Dolomit Valley is crossed by a normal fault as this valley constitutes the boundary between the central and eastern geological sections of Clavering Island (Koch & Haller, 1971). The western slopes consist of metasediments, gneiss, and granite formations of Caledonian Crystalline complexes, whereas the eastern slopes are formed by Jurassic and Cretaceous sedimentary rocks (mudstones, sandstones, and carbonates; Grønnow et al. 2009). As a result, thick deposits of Quaternary sediments affected by active hillside processes cover the middle and lower sections of the slopes.

The regional climate regime is defined as a High Arctic polar tundra climate (Kottek et al., 2006). The nearby Zackenberg Research Station records an average annual air temperature (MAAT) of -9.0°C (1996-2015), with monthly mean temperatures ranging from -19.8°C in February to 6.3°C in July (Højlund Pedersen, 2017). The mean annual precipitation is 367 mm, mainly falling as snow (Hansen et al., 2008). The area is snow-covered most of the year, generally from September to the end of May, although with a large interannual variability (Hinkler et al., 2008; López-Blanco et al., 2020). Permafrost controls geomorphological processes in the region; it is continuous and shows thicknesses up to 200-400 m, as observed in the nearby Zackenberg Valley (Christiansen et al., 2008; Christoffersen et al., 2008; Hansen et al., 2008). The vegetation in this area is predominantly composed of dwarf shrub heaths, with diversity and size diminishing as elevation increases. Below 200 m a.s.l. small shrubs, fell fields and grasses prevail (CAVM Team in 2003), whereas above 600 m a.s.l. vegetation becomes very scarce (Buus-Hinkler et al., 2006; Elberling et al., 2008).

3. METHODOLOGY

In this study, we integrated geomorphological and geochronological (CRE ¹⁰Be dating) approaches. The fieldwork was conducted in early September 2019, when the snow-free environment enabled a precise identification of geomorphological features and the collection of samples for CRE dating.

3.1 GEOMORPHOLOGICAL MAPPING

Prior to fieldwork, we prepared a geomorphological map based on satellite imagery, focusing on key glacial features such as moraines and polished surfaces. This preliminary map underwent validation through in-situ observations and also incorporated newly identified landforms. The final geomorphological maps were delineated within the ArcMap 10.8 work environment, based on WorldView-2 orthorectified panchromatic satellite images with imagery (0.5 m resolution) from 2018 for Olsen Valley and WorldView-3 imagery (0.3 m resolution) from 2019 for Dolomit Valley in conjunction with the shaded relief elevation raster derived from the Arctic DEM digital elevation model (2 m spatial resolution) (Porter et al. 2018).

3.2 SAMPLE COLLECTION STRATEGY

We collected 15 samples from the Olsen Valley and 12 more from the Dolomit Valley for ¹⁰Be CRE dating. Each sample consisted of ~1 kg of the uppermost rock layer (with a thickness of ≤ 5 cm) using a hammer and chisel. We refrain from sampling at corners, edges, and steep faces (>20°) to optimize the reception of cosmic ray flux. The selection of moraine boulders for sampling is contingent upon their deep anchoring in the ground to ensure stability and minimize the risk of boulder collapse. These boulders are positioned on moraine crests, protruding in a manner that makes it unlikely for them to have been covered by sediments since their deposition. Concurrently, we meticulously documented key details such as the geomorphological setting, geographic coordinates, elevation, and measurements necessary for subsequent geometric adjustments to account for topographic shielding effects from the surrounding relief. A comprehensive compilation of field data and sample attributes is presented in Table 1.

3.3 CRE LABORATORY PROCEDURES AND AGE CALCULATION

Sample crushing and sieving (0.25-1 mm fraction) was carried out at the Laboratory of Physical Geog-raphy in the Universidad Complutense de Madrid, Spain. Subsequent physical and chemical procedures were conducted at the Laboratoire National des Nucleides Cosmogéniques (LN2C) of the Centre Euro-péen de Recherche et d’Enseignement des Géosciences de l’Environnement (CEREGE, Aix-en Provence, France). Laboratory procedures followed the same protocols outlined in Garcia-Oteyza et al. (2022).

¹⁰Be/⁹Be ratio measurements were performed on the BeO targets at the French 5 MV Accélérateur pour les Sciences de la Terre, Environnement et Risques (ASTER) national facility at CEREGE, with identical calibrations and standards to those described in Garcia-Oteyza et al. (2022). Due to problems in the separation of quartz and the impossibility of

mcontinuing with the treatment, one sample (DOL-05) was discarded. Two samples exhibited invalid AMS measurements (DOL-03 and DOL-06) and three others showed low current values (DOL-02, DOL-09 and OLS-03). Consequently, these samples were identified as chemical outliers and were thus excluded from subsequent calculations and discussion. A com-prehensive record with all analytical data is provided in Table 2.

Table 1. Geographic location of samples, topographic shielding factors, and sample thicknesses.

Sample ID	Landform	Latitude (DD)	Longitude (DD)	Elevation (m a.s.l.)	Topographic shielding factor (dimensionless)	Thickness (cm)
OLSEN VALLEY						
OLS-01	Polished surface	74.53515	-21.196561	389	0.9932	2.5
OLS -02	Polished surface	74.534466	-21.192555	334	0.9894	2.5
OLS - 03	Lateral moraine	74.530252	-21.190141	251	0.9971	0.5
OLS -04	Lateral moraine	74.526673	-21.18916	242	0.9972	1.5
OLS -05	Lateral moraine	74.526646	-21.174735	231	0.9974	1.5
OLS -06	Lateral moraine	74.526578	-21.174642	231	0.9981	1.5
OLS -07	Polished surface	74.592999	-21.302957	263	0.9937	1.5
OLS -08	Polished surface	74.592188	-21.301233	263	0.9937	1.5
OLS -09	Polished surface	74.58642	-21.290792	231	0.9934	2.5
OLS -10	Polished surface	74.585605	-21.289947	228	0.9934	2.5
OLS -11	Polished surface	74.575724	-21.28058	293	0.9925	2.5
OLS -12	Lateral moraine	74.566978	-21.261636	183	0.9903	1.5
OLS -13	Lateral moraine	74.566978	-21.261823	183	0.9903	1.5
ZAC-15	Frontal moraine	74.56523	-21.53018	516	0.9788	2.6
ZAC-16	Frontal moraine	74.5645	-21.52769	556	0.9692	3.8
DOLOMIT VALLEY						
DOL-01	Slide boulder	74.380382	-20.615017	336	0.9942	1.5
DOL -02	Slide boulder	74.380576	-20.614789	335	0.9937	2.5
DOL - 03	Lateral moraine	74.382262	-20.658827	500	0.9873	0.5
DOL -04	Lateral moraine	74.382227	-20.65788	502	0.9873	0.5
DOL -05	Lateral moraine	74.377432	-20.638129	417	0.9927	1.5
DOL -06	Lateral moraine	74.377492	-20.638035	418	0.9927	0.5
DOL -07	Lateral moraine	74.377384	-20.640582	424	0.9924	0.5
DOL -08	Lateral moraine	74.37714	-20.634161	395	0.9855	2.5
DOL -09	Lateral moraine	74.377078	-20.634958	405	0.9855	2.5

Exposure ages were determined through the CRONUS-Earth online calculator, version 3.0 (Balco et al., 2008; <https://hess.ess.washington.edu/>), choosing the the Arctic-wide sea-level/high-latitude ¹⁰Be produc-tion rate (3.96 ± 0.15 atoms g⁻¹ a⁻¹) (Young et al., 2013) and the “Lm” (Lal/Stone) time-dependent scal-ing model (Lal, 1991; Stone, 2000). A 2.7 g cm⁻³ density was assumed for all samples. No corrections for erosion or snow shielding were considered in accordance with earlier studies on the area (Garcia-Oteyza et al, 2022; Garcia-Oteyza et al., 2023a). The partial shielding effect of the surrounding topogra-phy was accounted for with the “Topographic Shielding Calculator v.2” (http://stoneage.ice-d.org/math/skyline/skyline_in.html) for all sam-pling sites (see Table 2 for details). Exposure ages are given in Table 2 with their internal (only analyti-cal) and external uncertainties (including production rate uncertainty).

In the text and the figures, ages are given with their internal uncertainties unless otherwise stated. The mean ages shown were calculated arithmetically, and their uncertainties include the standard deviations of the single ages and the squared production rate uncertainties.

Table 2. AMS analytical data and calculated exposure ages.

Sample name	Quartz weight (g)	Mass of carrier (⁹ Be mg)	¹⁰ Be/ ⁹ Be (10 ⁻¹⁴)	Blank correction (%)	[¹⁰ Be] (10 ⁴ atoms g ⁻¹) ±1σ (atoms g ⁻¹)	¹⁰ Be age (ka)*	Internal uncertainty (ka)	External uncertainty (ka)
OLSEN VALLEY								
OLS-01	33.9929	0.44667	11.154 ± 0.372	2.06	5.129 ± 0.327	13.8	0.5	0.7
OLS-02	8.0601	0.44259	2.223 ± 0.098	8.88	7.537 ± 0.378	11.3	0.6	0.7
OLS-03	23.3613	0.44812	16.144 ± 6.105	1.42	20.399 ± 7.825	30.8	11.9	12.0
OLS-04	19.1958	0.44649	5.129 ± 0.160	4.48	7.615 ± 0.253	12.2	0.4	0.6
						- arithmetic mean age: 9.7 ± 1.2 ka (n=2) -		
OLS-05	12.5166	0.46718	2.721 ± 0.134	6.97	6.314 ± 0.341	10.4	0.6	0.7
OLS-06	16.5553	0.45248	3.154 ± 0.146	6.21	5.403 ± 0.272	8.9	0.4	0.6
OLS-07	24.3783	0.36370	8.217 ± 0.289	3.44	7.91 ± 0.291	10.4	0.4	0.5
OLS-08	13.3286	0.44685	3.441 ± 0.141	6.68	7.195 ± 0.323	9.4	0.4	0.5
OLS-09	38.9868	0.44428	15.261 ± 0.478	1.48	11.449 ± 0.366	15.0	0.5	0.7
OLS-10	7.2783	0.40868	2.344 ± 0.110	9.25	7.98 ± 0.427	10.6	0.6	0.7
OLS-11	18.9395	0.43772	5.858 ± 0.191	4.00	8.684 ± 0.299	11.6	0.4	0.6
						- arithmetic mean age: 9.4 ± 0.7 ka (n=2) -		
OLS-12	35.5021	0.44740	8.285 ± 0.267	2.77	6.784 ± 0.226	9.7	0.3	0.5
OLS-13	8.6230	0.45505	2.004 ± 0.107	9.72	6.38 ± 0.389	9.1	0.6	0.7
						- arithmetic mean age: 1.5 ± 0.4 ka (n=2) -		
ZAC-15	15.996	0.95051	1.114 ± 0.269	28.09	1.05 ± 0.358	1.5	0.5	0.5
ZAC-16	21.591	0.94236	1.352 ± 0.223	23.35	1.00 ± 0.220	1.4	0.3	0.3
DOLOMIT VALLEY								
DOL-01	16.3260	0.43814	0.991 ± 0.103	20.40	1.795 ± 0.191	2.5	0.3	0.3
DOL-02	7.4488	0.44655	1.839 ± 0.241	10.79	6.571 ± 0.972	11.4	1.7	1.7
DOL-03								
DOL-04	36.3018	0.44710	1.795 ± 0.166	12.80	1.288 ± 0.139	1.9	0.2	0.2
DOL-05								
DOL-06								
DOL-07	30.8826	0.44788	0.755 ± 0.087	29.66	0.515 ± 0.093	0.8	0.1	0.2
DOL-08	16.4179	0.45605	2.45 ± 0.105	7.93	4.187 ± 0.201	7.0	0.3	0.4
DOL-09	51.8427	0.44903	5.593 ± 0.493	3.53	3.123 ± 0.286	5.1	0.5	0.5
						- arithmetic mean age: 10.0 ± 1.4 ka (n=3) -		
DOL-10	28.4067	0.44821	5.763 ± 0.193	3.43	5.868 ± 0.205	11.5	0.4	0.6
DOL-11	38.2503	0.44658	6.288 ± 0.224	3.57	4.731 ± 0.177	9.1	0.3	0.5
DOL-12	31.3997	0.44734	5.302 ± 0.196	4.33	4.829 ± 0.189	9.3	0.4	0.5
Chemistry blank details ¹								
Blank name	mass of carrier (⁹ Be mg)	¹⁰ Be/ ⁹ Be (10 ⁻¹⁴)	[¹⁰ Be] (10 ⁴ atoms)					
BK1	0.45088	0.222 ± 0.04	6.703 ± 1.219					
BK2	0.44576	0.23 ± 0.032	6.862 ± 0.964					
BK3	0.45242	0.196 ± 0.028	5.921 ± 0.832					
BK4	0.96595	0.380 ± 0.0066	6.57 ± 0.994					

* ¹⁰Be ages assuming a density of 2.7 g cm⁻³ and a zero-erosion scenario.

¹ In parallel to the sample treatment, three blanks were prepared: BK1 (processed with samples OSL-09, DOL-07 and DOL-11), BK2 (processed with samples OSL-01, OS 03, OSL-04, OSL-07, OSL-08, OSL-11, OSL-12, DOL-04 and DOL-12), BK-03 (processed with samples OSL-02, OSL-05, OSL-06, OSL-10, OSL-13, DOL-01, DOL-02, DOL-08 and DOL-09) and BK4 (processed with samples ZAC-15 and ZAC-16).

4. RESULTS

The spatial distribution and typology of geomorphological features distributed in both valleys provide insights into the landscape evolution of the area over the last several millennia (Figure 2 and 3). The chronological framework of the environmental evolution in these two valleys is constrained by the 27 ¹⁰Be CRE ages obtained from glacial and slope records (Table 2).

4.1 GEOMORPHOLOGICAL SETTING AND EXPOSURE AGES

Both valleys have U-shaped, largely deglaciated glacial morphologies that preserve geomorphic evidence of past periods with larger ice masses. Some glacial landforms have been affected by paraglacial slope processes and special caution must therefore be taken when reconstructing the geomorphological evolution in the area. Based on the distribution of the major glacial landforms, we can track the past environmental dynamics occurring in the region since the onset of the deglaciation of the valleys. Chronological data and geographical characteristics of the samples are presented in Figures 2 and 3 together with photographs of the study area showing the different geomorphological units (Figure 4). Here, we present the CRE dating results in the two valleys from the lower sections up to the ice fronts.

Olsen Valley

The Olsen Valley is largely deglaciated and only includes one major ice tongue descending 6.5 km from the A.P. Olsen Ice Cap (SEOG glacier) forming two well-defined frontal moraine ridges. Towards the middle of the valley, two ice-free tributary valleys merge with the Olsen Valley from its NE and SW edges. Above ~550 m a.s.l. the metamorphic bedrock of this area remains exposed on relatively flat and mostly deglaciated mountain plateaus. Discontinuous till deposits with some minor moraine ridges cover the steep mountain slopes, with small and frequent exposures of polished bedrock surfaces across the lowest parts. This dynamic geomorphological setting favored the occurrence of very active periglacial processes on the slopes that triggered the development of protalus lobes, talus cones, debris flows, alluvial fans, etc., which, in turn, impeded the preservation of well-preserved datable glacial records as most were largely covered or eroded by postglacial slope processes. An outwash plain fed by glacial meltwater extends over much of the valley floor, and narrows downslope where it is gradually occupied by a braided river system with traces of erosion in river the banks triggered by GLOF events that also disrupted glacial sedimentary records existing on the valley floor (Figure 2). The CRE dating results (a total of 15 samples) of the Olsen Valley show ages between the last stages of T-1 and the Early Holocene and can be explained within the three different sectors of this valley that were observed:

- Lower valley – The moraines at the confluence with the Store Sødal valley is indicative that the area must have been occupied by a single glacial tongue formed by the coalescence of the SEOG glacier and the Store Sødal valley glacier descending from the ice sheet. In this large flat area, a lobate piedmont glacier generated multiple moraine ridges with abundant till dispersed across the valley bottom. Recurrent high-energy GLOFs cut the lowest part of this moraine complex and eroded the flanks of the valley floor up to the glacial front. In the highest part of this moraine complex, at the entrance of the valley, there

is a polished surface partially covered by till. Considering the limited availability of well-preserved glacial records and the intensity of alluvial and slope processes in the area, we collected six samples from this area distributed at different elevations: two from polished and striated bedrock surfaces at ~390 and ~330 m a.s.l., respectively (OLS-01, OLS-02) yielding exposure ages of 13.8 ± 0.5 ka (OLS-01) and 11.6 ± 0.6 ka (OLS-02); two from a moraine ridge on the internal sector at v250 m a.s.l. extending laterally from the foot of the

wall to the head of the lake where it has been dismantled by a large alluvial fan (OLS-03, OLS-04) and returned an age of 12.2 ± 0.4 ka (OLS-04) (Figure 4G); and two from the external moraine ridge at ~230 m a.s.l. (OLS-05, OLS-06) yielded ages of 10.4 ± 0.4 ka (OLS-05) and 8.9 ± 0.4 ka (OLS-06), respectively.

- Middle valley – Towards the middle of the valley, the second frontal moraine complex is composed of three minor moraine ridges indicative of the occurrence of glacial standstills or advances within the long-term retreat. Two samples were taken on the intermediate ridge of the complex at ~180 m a.s.l. (OLS-12, OLS-13), which was the best-preserved unit and that least affected by postglacial processes.

These samples returned exposure ages of 9.7 ± 0.3 ka (OLS-12) and 9.1 ± 0.6 ka (OLS-13), with a mean age of 9.4 ± 0.7 ka (n=2).

- Upper valley – Upstream, the valley is entirely covered by till up to the glacier front. There are only a few exposed sectors of polished and striated bedrock that have not been covered by postglacial sedimentary processes or affected by erosion associated with GLOF events. From this area, we collected seven samples at increasing distances from the present-day glacier front: two polished surface samples at the confluence with the two tributary valleys ~2.5 km from the glacier at ~260 m a.s.l. (OLS-07, OLS-08); two more ~3.5 km from the front at v230 m a.s.l. (OLS-09, OLS-10), and the last v5 km from the ice limit at ~290 m a.s.l. (OLS-11). No clear datable surfaces were found closer to the glacier front. This sequence of samples from an exposed polished surface along the upper valley towards the glacial front returned exposure ages of 11.6 ± 0.4 ka (OLS-11), 15.0 ± 0.4 ka (OLS-09) and 10.6 ± 0.6 ka (OLS-10) (Figure 4D), whereas the two samples collected next to the current ice margin yielded exposure ages of 10.4 ± 0.6 ka (OLS-07) and 9.4 ± 0.4 ka (OLS-08). Two samples were taken from moraine boulders from the frontal moraine ridge at ~200 m from the present glacier front at ~500 m a.s.l., returning ages of 1.5 ± 0.5 ka (ZAC-15) and 1.4 ± 0.3 ka (ZAC-16).

Dolomit Valley

The Dolomit Valley is mostly deglaciated, with a small mountain glacier (~3 km²) at its head whose front is currently located ~4.5 km from the coastline. In the upper part of the valley, a single N-S deglaciated tributary merges with the valley, providing abundant sediment supply to the main river. Above ~450 m a.s.l. on the mountain plateaus, the bedrock is largely exposed, intensely weathered and affected by very active periglacial processes. The highly weatherable sedimentary rocks supplying fine loose sediments and the abundant till deposits determine the high sediment load transported by the Dolomit River to the coastal zone, forming a delta. The preservation of glacial landforms in the Dolomit Valley is largely affected by periglacial slope processes, which have altered local slope stabilities and reshaped the hillsides forming talus slopes and cones, solifluction, alluvial fans, landslides, etc. Three different sections were identified in this valley and (Figure 3) and the age dataset (seven samples) for the Dolomit Valley is distributed as follows:

- Lower valley – Above the delta, there is a ~30-40 m-thick moraine ridge (NE), from where we collected three boulder samples ~245 m a.s.l. (DOL-10, DOL-11 and DOL-12). These

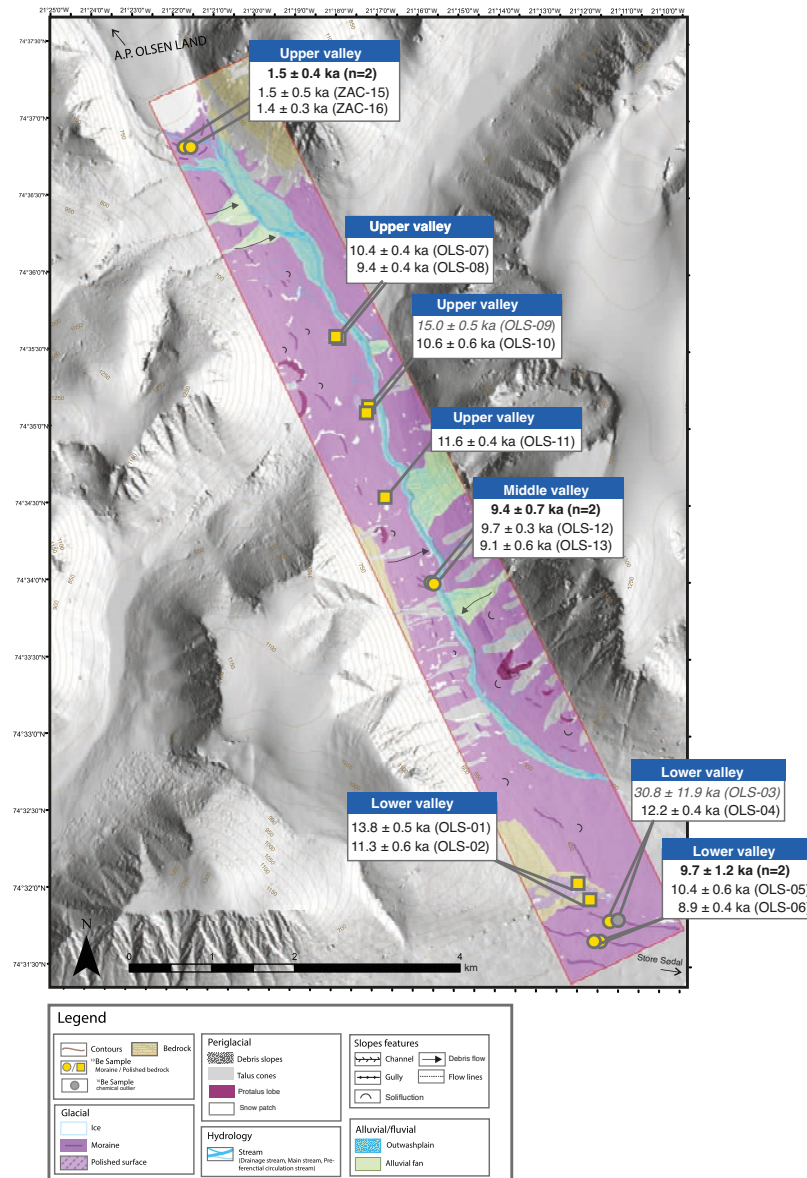


Figure 2. Olsen Valley geomorphological map including the main landforms together with the CRE results shown in Tables 1 and 2.

samples yielded ages of 11.5 ± 0.4 ka (DOL-10), 9.1 ± 0.3 ka (DOL-11) and 9.3 ± 0.4 ka (DOL-12) (Figure 4B) with a mean age of 10.0 ± 1.4 ka ($n=3$).

- Middle valley – On the NW side of the valley, a large landslide occurred following deglaciation. The landslide includes minor landforms, with the presence of several debris flows and very active soli-fluction dynamics that are indicative of intense reworking of the major slope deposit. The boulder samples DOL-1 and DOL-2 were taken ~ 335 m a.s.l. in

the most horizontal distal and stable part of the slide. The only valid sample returned an age of 2.5 ± 0.3 ka (DOL-01).

- Upper valley – The main ice tongue built a voluminous moraine complex integrated by three frontal ridges ~ 0.7 km from the current glacier front (Figure 4A). Two lichenized moraine boulders of the outermost ridge were sampled (DOL-08, DOL-09; at ~ 400 m a.s.l.),

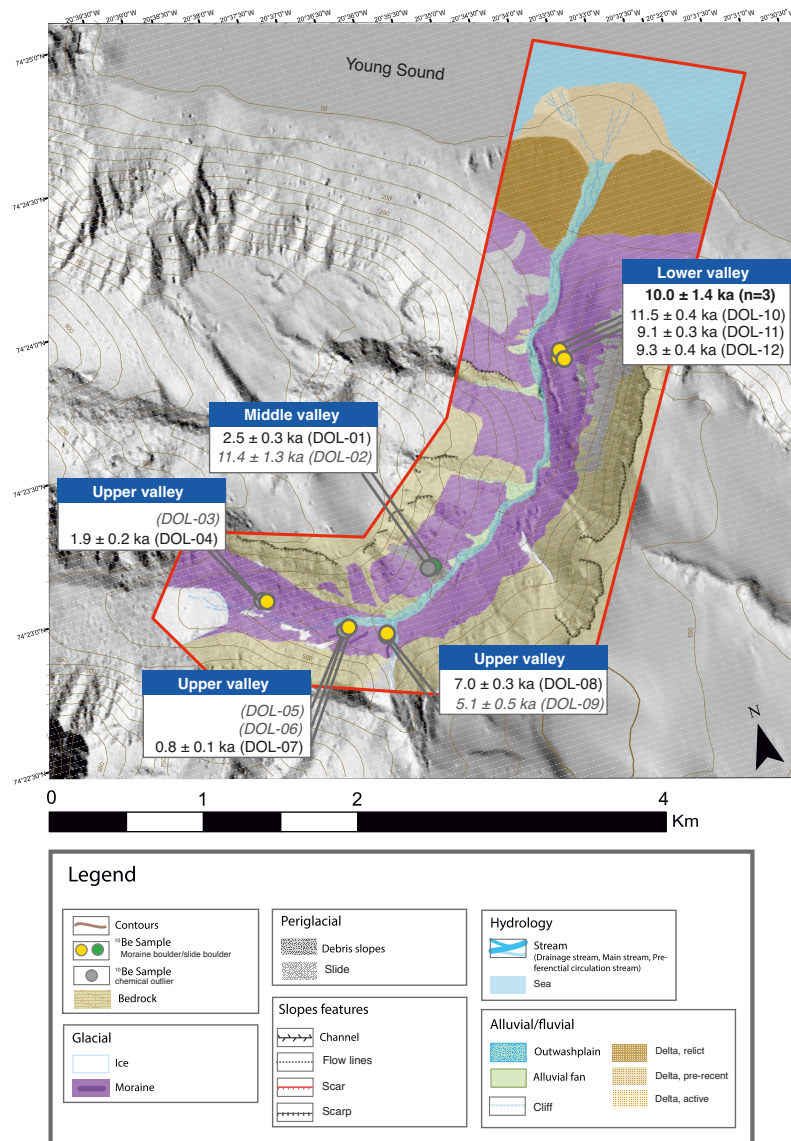


Figure 3. Dolomit Valley geomorphological map including the main landforms together with the CRE results shown in Tables 1 and 2.

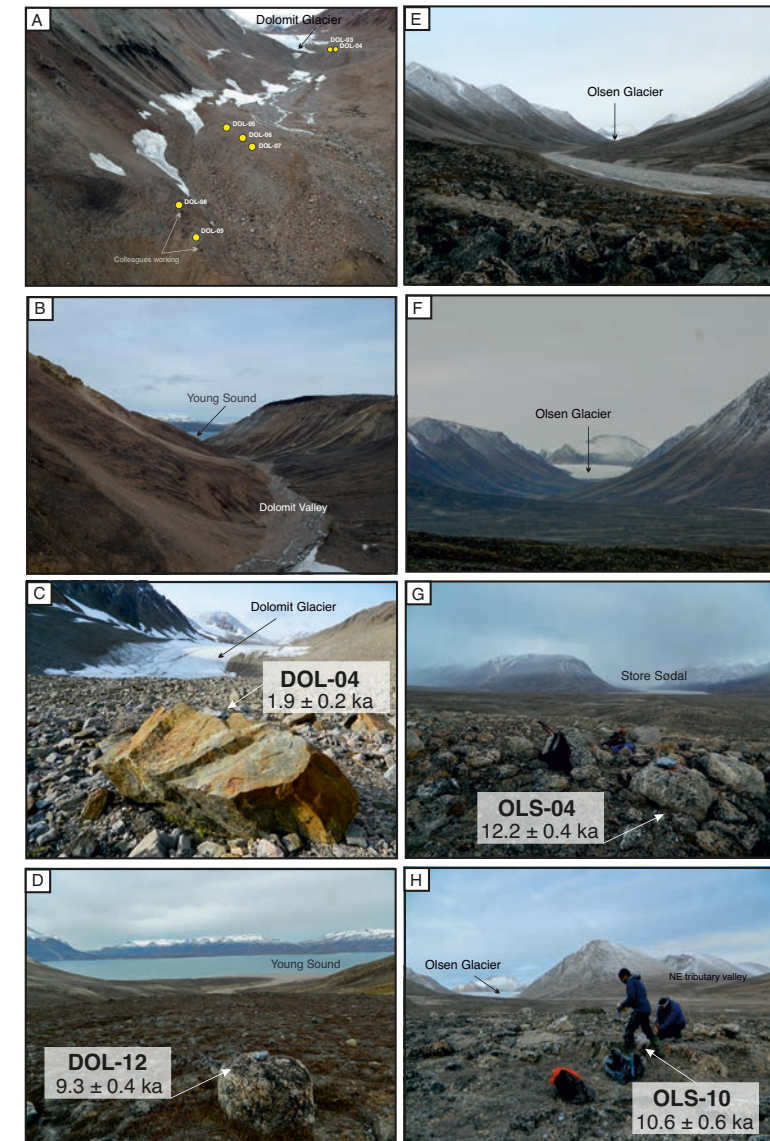


Figure 4. Examples of the different types of sampled and dated glacial landforms. See Figures 2 and 3 for the locations of the samples shown in the photographs. (A) and (B) general views of the Dolomit Valley; (C) and (D) examples of sampled boulders in Dolomit Valley; (E) and (F) general views of the Olsen Valley; (G) and (H) examples of sampled boulders in Olsen Valley.

and only one valid sample that yielded an age of 7.1 ± 0.3 (DOL-08). Three moraine boulders from the next well-preserved moraine (DOL-05, DOL-06, DOL-07; at ~ 420 m a.s.l.; Figure 3) were sampled and returned the only exposure age of 0.8 ± 0.1 ka (DOL-07). The closest samples to the ice margin were obtained from two boulders of the (sub)recent moraine ridge ~ 200 m from the present-day glacier front (DOL-03, DOL-04; at ~ 500 m a.s.l.), with one exposure age of 1.9 ± 0.2 ka (DOL-04) (Figure 4C). A well-preserved medial moraine (2-4 m-high) extended for ~ 160 m between the two most recent moraine complexes which were not sampled due to suspicion that they were ice-cored.

5. DISCUSSION

The chronological framework provided by our age dataset serves to reconstruct general spatial and temporal patterns with regards to glacial oscillations and climate variability in the region since the onset of the deglaciation. However, some interpretations must be taken with caution as paleoenvironmental studies reconstructing the timing of glacial oscillations in Greenland have reported problems associated with nuclide inheritance and postglacial dynamics affecting the interpretation of the sample results (Biette et al., 2020; Corbett et al., 2013; Farnsworth et al., 2018; Garcia-Oteyza et al., 2022; Goehring et al., 2010; Kelly et al., 2008; Larsen et al., 2021; Skov et al., 2020; Young et al., 2021).

5.1 CONSIDERATIONS ON THE GEOCHRONOLOGICAL DATASET

The CRE dates from the Olsen and Dolomit valleys show several chronological inconsistencies with the geomorphological sequences that need to be examined independently in detail in order to assess the validity of the results and their geochronological meaning for the correct interpretation of landscape evolution.

Some of the ice caps in the region have been defined as cold-based (Behm et al. 2020), which has major implications for past surface erosion. This type of glaciers can preserve the signal of past glacial periods and leave behind undisturbed relict landscapes (Briner et al. 2006; Davis et al. 2006; Fabel et al. 2002; Sugden et al. 2005; Corbett et al. 2011, 2013; Davis et al. 2006; Stroeven et al. 2002), which are a potential source of nuclide inheritance and uncertainties associated with CRE dating as ^{10}Be atoms accumulated from past deglacial periods is often incompletely eliminated as rock surfaces are not eroded deeply enough (Atkins et al. 2002). Our dataset for both valleys must be interpreted considering the different erosive capacities of each glacial advance - either because it is a cold-based glacier (insufficient reworking) or because of the brevity of Holocene advances - together with the potential effect of postglacial paraglacial processes in the area. Indeed, this has been identified in the neighboring Zackenberg Valley where samples provided younger ages than the real deglaciation age due to postglacial boulder remobilization by rock falls, debris flows, solifluction, etc. (Garcia-Oteyza et al., 2022).

Olsen Valley

Along the valley, the dated landforms showed some inconsistencies that are worth highlighting. At the lower Olsen Valley, the moraine ridges returned inverted ages: the external one yielded an age of 9.7 ± 1.2 ka (OLS-05 and OLS-06) and the internal one returned an age of 12.2 ± 0.4 ka (OLS-04). Further-more, the polished surface sample at this part of the valley also showed an age inversion, with an exposure age of 13.8 ± 0.5 ka

(OLS-01). In the middle and upper part of the valley, closer to the ice front, the ages of samples did not follow a stratigraphical order, although they yielded close ages. One polished surface sample from the upper part of the valley yielded an age of 15.0 ± 0.5 ka (OLS-09), which is stratigraphically inconsistent within the surrounding dated bedrock samples that reported ages ranging from 13.8 to 9.4 ka (OLS-01, OLS-07, OLS-08, OLS-10, and OLS-11). This time range is interpreted to be associated with ice thinning and the gradual exposure of the landscape to cosmic-ray flux. However, the polished surface sample OLS-09 is significantly out of range and is therefore interpreted to have nuclide inheritance, considered a geomorphological outlier and excluded from the age dataset.

These inconsistencies may reflect different sources of error that will be debated further in the following sections of the discussion: i) the distortion of moraine ages by GLOFs (dragging of blocks from slopes, removal of blocks, etc.), although the significance of the erosive capacity of GLOFs remains to be defined; ii) possible ice core moraines that produce a different evolution of the boulders; and iii) due to inheritance problems, the polished surface samples tend to return older ages than expected.

Paleoclimatically, the abundance of ages between 11 and 9 ka along the valley could suggest a rapid Early Holocene deglaciation with possible advances at cold events including the Preboreal oscillation (PBO) (11.4-11.5 ka) and the 9.2 ka event.

Dolomit Valley

The only landform with a consistent age dataset is the lower valley frontal moraine (10.0 ± 1.4 ka (DOL-10, DOL-11 and DOL-12)), where samples were obtained from an area less affected by slope processes than the rest of the valley slopes (as observed in the field). These ages confirmed that the glacier was already disconnected from Young Sound in the Early Holocene.

The age (2.5 ± 0.3 ka; DOL-01) of the landslide boulder in the middle valley marks the age of one of the multiple landslide events that probably occurred throughout the deglaciation.

The upper part of the valley showed a moraine boulder age of 7.0 ka (DOL-08), which may have been moved but which is globally consistent with the stratigraphy despite being just one sample, and it might mark the retreat of the glacier during the Middle Holocene.

Near the glacier front, we found inverted CRE ages: the sample closer to the ice front moraine yielded an age of 1.9 ± 0.2 ka (DOL-04), older than the sample from the lower moraine of the system that returned an age of 0.8 ± 0.1 ka (DOL-07). These CRE ages could indicate either that the more distal boulder was moved from its original position, thus resulting in a younger age than might be expected, or that the sample nearest to the ice front boulder may have been affected by inheritance probably associated with insufficient (en)glacial reworking. Other factors could also have produced this age inversion, including the occurrence of postglacial stabilization of moraine boulders associated with ice-cored moraines or slope readjustment to the new ice-free conditions. As the two samples were taken close to the glacial front (< 1 km), it is likely that both are associated with Neoglacial advances that occurred prior to the LIA, although neither was considered to be a geomorphological outlier.

The comparison of datasets from the two valleys reveals (i) more clustered ages dataset in the Olsen Valley, and more scattered ages in the Dolomit Valley (Figure 5); and (ii) more

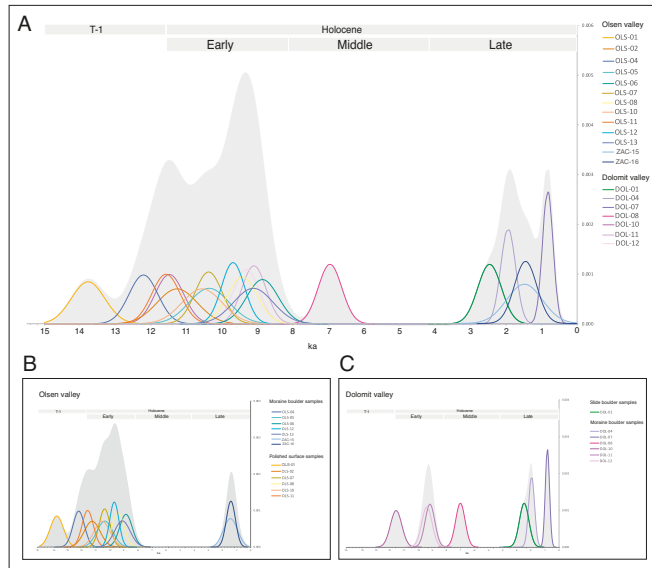


Figure 5. (A) Probability distribution functions of ^{10}Be ages with (with internal uncertainties) for all the samples of our final dataset of accepted ages; (B) Olsen Valley probability distribution function; (C) Dolomit probability distribution functions.

and Haeberli, 2007) and rock mechanical properties that may control slope destabilization (Krautblatter et al. 2013). Soft rocks or porous bedrock (such as sedimentary rocks) are generally more susceptible to frost shattering due to high porosity and low strength than massive / hard jointed rocks (e.g., metamorphic bedrock) (Murton, 2008). All the samples from the Dolomit Valley were obtained in sedimentary bedrock settings that enhance more intense paraglacial dynamics (e.g., solifluction, alluvial fans, landslides) that destabilized

outliers (5 samples) within the Dolomit Valley age dataset than the Olsen Valley (2).

One of the main factors explaining these differences might be the lithology of the study areas, which plays a key role in the intensity of (postglacial) periglacial processes affecting the valley slopes. The more weatherable the underlying lithologies (e.g., sedimentary rocks), the more intensely paraglacial processes affect the slopes and their stability. Periglacial processes following glacial retreat have a significant impact on slope mass wasting, which is even more enhanced in permafrost terrain where its effects on different lithologies are highly variable because of pore structure dependence (Gruber

the slopes and favored the reworking of the samples, thus altering the real deglaciation ages. By contrast, all samples from the Olsen Valley were taken from metamorphic substrates and reflected the lower intensity of mobilization processes on the slopes and, therefore, the greater stability of the landforms and dated boulders. The effect of underlying lithology for CRE dating was also seen in the neighboring Zackenberg Valley, which showed differences between samples taken on sedimentary (Figure 6B) and metamorphic (Figure 6A) slope substrates (Garcia-Oteyza et al., 2022). In Zackenberg Valley, the slopes with sedimentary lithology returned more outliers (both chemical and geomorphological) and more scattered ages, while samples on metamorphic substrates returned fewer outliers and more clustered ages (Figure 6A; Garcia-Oteyza et al. 2022). This may indicate that the differences between the age datasets of our two valleys are due, at least in part, to the substrates on which the landforms lied.

5.2 INFERENCE OF GLACIAL OSCILLATIONS AND CLIMATIC CONDITIONS

The geomorphological and geochronological evidence enables the reconstruction of a general chronological history of the deglaciation of these two valleys that can be compared with the paleoenvironmental evolution detected across Greenland during T-1 and the Early Holocene.

The abundance and variety of glacial landforms existing in both valleys down to sea level demonstrates that the area was heavily glaciated during the last glacial cycle. Both valleys were probably filled by ice to the mountain plateaus, similar to what occurred in other valleys of the Young Sound-Tyrolerfjord area (Garcia-Oteyza et al., 2022, 2023). The expansion of the GrIS and the surrounding ice caps during the last glacial cycle is well-documented in several areas in NE Greenland despite limited chronological control of the sequence of glacial advances and retreats. Prior to the Last Glacial Maximum (LGM), between 115-75 ka, glacier fronts in this region extended to reach the inner continental shelf (Funder et al., 2011; Lecavalier et al., 2014). The Olsen and Dolomit valleys must therefore have been occupied by an extensive glacial system interconnected with their tributary valleys feeding the major Young Sound glacier. Direct evidence shows rapid deglaciation following the LGM in NE Greenland (Vasskog, 2015) confirming the process also suggested by modelling studies (Lecavalier et al., 2014; Simpson et al., 2009; Vasskog et al., 2015).

A number of paleoclimate records reveal abrupt temperature changes during T-1 (5–15 °C), with a strongly seasonal regime that must have driven changes in GrIS volume (Buizert et al., 2014; Vasskog et al., 2015). Most of the currently ice-free areas in the southern sector of NE Greenland became deglaciated during this period and, broadly across Greenland, the GrIS had already retreated behind present-day boundaries by 10-9 ka (Carlson et al., 2014; Larsen et al., 2015; Reusche et al., 2018; Skov et al., 2020). During T-1 through the Early Holocene transition, glacial advances and retreats favored the formation of multiple moraine ridges at different elevations on slopes and valley bottoms, indicative of rapid climate variability. The long-term retreat and glacial shrinking during T-1 in Greenland was not a continuous process; it included by several cold events that favored readvances or glacial stabilization phases, with periods of moraine formation during the

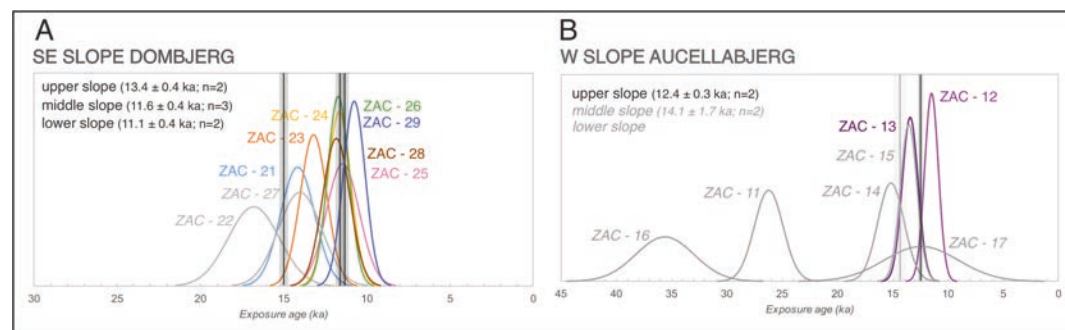


Figure 6. (A) Probability distribution functions of ^{10}Be ages from SE Dombjerg slope (Zackenberg Valley) that have metamorphic bedrock. (B) Probability distribution functions of ^{10}Be ages from W Aucellabjerg slope (Zackenberg Valley) that have sedimentary bedrock (Modified from Garcia-Oteyza et al. 2022, see this original publication for the exact location of the samples).

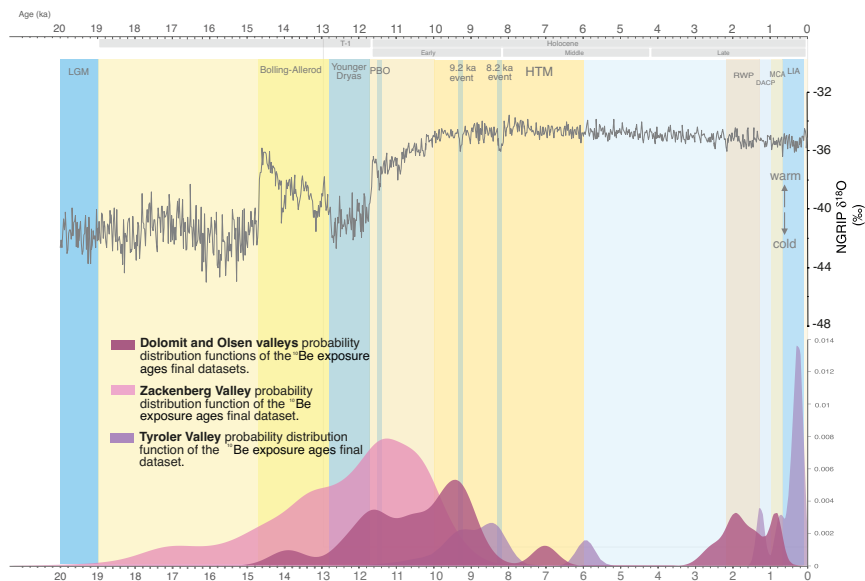


Figure 7. (A) $\delta^{18}O$ record of the NGRIP ice core smoothed with a 15 interval moving average (GICC05modelext, 5-point running mean; Rasmussen et al., 2006). (B) Sum probability distribution functions of all ^{10}Be ages (Olsen and Dolomit valleys). Sum probability distribution functions of Zackenberg Valley (Garcia-Oteyza et al. 2023) and Tyroler Valley (Garcia-Oteyza et al. 2023) ^{10}Be ages.

Late Glacial (Carlson et al., 2014; Larsen et al., 2015; Reusche et al., 2018; Skovet al., 2020).

Our age dataset reports the oldest deglaciation ages from samples located in the lowest parts of the valleys, suggesting a rapid deglaciation within the range from ~14.3 to 11.9 ka, when the glacier valleys became disconnected from the main ice tongues. This general retreat trend was not homogeneous, and it may have included interspersed glacial advances. Close age differences on the Olsen upper valley polished surface samples reinforce the idea of a rapid ice retreat during the Early Holocene with a variable ice cover thickness.

Most of the age results from moraine boulders are within the range of 11.5 to 9.1 ka (Figure 7). Comparing with the climate periods and events visible on the NGRIP ice core $\delta^{18}O$ record (Rasmussen et al., 2006) (Figure 7), our results may be related to the interruption of the long-term deglaciation trend by two cold events: the Preboreal oscillation (PBO) (11.5-11.4 ka) and the 9.2 ka event (9.5-9.2 ka interval) (Figure 7). These abrupt cooling events are well-defined in Greenland ice-core isotope records and appear prominently and synchronously in most of them (Kobashi et al., 2007; Rasmussen et al., 2007; Thomas et al., 2007). Both events likely involved the alteration of Atlantic Meridional Overturning Circulation (AMOC) driven by freshwater input into the North Atlantic Ocean via rapidly melting ice sheets (Jomelli et al., 2022; Renssen et al., 2009; Thornalley et al., 2018). The best-known of these events is that at 9.2 ka, for which evidence of a notable climatic anomaly around the Northern Hemisphere is sparse but detectable in multiple paleorecords

(Fleitmann et al., 2008), including ^{10}Be moraine chronologies on Baffin Bay region and western Greenland (Crump et al., 2020; Young et al., 2021). Multiple ^{10}Be CRE studies show that, while brief, this event was of sufficient duration to elicit a significant response by (at least) the western GrIS (Young et al., 2020, 2013). Based on gas-phase temperatures from Greenland ice (Kobashi et al., 2007, 2017), the 9.2 ka event is characterized by 2-3 °C mean-annual cooling over ~100 years. The PBO event is less well defined, but this stillstand may reflect an interruption of the overall warming near the YD termination in response to a brief episode of freshwater-forced cooling that weakened the AMOC. Similar studies based on ^{10}Be CRE dating detected this event at the GrIS margins in Baffin Bay (Young et al., 2020), dating stillstands at ~11.6 ka and ~9.1 ka, and in NE Greenland with moraines dated at ~11.4 ka (Levy et al., 2016).

Temperatures continued to rise through the Early Holocene (as well marked on the NGRIP record (Figure 7)) and accelerated the deglaciation pattern observed across Greenland and most Northern Hemisphere glaciers at that time (Buizert et al., 2014; Clark et al., 2012). The glacial shrinking recorded in our study occurred parallel to increased glacio-isostatic uplift, delta progradation (~13-11 to 6.3 ka) and permafrost aggradation (Christiansen et al., 2002; Gilbert et al., 2017). Our age assemblages at the end of the Early Holocene denote a rapid glacial retreat in the Dolomit and Olsen valleys, with the deglaciation of the lowest sectors by 11-10 ka. This is consistent with the paleoclimate reconstructions as well as with previous ^{10}Be CRE chronologies from the neighboring valleys of the area that show the tributaries disconnection from the main ice stream at ~11-10 ka in the Zackenberg Valley (Garcia-Oteyza et al., 2022) (Figure 7), at ~10-8.5 ka in the Tyroler Valley (Garcia-Oteyza et al., 2023a) (Figure 7), and after ~10 ka in the northern sector of Clavering Island (Biette et al., 2020).

The Holocene Thermal Maximum (HTM) was a relatively warm phase between 11 and 5 ka commonly associated with the orbitally-forced summer insolation maximum, but its timing and magnitude varied between regions and was pronounced at high latitudes where it was amplified by polar amplification (Renssen et al., 2012, 2009). Ice masses across the North Atlantic region, including Greenland, retreated during the mid-Holocene and re-advanced during the Late Holocene mainly due to changes in the intensity of the AMOC (Jomelli et al., 2022). In Greenland, the GrIS was behind its present-day ice limits at the end of the HTM and during the mid-Holocene, while most peripheral glaciers were smaller than at present or even disappeared completely at that time (Solomina et al., 2015). As in most areas in NE Greenland, glacial records from the mid-Holocene to the onset of the Late Holocene are absent in Olsen and Dolomit valleys, as glacial fronts were likely situated behind their present positions. This is also confirmed by other studies in the region, such as on Clavering Island (Biette et al. 2022) and in Tyroler Valley (Garcia-Oteyza et al., 2023a), where the lack of geomorphic evidence suggests that glaciers were smaller during most of the Holocene than at present.

Paleoclimatic data suggests that the region experienced relatively warm conditions from 8 to 6 ka BP (Figure 7), followed by a general overall decline in temperatures after ~5 ka that was interrupted by a series of multi-decadal to century-scale fluctuations (Bradley and Bakke, 2019). CRE dating results from SW Greenland indicate that the minimum Holocene extent of the GrIS likely occurred after ~5 ka, and at some GrIS edges occurred at 4-3 ka (Larocca et al., 2020; Larsen et al., 2018; Schweinsberg et al., 2019); subsequently, glacier expansion occurred in some areas in SW and E Greenland (Larocca et al 2020; Medford

et al. 2021) and the GrIS margin may have approached its eventual historical maximum extent as early as ~2 ka (Young et al. 2021).

The geomorphology and ages of the Dolomit Valley samples give information about events through the Late Holocene. The landslide sample at ~2.5 ka indicates that part of the Middle valley was already deglaciated at that time. Rapid deglaciation, reaching the Upper Valley, is indicated by the presence of a well-preserved medial moraine, although the moraine samples in the upper part of the valley also imply that this deglaciation was interrupted by minor advances. In both valleys, the closest to the ice margins moraine samples registered glacial advances at ~1.9 and ~1.5 ka.

Late Holocene glacial advances have also been CRE dated from the Theodolit Plateau, on W Clavering Island (Biette et al., 2020; Jomelli et al., 2022), at ~3 ka, 1 ka and the LIA. Around the area, lake sediments also documented glacier advances including from Madsen Lake (~20 km W of Zackenberg), which suggested that three glacier advances occurred over the last 2000 years (Adamson et al., 2019), the first two at 1.3 and 0.8 ka, and the third at 0.7 ka. At Aucella Lake in the Zackenberg Valley area, lake sediments documented cold climate conditions at ~3.8- 3.4 ka, at ~2.4- 2.0 ka with a minimum at ~1.2- 0.8 ka and colder more humid climate at LIA with the maximum glacial extent in the area before ~0.5 ka (Garcia-Oteyza et al. 2023b). In Kulusuk (~1000 km south of Zackenberg), sediment cores document glacier advances during Late Holocene, with the most extensive advances occurred at the end of the LIA (Balascio et al. 2015).

The most recent CRE sample in Dolomit Valley (0.8 ± 0.1) was from a moraine boulder located ~1 km from the ice front. Although no other results are available to validate this age, it is very similar to that reported ~1000 km S along the NE Greenland coast (Biette et al. 2022). These authors reported an early LIA advance at ~0.66–0.70 ka that formed a moraine located at ~500 m from the current ice front. Other studies at Scoresby Sund assumed that the ice caps reached the maximum extent during the LIA at ~0.7–0.3 ka (Kelly et al., 2008; Levy et al., 2014).

5.3 LIMITS OF COSMOGENIC DATING IN GREENLAND

The problems detected in the Olsen and Dolomit valleys samples are common to the application of CRE methods in Greenland and other Arctic sectors, where cold-based glaciers dominate, the level of continuous or discontinuous permafrost is close to sea level, or where samples are taken at the bottom of valleys under steep slope walls, where they could be subjected to frequent avalanches and flooding.

Cosmogenic nuclide inheritance, which increases progressively with altitude, rising to over 600 ka on plateaus, is a considerable problem in Greenland. Inheritance may be present but is generally much more limited in the valley bottoms at low altitude (Roberts et al., 2013; Skov et al., 2020), and comparative studies have shown that cosmogenic inheritance may or may not be present in neoglacial moraines at the bottom of the valleys. The level of inheritance largely depends on the entirety of Holocene advances, as in many cases the erosion caused by these advances is unable to completely erase the heritage accumulated from previous glacial erosional activity (Larsen et al., 2021). This type of lower erosional capacity of these re-advances is more frequent for local mountain glaciers in Greenland, where boulders with ages older than those of the same moraine frequently occur because

these re-advance moraines can mix strongly inherited boulders with intensely eroded boulders with no inheritance (Larsen et al., 2021, 2020). Although studies about inheritance on bedrock polished surfaces in valley floors are very limited (Bierman et al., 2018; Ewertowski and Tomczyk, 2015; Levy et al., 2020), the erosive capacity of Holocene reworking on these rock surfaces appears to be decisive in erasing previous inheritance and may largely depend on the degree of weakness of the rock itself (Levy et al., 2020). For these reasons, polished bedrock with significant inheritance can be found at the bottom of the valleys where rock strength has prevented the erosion by new glacial advances, and this bedrock surfaces can be located near other outcrops that have been eroded and do not present inheritance. As such, bedrock outcrops located very close to each other may give ages that differ by 1-3 ka in an illogical geomorphological order (Levy et al., 2020; Garcia-Oteyza et al. 2022). Another common problem in Greenland and throughout the Arctic is related to the stabilization phases of the Holocene ice-core moraines that are common in these regions. After formation, due to the uneven insulation capacity of the till, the ice melts under the moraines in an irregular way, which causes an irregular stabilization period of the boulders, and therefore that their exposure to cosmogenic radiation is highly variable. As a result of this slow moraine degradation, different CRE ages may be found in the same moraine (Briner et al., 2005; Zech et al., 2005). In these cases, the oldest ages unaffected by inheritance are likely to reflect the age of moraine formation (Crump et al., 2017).

The other important process that can alter CRE ages is strong post-glacial erosion due to the importance of steep slope processes, permafrost degradation (Christiansen et al., 2008; Rasmussen et al., 2018) and intense nival action (Christiansen, 1998). These processes can both reset the clock that records ^{10}Be accumulation since glacial sedimentation of boulders, or introduce boulders onto the valley floor from higher altitude sectors, where cosmogenic inheritance is more pronounced (Levy et al., 2020; Garcia-Oteyza et al. 2022). Another important post-glacial process are the GLOFs. Their frequency in the Olsen Valley is well known thanks to the location of the Zackenberg Research Station, but they may also be common in many other Greenland valleys due to the abundance of proglacial lakes and retreating glacial fronts (Dømggaard et al., 2023). In the case of Olsen Valley, significant GLOFs have been detected with high erosive velocity and power, and that have caused significant alterations of the glacial geomorphology of the valley floor (Behm et al., 2020; Dømggaard et al., 2023). As shown by recent events, GLOFs not only erode and alter the valley floor and sides, but also favor subsequent gravitational processes, destabilizing the slopes (Dømggaard et al., 2023).

6. CONCLUSIONS

Therefore, despite the limited number of valid CRE ages, CRE results from Olsen and Dolomit valleys confirm the general pattern observed in NE Greenland: (i) massive deglaciation and disconnection of glaciers from the main glacial systems during the Early Holocene; (ii) no evidence of glacial activity during the mid-Holocene, probably due to the existence of smaller ice masses than at present; and (iii) glacier expansion during the Late Holocene, with a LIA advance representing the last major period of glacial regrowth. Future

studies must complement the chronological framework of these glacial oscillations and the climatic background of these environmental changes.

From this study, we draw the following conclusions:

- This study provides new geomorphological and geochronological data to better understand the complex spatial and temporal patterns with regards to glacial oscillations and climate variability in the region since the onset of the deglaciation.
- The interpretation of our ages must consider the limitations related to the application of CRE methods in areas with very active paraglacial dynamics and cold-based glaciers.
- To successfully apply CRE dating techniques, the lithology of samples and of the study area, as well as the intensity of paraglacial processes, must be taken into account.

ACKNOWLEDGEMENTS

This study was funded by the NEOGREEN (PID2020-113798GB-C31) and PALEOGREEN (CTM2017-87976-P) projects of the Spanish Ministerio de Economía y Competitividad. Field research was also supported by the research group ANTALP (Antarctic, Arctic, Alpine Environments; 2017-SGR-1102) funded by the Agència de Gestió d'Ajuts Universitaris i de Recerca of the Government of Catalonia. Julia Garcia-Oteyza was supported by an FPI fellowship from the Spanish Ministry of Science. The ¹⁰Be measurements were performed at the ASTER AMS national facility (CEREGE, Aix-en-Provence), which is supported by the INSU/CNRS and the ANR through the “Projets thématiques d'excellence” programme for the “Equipements d'excellence” ASTER-CEREGE action and IRD. We are also grateful to Jesús Ruiz and Zackenberg Research Station for field support.

Adamson, K., Lane, T., Carney, M., Bishop, T., Delaney, C., 2019. High-resolution proglacial lake records of pre-Little Ice Age glacier advance, northeast Greenland. *Boreas* 48, 535–550. <https://doi.org/10.1111/bor.12361>

Atkins, C., Barrett, P., Hicock, S., 2002. Cold glaciers erode and deposit: Evidence from Allan Hills, Antarctica. *Geology* 30, 659–662. [https://doi.org/10.1130/0091-7613\(2002\)030<0659:CGEAD>2.0.CO;2](https://doi.org/10.1130/0091-7613(2002)030<0659:CGEAD>2.0.CO;2)

Balco, G., 2019. Glacier Change and Paleoclimate Applications of Cosmogenic-Nuclide Exposure Dating. *Annu. Rev. Earth Planet. Sci.* 48. <https://doi.org/10.1146/annurev-earth-081619-052609>

Balco, G., Stone, J.O., Lifton, N.A., Dunai, T.J., 2008. A complete and easily accessible means of calculating surface exposure ages or erosion rates from ¹⁰Be and ²⁶Al measurements. *Quat. Geochronol.* 3, 174–195. <https://doi.org/10.1016/j.quageo.2007.12.001>

Behm, M., Walter, J.I., Binder, D., Cheng, F., Citterio, M., Kulesa, B., Langley, K., Limpach, P., Mertl, S., Schöner, W., Tamstorf, M., Weyss, G., 2020. Seismic characterization of a rapidly-rising jökulhlaup cycle at the A.P. Olsen Ice Cap, NE-Greenland. *J. Glaciol.* 66, 329–347. <https://doi.org/10.1017/jog.2020.9>

Bierman, P.R., Rood, D.H., Shakun, J.D., Portenga, E.W., Corbett, L.B., 2018. Directly dating postglacial Greenlandic land-surface emergence at high resolution using in situ ¹⁰Be. *Quat. Res. (United States)* 90, 110–126. <https://doi.org/10.1017/qua.2018.6>

Biette, M., Jomelli, V., Chenet, M., Braucher, R., Rinterknecht, V., Lane, T., 2020. Mountain glacier fluctuations during the Lateglacial and Holocene on Clavering Island (northeastern Greenland) from ¹⁰Be moraine dating. *Boreas* 49, 873–885. <https://doi.org/10.1111/bor.12460>

Bradley, R.S., Bakke, J., 2019. Is there evidence for a 4.2 ka BP event in the northern North Atlantic region? *Clim. Past* 15, 1665–1676. <https://doi.org/10.5194/cp-15-1665-2019>

Briner, J.P., Kaufman, D.S., Manley, W.F., Finkel, R.C., Caffee, M.W., 2005. Cosmogenic exposure dating of late Pleistocene moraine stabilization in Alaska. *Bull. Geol. Soc. Am.* 117, 1108–1120. <https://doi.org/10.1130/B25649.1>

Briner, J.P., Miller, G.H., Davis, P.T., Finkel, R.C., 2006. Cosmogenic radionuclides from fiord landscapes support differential erosion by overriding ice sheets. *Bull. Geol. Soc. Am.* 118, 406–420. <https://doi.org/10.1130/B25716.1>

Buizert, C., Gkinis, V., Severinghaus, J.P., He, F., Lecavalier, B.S., Kindler, P., Leuenberger, M., Carlson, A.E., Vinther, B., Masson-Delmotte, V., White, J.W.C., Liu, Z., Otto-Bliesner, B., Brook, E.J., 2014. Greenland temperature response to climate forcing during the last deglaciation. *Science* (80-.). 345, 1177–1180. <https://doi.org/10.1126/science.1254961>

Buus-Hinkler, J., Hansen, B.U., Tamstorf, M.P., Pedersen, S.B., 2006. Snow-vegetation relations in a High Arctic ecosystem: Inter-annual variability inferred from new monitoring and modeling concepts. *Remote Sens. Environ.* 105, 237–247. <https://doi.org/10.1016/j.rse.2006.06.016>

Carlson, A.E., Winsor, K., Ullman, D.J., Brook, E.J., Rood, D.H., Axford, Y., LeGrande, A.N., Anslow, F.S., Sinclair, and G., 2014. Earliest Holocene south Greenland ice sheet retreat within its late Holocene extent 5514–5521. <https://doi.org/10.1002/2014GL060800>.

Christiansen, H.H., 1998. Nivation forms and processes in unconsolidated sediments, NE Greenland. *Earth Surf. Process. Landforms* 23, 751–760. [https://doi.org/10.1002/\(SICI\)1096-9837\(199808\)23:8<751::AID-ESP886>3.0.CO;2-A](https://doi.org/10.1002/(SICI)1096-9837(199808)23:8<751::AID-ESP886>3.0.CO;2-A)

Christiansen, H.H., Bennike, O., Böcher, J., Elberling, B., Humlum, O., Jakobsen, B.H., 2002. Holocene environmental reconstruction from deltaic deposits in Northeast Greenland. *J. Quat. Sci.* 17, 145–160. <https://doi.org/10.1002/jqs.665>

Christiansen, H.H., Sigsgaard, C., Humlum, O., Rasch, M., Hansen, B.U., 2008. Permafrost and Periglacial Geomorphology at Zackenberg. *Adv. Ecol. Res.* 40, 151–174. [https://doi.org/10.1016/S0065-2504\(07\)00007-4](https://doi.org/10.1016/S0065-2504(07)00007-4)

Clark, P.U., Dyke, A.S., Shakun, J.D., Carlson, A.E., Clark, J., Wohlfarth, B., Mitrovica, J.X., Hostetler, S.W., McCabe, A.M., 2009. The Last Glacial Maximum. *Science*. 325, 710–714. <https://doi.org/10.1126/science.1172873>

Clark, P.U., Shakun, J.D., Baker, P.A., Bartlein, P.J., Brewer, S., Brook, E., Carlson, A.E., Cheng, H., Kaufman, D.S., Liu, Z., Marchitto, T.M., Mix, A.C., Morrill, C., Otto-Bliesner, B.L., Pahnke, K., Russell, J.M., Whitlock, C., Adkins, J.F., Blois, J.L., Clark, J., Colman, S.M., Curry, W.B., Flower, B.P., He, F., Johnson, T.C., Lynch-Stieglitz, J., Markgraf, V., McManus, J., Mitrovica, J.X., Moreno, P.I., Williams, J.W., 2012. Global climate evolution during the last deglaciation. *Proc. Natl. Acad. Sci. U. S. A.* 109. <https://doi.org/10.1073/pnas.1116619109>

Corbett, L.B., Bierman, P.R., Graly, J.A., Neumann, T.A., Rood, D.H., 2013. Constraining

Landscape History and Glacial Erosivity Using 4, 9–11.

Crump, S.E., Anderson, L.S., Miller, G.H., Anderson, R.S., 2017. Interpreting exposure ages from ice-cored moraines: a Neoglacial case study on Baffin Island, Arctic Canada. *J. Quat. Sci.* 32, 1049–1062. <https://doi.org/10.1002/jqs.2979>

Crump, S.E., Young, N.E., Miller, G.H., Pendleton, S.L., Tulenko, J.P., Anderson, R.S., Briner, J.P., 2020. Glacier expansion on Baffin Island during early Holocene cold reversals. *Quat. Sci. Rev.* 241. <https://doi.org/10.1016/j.quascirev.2020.106419>

Davis, P.T., Briner, J.P., Coulthard, R.D., Finkel, R.W., Miller, G.H., 2006. Preservation of Arctic landscapes overridden by cold-based ice sheets. *Quat. Res.* 65, 156–163. <https://doi.org/10.1016/j.yqres.2005.08.019>

Dømgaard, M., Kjeldsen, K.K., Huiban, F., Carrivick, J.L., Khan, S.A., Bjørk, A.A., 2023. Recent changes in drainage route and outburst magnitude of the Russell Glacier ice-dammed lake, West Greenland. *Cryosphere* 17, 1373–1387. <https://doi.org/10.5194/tc-17-1373-2023>

Elberling, B., Tamstorf, M.P., Sigsgaard, C., Illeris, L., Bay, C., B.H., H., Christensen, T.R., Hansen, E.S., Jakobsen, B.H., Beyens, L., 2008. Soil and Plant Community-Characteristics and Dynamics at Zackenberg in Meltofte, H. et al. (ed.), *High-Arcti. ed.*

Ewertowski, M.W., Tomczyk, A.M., 2015. Quantification of the ice-cored moraines' short-term dynamics in the high-Arctic glaciers Ebbabreen and Ragnarbreen, Petuniabukta, Svalbard. *Geomorphology* 234, 211–227. <https://doi.org/10.1016/j.geomorph.2015.01.023>

Fabel, D., Stroeven, A.P., Harbor, J., Kleman, J., Elmore, D., Fink, D., 2002. Landscape preservation under fennoscandian ice sheets determined from in situ produced ¹⁰Be and ²⁶Al. *Earth Planet. Sci. Lett.* 201, 397–406. [https://doi.org/10.1016/S0012-821X\(02\)00714-8](https://doi.org/10.1016/S0012-821X(02)00714-8)

Farnsworth, L.B., Kelly, M.A., Bromley, G.R.M., Axford, Y., Osterberg, E.C., Howley, J.A., Jackson, M.S., Zimmerman, S.R., 2018. Holocene history of the Greenland Ice-Sheet margin in Northern Nunatarssuaq, Northwest Greenland. *Arktos* 4, 0. <https://doi.org/10.1007/s41063-018-0044-0>

Fleitmann, D., Mudelsee, M., Burns, S.J., Bradley, R.S., Kramers, J., Matter, A., 2008. Evidence for a widespread climatic anomaly at around 9.2 ka before present. *Paleoceanography* 23. <https://doi.org/10.1029/2007PA001519>

Funder, S., Kjeldsen, K.K., Kjær, K.H., O Cofaigh, C., 2011. The Greenland Ice Sheet During the Past 300,000 Years: A Review. *Dev. Quat. Sci.* 15, 699–713. <https://doi.org/10.1016/B978-0-444-53447-7.00050-7>

Garcia-Oteyza, J., Giralt, S., Pla-Rabes, S., Antoniades, D., Oliva, M., Ghanbari, H., Osorio-Serrano, R., Palacios, D., 2023b. A \square 5000 year multiproxy record of summer climate in NE Greenland. *Sci. Total Environ.* 906, 167713. <https://doi.org/10.1016/j.scitotenv.2023.167713>

Garcia-Oteyza, J., Oliva, M., Palacios, D., Fernández-Fernández, J.M., Schimmelpfennig, I., Andrés, N., Antoniades, D., Christiansen, H.H., Humlum, O., Léanni, L., Jomelli, V., Ruiz-Fernández, J., Rinterknecht, V., Lane, T.P., Adamson, K., Aumaître, G., Bourlès, D., Keddadouche, K., 2022. Late Glacial deglaciation of the Zackenberg area, NE Greenland. *Geomorphology* 401, 108125. <https://doi.org/10.1016/j.geomorph.2022.108125>

Garcia-Oteyza, Julia, Oliva, M., Palacios, D., Schimmelpfennig, I., Medialdea, A.,

Fernández-fernández, J.M., Fernandes, M., Giralt, S., Jomelli, V., Antoniades, D., Team, A., 2023a. Holocene glacial oscillations in the Tyroler Valley (NE Greenland). *L. Degrad. Dev.* <https://doi.org/10.1002/ldr.4633>

Gilbert, G.L., Cable, S., Thiel, C., Christiansen, H.H., Elberling, B., 2017. Cryostratigraphy, sedimentology, and the late Quaternary evolution of the Zackenberg River delta, northeast Greenland. *Cryosphere* 11, 1265–1282. <https://doi.org/10.5194/tc-11-1265-2017>

Goehring, B.M., Kelly, M.A., Schaefer, J.M., Finkel, R.C., Lowell, T. V., 2010. Dating of raised marine and lacustrine deposits in east Greenland using beryllium-10 depth profiles and implications for estimates of subglacial erosion. *J. Quat. Sci.* 25, 865–874. <https://doi.org/10.1002/jqs.1380>

Gosse, J., Klein, J., 2014. Encyclopedia of Scientific Dating Methods. *Encycl. Sci. Dating Methods* 1–23. <https://doi.org/10.1007/978-94-007-6326-5>

Grønnow, B., Jensen, J.F., Sørensen, M., Gullov, H.C., Gotfredsen, A.B., Melgaard, M., 2009. Geographical Report of the GeoArk expeditions to North-East Greenland 2007 and 2008.

Gruber, S., Haeberli, W., 2007. Permafrost in steep bedrock slopes and its temperatures-related destabilization following climate change. *J. Geophys. Res. Earth Surf.* 112, 1–10. <https://doi.org/10.1029/2006JF000547>

Håkansson, L., Alexanderson, H., Hjort, C., Möller, P., Briner, J.P., Possnert, A.A., 2009. Late Pleistocene glacial history of Jameson Land, central East Greenland, derived from cosmogenic ¹⁰Be and ²⁶Al exposure dating. *Boreas* 38, 244–260. <https://doi.org/10.1111/j.1502-3885.2008.00064.x>

Håkansson, L., Briner, J., Alexanderson, H., Aldahan, A., Possnert, G., 2007a. ¹⁰Be ages from central east Greenland constrain the extent of the Greenland ice sheet during the Last Glacial Maximum. *Quat. Sci. Rev.* 26, 2316–2321. <https://doi.org/10.1016/j.quascirev.2007.08.001>

Håkansson, L., Briner, J., Alexanderson, H., Aldahan, A., Possnert, G., 2007b. ¹⁰Be ages from central east Greenland constrain the extent of the Greenland ice sheet during the Last Glacial Maximum. *Quat. Sci. Rev.* 26, 2316–2321. <https://doi.org/10.1016/j.quascirev.2007.08.001>

Håkansson, L., Briner, J.P., Aldahan, A., Possnert, G., 2011. ¹⁰Be data from meltwater channels suggest that Jameson Land, east Greenland, was ice-covered during the last glacial maximum. *Quat. Res.* 76, 452–459. <https://doi.org/10.1016/j.yqres.2011.06.007>

Hansen, B.U., Sigsgaard, C., Rasmussen, L., Cappelen, J., Hinkler, J., Mernild, S.H., Petersen, D., Tamstorf, M.P., Rasch, M., Hasholt, B., 2008. Present-Day Climate at Zackenberg, in: *Advances in Ecological Research*. pp. 111–149. [https://doi.org/10.1016/S0065-2504\(07\)00006-2](https://doi.org/10.1016/S0065-2504(07)00006-2)

Hinkler, J., Hansen, B.U., Tamstorf, M.P., Sigsgaard, C., Petersen, D., 2008. Snow and Snow-Cover in Central Northeast Greenland. *Adv. Ecol. Res.* 40, 175–195. [https://doi.org/10.1016/S0065-2504\(07\)00008-6](https://doi.org/10.1016/S0065-2504(07)00008-6)

Højlund Pedersen, S., 2017. Scaling-up Climate Change Effects in Greenland. PhD Thesis. Aarhus University. Department of Bioscience, Denmark. 178 pp.

IMBIE Team, 2020. Mass balance of the Greenland Ice Sheet from 1992 to 2018. *Nature*

579, 233–239. <https://doi.org/10.1038/s41586-019-1855-2>

Jomelli, V., Swingedouw, D., Vuille, M., Favier, V., Goehring, B., Shakun, J., Braucher, R., Schimmelpennig, I., Menviel, L., Rabatel, A., Martin, L.C.P., Blard, P.H., Condom, T., Lupker, M., Christl, M., He, Z., Verfaillie, D., Gorin, A., Aumaître, G., Bourlès, D.L., Keddadouche, K., 2022. In-phase millennial-scale glacier changes in the tropics and North Atlantic regions during the Holocene. *Nat. Commun.* 13, 1–11. <https://doi.org/10.1038/s41467-022-28939-9>

Kelly, M.A., Lowell, T. V., 2008. Fluctuations of local glaciers in Greenland during latest Pleistocene and Holocene time. *Quat. Sci. Rev.* 28, 2088–2106. <https://doi.org/10.1016/j.quascirev.2008.12.008>

Kelly, M.A., Lowell, T. V., Hall, B.L., Schaefer, J.M., Finkel, R.C., Goehring, B.M., Alley, R.B., Denton, G.H., 2008. A ^{10}Be chronology of lateglacial and Holocene mountain glaciation in the Scoresby Sund region, east Greenland: implications for seasonality during lateglacial time. *Quat. Sci. Rev.* 27, 2273–2282. <https://doi.org/10.1016/j.quascirev.2008.08.004>

King, M.D., Howat, I.M., Candela, S.G., Noh, M.J., Jeong, S., Noël, B.P.Y., van den Broeke, M.R., Wouters, B., Negrete, A., 2020. Dynamic ice loss from the Greenland Ice Sheet driven by sustained glacier retreat. *Commun. Earth Environ.* 1, 1–7. <https://doi.org/10.1038/s43247-020-0001-2>

Kobashi, T., Severinghaus, J.P., Brook, E.J., Barnola, J.M., Grachev, A.M., 2007. Precise timing and characterization of abrupt climate change 8200 years ago from air trapped in polar ice. *Quat. Sci. Rev.* 26, 1212–1222. <https://doi.org/10.1016/j.quascirev.2007.01.009>

Krautblatter, M., Funk, D., Günzel, F.K., 2013. Why permafrost rocks become unstable: A rock-ice-mechanical model in time and space. *Earth Surf. Process. Landforms* 38, 876–887. <https://doi.org/10.1002/esp.3374>

Kroon, A., Abermann, J., Bendixen, M., Lund, M., Sigsgaard, C., Skov, K., Hansen, B.U., 2017. Deltas, freshwater discharge, and waves along the Young Sound, NE Greenland. *Ambio* 46, 132–145. <https://doi.org/10.1007/s13280-016-0869-3>

Lal, D., 1991. Cosmic ray labeling of erosion surfaces: in situ nuclide production rates and erosion models: Earth and Planetary Science Letters. *Earth Planet. Sci. Lett.* 104, 424–439.

Larocca, L.J., Axford, Y., Woodroffe, S.A., Lasher, G.E., Gawin, B., 2020. Holocene glacier and ice cap fluctuations in southwest Greenland inferred from two lake records. *Quat. Sci. Rev.* 246, 106529. <https://doi.org/10.1016/j.quascirev.2020.106529>

Larsen, N.K., Kjær, K.H., Lecavalier, B., Bjørk, A.A., Colding, S., Huybrechts, P., Jakobsen, K.E., Kjeldsen, K.K., Knudsen, K.L., Odgaard, B. V., Olsen, J., 2015. The response of the southern Greenland ice sheet to the Holocene thermal maximum. *Geology* 43, 291–294. <https://doi.org/10.1130/G36476.1>

Larsen, N.K., Levy, L.B., Carlson, A.E., Buizert, C., Olsen, J., Strunk, A., Bjørk, A.A., Skov, D.S., 2018. Instability of the Northeast Greenland Ice Stream over the last 45,000 years. *Nat. Commun.* 9, 3–10. <https://doi.org/10.1038/s41467-018-04312-7>

Larsen, N.K., Søndergaard, A.S., Levy, L.B., Laursen, C.H., Bjørk, A.A., Kjeldsen, K.K., Funder, S., Strunk, A., Olsen, J., Kjær, K.H., 2021. Cosmogenic nuclide inheritance in Little Ice Age moraines - A case study from Greenland. *Quat. Geochronol.* 65. <https://doi.org/10.1016/j.quageo.2021.101200>

[org/10.1016/j.quageo.2021.101200](https://doi.org/10.1016/j.quageo.2021.101200)

Larsen, N.K., Søndergaard, A.S., Levy, L.B., Olsen, J., Strunk, A., Bjørk, A.A., Skov, D., 2020. Contrasting modes of deglaciation between fjords and inter-fjord areas in eastern North Greenland. *Boreas* 49, 903–917. <https://doi.org/10.1111/bor.12475>

Lecavalier, B.S., Milne, G.A., Simpson, M.J.R., Wake, L., Huybrechts, P., Tarasov, L., Kjeldsen, K.K., Funder, S., Long, A.J., Woodroffe, S., Dyke, A.S., Larsen, N.K., 2014. A model of Greenland ice sheet deglaciation constrained by observations of relative sea level and ice extent. *Quat. Sci. Rev.* 102, 54–84. <https://doi.org/10.1016/j.quascirev.2014.07.018>

Lenton, T.M., Held, H., Kriegler, E., Hall, J.W., Lucht, W., Rahmstorf, S., Schellnhuber, H.J., 2008. Tipping elements in the Earth's climate system. *Proc. Natl. Acad. Sci. U. S. A.* 105, 1786–1793. <https://doi.org/10.1073/pnas.0705414105>

Levy, L.B., Kelly, M.A., Lowell, T. V., Hall, B.L., Hempel, L.A., Honsaker, W.M., Lusas, A.R., Howley, J.A., Axford, Y.L., 2014. Holocene fluctuations of Bregne ice cap, Scoresby Sund, east Greenland: A proxy for climate along the Greenland Ice Sheet margin. *Quat. Sci. Rev.* 92, 357–368. <https://doi.org/10.1016/j.quascirev.2013.06.024>

Levy, L.B., Kelly, M.A., Lowell, T. V., Hall, B.L., Howley, J.A., Smith, C.A., 2016. Coeval fluctuations of the Greenland ice sheet and a local glacier, central East Greenland, during late glacial and early Holocene time. *Geophys. Res. Lett.* 43, 1623–1631. <https://doi.org/10.1002/2015GL067108>

Levy, L.B., Larsen, N.K., Knudsen, M.F., Egholm, D.L., Bjørk, A.A., Kjeldsen, K.K., Kelly, M.A., Howley, J.A., Olsen, J., Tikhomirov, D., Zimmerman, S.R.H., Kjær, K.H., 2020. Multi-phased deglaciation of south and southeast Greenland controlled by climate and topographic setting. *Quat. Sci. Rev.* 242, 106454. <https://doi.org/10.1016/j.quascirev.2020.106454>

López-Blanco, E., Jackowicz-Korczynski, M., Mastepanov, M., Skov, K., Westergaard-Nielsen, A., Williams, M., Christensen, T.R., 2020. Multi-year data-model evaluation reveals the importance of nutrient availability over climate in arctic ecosystem C dynamics. *Environ. Res. Lett.* 15. <https://doi.org/10.1088/1748-9326/ab865b>

Lowell, T. V., Hall, B.L., Kelly, M.A., Bennike, O., Lusas, A.R., Honsaker, W., Smith, C.A., Levy, L.B., Travis, S., Denton, G.H., 2013. Late Holocene expansion of Istorvet ice cap, Liverpool Land, east Greenland. *Quat. Sci. Rev.* 63, 128–140. <https://doi.org/10.1016/j.quascirev.2012.11.012>

Meredith, M., Sommerkorn, M., Cassotta, S., Derksen, C., Ekaykin, A., Hollowed, A., 2019. Polar regions. IPCC Spec. Rep. Ocean Cryosph. a Chang. Clim. Ed. by H.-O. Pörtner, D.C. Roberts, V. Masson-Delmotte, P. Zhai, M. Tignor, E. Poloczanska, K. Mintenbeck, A. Alegria, M. Nicolai, A. Okem, J. Petzold, B. Rama, N.M. Weyer 203–320. [https://doi.org/10.1016/S1366-7017\(01\)00066-6](https://doi.org/10.1016/S1366-7017(01)00066-6)

Murton, M., 2008. Remote sensing of permafrost-related problems and hazards. *Permafr. Periglac. Process.* 136, 107–136. <https://doi.org/10.1002/ppp>

Rasmussen, L.H., Zhang, W., Hollesen, J., Cable, S., Christiansen, H.H., Jansson, P.E., Elberling, B., 2018. Modelling present and future permafrost thermal regimes in Northeast Greenland. *Cold Reg. Sci. Technol.* 146, 199–213. <https://doi.org/10.1016/j.coldregions.2017.10.011>

Rasmussen, S.O., Andersen, K.K., Svensson, A.M., Steffensen, J.P., Vinther, B.M., Clausen, H.B., Siggaard-Andersen, M.L., Johnsen, S.J., Larsen, L.B., Dahl-Jensen, D., Bigler, M., Röthlisberger, R., Fischer, H., Goto-Azuma, K., Hansson, M.E., Ruth, U., 2006. A new Greenland ice core chronology for the last glacial termination. *J. Geophys. Res. Atmos.* 111, 1–16. <https://doi.org/10.1029/2005JD006079>

Rasmussen, S.O., Vinther, B.M., Clausen, H.B., Andersen, K.K., 2007. Early Holocene climate oscillations recorded in three Greenland ice cores. *Quat. Sci. Rev.* 26, 1907–1914. <https://doi.org/10.1016/j.quascirev.2007.06.015>

Renssen, H., Seppä, H., Crosta, X., Goosse, H., Roche, D.M., 2012. Global characterization of the Holocene Thermal Maximum. *Quat. Sci. Rev.* 48, 7–19. <https://doi.org/10.1016/j.quascirev.2012.05.022>

Renssen, H., Seppä, H., Heiri, O., Roche, D.M., Goosse, H., Fichet, T., 2009. The spatial and temporal complexity of the holocene thermal maximum. *Nat. Geosci.* 2, 411–414. <https://doi.org/10.1038/ngeo513>

Reusche, M.M., Marcott, S.A., Ceperley, E.G., Barth, A.M., Brook, E.J., Mix, A.C., Caffee, M.W., 2018. Early to Late Holocene Surface Exposure Ages From Two Marine-Terminating Outlet Glaciers in Northwest Greenland. *Geophys. Res. Lett.* 45, 7028–7039. <https://doi.org/10.1029/2018GL078266>

Roberts, D.H., Rea, B.R., Lane, T.P., Schnabel, C., Rodés, A., 2013. New constraints on Greenland ice sheet dynamics during the last glacial cycle: Evidence from the Uummannaq ice stream system. *J. Geophys. Res. Earth Surf.* 118, 519–541. <https://doi.org/10.1002/jgrf.20032>

Schweinsberg, A.D., Briner, J.P., Licciardi, J.M., Bennike, O., Lifton, N.A., Graham, B.L., Young, N.E., Schaefer, J.M., Zimmerman, S.H., 2019. Multiple independent records of local glacier variability on Nuussuaq, West Greenland, during the Holocene. *Quat. Sci. Rev.* 215, 253–271. <https://doi.org/10.1016/j.quascirev.2019.05.007>

Simpson, M.J.R., Milne, G.A., Huybrechts, P., Long, A.J., 2009. Calibrating a glaciological model of the Greenland ice sheet from the Last Glacial Maximum to present-day using field observations of relative sea level and ice extent. *Quat. Sci. Rev.* 28, 1631–1657. <https://doi.org/10.1016/j.quascirev.2009.03.004>

Skov, D.S., Andersen, J.L., Olsen, J., Jacobsen, B.H., Knudsen, M.F., Jansen, J.D., Larsen, N.K., Egholm, D.L., 2020. Constraints from cosmogenic nuclides on the glaciation and erosion history of Dove Bugt, northeast Greenland. *Bull. Geol. Soc. Am.* 132, 2282–2294. <https://doi.org/10.1130/b35410.1>

Solomina, O.N., Bradley, R.S., Hodgson, D.A., Ivy-Ochs, S., Jomelli, V., Mackintosh, A.N., Nesje, A., Owen, L.A., Wanner, H., Wiles, G.C., Young, N.E., 2015. Holocene glacier fluctuations. *Quat. Sci. Rev.* 111, 9–34. <https://doi.org/10.1016/j.quascirev.2014.11.018>

Stone, J.O., 2000. Air pressure and cosmogenic isotope production. *J. Geophys. Res.* 105, 753–759.

Sugden, D.E., Balco, G., Cowdery, S.G., Stone, J.O., Sass, L.C., 2005. Selective glacial erosion and weathering zones in the coastal mountains of Marie Byrd Land, Antarctica. *Geomorphology* 67, 317–334. <https://doi.org/10.1016/j.geomorph.2004.10.007>

Thomas, E.R., Wolff, E.W., Mulvaney, R., Steffensen, J.P., Johnsen, S.J., Arrowsmith, C., White, J.W.C., Vaughn, B., Popp, T., 2007. The 8.2 ka event from Greenland ice cores.

Quat. Sci. Rev. 26, 70–81. <https://doi.org/10.1016/j.quascirev.2006.07.017>

Thornalley, D.J.R., Oppo, D.W., Ortega, P., Robson, J.I., Brierley, C.M., Davis, R., Hall, I.R., Moffa-Sanchez, P., Rose, N.L., Spooner, P.T., Yashayaev, I., Keigwin, L.D., 2018. Anomalously weak Labrador Sea convection and Atlantic overturning during the past 150 years. *Nature* 556, 227–230. <https://doi.org/10.1038/s41586-018-0007-4>

Vasskog, K., Langebroek, P.M., Andrews, J.T., Nilsen, J.E.Ø., Nesje, A., 2015. The Greenland Ice Sheet during the last glacial cycle: Current ice loss and contribution to sea-level rise from a palaeoclimatic perspective. *Earth-Science Rev.* 150, 45–67. <https://doi.org/10.1016/j.earscirev.2015.07.006>

Young, N.E., Briner, J.P., Miller, G.H., Lesnek, A.J., Crump, S.E., Thomas, E.K., Pendleton, S.L., Cuzzone, J., Lamp, J., Zimmerman, S., Caffee, M., Schaefer, J.M., 2020. Deglaciation of the Greenland and Laurentide ice sheets interrupted by glacier advance during abrupt coolings. *Quat. Sci. Rev.* 229. <https://doi.org/10.1016/j.quascirev.2019.106091>

Young, N.E., Briner, J.P., Rood, D.H., Finkel, R.C., Corbett, L.B., Bierman, P.R., 2013. Age of the Fjord Stade moraines in the Disko Bugt region, western Greenland, and the 9.3 and 8.2 ka cooling events. *Quat. Sci. Rev.* 60, 76–90. <https://doi.org/10.1016/j.quascirev.2012.09.028>

Young, N.E., Lesnek, A.J., Cuzzone, J.K., Briner, J.P., Badgeley, J.A., Balter-Kennedy, A., Graham, B.L., Cluett, A., Lamp, J.L., Schwartz, R., Tuna, T., Bard, E., Caffee, M.W., Zimmerman, S.R.H., Schaefer, J.M., 2021. In situ cosmogenic ^{10}Be - ^{14}C - ^{26}Al measurements from recently deglaciated bedrock as a new tool to decipher changes in Greenland Ice Sheet size. *Clim. Past* 17, 419–450. <https://doi.org/10.5194/cp-17-419-2021>

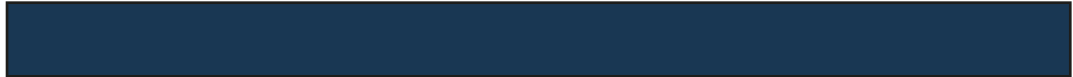
Zech, R., Glaser, B., Sosin, P., Kubik, P.W., Zech, W., 2005. Evidence for long-lasting landform surface instability on hummocky moraines in the Pamir Mountains (Tajikistan) from ^{10}Be surface exposure dating. *Earth Planet. Sci. Lett.* 237, 453–461. <https://doi.org/10.1016/j.epsl.2005.06.031>

3.2 LOCAL CLIMATE VARIABILITY IN NE GREENLAND

3.2.1 PAPER IV. A ~5000-YEAR MULTIPROXY RECORD OF SUMMER CLIMATE.

PAPER IV

J. Garcia-Oteyza, S. Giralt, S. Pla-Rabes, D. Antoniades, M. Oliva, H. Ghanbari, R. Osorio-Serrano, D. Palacios. A ~5000-year multiproxy record of summer climate in NE Greenland. (2023). Volume 906, 2024, 167713, ISSN 0048-9697, <https://doi.org/10.1016/j.scitotenv.2023.167713>.





Contents lists available at ScienceDirect
Science of the Total Environment
 journal homepage: www.elsevier.com/locate/scitotenv



A ~5000 year multiproxy record of summer climate in NE Greenland

J. Garcia-Oteyza^{a,*}, S. Giralt^b, S. Pla-Rabes^{c,f}, D. Antoniades^d, M. Oliva^a, H. Ghanbari^d, R. Osorio-Serrano^b, D. Palacios^c

^a Department of Geography, Universitat de Barcelona, Catalonia, Spain

^b Geosciences Barcelona (GEO3BCN-CSIC), Spain

^c Universitat Autònoma de Barcelona, Bellaterra (Cerdanyola del Vallès), Catalonia, Spain

^d Department of Geography & Centre for Northern Studies, Laval University, Quebec, Canada

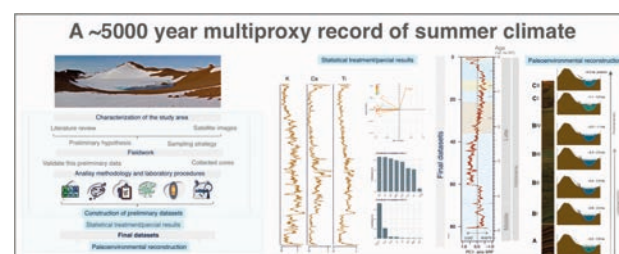
^e Department of Geography, Universidad Complutense de Madrid, Spain

^f CREAf, Bellaterra (Cerdanyola del Vallès), Catalonia, Spain

HIGHLIGHTS

- Arctic lakes are climate change sentinels. Their sediments show natural climatic fluctuations and anthropogenic influences.
- High-resolution climate variability from NE Greenland based on lake sediments properties.
- Changing air temperatures were controlled by a mix of regional climatic changes and local landscape feedbacks.

GRAPHICAL ABSTRACT



ARTICLE INFO

Guest Editor: Sergi González-Herrero

Keywords:
 NE Greenland
 Aucella Lake
 Arctic lakes
 Paleolimnology
 Climate variability
 Multiproxy analysis

ABSTRACT

The High Arctic plays a vital role in Earth's climate system, and its ecosystems are highly sensitive to global climate change. High Arctic lakes are valuable sentinels of climate change, as their sediments integrate long-term natural climatic fluctuations and anthropogenic influences. Here, we present a high-resolution ~5000 year-reconstruction of NE Greenland climate variability from Aucella Lake (74°N, 20°E) based on physical, chemical, and biological properties of lake sediments. We use CT-scans, hyperspectral imaging, organic matter, XRD, and diatom analyses to show that changing air temperatures were controlled by a mix of regional climatic changes and local landscape feedbacks. The latest Mid-Holocene (~5.0–3.8 cal. ka BP) was characterized by relatively warmer conditions, while the onset of the Late-Holocene was marked by abrupt temperature decreases that coincided with the beginning of glacial advances elsewhere (~3.8–3.4 cal. ka BP). From ~3.4–2.4 cal. ka BP, the sedimentary record indicated progressive warming, with temperature peaking during the Medieval Climate Anomaly, although temperature rises were punctuated by abrupt, short-lived cold periods. From ~1.1–0.05 cal. ka BP, the influence of landscape factors over the system diminished. Sedimentary indicators suggested a transition towards a colder, more humid climate, coinciding with the beginning of the Little Ice Age, that was characterized by a marked decrease in air temperature that reached minimum values at the end of this period.

1. Introduction

The High Arctic region is a crucial component of Earth's climate system, and its ecosystems are highly sensitive to global climate change (Anderson et al., 2017; Post et al., 2009; Saros et al., 2019). Both instrumental observations and future climate models reveal that the region is undergoing rapid warming, and it is expected to experience some of the most intense changes in response to climate warming by the end of the century (Preusser et al., 2008; Saros et al., 2019). According to >40 years of weather data, after 1994 CE mean June air temperatures increased by 2.2 °C in West Greenland and mean winter precipitation doubled from 21 to 40 mm, while since 2006 CE mean July air temperatures have increased by 1.1 °C (Saros et al., 2019). However, much remains to be understood about the drivers of Arctic amplification, climate variability and feedbacks (Lund et al., 2017; Pithan and Mauritsen, 2014; Serreze and Barry, 2011). Arctic climate change is non-uniform both spatially and temporally (Miller et al., 2010); to project future climate scenarios accurately it is therefore essential to contextualize present-day warming within a long-term perspective and thus decipher natural climatic fluctuations from anthropogenic influences. This is of paramount importance since the Greenland Ice Sheet may contribute between 5 and 33 cm to sea level rise by 2100 CE (Aschwanden et al., 2019). Furthermore, a detailed understanding of the short- and long-term temporal and spatial evolution of Greenland climate, mainly related to Greenland blocking, might help to provide insights describing the spatial and temporal evolution of the North Atlantic Oscillation (NAO), the major regional pattern of wintertime variability in the Northern Hemisphere (Davini et al., 2012; Hanna et al., 2016). According to some studies, an increasing trend of Greenland blocking in summer and a more variable blocking in winter may lead to enhanced early winter NAO variability, mainly at the southern node of this climate mode (Hanna et al., 2015).

Lakes are considered to be sentinels of environmental changes as their physical, chemical, and biological properties respond rapidly to climate-related changes (Adrian et al., 2009; Catalan et al., 2013; Saros et al., 2019; Williamson et al., 2009). Lakes sensitively capture climate signals and environmental changes in the surrounding landscape and atmosphere (Goosse et al., 2018). Remote lakes, which are not directly influenced by anthropogenic factors (e.g. point sources of pollution, land-use changes and resource exploitation in their catchments), are often found at higher elevation and latitude and are among the most sensitive of such ecosystems (Carpenter et al., 2007; Pham et al., 2008; Williamson et al., 2008). Lake sediment properties offer continuous terrestrial paleoenvironmental archives that may be interpreted in the context of long-term climatic changes (Rosenzweig, 2007).

Although sediment sequences reconstructing local and regional Holocene climate have been published from several ice-free regions of Greenland, the spatial coverage is still incomplete, and temporal resolution is still coarse for many sites. Previous studies have shown spatial variation in Holocene temperature changes, and the timing of some critical events needs to be better constrained (Briner et al., 2016; Gajewski, 2015 and references therein). Moreover, most high Arctic Holocene climate reconstructions deal with temperature changes, and hydroclimate records should be a priority in order to reconcile ice sheet extension inferred from cosmic-ray exposure ages and geomorphological features with models of ice sheet evolution (McFarlin et al., 2018).

We sought to fill several of these knowledge gaps in a study of the remote Aucella Lake at 74° N, with the following objectives: (i) to refine our understanding of the timing and patterns of regional environmental and climate variability in NE Greenland; (ii) to produce a high-

The last 50 years at Aucella Lake were marked by abrupt temperature rises, consistent with recently observed anthropogenic global warming. Our results illustrate the importance of high-resolution multiproxy studies for accurately characterizing lake linkages to their environment and climate.

resolution geochemical, biological, and physical reconstruction from a remote lake on continuous permafrost terrain; and (iii) determine the climatic context driving glacial oscillations in the area. To achieve these goals, our specific objectives were to address the following questions:

- What was the natural climate variability in this area during the last several millennia?
- Were any observed climate oscillations synchronous with those recorded in other NE Greenland regions?

2. Study area

Aucella Lake (911 m a.s.l.; 74° 31.5044' N, 20° 26.5231' W), is a ~3.4 ha lake located near the top of the Aucellabjerg Mountain plateau (911 m), within the Wollaston Foreland peninsula in the SE corner of Northeast Greenland National Park (Fig. 1).

The lake's steeply sloped, glacial inherited catchment depression has an approximate area of 16.9 ha, and the lake has no defined inflowing streams. An NW outlet drains the lake, fed by a perennial snow patch of 0.06 km² area (Docherty et al., 2018) (on the north-facing slope), and descends through the Aucellabjerg slope forming the Aucellaelv stream, building an alluvial fan at the Zackenberg Valley bottom, and ultimately joining the main flow of the Zackenberg River. Geologically, while the Aucellabjerg Mountain slopes are composed of Cretaceous to Jurassic sedimentary rock units (mudstones, sandstones, and conglomerates) (Henriksen et al., 2009), the mountain plateau and the Aucella Lake catchment area expose Paleogene reddish-brown basalts (dominantly silica-oversaturated tholeiites) (Henriksen et al., 2009). The climate in this area is a polar tundra (Bonow and Japsen, 2021), with a mean annual air temperature (MAAT) recorded between 1996 CE and 2015 CE at Zackenberg Research Station weather station (situated at the valley bottom, at 700 m lower elevation) of −9.0 °C, and an average annual precipitation of 367 mm (Kottke et al., 2006) of which only 10 % falls as rain during the summer months (June to September) (Højlund Pedersen, 2017). Whereas the large lowland valley areas include moist to dry tundra dominated by shrubs with grasslands and fens (Hasholt et al., 2008), the variety and size of the plants decreases at higher elevations, with vegetation practically non-existent in the Aucella Lake catchment. The whole area is underlain by continuous permafrost with a thickness measured in the valley bottom ranging from 200 to 400 m and a spatially variable active layer that fluctuates between 45 and 80 cm thick (CAVM Team, 2003). The latest deglaciation studies in the area show that no glaciers have been present on the Zackenberg Valley bottom since the Early Holocene (ca. 10.5 ka; Garcia-Oteyza et al., 2022). However, cosmogenic surface exposure dating indicated that ice reached the landscape surrounding the lake during most of the last glacial cycle, arriving >800 m above the current valley floor during the maximum advance (ca. 80–50 ka) and probably also during the Last Glacial Maximum (Christiansen et al., 2010, 2008).

3. Methodology

3.1. Sediment coring

Fieldwork was carried out on July 26th, 2018. Sediment coring was carried out at the deepest known point (74° 31.3047' N, 20° 26.1528' W) in the lake (~15 m) after using satellite images to establish target regions from catchment topography. One gravity core, AUC02 (83.6 cm) was recovered from the deepest part of the central basin (Fig. 1C), to avoid potential reworked sediment or sediment gravity flows from the margins, using a UWITEC gravity corer with a core diameter of 60 mm.

* Corresponding author at: Department of Geography, Universitat de Barcelona, Montalegre 6-8, 3rd floor, 08001 Barcelona, Spain.
 E-mail address: juliaoteyzaciria@gmail.com (J. Garcia-Oteyza).

<https://doi.org/10.1016/j.scitotenv.2023.167713>

Received 3 July 2023; Received in revised form 29 September 2023; Accepted 8 October 2023

Available online 10 October 2023

0048-9697/© 2023 The Authors. Published by Elsevier B.V. This is an open access article under the CC BY-NC-ND license (<http://creativecommons.org/licenses/by-nc-nd/4.0/>).

J. Garcia-Oteyza et al.

Science of the Total Environment 906 (2024) 167713

The water-sediment interface of both cores was immediately fixed using sodium polyacrylate (Tomkins et al., 2008); tubes were completely sealed at both ends and transported vertically in order to prevent disturbance and were then stored at +4 °C until they were opened for sampling in the laboratory.

3.2. Chronology

The chronological framework of the sedimentary sequence of Aucella Lake was constructed based on nine AMS radiocarbon dates exclusively measured on moss fragments, including a date of the core's surface in order to establish the presence/absence of a carbon reservoir effect in the lake. AMS radiocarbon samples were prepared at the Radiochronology laboratory of the Centre d'études nordiques, Laval University (Quebec City, Canada) and analyzed at the W. M. Keck Carbon Cycle Accelerator Mass Spectrometer Facility (Irvine, United States). The final age-depth model (see Section 4.1) was constructed Bayesian age-depth modeling in the R package rbacon (Blaauw and Andrés Christeny, 2011), with ages calibrated using the IntCal20 calibration curve (Reimer et al., 2020). In this study, our 0 cal. ka BP (or 'present') corresponds to 2018 CE.

3.3. Data and laboratory analysis

The sediment core (AUC02) was split lengthwise, with one half stored as an archive (in the cold room of the Geosciences Institute of Barcelona (GEO3BCN - CSIC) at +4 °C); the other half was used for non-destructive high-resolution analysis and subsampled at 1 cm resolution and stored in the same cold room until subsampling for destructive

analysis.

3.3.1. Non-destructive analysis (CT-scan, XRF, hyperspectral imaging)

Before opening, all cores were scanned using a computerized 3D X-ray computed tomography Siemens Somatom 64 scanner (CT-scan) at the Institut National de la Recherche Scientifique, Centre Eau Terre Environnement (INRS-ETE) in Quebec City (Canada), to identify sedimentary structures (St-Onge et al., 2007). The sediment elemental composition (by X-Ray Fluorescence, XRF analysis) was then determined (Supplementary Fig. 1) using the ITRAX XRF Core Scanner at INRS-ETE with a resolution of 0.5 mm, a voltage of 1100 µA and a counting time of 10 s for eleven light elements (Al, Si, S, Cl, K, Ca, Ti, V, Cr, Mn, Fe) and seventeen heavy elements (Ni, Cu, Zn, Ga, Br, Rb, Sr, Y, Zr, Nd, Ba, Ce, Nd, Ta, Pb, Ra). The rest of the following analysis were performed only on the longest sediment core (AUC02). The cores were scanned using a hyperspectral scanner at the Aquatic Paleoecology Laboratory (LPA) in Laval University (Quebec City, Canada), equipped with visible-near infrared (VNIR) and shortwave infrared (SWIR) cameras (SPECIM, Oulu, Finland) covering the spectral ranges between 400 and 1000 nm and 1000–2500 nm, and having spatial resolutions of ~70 µm and ~180 µm, respectively. Hyperspectral images were used to infer high-resolution profiles of mean grain size distribution and total chlorophyll a (including degradation products) following the methodology established in Ghanbari and Antoniadis (2022).

3.3.2. Destructive analyses (organic matter, XRD, diatoms)

Sediment samples were taken every centimetre for analysis of organic geochemical variables, including sediment organic matter (total organic carbon (TOC), total nitrogen (TN) and their stable isotopes ¹⁵N

J. Garcia-Oteyza et al.

Science of the Total Environment 906 (2024) 167713

and ¹³C) as well as for mineralogical determinations. In both cases, samples were dried at 60 °C for 48 h and ground by hand using an agate mill. TOC, TN, δ¹³C and δ¹⁵N were determined using a Finnigan DELTAplus elemental analyzer-continuous flow-isotope ratio mass spectrometer (EA-CF-IRMS) at the Centres Científics i Tecnològics of the Universitat de Barcelona (CGITUB). Mineralogy was determined by X-ray diffraction using a Bruker-AXS D5005 X-ray diffractometer in the following conditions: wavelength of 1.5405 Å and ultrafast PSD detector between the angles of 4° and 60° 2theta, at GEO3BCN (Barcelona, Spain). Identification and quantification of the different mineralogical species present in the crystalline fraction were carried out following a standard procedure (Chung, 1974). 40 subsamples for diatom analysis were taken at ~2 cm intervals throughout the core. Diatom subsamples were processed with 33 % hydrogen peroxide (H₂O₂) and HCl (1 M) following the method described in Battarbee et al. (2001). At least 300 valves were counted at 1000× magnification with a light microscope and species are expressed as relative abundances (%) for each taxon. Taxonomic identifications mainly followed Krammer and Lange-Bertalot (1986, 1988, 1991a, 1991b), although basionyms were updated to follow current accepted nomenclature (https://www.algaebase.org/).

3.4. Data treatment

Statistical treatment of the datasets was performed in the R software environment v2022.12.0 + 353 (R Core Team, 2022), together with the packages 'rioja' (Juggins, 2022), 'vegan' (Oksanen et al., 2020) and 'factoextra' (Kassambara and Mundt, 2020). Only elements that had average values >300 cps in the XRF analyses were included, in order to ensure that the signal-to-noise ratio was high enough to characterize short- and long-term chemical variations with confidence (i.e., K, Ca, Ti, Mn, Fe, Cu and Sr). All variables were standardized and transformed prior to statistical analysis. Only diatom taxa representing >1 % of the total diatom sum were used in statistical analyses, and those with >4 % of the total diatom sum in at least one sample were plotted stratigraphically. Simpson's Index of diversity and principal component analysis of the Hellinger-transformed diatom relative abundance data were used to summarize the main trends in diatom assemblages (Legendre and Birks, 2012; Legendre and Gallagher, 2001). We also performed a stratigraphically constrained cluster analysis for each separate data group (XRF, XRD, mean grain size, organic geochemistry, chlorophyll, and diatoms) using constrained incremental sums of squares (CONISS; Grimm, 1987) (Supplementary Fig. 2).

We applied multivariate ordination methods to reduce the complexity of the large multi-proxy data set in order to identify underlying system dynamics, which required data pre-treatment. First, we averaged XRF data to the TOC resolution and carried out a PCA to reveal the relationships between the organic and inorganic sediment fractions. Second, we performed two redundancy analyses (RDA): one between the mineralogical composition of the sediments (explanatory variable) and the geochemical elements (response variable) to identify the possible provenances of the chemical elements; the second used the diatom

assemblages as a response variable with the geochemical parameters as the environmental matrix (Supplementary Fig. 1A). To support (visual) identification of the main lithostratigraphic core units, we also conducted a constrained cluster analysis with measured datasets down-sampled to 2-cm resolution and ran a broken stick model to identify the number of significant units.

4. Results

4.1. Age-depth model

Nine radiocarbon dates were determined from Aucella Lake sediments (Table 1).

Moss fragments in the surface layer of the sediment core returned an age of 1265 ± 20 cal BP. The water-sediment interface was clear and sharp, with no indication of sediment loss or mixing, therefore, a deltaR value equal to the age of the core surface was applied to the rest of our radiocarbon ages. A slump between 42 and 45 cm core depth was identified from visual inspection and confirmed by two anomalously old radiocarbon ages that were excluded from model construction; this section of the core was also assumed to have been deposited concurrently for the purposes of the age-depth model. The sample at 44.5 cm was rejected as it represented a stratigraphic inversion. The age-depth model (Fig. 2) was thus constructed using a final dataset of six ¹⁴C reservoir corrected ages using the Bacon R script and showed that the AUC02 core represents ~5000 years of sediment deposition, with limited variation in sedimentation rates throughout the core.

4.2. Lake stratigraphy and sediment characteristics

The core was divided into three main different lithological units (A, B, C). Zones inside unit B (BI, BII, BIII and BIV) and C (CI and CII) were established by visual identification (Figs. 3 and 4).

4.2.1. Unit A (83.6–68 cm depth) – age ~5.0–3.8 cal. ka BP

The sediments were mainly composed of centimetre-thick laminated light and dark brownish clays with macrofossils. Geochemically, there were peaks in several elements including K, Ca, and Ti in lowest part of the record, followed by a decrease and subsequent rise. Mn/Fe values remained high throughout the unit. Low values for grain size, and the dominance of clay minerals such as kaolinite, biotite/muscovite and, punctually, montmorillonite, highlighted the clay-rich nature of these sediments. In agreement with the visually evident macrofossils (mosses), organic indicators, including TOC, TN, and chlorophyll, had high values in this section (Fig. 4). Diatom assemblages were defined by the presence of *Staurosira venter*, followed by *Pseudostaurosira pseudoconstruens*, and other common taxa included *Staurosirella pinnata*, *Sellaphora seminulum*, *Sellaphora rectangularis*, *Rossetidium lineare* (although decreasing through the unit), and *Achnanthydium minutissimum* (Fig. 3). The transition to Unit B was clear both visually and in the CT-scan image, which had a sediment density boundary change from clay-rich to more sandy sediment.

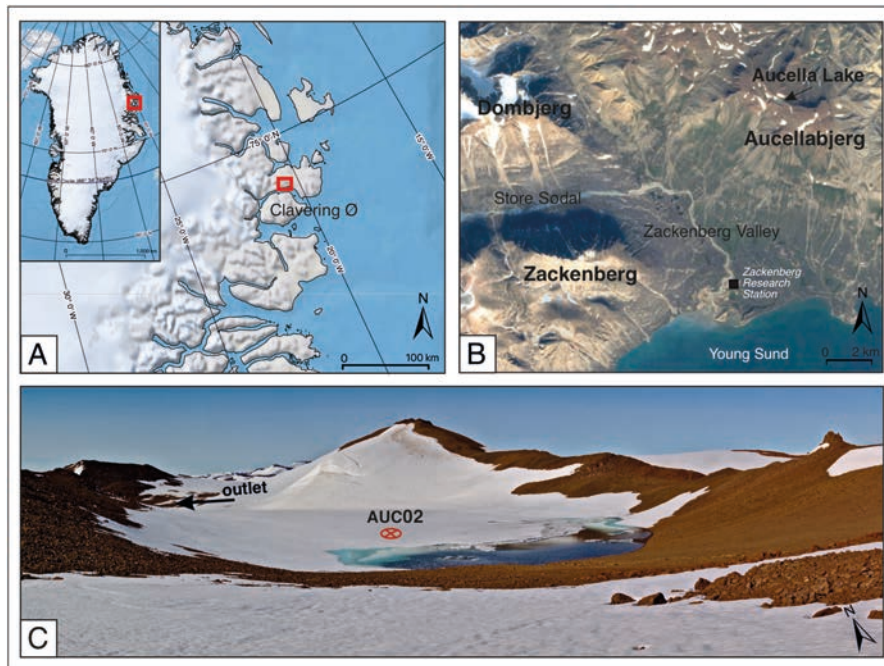


Fig. 1. Map of (A) study area within NE Greenland (B) Aucella Lake location in the Zackenberg area. (C) Picture of Aucella Lake with the location of AUC02 coring location.

Table 1

¹⁴C dates of samples from the sediment core AUC02. Samples in italics were not included during the construction of the final age-depth model.

Sample ID	Midpoint (for age model, cm)	Dated Material	Lab Number	δ ¹³ C (‰)	¹⁴ C age (BP)	±	Reservoir corrected ¹⁴ C yr BP
AUC 1802-0-1	0.5	Moss	UCIAMS-247345	-26.8	1265	20	
AUC 1802-11-12	11.5	Moss	UCIAMS-240752	-27.9	2425	15	1160 ± 25
AUC 1802-29-31	30.0	Moss	UCIAMS-240751	n/d	3255	15	1990 ± 29
AUC 1802-56-57	56.5	Moss	UCIAMS-240750	-26.4	4390	15	3125 ± 38
AUC 1802-70-71	70.5	Moss	UCIAMS-240744	-25.3	4820	20	3555 ± 38
AUC 1802-78	78.0	Moss	UCIAMS-221357	-25.2	5430	20	4165 ± 43
AUC 1802-42-43	42.5	Moss	UCIAMS-240753	-28.1	120	15	
AUC 1802-43-44	43.5	Moss	UCIAMS-261723	-28.1	Modern	2.1	
AUC 1802-44-45	44.5	Moss	UCIAMS-261724	-24.8	4460	15	

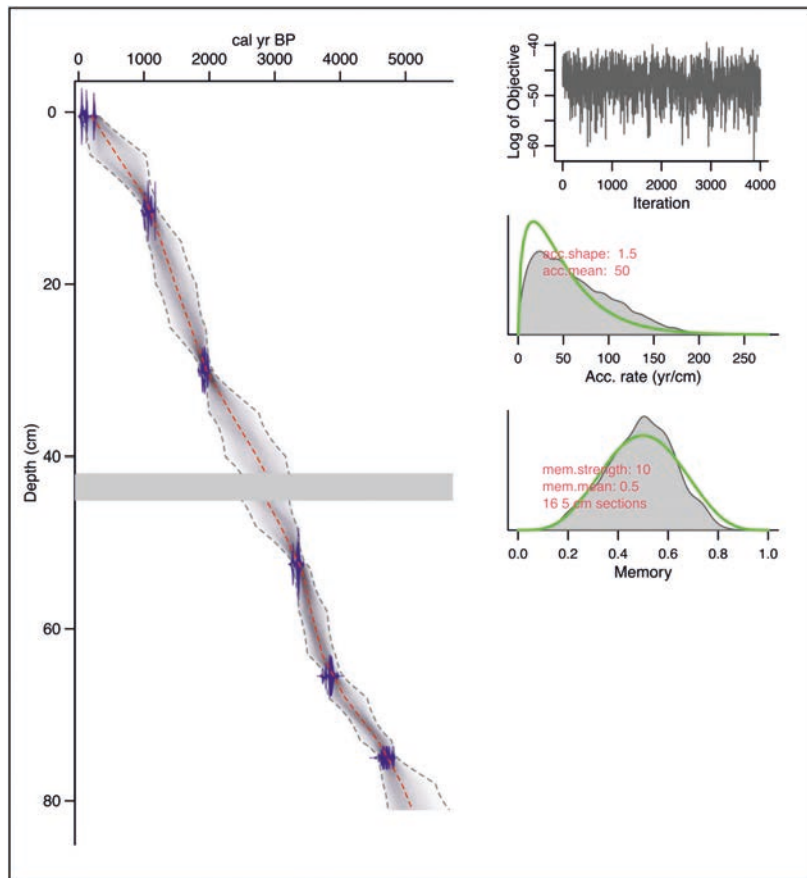


Fig. 2. Age-depth model for AUC02 based on bacon (Blaauw and Andrés Christeny, 2011). Right plot: shows the distribution of the radiocarbon dates in blue, assuming slump at 42–45 cm depth (grey rectangle). The age-depth model is shown in grey-scale, where darker hues indicate more certain areas. The red dashed curve shows the mean model and the dashed grey curves the 95 % confidence intervals. Left upper plot shows the MCMC (Markov Chain Monte Carlo) iterations of the run showing a stationary distribution with little structure among iterations. Left middle plot shows prior (green curve) and posterior (grey filled curve) distribution accumulation rates. The mean accumulation rate was 50 yr/cm. Left lower plot: shows the prior (green) and posterior (grey) probability distributions for the memory (i.e. autocorrelation strength).

4.2.2. Unit B (68–13 cm depth) - age ~3.8–1.1 cal. ka BP

Unit B's limits were marked by clusters in all proxy datasets, although the precise depths varied slightly. Overall, this unit was made up mainly of silty clays and sands in which four zones were distinguished:

4.2.2.1. Zone BI (68–59 cm depth) - age ~3.8–3.4 cal. ka BP. This zone's base started with sediment composed of well-laminated green/Gy silt. Geochemically, visible peaks were present in almost every element except for Sr, while Mn/Fe showed a slight decrease overall and less variability. The silty nature of the sediments was highlighted by a grain size increase, although with lower variability than in the previous unit, as well as by an abrupt change in the CT-scan. The organic parameters TN, TOC, and chlorophyll decreased markedly (Fig. 4). A peak of diatom diversity and richness appeared, and diatom assemblages in this zone

were formed by increases in *Encyonema silesiacum* with the appearance of *Encyonema procerum*, *Adlafia* sp. B, *Amphora copulata* and *Navicula-dicta* sp. A (Fig. 3).

4.2.2.2. Zone BII (59–39 cm depth) - age ~3.4–2.4 cal. ka BP. This zone was generally characterized by a massive brown silt sediment structure with macrofossils, although several centimetre-thick laminations were present at ~47 cm and ~41 cm core depth. A mass movement between 42 and 45 cm depth was identified based on visual evidence of perturbed sediment within a laminated unit, as well as by three anomalous radiocarbon ages within the zone (Table 1). As such, these 3 cm were removed from the record for the construction of the chronology as well as for paleoecological interpretations. All biogeochemical proxies showed trends in zone BII similar to those in BI. Mineralogically, zone BII was characterized by the presence of a montmorillonite peak and the

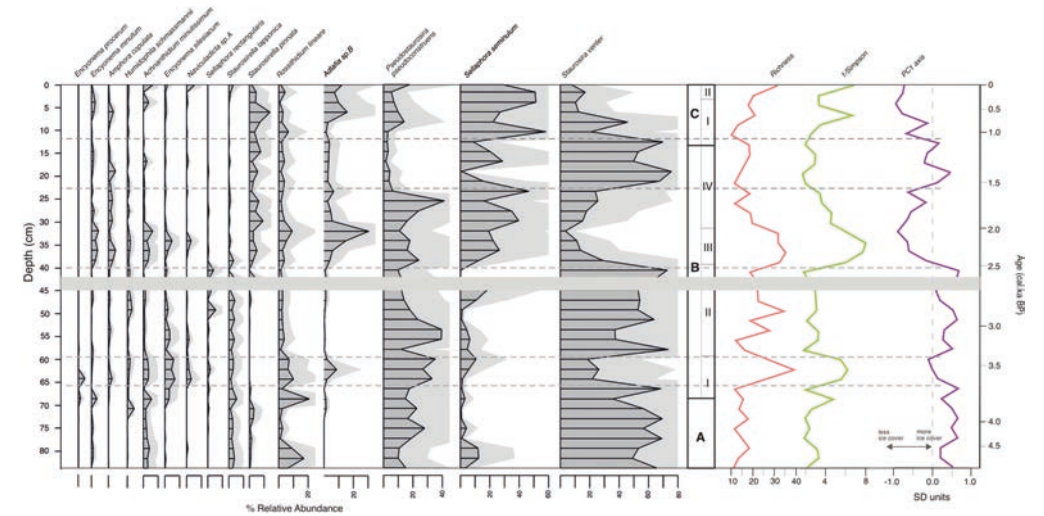


Fig. 3. Diagram of total diatom taxa valve abundance and (% total diatom valves) for AUC02 core; diatoms richness; Simpson's diversity index, sample scores on diatom PCA axis 1; diatom PC1 axis.

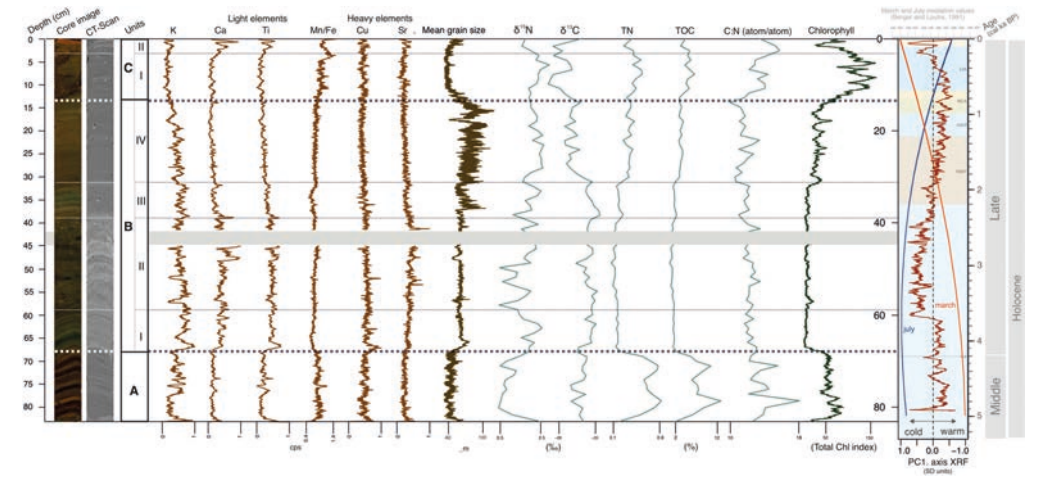


Fig. 4. Multi-proxy data from AUC02 sediment core. From left to right: depth scale; picture and Ct-scan image of the core; Physical characteristics: XRF; Grain size; Organic characteristics: C/N; Chlorophyll; XRF PC1 axis from Aucella Lake record (slump centimetres extracted); March and July insolation at 65°N (Berger and Loutre, 1991). Specific climatic periods/events are shown: Roman Warm Period (RWP), Dark Ages Cold Period (DACP), Medieval Climate Anomaly (MCA) and Little Ice Age (LIA), after Kolliing et al. (2017).

highest values of kaolinite and plagioclase (Fig. 4). Diatom assemblages were strongly dominated by *Staurosirella lapponica*, *S. pinnata*, *Pseudostaurosira pseudoconstruens* and *Staurosira venter* (Fig. 3).

4.2.2.3. Zone BIII (39–31 cm depth) - age ~2.4–2.0 cal. ka BP. Sediments were millimetre-thick orange/greenish laminations. All elements showed a decreasing trend except K, which displayed values higher than

the zone below. There was an abrupt increase in grain size upwards beginning at ca. 37 cm depth, followed by a gradual upwards decline. Organic matter indicators did not change significantly with respect to the zone below (Fig. 4). Diatom assemblages were diverse, with no clearly dominant taxa, a marked decline in the relative abundance of *Staurosira venter*, and a peak in the abundance of *Adlafia* sp. B (Fig. 3) and in Simpson's index.

J. Garcia-Oteyza et al.

Science of the Total Environment 906 (2024) 167713

J. Garcia-Oteyza et al.

Science of the Total Environment 906 (2024) 167713

4.2.2.4. *Zone BIV (31–13 cm depth)* - age ~2.0–1.1 cal. ka BP. This zone was composed of light and dark brown millimetre-thick silty clay laminations. Light element trend values decreased, with K doing so more markedly. In contrast, for Mn/Fe there is a slight increase on trend values and no major changes for the rest of heavy elements. Grain size increased gradually upwards in this section to ~15 cm depth and declined thereafter, although this trend was superimposed on significant variability, highlighting the unit's silty clay nature. Plagioclase, quartz, kaolinite, and biotite/muscovite displayed overall decreasing trends, while organic matter indicators and chlorophyll showed increased their values and variability with respect to unit BIII below (Fig. 4). Zone BIV was marked by the return to dominance of *Staurorsira venter* and *Sellaphora seminulum*, as well as by the decrease of *Pseudostaurorsira pseudoconstruens* and the disappearance of *Staurorsirella lapponica* (Fig. 3).

4.2.3. *Unit C (13–0 cm depth)* - age ~1.1 cal. ka BP - present

4.2.3.1. *Zone CI (13–3 cm depth)* - age ~1.1–0.3 cal. ka BP. CT-scan results indicated that this zone was mainly composed of millimetre-thick laminae, although they were not visually evident and could be observed as brown clay sediment with microfossils. Geochemical indicators did not display significant trends, apart from Mn/Fe values that increased upwards and had increased variability. Grain size decreased upwards in terms of both values and variability. The most significant peaks of montmorillonite appeared in this zone, along with the disappearance of nontronite and kaolinite and increases in the percentages of quartz and plagioclase. There was an increasing upward trend observed in TN, TOC, $\delta^{15}\text{N}$ and chlorophyll, and a decreasing trend for $\delta^{13}\text{C}$ (Fig. 4). Diatom assemblages were strongly dominated by *Sellaphora seminulum*, with declines in most other taxa except *Adlafia* sp. B and *Pseudostaurorsira pseudoconstruens* (Fig. 3).

4.2.3.2. *Zone CII (3–0 cm depth)* - age ~0.3 cal. ka BP - present. This zone contained abrupt changes, with a visually notable decline in the quantity of microfossils, and an orange hue in the upper centimetre. Elements including K, Ca, Ti, Cu, and Sr peaked in this zone, while Mn/Fe abruptly decreased. Mean grain size increased slightly, reflecting the silty clay nature of the sediments, and kaolinite reappeared along with a corresponding decrease in quartz. $\delta^{15}\text{N}$, TN, and TOC decreased, chlorophyll decreased abruptly, and $\delta^{13}\text{C}$ increased upwards to the sediment surface (Fig. 4). No large changes in the diatoms assemblages were recorded, only small increases in *Naviculadicta* sp. A, *Pseudostaurorsira pseudoconstruens* and *Staurorsirella lapponica*.

4.3. Multivariate analysis

4.3.1. Diatom assemblages

In terms of abundance, three diatom species dominated throughout the core and the main diatom zones were defined according to their shifts: *Staurorsira venter* and *Sellaphora seminulum* and *Pseudostaurorsira pseudoconstruens* (Fig. 3). The first two axes of the diatom PCA were significant according to the broken stick; the first explained 47.2% and the second explained 18.2% of the total variance. The three taxa with the strongest influence on the first axis were *Sellaphora seminulum*, *Staurorsira venter* and *Adlafia* sp. B, while for the second axis they were *Pseudostaurorsira pseudoconstruens*, *Staurorsira venter* and *Sellaphora seminulum* (Fig. 5A). We focused our interpretations on PCA1 since it independently explained almost half the variance in the dataset.

4.3.2. Biogeochemical composition of the sediments

The first axis of the PCA of the XRF/organic matter data explained 73.6% of the total variance (Fig. 5B) and was negatively associated with the lighter elements (i.e., Fe, Ti). The RDA of the XRF data with the mineralogical composition of the sediments as the constraining matrix showed the possible provenance of light and heavy elements obtained by

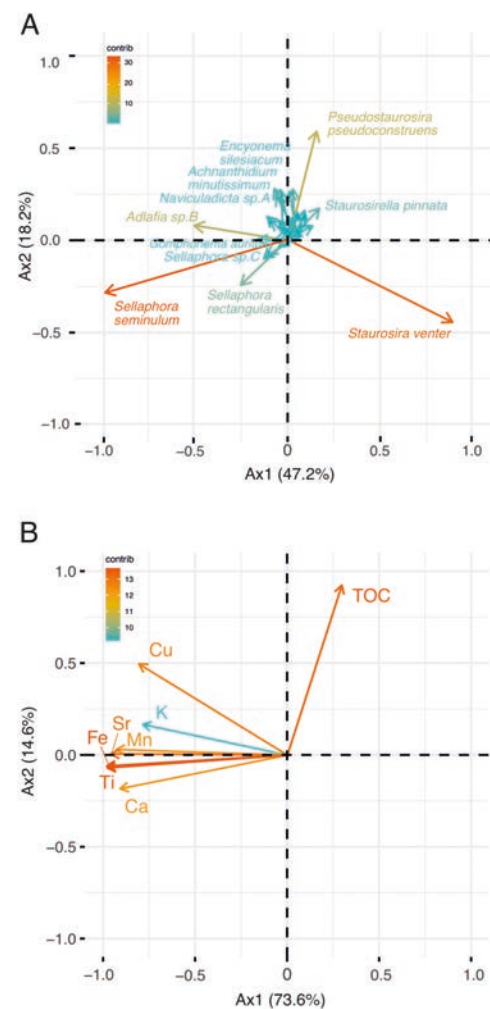


Fig. 5. Graphs (A) Diatom taxa PCA (B) XRF data combined with TOC PCA.

the XRF. This RDA (Supplementary Fig. 1A) had one significant first axis that explained 87.8% of the total variance. Ca, Ti, Fe, Mn, Sr, Cu, and K were mainly grouped with clays composed of muscovite/biotite, high $\delta^{13}\text{C}$ and kaolinite.

The first axis of the RDA constraining the diatom variance to the environmental dataset (Supplementary Fig. 1B) explained 34.8% of the total variance and indicated that the three lower diatom clusters were associated with terrigenous inputs into the system and with an assemblage dominated by *Staurorsirella* taxa. In contrast, the genus *Sellaphora* increased greatly in the three upper clusters of the record, where its interplay with *Staurorsira venter* determined diatom zonation, and high abundance values of *Sellaphora* taxa were more strongly associated with high values of the internal ecosystem parameters such as $\delta^{15}\text{N}$.

5. Discussion

Interpretations of the PCA axes synthesize the local limnological and paleoenvironmental response to climate-related processes in Aucella Lake and its catchment. After understanding the baseline behavior of our ecosystem, we then compare our interpretations with other proxy data, both local and regional, and with globally known cold and warm periods, to compare local NE Greenland environmental change with that observed at larger scales.

5.1. Linking datasets: limnological processes

The first axis of the diatom PCA reflected climate-related processes (Fig. 5). Taxa associated with strongly ice-dominated polar lakes, including *Staurorsira venter*, *Staurorsirella pinnata*, *Staurorsirella lapponica*, and *Pseudostaurorsira pseudoconstruens* (Bouchard et al., 2004; Finkelstein and Gajewski, 2008; Kuhn et al., 1981), were strongly associated with the positive end of the axis. Conversely, the negative end was influenced by more diverse assemblages and epiphytic taxa such as *Sellaphora seminulum* (Emson et al., 2018), *Encyonema minutum* and *Amphora copulata* (Antonides et al., 2008). The richness curve, which paralleled trends in PCA axis 1, further reinforced the dependence of this axis on climate, as longer ice-free seasons increase microhabitat diversity and therefore diatom diversity in high Arctic lakes (Smol, 1983). As such, the positive scores on the first diatom PCA axis represented cold water conditions with thicker and longer-lasting ice cover, while the negative scores were linked to longer ice-free summers that implied melting of the surrounding ice caps during wetter and/or warmer periods. The lack of planktonic diatoms in our sediments, similar to that observed in other Arctic lakes, may result from ice-free conditions that are too brief for their development, and/or from the high relief of the catchment preventing the wind-induced mixing of the lake required for diatom resuspension in the photic zone (Bouchard et al., 2004; Finkelstein and Gajewski, 2008; Paull et al., 2008).

The first diatom PCA axis divided the record into two clear sections (Fig. 2): the first (~5.0–2.4 cal. ka BP) showed positive values reflective of greater lake ice thickness and duration, and the second (~2.4 cal. ka BP - present) had predominantly negative values that indicated less severe ice conditions, albeit interspersed with some excursions towards more positive values. Richness and Simpson's index reinforced the linkages between diatom diversity and climatic changes, showing rises during periods of shorter ice cover duration shown by the first axis and the rise in water temperature of the Roman Warm Period (RWP) period. The sampling resolution of the diatom analyses (2-cm) implied an average interval of ~125 years, and these inferences therefore better capture long-term climate trends than high-frequency variations.

Sediment geochemistry was closely linked to catchment system dynamics, such as surface run-off during the ice-free season and ice cap melting periods, as confirmed by the RDA between the mineral species and the XRF, TOC and TN datasets (Supplementary Fig. 1A). Ca, Ti, Fe, Mn, and Sr were grouped mainly with clays derived from the catchment's primarily volcanic rocks, whereas the negative end of this axis was mainly triggered by changes in sediment biomass indicators TOC and TN. The absence of well-developed soils and vegetation around the lake and, therefore, of terrestrial organic matter in the basin, indicates that the majority of sediment organic matter was related to algal processes, a hypothesis also supported by the coincidence with low C/N ratios and $\delta^{13}\text{C}$ values. The association of montmorillonite with this negative end provides further evidence that lake primary productivity was associated with relatively warm conditions, since this clay is formed by the pedogenic alteration of pre-existent catchment rocks by hydrolysis under relatively warmer conditions (Fagel and Boës, 2008). The almost opposing trends of inorganic elements and lacustrine organic matter along the first RDA axis can be interpreted in terms of surface run-off. During relatively cold conditions, Aucella Lake may have remained partially ice-covered in summer, allowing the input of fine and

non-chemically altered terrigenous particles from the catchment, whereas in relatively warm periods the lake was ice-free, permitting the input of previously formed soil clays into the lake as well as enhancing algal organic matter production. The thickness and duration of lake ice cover, as well as the amount of surface run-off in summer, are influenced by changes in air temperature (Sánchez-López et al., 2015). As such, variations along this first RDA axis reflect temperature changes. As the geochemical distribution in the RDA is almost the same in the PCA (almost opposing trends of inorganic elements and TOC) and the XRF data has better resolution than the RDA axis, the first axis of this is interpreted in terms of air temperature fluctuations.

The first XRF PCA axis (Fig. 4) shows a relatively warm period between ~5.0 and 3.8 cal. ka BP, during which ice cover was relatively thinner and/or less persistent and algal diversity was high, as shown by diatom diversity measures and PCA scores (Fig. 4). At 3.8 cal. ka BP, temperatures decreased abruptly, which coincided with the first decrease in algal diversity (Fig. 6A). Air and water temperatures remained relatively cold until ~3 cal. ka BP when air temperature started to gradually increase in consonance with the water temperature. Water temperature peaked at the onset of the RWP at ~2 cal. ka BP, while the air temperature peak occurred during the Medieval Climate Anomaly (MCA). The Little Ice Age (LIA) was marked by an abrupt air temperature decrease that reached minimum values at the end of this period. The Industrial Period was marked by a steep air temperature increase, thin ice lake covers and/or longer ice-free seasons, and a significant increase in diatom diversity.

The relationship between environmental factors in the RDA (Supplementary Fig. 2B) and the genus *Staurorsirella* (a cold-tolerant and post-glacial pioneering taxon; (Smol, 1983) suggests its association with more turbulent environments, and with more movement or entry of material into the system. We hypothesize that the lower part of the core represented by the first three diatom clusters reflects a more turbulent or unstable environment dominated by more rapid changes, likely related to the dynamics of proximal factors such as the snow patch in the catchment area.

5.2. Local limnological and paleoenvironmental history

Other sediment core studies from the same area have documented changing conditions that were generally controlled by a mix of regional climatic changes and local landscape feedbacks (Bennike et al., 2008). Climate variability is regional (seasonal, inter-annual, and inter-decadal), while landscape factors, such as the behavior of the perennial snow patch inside the catchment area can be considered to be local (Hernández et al., 2015). Previous local studies suggested that this snow patch existed consistently in the uplands on Aucellabjerg Mountain from the early to mid-Holocene (Cable et al., 2018), which includes the early part of our sedimentary record, and that the winter snow patch size is an important driver of stream physico-chemical habitat in an Arctic region with low glacial cover (Docherty et al., 2018). Given that the sensitivity of the snow patch to changes in snowline elevation is primarily influenced by summertime temperatures (Oerlemans, 2001), the direct relationship between our temperature variation axis and the July insolation curve (Fig. 4) indicates that the evolution of Aucella Lake observed in our sediment core reflects summertime climate (Fig. 6).

Our air temperature record indicates that generally warm conditions prevailed during the mid-Holocene at Aucella Lake (~5.0–3.8 cal. ka BP) (Fig. 6, zone A). There were low, but present, inputs of terrigenous material to the system, showing that the lake became seasonally ice free during this period. Oxidic conditions were present during the first thousand years of our record, with chlorophyll indicating high biomass, with at least the lake littoral zone thawing which allowed some nutrients to enter the system. Chlorophyll values suggest a lower snow accumulation above the lake ice cover and therefore dry conditions in the mid-Holocene. The input of newly formed clays, combined with high biomass variables, are related to higher rates of organic matter

J. Garcia-Oteyza et al.

Science of the Total Environment 906 (2024) 167713

J. Garcia-Oteyza et al.

Science of the Total Environment 906 (2024) 167713

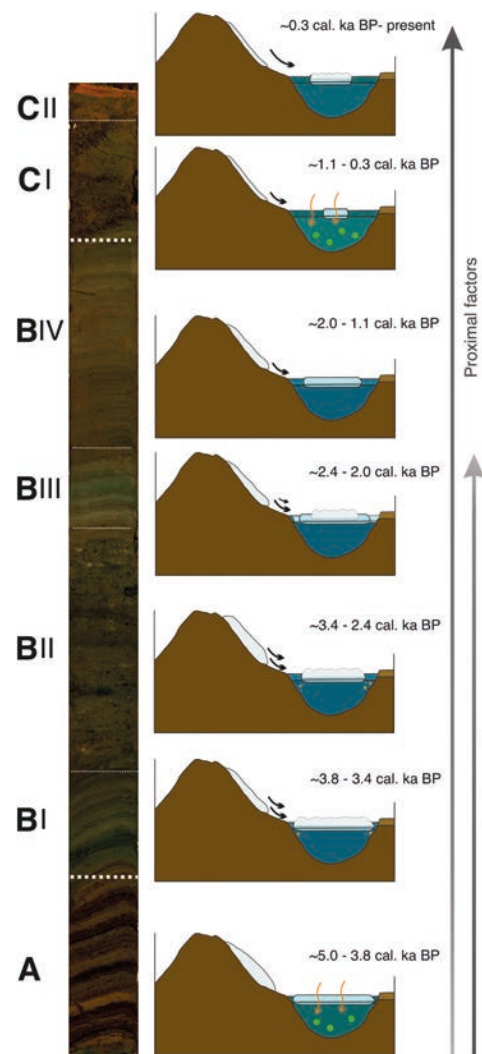


Fig. 6. Conceptual model of the of Aucella Lake evolution for each core zone.

productivity due to short periods of ice cover duration relative to other NE Greenland lakes (Smol, 1983). The rapid transition at ~3.8–3.4 ka BP was the most abrupt in our record and was recorded by every proxies, although to a lesser extent by diatom assemblages. The abrupt change visible in terrigenous elements indicates enhanced delivery to lake sediments, and thus a more humid and colder climate that increased the transport of primary and non-chemically altered rock fragments from the catchment to the lake. Moreover, this increased input of terrigenous particles from around the lake increased turbidity and hindered light penetration, with a resulting decrease in diatom diversity and a longer ice-cover duration. During the next millennium (~3.4–2.4

cal. ka BP) (Fig. 6, zone BII), the sedimentary record was indicative of progressively warming conditions with high inputs of weathered terrigenous material, sustained by the continued domination of the snow patch as a landscape factor. Limited lake ice allowed high-continuous entry of material, as reflected by the fine grain size, and the continuity of low chlorophyll values suggests the presence of significant snow cover on the lake, in addition to high turbidity. Throughout the period ~2.4–2.0 cal. ka BP (Fig. 6, zone BIII), with the onset of the RWP, the diatom index and axis curves show (Fig. 2), on the one hand, a decrease of species diversity together with a significant change in the trend of PCA axis, on which more negative values show a shift to colder conditions with thicker and/or more persistent ice cover on the lake. This shift reflects a regime change that occurred in the system, when it ceased to be dominated by landscape factors (with large inputs of weathered terrigenous due to the activity of the snow patch) and began to record signals more dominated by regional climate variability. This is reinforced by an abrupt air temperature oscillation.

The sedimentary record then indicates a progressive transition to a warmer and drier climate at ~2.0–1.1 cal. ka BP (Fig. 6, zone BIV) peaking at the MCA. The highest temperatures coincided with a drop in grain size and terrigenous inputs, as well as an increase in chlorophyll values and the highest values of diatom diversity, suggesting longer ice-free periods during summer. Over the next several centuries, from ~1.1–0.3 cal. ka BP (Fig. 6, zone CI), the influence of landscape factors over the system diminished, and sedimentary indicators suggested a transition towards a colder, more humid climate that coincided with the LIA; air temperatures reached their minimum values at the end of this period. Diatom assemblages also had low diversities during this period, most likely linked to an increase in the duration and/or thickness of ice cover. An abrupt change was recorded during the last 50 years of the record (Fig. 6, zone CII), with increased diatom diversity and warmer conditions marked by thin ice covers and/or long seasonally ice-free periods, and an abrupt air temperature increase which almost reached the MCA peaks/relative trends. A parallel shift towards increasing mean grain size and high chlorophyll values imply rising temperatures and a potentially more turbulent environment that reflect recent warming as observed at high latitudes.

5.3. Local to supra-regional inferences proxy correlations

The closest multiproxy lake study to our site is located at the bottom of the Zackenberg Valley (at ca.8 km distance), and extends to 9.0 cal. ka BP (Bennike et al., 2008). The authors inferred an overall trend of declining summer temperatures and longer-lasting snow cover from 5.5 cal. ka BP to the present, unlike the trends we observed in Aucella Lake for the last 5.0 cal. ka BP. The Aucella Lake abrupt change recorded ~3.8 cal. ka BP was not observed in the Renland Ice Core oxygen isotope record (ca. 400 km south from Zackenberg), which may indicate that this abrupt shift was associated with landscape factors. The importance of local influences (size, depth, morphology and chemistry of the catchment) for the sedimentary record and lake biology has already been noted from NE Greenland sites (Bennike et al., 2008). A high-resolution record of proglacial Madsen Lake, ~20 km to the W, showed three phases of enhanced glacial activity during the last two millennia, with two phases between ~1.3–0.8 cal. ka BP and a third phase at ~0.7 cal. ka BP (Adamson et al., 2019). The Aucella Lake core records the onset of Late Holocene climatic deterioration at ~2.5 cal. ka BP, early for NE Greenland and preceding the Madsen Lake record, and also shows temperature minima coincident with the first two phases of glacial advance (~1.2 and ~0.8 cal. ka BP) recorded in this nearby study (Adamson et al., 2019). This suggests that remote (high latitude and altitude) Aucella Lake is highly sensitive and therefore a sentinel of climate change. The third phase recorded at Madsen Lake differs from the previous ones, representing more a reflection of regional climatic changes associated with the LIA onset (Catalan et al., 2013). The maximum glacial extent in the area occurred before ~0.5 cal. ka BP,

effectively during the beginning of the LIA, when an increase of nivation processes in Zackenberg Valley was recorded (Adamson et al., 2019), after which temperatures increased.

There have been several studies from the Aucella Lake region that have examined paleo-records from lacustrine and continental shelf sediments. Research has focused on areas to the north (Christiansen, 1998) and the south of our study area (Davies et al., 2022; Klug, 2009; Pados-Dibattista et al., 2022; Schmidt et al., 2011; Wagner et al., 2008b). Records from these two regions broadly agree with the structure of a cold Early Holocene, a warmer Mid-Holocene with a Holocene Thermal Maximum ending at ~5.5 cal. ka BP, and a relatively cold Late Holocene (Axford et al., 2017; Cremer et al., 2001a, 2001b; Klug and Wagner, 2008; Kolling et al., 2017; Levy et al., 2014a; Lowell et al., 2013; Lusas et al., 2017; Medford et al., 2021; Wagner et al., 2000, 2005; Wagner and Melles, 2002). Around 6.2 cal. ka BP, sub-surface waters on the Central Northeast Greenland shelf started to cool (Klug, 2009). After ~5.5 cal. ka BP a distinct cooling commenced with an increase in sea ice-extents (Pados-Dibattista et al., 2022) showing a Neoglacial average cooling of 0.6–0.8 °C per thousand years from ~5.5 to ~0.5 cal. ka BP that was more intense between ~4 to ~3.5 cal. ka BP and became progressively colder throughout the late Holocene (4.2 cal. ka BP-present) (Klug, 2009; Klug and Wagner, 2008). In some cases, the records also show greater productivity in the early and middle Holocene than in the late Holocene (Axford et al., 2017; Pados-Dibattista et al., 2022). Across the entire set of records, there is no strong consensus on the timing of the Neoglacial or other events such as the LIA. The closest to our study area was reported as the onset of the Neoglacial at ~3.2–3.5 cal. ka BP glacial advance was reported as the onset of the Neoglacial (Lusas et al., 2017) accompanied by a reconstructed negative temperature anomaly (Medford et al., 2021) and a cooling of the sub-surface water on the central Northeast Greenland shelf at 3.2 cal. ka BP (Axford et al., 2017). A shift towards more arid conditions at was recorded ~2.7 cal. ka BP, when the atmospheric circulation over North Atlantic significantly changed (Pados-Dibattista et al., 2022), with the first signs of glacial regrowth at ~2.6 cal. ka BP (Wagner et al., 2008a) appearing initially in high-elevation interior locations. Diatom analyses suggested that some areas of NE Greenland were seasonally ice-free during much of the Holocene, with perennial ice cover developing only after 1.8 cal. ka BP (Cremer et al., 2001a, 2001b). A gradual change towards colder temperature conditions began after 1.8 cal. ka BP, as registered in other regions (Levy et al., 2014b). There is no consensus about the timing of the LIA, although most records have indicated cold events or glacial advances prior to or around ~700 cal. ka BP, including at ~1.3 cal. ka BP (Lusas et al., 2017) and ~1.0–0.8 cal. ka BP (Adamson et al., 2019; Medford et al., 2021), with a subsequent period of ice-marginal retreat at ~0.5 cal. ka BP (Adamson et al., 2019; Lusas et al., 2017; Medford et al., 2021).

5.3.1. Greenland correlations

We compared our XRF-inferred temperature first vector and the first diatom PCA axis with Greenland temperature records: the temperature reconstructions from the nearest coastal ice core, from Renland Ice Cap (Medford et al., 2021), and the high-resolution XRF-inferred temperature reconstruction from a SE Greenland lake (Vinther et al., 2008). Moreover, we compared our temperature change record to regional changes in summer and winter solar insolation at 65°N (Balascio et al., 2015).

There was spatial and temporal thermal heterogeneity between the different records. The Renland ice-core temperature record showed a general cooling trend for the 5000 years of data, which differed from the response of our diatom assemblages, possibly due to the different sensitivity of the proxies employed to reconstruct this lake process. Although Aucella Lake does not directly receive glacial meltwater and our data do not preserve a direct sedimentary record of glacier activity (advances and retreats), the climate variability inferred from its record mirrors local glacial oscillations. Six major Neoglacial advances (4.1,

3.9, 3.2, 2.8, 2.1, and 1.3 cal. ka BP) of the Kulusuk glaciers were inferred from the Kulusuk Lake sediment record study (Balascio et al., 2015); these were broadly consistent with those detected in Aucella Lake. The first Neoglacial advance coincided with the abrupt air temperature drop recorded in Aucella Lake, indicating that this event was not due to local factors but rather to regional forcing. This ice advance may have been caused by the progressively declining NH summer insolation and the timing of cooling episodes in the North Atlantic Ocean attributed to the increased strength of the East Greenland Current (Balascio et al., 2015). These advances are also reflected as cooling peaks in our temperature reconstruction from XRF PC1 and likely record local glacier advances during these periods.

The Aucella Lake data presents linkages with changes in winter (before ~0.8 cal. ka BP) and summer (after ~0.8 cal. ka BP) insolation (Fig. 4), with a shift during the Late Holocene into warmer conditions beginning shortly after the summer and winter insolation curves intersect (~1.2 cal. ka BP) (Berger and Loutre, 1991). When comparing our results with the general East Greenland Mean July temperature obtained from the average of several records using a compilation of pollen data from different sediment cores (Gajewski, 2015), the difference in temporal resolution becomes clear, as does the need for multiproxy studies in order to better understand lake system linkages to the environment and climate.

6. Conclusions

This study presents the first multi-proxy-high-resolution approach for the climate variability in this region for the last ~5000 years and shows that high altitude lakes act as sentinels and amplifiers of rapid high arctic changes, and that local, seasonally specific temperature reconstructions with high resolution multiproxy studies are needed for accurately characterizing climates of the past. Aucella Lake limnological conditions were determined by a mixture of local and regional factors, including the presence of a snow patch in the lake catchment and regional climate evolution. Water turbidity due to the input of fine terrigenous particles, as well as the duration and thickness of lake ice cover, play important roles in determining these limnological conditions. Our paleolimnological reconstruction reflected changes in summer climate. It highlighted the relatively warmer conditions of the mid-Holocene, and abrupt temperature decreases at the onset of the Late Holocene which coincided with the beginning of glacial advances elsewhere, and occurred when winter and summer insolation temperatures had a minimum difference in values. The temperature recovery started at ca. 2.8 cal. ka BP and peaked during the Medieval Climate Anomaly. However, this progressive temperature rise was punctuated by abrupt and short-lived cold periods such as that which marked the onset of the Roman Warm Period at ca. 2 cal. ka BP. The beginning of the Little Ice Age was characterized by marked decreases in air temperatures, reaching minimum values at the end of this period. The last 50 years of the Aucella Lake record were marked by abrupt temperature rises, the highest peaks of the last 5000 years and are reflective of current anthropogenic global warming.

Supplementary data to this article can be found online at <https://doi.org/10.1016/j.scitotenv.2023.167713>.

Declaration of competing interest

All authors have participated in (i) conception and design, or analysis and interpretation of the data; (ii) drafting the article or revising it critically for important intellectual content; and (iii) approval of the final version. This manuscript has not been submitted to, nor is under review at, another journal or other publishing venue.

Data availability

Data will be made available on request.

Acknowledgements

This research was funded by the project PALEOGREEN (CTM2017-87976-P) of the Spanish Ministry of Economy and Competitiveness. Field work was also supported by an INTERACT Transnational Access grant (Ref. 730938, GLACI GREEN) and by the Research Group ANTALP (Antarctic, Arctic, Alpine Environments; 2017-SGR-1102), funded by the Government of Catalonia. Julia Garcia-Oteyza was supported by an FPI fellowship from the Spanish Ministry of Science, Innovation and Universities.

CRediT authorship contribution statement

All the authors have been actively involved in the investigation presented in this work:

1. Julia Garcia-Oteyza. Writing of a first draft of the manuscript (text, table, and figures), analysis, data processing, laboratory tasks, discussion of the results.
2. Santiago Giralt. Coordination of the research and writing of a first draft of the manuscript, leading the fieldwork, laboratory analysis, sampling and data processing.
3. Sergi Pla-Rabes. Laboratory diatoms analysis, discussion of the results, contribution to the discussion and writing.
4. Dermot Antoniades. Writing of a first draft of the manuscript and subsequent text revisions, fieldwork, laboratory analysis, sampling and data processing.
5. Marc Oliva. Fieldwork. Interpretation and discussion of the results thorough correction of the manuscript.
6. Hamid Ghanbari. Laboratory processing of grain size and chrophyl data results and contribution to the interpretation and revision of the manuscript.
7. Rodrigo Osorio-Serrano. Discussion of the results and contribution to the revision of the manuscript.
8. David Palacios. Fieldwork and discussion of the results and contribution to the revision of the manuscript.

References

- Adamson, K., Lane, T., Carney, M., Bishop, T., Delaney, C., 2019. High-resolution proglacial lake records of pre-little ice age glacial advance, northeast Greenland. *Boreas* 48, 535–550. <https://doi.org/10.1111/bor.12361>.
- Adrian, R., O'Reilly, C.M., Zagarese, H., Baines, S.B., Hesse, D.O., Keller, W., Livinstone, D.M., Sommaruga, R., Straile, D., Van Donk, E., Weyhenmeyer, G.A., Winder, M., 2009. Lakes as sentinels of climate change. *Limnol. Oceanogr.* 33, 2283–2297. <https://doi.org/10.4319/lo.2009.54.6.part.2.2283>.
- Anderson, N., Saros, J.E., Bullard, J.E., Cahoon, S.M.P., McGowan, S., Bagshaw, E.A., Barry, C.D., Bindler, R., Burpee, B.T., Carrivick, J.L., Fowler, R.A., Fox, A.D., Fritz, S. C., Giles, M.E., Hamerlik, L., Ingeman-Nielsen, T., Law, A.C., Mernild, S.H., Northington, R.M., Osburn, C.L., Pla-Rabes, S., Post, E., Telling, J., Stroud, D.A., Whiteford, E.J., Yallop, M.L., Yde, A.J.C., 2017. The arctic in the twenty-first century: changing biogeochemical linkages across a paraglacial landscape of Greenland. *Bioscience* 67, 118–133. <https://doi.org/10.1093/biosci/biw158>.
- Antoniades, D., Hamilton, P., Douglas, M., Smol, J., 2008. Diatoms of North America: the freshwater floras of Prince Patrick, Ellef Ringnes and northern Ellesmere Islands from the Canadian Arctic Archipelago. *Iconogr. Diatomol.* 17, 1–649.
- Aschwanden, A., Fahnestock, M.A., Truffer, M., Brinkerhoff, D.J., Hock, R., Khroulev, C., Mottram, R., Abbas Khan, S., 2019. Contribution of the Greenland ice sheet to sea level over the next millennium. *Sci. Adv.* 5, 1–7. <https://doi.org/10.1126/sciadv.aav9396>.
- Axford, Y., Levy, L.B., Kelly, M.A., Francis, D.R., Hall, B.L., Langdon, P.G., Lowell, T.V., 2017. Timing and magnitude of early to middle Holocene warming in East Greenland inferred from chironomids. *Boreas* 46, 678–687. <https://doi.org/10.1111/bor.12247>.
- Balascio, N.L., D'Andrea, W.J., Bradley, R.S., 2015. Glacier response to North Atlantic climate variability during the Holocene. *Clim. Past* 11, 1587–1598. <https://doi.org/10.5194/cp-11-1587-2015>.
- Battarbee, R.W., Carvalho, L., Jones, V.J., Flower, et al., 2001. Diatom analysis. In: Smol, J.P., Birks, H.J.B. (Eds.), *Tracking Environmental Change using Lake Sediments*. Kluwer Academic Publishers, Last, Dordrecht, pp. 185–202.
- Bennike, O., Sørensen, M., Fredskild, B., Jacobsen, B.H., Bøcher, J., Amsinck, S.L., Jeppesen, E., Andreassen, C., Christiansen, H.H., Humlum, O., 2008. Late Quaternary environmental and cultural changes in the Wollaston Forland Region, Northeast

- Greenland. *Adv. Ecol. Res.* 40, 45–79. [https://doi.org/10.1016/S0065-2504\(07\)00003-7](https://doi.org/10.1016/S0065-2504(07)00003-7).
- Berger, A., Loutre, M.F., 1991. Insolation values for the climate of the last 10 million years. *Quat. Sci. Rev.* 10, 297–317. [https://doi.org/10.1016/0277-3791\(91\)90033-Q](https://doi.org/10.1016/0277-3791(91)90033-Q).
- Blaauw, Maarten, Andrés Christeny, J., 2011. Flexible paleoclimate age-depth models using an autoregressive gamma process. *Bayesian Anal.* 6 (3), 457–474.
- Bonow, J.M., Japsen, P., 2021. Peneplains and tectonics in north-east Greenland after opening of the North-East Atlantic. *GEUS Bull.* 45, 1–35. <https://doi.org/10.34194/GEUSB.V45.5297>.
- Bouchard, G., Gajewski, K., Hamilton, P.B., 2004. Freshwater diatom biogeography in the Canadian Arctic archipelago. *J. Biogeogr.* 31, 1955–1973. <https://doi.org/10.1111/j.1365-2699.2004.01143.x>.
- Briner, J.P., McKay, N.P., Axford, Y., Bennike, O., Bradley, R.S., de Vernal, A., Fisher, D., Francus, P., Fréchette, B., Gajewski, K., Jennings, A., Kaufman, D.S., Miller, G., Rouston, C., Wagner, B., 2016. Holocene climate change in Arctic Canada and Greenland. *Quat. Sci. Rev.* 147, 340–364. <https://doi.org/10.1016/j.quascirev.2016.02.010>.
- Cable, S., Christiansen, H.H., Westergaard-Nielsen, A., Kroon, A., Elberling, B., 2018. Geomorphological and cryostratigraphical analyses of the Zackenberg Valley, NE Greenland and significance of Holocene alluvial fans. *Geomorphology* 303, 504–523.
- Carpenter, S.R., Benson, B.J., Biggs, R., Chipman, J.W., Foley, J.A., Golding, S.A., Hammer, R.B., Hanson, P.C., Johnson, P.T.J., Kamarainen, A.M., Kratz, T.K., Lathrop, R.C., McMahon, K.D., Provencher, B., Rusak, J.A., Solomon, C.T., Stanley, E.H., Turner, M.G., Vander Zanden, M.J., Wu, C.H., Yuan, H., 2007. Understanding regional change: a comparison of two lake districts. *Bioscience* 57, 323–335. <https://doi.org/10.1641/B570407>.
- Catalan, J., Pla-Rabes, S., Wolfe, A.P., Smol, J.P., Rühland, K.M., Anderson, N.J., Kopaček, J., Stuchlik, E., Schmidt, R., Koinig, K.A., Camarero, L., Flower, R.J., Heiri, O., Kamenik, C., Korhola, A., Leavitt, P.R., Psenner, R., Renberg, I., 2013. Global change revealed by palaeolimnological records from remote lakes: a review. *J. Paleolimnol.* 49, 513–535. <https://doi.org/10.1007/s10933-013-9681-2>.
- CAVM Team, 2003. Circumpolar Arctic Vegetation Map. (1:7,500,000 scale), Conservation of Arctic Flora and Fauna (CAFF) Map No. 1. US Fish Wildl. Serv. AK. Available <http://www.Geobot.uaf.edu/cavm/> [Verified 1 August 15 July 2015].
- Christiansen, H.H., 1998. "Little Ice Age" nivation activity in northeast Greenland. *Holocene* 8, 719–728. <https://doi.org/10.1191/09596839866994797>.
- Christiansen, H.H., Sigsgaard, C., Humlum, O., Rasch, M., Hansen, B.U., 2008. Permafrost and periglacial geomorphology at Zackenberg. *Adv. Ecol. Res.* 40, 151–174. [https://doi.org/10.1016/S0065-2504\(07\)00007-4](https://doi.org/10.1016/S0065-2504(07)00007-4).
- Christiansen, H.H., Eitzel Müller, B., Isaksen, K., Juliusen, H., Farbot, H., Humlum, O., Johansson, M., Ingeman-Nielsen, T., Kristensen, L., Hjort, J., Holmlund, P., Sannel, A.B.K., Sigsgaard, C., Åkerman, H.J., Foged, N., Blüke, L.H., Pernosky, M.A., Ødegård, R.S., 2010. The thermal state of permafrost in the nordic area during the international polar year 2007–2009. *Permaf. Periglac. Process.* 21, 156–181. <https://doi.org/10.1002/ppp.687>.
- Chung, 1974. Quantitative interpretation of X-ray diffraction patterns of mixtures: II. Adiabatic principles of X-ray diffraction analysis of mixtures. *Structure* 526–531.
- Cremer, H., Melles, M., Wagner, B., 2001a. Holocene climate changes reflected in a diatom succession from Basalts, east Greenland. *Can. J. Bot.* 79, 649–656. <https://doi.org/10.1139/cjb-79-6-649>.
- Cremer, H., Wagner, B., Melles, M., Hubberten, H.W., 2001b. The postglacial environmental development of Raffles So, East Greenland: inferences from a 10,000 year diatom record. *J. Paleolimnol.* 26, 67–87. <https://doi.org/10.1023/A:1011179321529>.
- Davies, J., Mathiasen, A.M., Kristiansen, K., Hansen, K.E., Wacker, L., Alstrup, A.K.O., Munk, O.L., Pearce, C., Seidenkrantz, M.S., 2022. Linkages between ocean circulation and the Northeast Greenland Ice Stream in the Early Holocene. *Quat. Sci. Rev.* 286, 107530 <https://doi.org/10.1016/j.quascirev.2022.107530>.
- Davini, P., Cagnazzo, C., Neale, R., Tribbia, J., 2012. Coupling between Greenland blocking and the North Atlantic Oscillation pattern. *Geophys. Res. Lett.* 39, 1–6. <https://doi.org/10.1029/2012GL052315>.
- Docherty, C.L., Riis, T., Milner, A.M., Christofferson, K.S., Hannah, D.M., 2018. Controls on stream hydrochemistry dynamics in a high Arctic snow-covered watershed. *Hydrol. Process.* 32, 3327–3340. <https://doi.org/10.1002/hyp.13256>.
- Emson, D., Sayer, C.D., Bennion, H., Patmore, I.R., Rioual, P., 2018. Mission possible: diatoms can be used to infer past duckweed (lemnoid Araceae) dominance in ponds. *J. Paleolimnol.* 60, 209–221. <https://doi.org/10.1007/s10933-017-0008-6>.
- Fagel, N., Boës, X., 2008. Clay-mineral record in Lake Baikal sediments: the Holocene and Late Glacial transition. *Palaeogeogr. Palaeoclimatol. Palaeoecol.* 259, 230–243. <https://doi.org/10.1016/j.palaeo.2007.10.009>.
- Finkelstein, S.A., Gajewski, K., 2008. Responses of Fragilarioid-dominated diatom assemblages in a small Arctic lake to Holocene climatic changes, Russell Island, Nunavut, Canada. *J. Paleolimnol.* 40, 1079–1095. <https://doi.org/10.1007/s10933-008-9215-5>.
- Gajewski, K., 2015. Quantitative reconstruction of Holocene temperatures across the Canadian Arctic and Greenland. *Glob. Planet. Chang.* 128, 14–23. <https://doi.org/10.1016/j.gloplacha.2015.02.003>.
- Garcia-Oteyza, J., Oliva, M., Palacios, D., Fernández-Fernández, J.M., Schimmelpfennig, I., Andrés, N., Antoniades, D., Christiansen, H.H., Humlum, O., Léanni, L., Jomelli, V., Ruiz-Fernández, J., Rinterknecht, V., Lane, T.P., Adamson, K., Aumaitre, G., Bourlés, D., Keddadouche, K., 2022. Late Glacial deglaciation of the Zackenberg area, NE Greenland. *Geomorphology* 401, 108125.
- Ghanbari, H., Antoniades, D., 2022. Convolutional neural networks for mapping of lake sediment core particle size using hyperspectral imaging. *Int. J. Appl. Earth Obs. Geoinf.* 112, 102906 <https://doi.org/10.1016/j.jag.2022.102906>.

- Goose, H., Kay, J.E., Armour, K.C., Bodas-Salcedo, A., Chepfer, H., Docquier, D., Jonko, A., Kushner, P.J., Lecomte, O., Massonnet, F., Park, H.S., Pithan, F., Svensson, G., Vancoppenolle, M., 2018. Quantifying climate feedbacks in polar regions. *Nat. Commun.* 9 <https://doi.org/10.1038/s41467-018-04173-0>.
- Grimm, E.C., 1987. CONISS: a FORTRAN 77 program for stratigraphically constrained cluster analysis by the method of incremental sum of squares. *Comput. Geosci.* 13, 13–35. [https://doi.org/10.1016/0098-3004\(87\)90022-7](https://doi.org/10.1016/0098-3004(87)90022-7).
- Hanna, E., Cropper, T.E., Jones, P.D., Scaife, A.A., Allan, R., 2015. Recent seasonal asymmetric changes in the NAO (a marked summer decline and increased winter variability) and associated changes in the AO and Greenland Blocking Index. *Int. J. Climatol.* 35, 2540–2554. <https://doi.org/10.1002/joc.4157>.
- Hanna, E., Cropper, T.E., Hall, R.J., Cappelen, J., 2016. Greenland Blocking Index 1851–2015: a regional climate change signal. *Int. J. Climatol.* 36, 4847–4861. <https://doi.org/10.1002/joc.4673>.
- Hasholt, B., Mernild, S.H., Sigsgaard, C., Elberling, B., Petersen, D., Jakobsen, B.H., Hansen, B.U., Hinkler, J., Søgaard, H., 2008. Hydrology and transport of sediment and solutes at Zackenberg. *Adv. Ecol. Res.* 40, 197–221. [https://doi.org/10.1016/S0065-2504\(07\)00009-8](https://doi.org/10.1016/S0065-2504(07)00009-8).
- Henriksen, N., Higgins, A.K., Kalsbeek, F., Pulvertaft, T.C.R., 2009. Greenland from Archaean to quaternary descriptive text to the 1995 geological map of Greenland, 1: 2500000. *Geol. Surv. Denmark Greenl. Bull.* 18, 126.
- Hernández, A., Trigo, R.M., Pla-Rabes, S., Valero-Garcés, B.L., Jerez, S., Rico-Herrero, M., Vega, J.C., Jambriña-Enríquez, M., Giralt, S., 2015. Sensitivity of two Iberian lakes to North Atlantic atmospheric circulation modes. *Clim. Dyn.* 45, 3403–3417. <https://doi.org/10.1007/s00382-015-2547-8>.
- Højlund Pedersen, S., 2017. Scaling-up Climate Change Effects in Greenland. PhD Thesis. Aarhus University. Department of Bioscience, Denmark (178 pp).
- Juggins, S., 2022. rioja: Analysis of Quaternary Science Data. R package version 1.0-5. <https://cran.r-project.org/package=rioja>.
- Kassambara, A., Mundt, F., 2020. Factoextra: Extract and Visualize the Results of Multivariate Data Analyses. R Package Version 1.0.7. <https://CRAN.R-project.org/package=factoextra>.
- Klug, M., 2009. The Late Quaternary environmental and climatic history of North-East Greenland, inferred from coastal lakes. PhD Thesis. Univ. Köln 148. <https://doi.org/10.23689/figdeq.241>.
- Klug, M., Wagner, B., 2008. Late Pleistocene and Holocene environmental history of northeastern Geographical Society Ø, East Greenland, inferred from Loon Lake s sediment record. *Leipzigiger Geowissenschaften, Leipzig* 1–22.
- Kölling, H.M., Stein, R., Fahl, K., Perner, K., Moros, M., 2017. Short-term variability in late Holocene sea ice cover on the East Greenland Shelf and its driving mechanisms. *Palaeogeogr. Palaeoclimatol. Palaeoecol.* 485, 336–350. <https://doi.org/10.1016/j.palaeo.2017.06.024>.
- Kottek, M., Grieser, J., Beck, C., Rudolf, B., Rubel, F., 2006. World map of the Köppen-Geiger climate classification updated. *Meteorol. Z.* 15, 259–263. <https://doi.org/10.1127/0941-2948/2006/0130>.
- Krammer, K., Lange-Bertalot, H., 1986. 2/1. Bacillariophyceae. 1. Teil: Naviculaceae. In: Ettl, H., Gerloff, J., Heynig, H., Mollenhauer, D. (Eds.), *Süßwasserflora von Mitteleuropa*. G. Fischer Verlag, Stuttgart, Germany, 206 Tafeln mit 2976 Figuren. 876 pp.
- Krammer, K., Lange-Bertalot, H., 1988. 2/2. Bacillariophyceae. 2. Teil: Bacillariaceae. Epithemiaceae, Surirellaceae. In: Ettl, H., Gerloff, J., Heynig, H., Mollenhauer, D. (Eds.), *Süßwasserflora von Mitteleuropa*. G. Fischer Verlag, Stuttgart, Germany, 184 Tafeln mit 1914 Figuren. 596 pp.
- Krammer, K., Lange-Bertalot, H., 1991a. 2/3. Bacillariophyceae. 3. Teil: Centrales, Fragilariaceae, Eunotiaceae. In: Ettl, H., Gerloff, J., Heynig, H., Mollenhauer, D. (Eds.), *Süßwasserflora von Mitteleuropa*. G. Fischer Verlag, Stuttgart, 166 Tafeln mit 2180 Figuren. 576 pp.
- Krammer, K., Lange-Bertalot, H., 1991b. 2/4. Bacillariophyceae. 4. Teil: Achmannthaceae. Kritische Ergänzungen zu Navicula (Lineolatae) und Gomphonema. In: Ettl, H., Gerloff, J., Heynig, H., Mollenhauer, D. (Eds.), *Süßwasserflora von Mitteleuropa*. G. Fischer Verlag, Stuttgart, 88 Tafeln mit 2048 Figuren. 437 pp.
- Kuhn, D.L., Plafkin, J.L., Cairns, J., Lowe, R.L., 1981. Qualitative characterization of aquatic environments using diatom life-form strategies. *Trans. Am. Microsc. Soc.* 100, 165. <https://doi.org/10.2307/3225800>.
- Legendre, P., Birks, H.J.B., 2012. Clustering and partitioning. *Track. Environ. Chang. Lake Sediments* 5, 1–32.
- Legendre, P., Gallagher, E.D., 2001. Ecologically meaningful transformations for ordination of species data. *Oecologia* 129, 271–280. <https://doi.org/10.1007/s004420100716>.
- Levy, L.B., Kelly, M.A., Lowell, T.V., Hall, B.L., Hempel, L.A., Honsaker, W.M., Lusas, A. R., Howley, J.A., Axford, Y.L., 2014a. Holocene fluctuations of Bregne ice cap, Scoresby Sund, east Greenland: a proxy for climate along the Greenland Ice Sheet margin. *Quat. Sci. Rev.* 92, 357–368. <https://doi.org/10.1016/j.quascirev.2013.06.024>.
- Levy, L.B., Kelly, M.A., Lowell, T.V., Hall, B.L., Hempel, L.A., Honsaker, W.M., Lusas, A. R., Howley, J.A., Axford, Y.L., 2014b. Holocene fluctuations of Bregne ice cap, Scoresby Sund, east Greenland: a proxy for climate along the Greenland Ice Sheet margin. *Quat. Sci. Rev.* 92, 357–368. <https://doi.org/10.1016/j.quascirev.2013.06.024>.
- Lowell, T.V., Hall, B.L., Kelly, M.A., Bennike, O., Lusas, A.R., Honsaker, W., Smith, C.A., Levy, L.B., Travis, S., Denton, G.H., 2013. Late Holocene expansion of Istovret ice cap, Liverpool Land, east Greenland. *Quat. Sci. Rev.* 63, 128–140. <https://doi.org/10.1016/j.quascirev.2012.11.012>.
- Lund, M., Abermann, J., Skov, K., 2017. Environmental effects of a rare rain event in the high Arctic. In: *EGUGeneralAssembly Conf. Abstr.* 1 19, Abstract no. 9462.

- Lusas, A.R., Hall, B.L., Lowell, T.V., Kelly, M.A., Bennike, O., Levy, L.B., Honsaker, W., 2017. Holocene climate and environmental history of East Greenland inferred from lake sediments. *J. Paleolimnol.* 57, 321–341. <https://doi.org/10.1007/s10933-017-9951-5>.
- McFarlin, J.M., Axford, Y., Osburn, M.R., Kelly, M.A., Osterberg, E.C., Farnsworth, L.B., 2018. Pronounced summer warming in northwest Greenland during the Holocene and Last Interglacial. *Proc. Natl. Acad. Sci. U. S. A.* 115 (25), 6357–6362.
- Medford, A.R., Hall, B.L., Lowell, T.V., Kelly, M.A., Levy, L.B., Wilcox, P.S., Axford, Y., 2021. Holocene glacial history of Renland Ice Cap, East Greenland, reconstructed from lake sediments. *Quat. Sci. Rev.* 258, 106883 <https://doi.org/10.1016/j.quascirev.2021.106883>.
- Miller, G.H., Alley, R.B., Brigham-Grette, J., Fitzpatrick, J.J., Polyak, L., Serreze, M.C., White, J.W.C., 2010. Arctic amplification: can the past constrain the future? *Quat. Sci. Rev.* 29, 1779–1790. <https://doi.org/10.1016/j.quascirev.2010.02.008>.
- Oksanen, J., Blanchet, F.G., Friendly, M.; Kindt, R.; Legendre, P.; McGinn, D.; Minchin, P.; O'Hara, R.B.; Simpson, G.; Solymos, P.; Stevens, M.H.H.; Szöcs, E.; Wagner, H., 2020. *vegan* community ecology package, version 2.5-7.
- Oerlemans, J., 2001. Climatic interpretation of glacier fluctuations. In: Oerlemans, J. (Ed.), *Glaciers and Climate Change*. A.A. Balkema Publishers, Lisse, Netherlands, pp. 93–107.
- Pados-Dibattista, T., Pearce, C., Detlef, H., Bendtsen, J., Seidenkrantz, M.S., 2022. Holocene palaeoceanography of the Northeast Greenland shelf. *Clim. Past* 18, 103–127. <https://doi.org/10.5194/cp-18-103-2022>.
- Paull, T.M., Hamilton, P.B., Gajewski, K., LeBlanc, M., 2008. Numerical analysis of small Arctic diatoms (Bacillariophyceae), representing the *Staurastrira* and *Staurastrira* species complexes. *Phycologia* 47, 213–224. <https://doi.org/10.2216/07-17.1>.
- Pham, S.V., Leavitt, P.R., McGowan, S., Peres-Neto, P., 2008. Spatial variability of climate and land-use effects on lakes of the northern Great Plains. *Limnol. Oceanogr.* 53, 728–742. <https://doi.org/10.4319/lo.2008.53.2.0728>.
- Pithan, F., Mauritsen, T., 2014. Arctic amplification dominated by temperature feedbacks in contemporary climate models. *Nat. Geosci.* 7, 181–184. <https://doi.org/10.1038/ngeo2071>.
- Post, E., Forchhammer, M.C., Bret-Harte, M.S., Callaghan, T.V., Christensen, T.R., Elberling, B., Fox, A.D., Gilg, O., Hik, D.S., Hoye, T.T., Ims, R.A., Jeppesen, E., Klein, D.R., Madsen, J., McGuire, A.D., Rysgaard, S., Schindler, D.E., Stirling, I., Tamstorf, M.P., Tyler, N.J.C., Van Der Wal, R., Welker, J., Wookey, P.A., Schmidt, N. M., Aastrup, P., 2009. Ecological dynamics across the Arctic associated with recent climate change. *Science* 325, 1355–1358. <https://doi.org/10.1126/science.1173113>.
- Preusser, F., Degering, D., Fuchs, M., Hilgers, A., Kadereit, A., Klases, N., Krbetschek, M., Richter, D., Spencer, J.Q.G., 2008. Luminescence dating: basics, methods and applications. *Quat. Sci. J.* 57, 95–149. <https://doi.org/10.10285/eg.57.1-2.5>.
- R Core Team, 2022. R: A Language and Environment for Statistical Computing. R Foundation for Statistical Computing, Vienna, Austria. URL: <https://www.R-project.org/>.
- Reimer, P.J., Austin, W.E.N., Bard, E., Bayliss, A., Blackwell, P.G., Ramsey, C.B., Butzin, M., Cheng, H., Edwards, R.L., Friedrich, M., Grootes, P.M., Guilderson, T.P., Hajdas, I., Heaton, T.J., Hogg, A.G., Hughen, K.A., Kromer, B., Manning, S.W., Muscheler, R., Palmer, J.G., Pearson, C., van der Plicht, J., Reimer, R.W., Richards, D.A., Scott, E.M., Southon, J.R., Turney, C.S.M., Wacker, L., Adolphi, F., Büntgen, U., Capano, M., Fahrni, S.M., Fogtmann-Schulz, A., Friedrich, R., Köhler, P., Kudsk, S., Miyake, F., Olsen, J., Reinig, F., Sakamoto, M., Sookdebo, A., Talamo, S., 2020. The IntCal20 Northern Hemisphere radiocarbon age calibration curve (0–55 Cal BP). *Radiocarbon* 62 (4), 725–757.
- Rosenzweig, C., 2007. Assessment of observed changes and responses in natural and managed systems. In: Parry, M.L., Canz, O.F., Palutikof, J.P., van der Linden, P.J., Hanson, C.E. (Eds.), *Clim. Chang. 2007—Impacts, Adapt, Vulnerability*. Contrib. Work. Gr. II to Fourth Assess. Rep. Intergov. Panel 79–131.
- Sánchez-López, G., Hernández, A., Pla-Rabes, S., Toro, M., Granados, I., Sigró, J., Trigo, R.M., Rubio-Ingles, M.J., Camarero, L., Valero-Garcés, B., Giralt, S., 2015. The effects of the NAO on the ice phenology of Spanish alpine lakes. *Clim. Chang.* 130, 101–113. <https://doi.org/10.1007/s10584-015-1353-y>.
- Saros, J.E., Anderson, N.J., Juggins, S., McGowan, S., Yde, J.C., Telling, J., Bullard, J.E., Yallop, M.L., Heathcote, A.J., Burpee, B.T., Fowler, R.A., Barry, C.D., Northington, R. M., Osburn, C.L., Pla-Rabes, S., Mernild, S.H., Whiteford, E.J., Grace Andrews, M., Kerby, J.T., Post, E., 2019. Arctic climate shifts drive rapid ecosystem responses across the West Greenland landscape. *Environ. Res. Lett.* 14 <https://doi.org/10.1088/1748-9326/ab2928>.
- Schmidt, S., Wagner, B., Heiri, O., Klug, M., Bennike, O., Melles, M., 2011. Chironomids as indicators of the Holocene climatic and environmental history of two lakes in northeast Greenland. *Boreas* 40, 116–130. <https://doi.org/10.1111/j.1502-3885.2010.00173.x>.
- Serreze, M.C., Barry, R.G., 2011. Processes and impacts of Arctic amplification: a research synthesis. *Glob. Planet. Chang.* 77, 85–96. <https://doi.org/10.1016/j.gloplacha.2011.03.004>.
- Smol, J.P., 1983. Paleophycology of a high arctic lake near Cape Herschel, Ellesmere Island. *Can. J. Bot.* 61, 2195–2204. <https://doi.org/10.1139/b83-238>.
- St-Onge, G., Mulder, T., Francus, P., Long, B., 2007. Chapter 2 continuous physical properties of core marine sediments. *Dev. Mar. Geol.* 1, 63–98. [https://doi.org/10.1016/S1572-5480\(07\)01007-X](https://doi.org/10.1016/S1572-5480(07)01007-X).
- Tomkins, J.D., Antoniades, D., Lamoureux, S.F., Vincent, W.F., 2008. A simple and effective method for preserving the sediment-water interface of sediment cores during transport. *J. Paleolimnol.* 40, 577–582. <https://doi.org/10.1007/s10933-007-9175-1>.
- Vinther, B.M., Clausen, H.B., Fisher, D.A., Koerner, R.M., Johnsen, S.J., Andersen, K.K., Dahl-Jensen, D., Rasmussen, S.O., Steffensen, J.P., Svensson, A.M., 2008.

J. García-Oteyza et al.

Science of the Total Environment 906 (2024) 167713

Synchronizing ice cores from the Renland and Agassiz ice caps to the Greenland Ice Core Chronology. *J. Geophys. Res. Atmos.* 113, 1–10. <https://doi.org/10.1029/2007JD009143>.
 Wagner, B., Melles, M., 2002. Holocene environmental history of western Ymer, East Greenland, inferred from lake sediments. *Quat. Int.* 89, 165–176. [https://doi.org/10.1016/S1040-6182\(01\)00087-8](https://doi.org/10.1016/S1040-6182(01)00087-8).
 Wagner, B., Melles, M., Hahne, J., Niessen, F., Hubberten, H.W., 2000. Holocene climate history of Geographical Society Ø, East Greenland - evidence from lake sediments. *Palaeogeogr. Palaeoclimatol. Palaeoecol.* 160, 45–68. [https://doi.org/10.1016/S0031-0182\(00\)00046-8](https://doi.org/10.1016/S0031-0182(00)00046-8).
 Wagner, B., Heiri, O., Hoyer, D., 2005. Chironomids as proxies for palaeoenvironmental changes in East Greenland: a Holocene record from Geographical Society Ø. *Zeitschrift der Dtsch. Gesellschaft für Geowissenschaften* 156, 543–556. <https://doi.org/10.1127/1860-1804/2005/0156-0543>.

Wagner, B., Bennike, O., Bos, J.A.A., Cremer, H., Lotter, A.F., Melles, M., 2008a. A multidisciplinary study of Holocene sediment records from Hjørt Sø on Store Koldevey, Northeast Greenland. *J. Paleolimnol.* 39, 381–398. <https://doi.org/10.1007/s10933-007-9120-3>.
 Wagner, B., Bennike, O., Bos, J.A.A., Cremer, H., Lotter, A.F., Melles, M., 2008b. A multidisciplinary study of Holocene sediment records from Hjørt Sø on Store Koldevey, Northeast Greenland. *J. Paleolimnol.* 39, 381–398. <https://doi.org/10.1007/s10933-007-9120-3>.
 Williamson, C.E., Dodds, W., Kratz, T.K., Palmer, M.A., 2008. Lakes and streams as sentinels of environmental change in terrestrial and atmospheric processes. *Front. Ecol. Environ.* 6, 247–254. <https://doi.org/10.1890/070140>.
 Williamson, C.E., Saros, J.E., Schindler, D.W., 2009. Climate change: sentinels of change. *Science* 323, 887–888. <https://doi.org/10.1126/science.1169443>.

3.2.2 OTHER DATA

The results and conclusions of the study of ZAC1906 Lake are presented here. These results come from the Bachelor thesis of Ada Rodríguez Martínez (2022, Universitat de Barcelona) and, since they have not been published, a summary of this study is reproduced here to complement the conclusions of this PhD thesis.

The ZAC1906 Lake (~250 m a.s.l.; 74° 28' 54.54" N, 21° 29' 14.70" W), is a ~67 ha lake (~1250 m long; ~ 600 m wide, ~14 m deep) located at the western end of the Store Sødal valley, within the Wollaston Foreland peninsula in the SE corner of Northeast Greenland National Park (Figure 1). The lake is a glacial depression with inflows mainly from the steep southern slopes and from a small NE lake a few metres above. A SE outlet drains the lake, which flows into another neighbouring lake. The geology of ZAC1906 Lake is based on Precambrian gneisses with a mineralogy consisting mainly of chlorite, illite, quartz, riebeckite, plagioclase and pyrite (Henriksen et al., 2009).

AGE-DEPTH MODEL

Seven radiocarbon dates were obtained from ZAC1906 Lake sediments from the bulk organic matter present in the selected samples (Table 1). No inversion ages were obtained. The first age-depth model suggested that the top of the core had an apparent age of ~ 500 cal

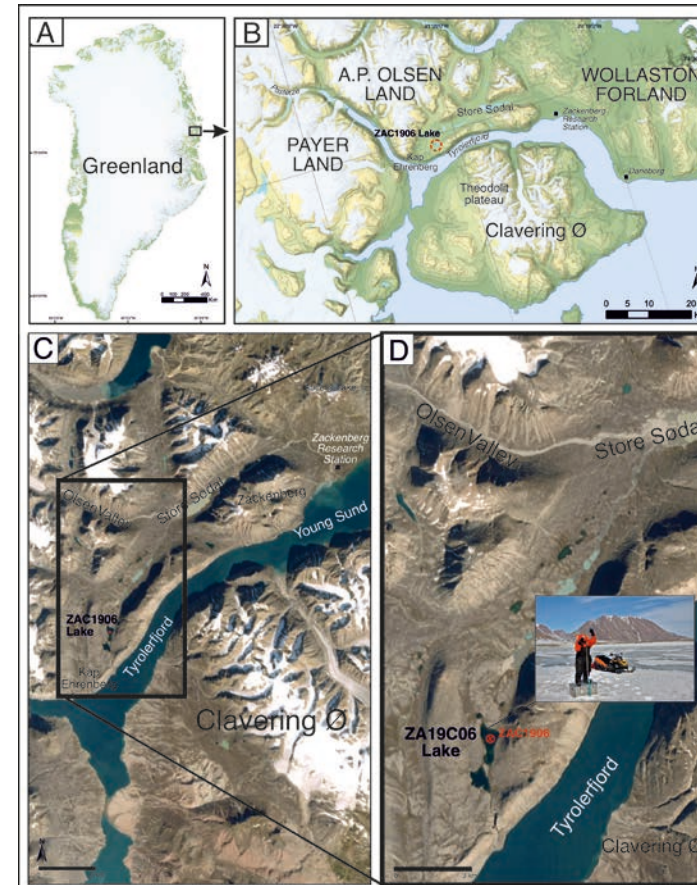


Figure 1. (A) General location of the study area within Greenland. (B) Zoom on the location of the ZAC1906 Lake within the area. (C) Zoom on the location of ZAC1906 Lake on the satellite image. (D) Image of the ZAC1906 Lake with the location of the ZAC1906 coring site.

yrs BP. However, the water-sediment interface was clear and sharp, with no evidence of sediment loss or mixing, therefore, so a deltaR value equal to the core surface age was applied to the rest of the radiocarbon ages as a reservoir effect of 500 cal yrs BP. The final age-depth model (Figure 1) was thus constructed from a final dataset of seven reservoir-

corrected ¹⁴C ages running classical modelling techniques with the clam2.4 R package "clam" (Blaauw, 2010). This age-depth model showed that the ZAC1906 core represents ~11 cal. ka BP of sediment deposition, with limited variation in its sedimentation rates. There are no visible signs of hiatuses or re-deposition, although there appear to be two well-differentiated periods associated with low sedimentation rates from bottom of the core to ~8.0 cal ka BP and from ~4.0 to ~2.0 cal.ka BP.

Table 1. ¹⁴C dates of samples from the sediment core ZAC1906.

Sample ID	Midpoint (cm) (Depth for Age model)	Dated Material	Lab Number	δ ¹³ C (‰)	¹⁴ C age (BP)	±	Reservoir corrected ¹⁴ C yr BP
UCIAMS-261759	2.25	Bulk organic matter	ZAC-06-02 (2-2.5 cm sediment)	-27.2	650	15	150
UCIAMS-261760	12.25	Bulk organic matter	ZAC-06-02 (12-12.5 cm sediment)	-28.1	1315	15	815
UCIAMS-261761	22.25	Bulk organic matter	ZAC-06-02 (22-22.5 cm sediment)	-26.8	2505	15	2005
UCIAMS-261762	32.25	Bulk organic matter	ZAC-06-02 (32-32.5 cm sediment)	-27.8	4495	20	3995
UCIAMS-261758	42.25	Bulk organic matter	ZAC-06-02 (42-42.5 cm sediment)	-26	5685	20	5185
UCIAMS-261763	52.25	Bulk organic matter	ZAC-06-02 (52-52.5 cm sediment)	-24.7	6445	20	5945
UCIAMS-234344	74.0	Bulk organic matter	ZAC19-06-01 (70 cm sediment)	--	9690	25	9190

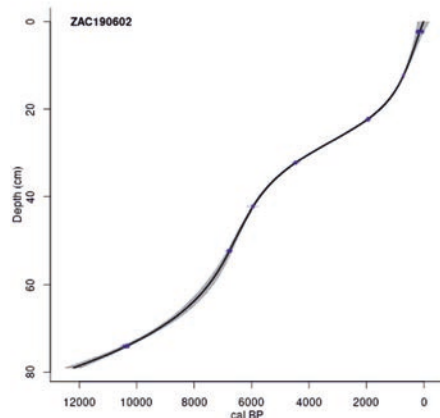


Figure 2. Age-depth model for ZAC1906.

Lake stratigraphy and main sediment characteristics

From the bottom to the top, the core was divided into four main distinct lithological units (A, B, C, D) (Figure. 3).

UNIT A (77.5-71.5 CM DEPTH) - ~11.0 - 10 CAL. KA BP

The sediments consisted mainly of compacted light grey clay. Biological remains are scarce and amorphous organic matter constitutes the main component of this unit. Geochemically, most of the chemical element values show an upward decrease in their intensities. From a mineralogical point of view, these sediments are characterized by a fairly homogeneous composition, highlighting the clay-rich nature of these sediments, with a dominance of clay minerals as chlorite compared to riebeckite, and with high values of pyrite.

UNIT B (71.5-39 CM DEPTH) - 10.0-5.8 CAL. KA BP

This unit consists of millimetre to decimetre thick layers of brown silt. The thickness of the layers decreases upwards and ranges from 1.5 cm to less than 5 mm. There is a general decreasing upward trend in all chemical element values except Cl, which remains broadly constant. There are abrupt peaks in Al, Si, K, Ca, Ti and Zr between ~65-62 cm core depth. Amorphous organic matter content is high, with few visible plant remains. Mineralogically,

Unit B is characterized by the presence of high values of quartz and riebeckite. The coarsest grain size of the core was recorded in the 52.5- 53 cm interval.

UNIT C (39-5 CM DEPTH) - ~5.8-0.8 CAL. KA BP

This unit begins with a homogeneous grey clay section ~2.5 cm thick, while between ~36 and ~28 cm of core depth there are indistinct millimetre thick brown laminations which become more prominent and thicker towards the top of this unit. From a geochemical point of view, the beginning of this unit shows a peak in all chemical elements except Cl and Mn, with a posterior upward increase is observed in all elements. At the end of this unit there is also a drastic decrease in Al, Si, K, and Ti. Plagioclase, quartz, and riebeckite displayed an overall decreasing trend, while illite and chlorite showed an increasing pattern.

UNIT D (5-0 CM DEPTH) - AGE ~0.8 CAL. KA BP- PRESENT

This zone is characterized by laminated silt with alternating very dark brown, organic-rich millimeter-thick (0.5-0.8 cm) bands and centimeter-thick (1-2.5 cm) brown bands. An orange hue is visible in the top ~2 cm. Chemical elements such as Si, Mn, and Fe peak in this zone, while Rb, Sr, and Zr decrease abruptly. The mineral content is very low, with chlorite, quartz and plagioclase decreasing in abundance and illite and riebeckite increasing.

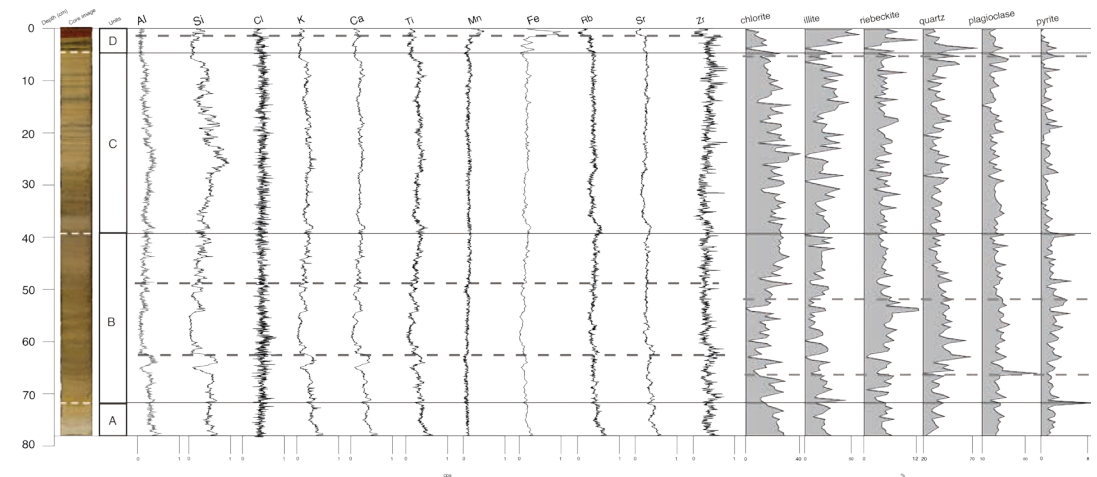


Figure 3. Data from ZAC1906 sediment core. From left to right: depth axis scale; ZAC1906 core image; units delimited through visual identification; XRF elements; clusters formed from XRF and XRD data.

RDA/PCA INTERPRETATIONS

The first RDA axis (Figure 4A), accounting for 63% of the total data variance, revealed a strong association between chlorite and elements such as Ca, Si, K, Ti, and Al on the

positive side of this axis. Conversely, riebeckite and Zr were present on the negative end of this axis.

The second RDA axis, representing 30% of the total variance, showed illite and Mn, and Fe at the positive end of this axis while quartz, plagioclase, pyrite, Cl, Sr and Rb were present at the negative end.

The PCA (Figure 4B) was performed on the chemical element data in order to summarize the main forcings triggering the development of the lake and to interpret its changes over time. The first PCA component (Ax1) explains almost 57% of the total variance and it is related to Al, Sr, Si, Zr, K, Ca, and Ti in the positive values while Cl is found at the negative end. The second PCA component explains 14.2% of the total variance and it is defined by Mn and Fe at the positive end, while Zr and Rb define the negative end of this axis.

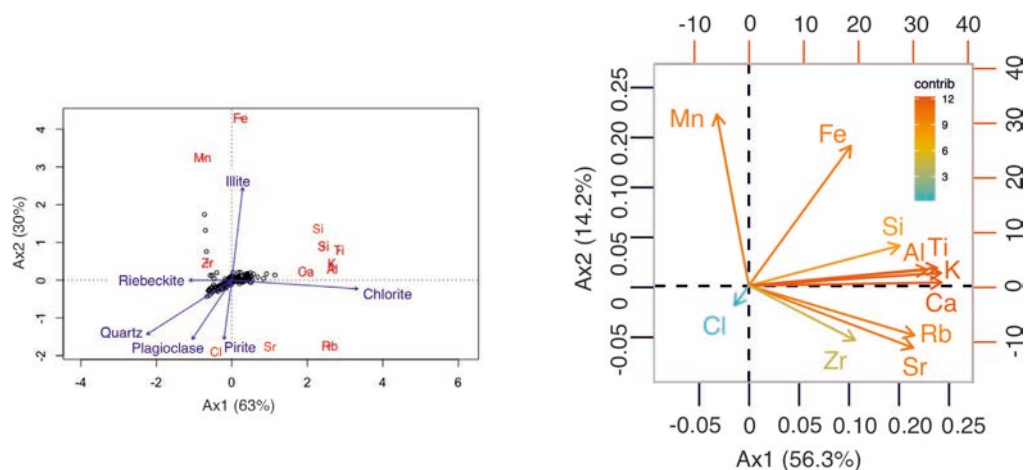


Figure 4. Graphs (left) XRD and XRF data RDA (right) XRF data PCA.

INTERPRETATION:

Sediment geochemistry is closely linked to catchment system dynamics as confirmed by the RDA between the mineral species (XRD) and the XRF data. Two independent but complementary processes have been attributed to the RDA, with one being represented on the abscissa axis and the other on the ordinate one. On the abscissa axis (Ax 1), the first component is defined by a contribution of riebeckite (primary mineral of the catchment rocks), which shows an opposite behavior with respect to chlorite, corresponding to a secondary mineral generated by the chemical alteration of amphiboles and piroxenes through the chloritization process (Schott et al., 1981). Examining their respective densities, chlorite has a density range of 2.6-2.8 g/cm³, while riebeckite has a higher density of 3.3 g/cm³. This suggests that more energy is required in the system to mobilise riebeckite from the altered rocks present in the catchment and to incorporate this mineral into the lake sediments. In our context, this corresponds to periods of high precipitation values, either snow or rain. Conversely, chlorite, which has a lower density, can be more easily mobilized from the catchment to the lake, for example during periods where wind is the dominant

mobilizing agent. Consequently, we can infer that periods with abundant riebeckite indicate a higher energy state in the system compared to periods dominated by chlorite.

The ordinate axis (Ax2) illustrates the association between plagioclase and illite. The distinction between plagioclase as a primary mineral of the catchment rocks and illite as a secondary mineral derived from the chemical alteration of plagioclases suggests that the plausible process associated with Ax2 involves the transformation of the former into the latter. This transformation is controlled by temperature, inducing seritization in plagioclase and resulting in the production of illite. Seritization, a hydrolysis process, requires the presence of liquid water. Consequently, temperatures above 0°C are essential. Put simply, the positive detection of illite formation in the system indicates that the temperature was above freezing when this alteration occurred.

Therefore, Ax1 can be interpreted in terms of run-off changes, while Ax2 can be linked to air temperature variations.

In terms of PCA, the first component is influenced by chemical elements associated with the influx of detrital material into the basin (Si, Ca, Al), which then remains relatively immobile afterward. Therefore, the first component can be correlated with increased rainfall and runoff. Conversely, the second component is driven by Mn and Fe, chemical elements sensitive to oxidation/reduction processes. In general, lake water temperature and stratification strongly influence the redox conditions at the lake water-sediment interface (Naehler et al., 2013; Vyse et al., 2020). At low temperatures, where the ice cover persists for long periods, reducing environments are generated due to oxygen depletion by organic matter during mineralization. This leads to significant iron precipitation. In contrast, during short-lived ice cover periods, the constant movement of the lake, driven by wind and shallowness, maintains a fully oxygenated water column, resulting in oxidizing conditions at the water-sediment interface. Consequently, manganese precipitation is favored over iron during these periods.

As such, and following the interpretation of the RDA axes, variations along this first PCA axis reflects changes in runoff, while the second PCA axis air represents temperature fluctuations (Figure 3).

LOCAL HOLOCENE CLIMATE HISTORY

During the first 600 years (~11.0 - 10.4 cal. ka BP), the record shows high discharge (represented by the first axis of the PCA) and cold temperatures (represented by the second axis of the PCA) (Figure 5). An increase in these two parameters occurs during a short period (~10.4 - 10.2 cal. ka BP) and gradually decreases during the remainder of Unit A (~10.0 cal. ka BP). The period following Unit B (~10.0 - 5.5 cal. ka BP) exhibits significant variability, with abrupt fluctuations in runoff and less pronounced temperature variations. Two significant changes occurred during this period, marked by geochemical and mineralogical differences in the clusters (Figure 5). The first change occurred between ~9. and 8.7 cal ka BP, and the second between ~7.2 and 6.8 cal ka BP. The first is characterized by an increase in both axes, indicating a wet and warm phase, and the second is the opposite, suggesting drier and colder conditions. From this point (~6.8 cal ka BP) until the end of the unit at ~5.5 cal ka BP, the system moves towards increasingly humid and warmer conditions, although with considerable variability. The system enters Unit C with high values of both climate parameters, indicating wetter and warmer conditions. During

this unit, while the values of temperature increase and are maintained with low variability, the runoff experienced some changes, with a decrease and maintenance of low values with low variability, indicating dry conditions for the period comprised between ~ 5 and 3 cal ka BP. The last three millennia are characterized by an abrupt change in climate conditions towards wetter and warmer conditions. They are maintained until ~ 1.8 cal ka BP when an abrupt change indicates a decrease in precipitation and temperature. Until the end of Unit C, ZAC1906 shows predominantly dry conditions with warmer but variable temperatures. In contrast, during the Dark Ages Cold Period (DACP) and the onset of the Medieval Climate Anomaly (MCA), this area generally experienced wetter and warmer conditions than during the last part of RWP (Figure 5). During the MCA, climate conditions culminated in dry and cold conditions that marked the beginning of the Little Ice Age (LIA). During the last few hundreds years (up to Unit D), runoff and temperature showed a general upward trend, with significant temperature variability. At the end of the LIA, there was an abrupt

both runoff and temperature are shown, with the highest values in the record accompanied by one of the lowest values of precipitation (Figure 5).

In order to better understand the climate variability within our study area, we have compared the results of the climate history of ZAC1906 Lake with that of Aucella Lake, which is part of this PhD thesis (Paper IV); this lake is located at a distance of ~32 km along a straight line, with an elevation difference of ~700 m between the two lakes. The two sedimentary records have two fundamental and related differences, the first being the reservoir effect that each one has, with that of Aucella Lake (~1200 years) being more than double that of the ZAC1906 Lake (~500 years). The second is the average sedimentation rate, which is more than twice as high in ZAC1906 (~139 years/cm) as in Aucella (~60 years/cm). The 83.6 cm of the Aucella Lake climate record is found within the last 35 cm of the ZAC1906 Lake record (Figure 5). These differences are due to the contrast that exists in the local environmental factors that influence each of the ecosystems. Among them, the most likely important one is related to the altitude, which directly affects the availability of liquid water and the sensitivity of lake temperature to climate variations.

The working hypothesis is that because the two sedimentary records are so close together, they should record the same climate variations and trends, albeit with different intensities due to their own particular geomorphological and limnological characteristics. Indeed, the comparison of the two records suggests that they detect the same climate history, but with a different time scale. Contrary to expectation, the first abrupt change recorded in the curves of both records, and indicated by the grey arrow (Figure 5), is observed at ~ 3,800 cal years BP in the Aucella record, while it is present at ~3200 cal years BP in the ZAC1906 record, although the latter is at a lower altitude the latter with respect to the former. A possible explanation for this 600 year discrepancy, completely outside the uncertainties of

Table 2. ¹⁴C dates of samples from the sediment core AUC02 (grey columns) with the corrected new ages after applying non-linear reservoir effect (black columns) along the core for the construction of the new age-depth model. To see the complete information about the original dates refer to the table on Paper IV.

Sample ID	Midpoint (for age model, cm)	Dated Material	¹⁴ C age (BP)	±	Reservoir corrected ¹⁴ C yr BP	Non-linear reservoir corrected ¹⁴ C yr BP	Corrected ¹⁴ C age (BP)	±
AUC 1802-0-1	0.5	Moss	1265	20			1265	20
AUC 1802-11-12	11.5	Moss	2425	15	1160	1160	2425	15
AUC 1802-29-31	30.0	Moss	3255	15	1990	1835	3100	15
AUC 1802-56-57	56.5	Moss	4390	15	3125	2625	3890	15
AUC 1802-70-71	70.5	Moss	4820	20	3555	3055	4320	20
AUC 1802-78	78.0	Moss	5430	20	4165	3665	4930	20

either age-depth model, is that the Aucella Lake record may have a higher reservoir effect than originally calculated, and/or that this effect is not constant throughout the core, as assumed in the initial analysis of this record. Consequently, a revision of the existing age-depth model is recommended.

The main key point for this age revision is the major moisture change that took place at ~3,000 cal. years BP. This moisture change has been extensively described for Greenland (Søndergaard et al., 2019). Taking this into account, the age revision has consisted of adding a progressive offset to the original radiocarbon dates, from ~100 years for the uppermost radiocarbon date to ~500 years for the lowest ones (see Table 2). Therefore, the

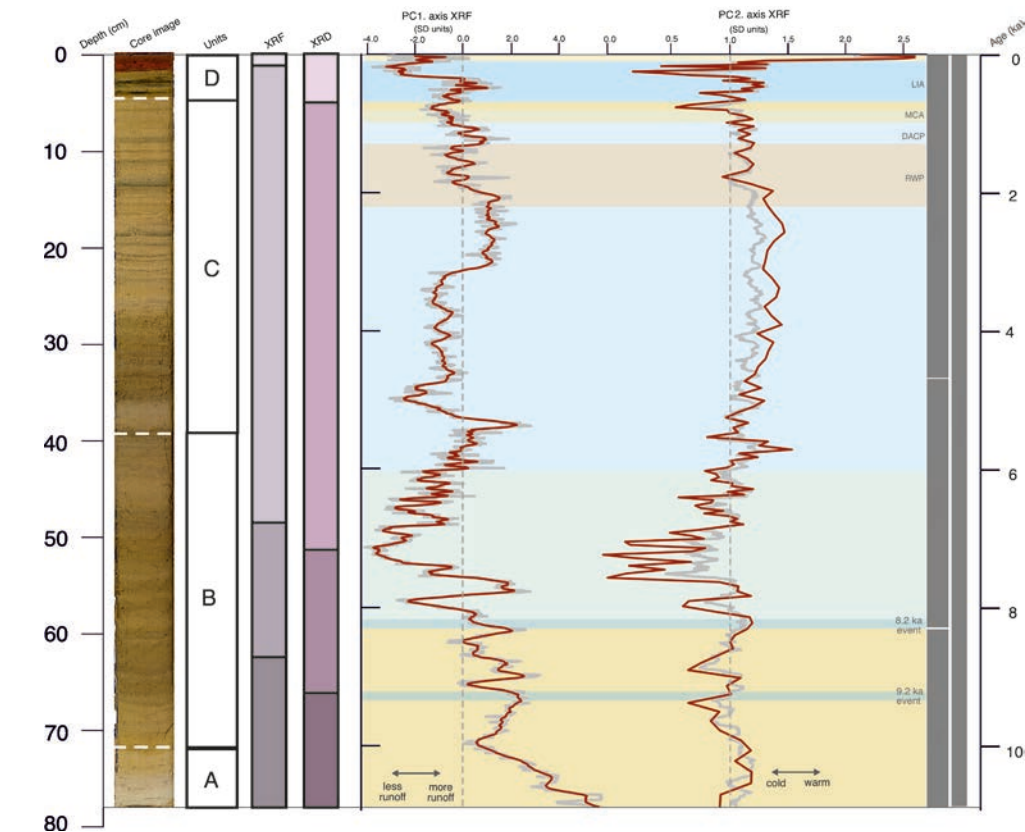


Figure 5. Results from the interpretation of the PCA from ZAC1906 dataset. From left to right: depth axis; ZAC1906 core image; units delimited through visual identification; change limits from the XRF data clusters; change limits from XRD data clusters; smothered XRF PC1 axis curve and its interpretation; smothered XRF PC2 axis curve and its interpretation; age axis. Source: own elaboration.

drop both in temperature and precipitation. The largest and most significant increase in temperature occurred in the last 50 years of the record. From ~1950 CE, extreme values of

oldest radiocarbon dates would be affected by a reservoir effect of $\sim 1,700$ years. Such large reservoir effects are common in high latitude lakes and are mostly related to the input of old carbon, primarily from subsurface thawing of permafrost and melting of adjacent glaciers, and large water residence times (Hendy and Hall, 2006; Vyse et al., 2020).

In addition to the review of the Aucella Lake age model after comparison with the ZAC1906 record, a review of its interpretation, in particular the discussion of the PC1 curve (Paper IV), is also recommended.

In a general overview, comparing the climatic history shown by the sediment core from Lake ZAC1906 with that from Aucella Lake (Figure 6), they show significantly similar climatic variability over most of the record, both in major trends and in decadal fluctuations. Only between ~ 1.2 and 0.2 cal ka BP do the curves differ in that in Aucella Lake shows a more continuous decrease in temperature with little variability, whereas ZAC1906 shows much more variability and an abrupt decrease in discharge. This could be due to landscape factors interacting and interfering with the climate signal. In order to improve our perspective, it would be useful to be able to compare these records with others from lakes in the same area and thus be able to distinguish the climatic signals from the landscape noise of each lake.

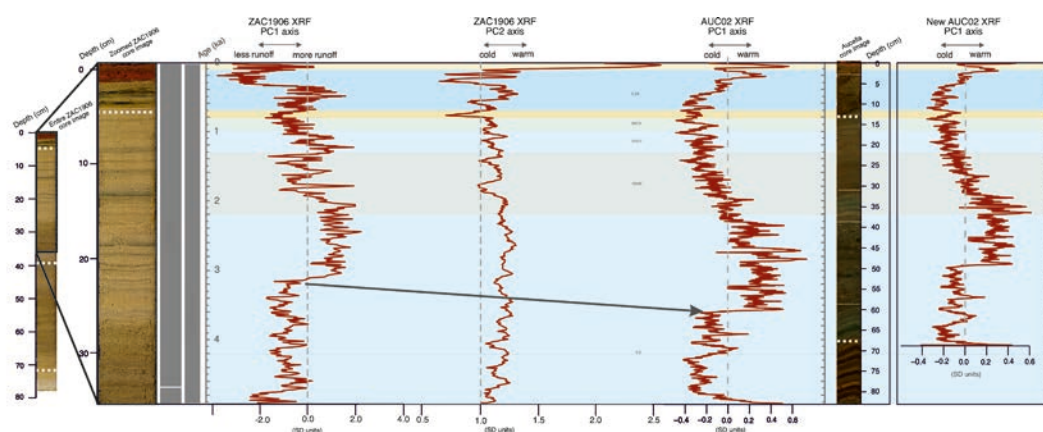


Figure 6. Comparison of the results of Lake ZAC1906 and Aucella Lake. Images of the cores studied marked with the unit differentiated in each one, along with the curves of the PCA's axes with XRF data obtained in each study.

REFERENCES

- Blaauw, M., 2010. Methods and code for “classical” age-modelling of radiocarbon sequences. *Quat. Geochronol.* 5, 512–518. <https://doi.org/10.1016/j.quageo.2010.01.002>
- Hendy, C.H., Hall, B.L., 2006. The radiocarbon reservoir effect in proglacial lakes: Examples from Antarctica. *Earth Planet. Sci. Lett.* 241, 413–421. <https://doi.org/10.1016/j.epsl.2005.11.045>
- Henriksen, N., Higgins, A.K., Kalsbeek, F., Pulvertaft, T.C.R., 2009. Greenland from Archaean to Quaternary Descriptive text to the 1995 Geological map of Greenland, 1:2500000. *Geol. Surv. Denmark Greenl. Bull.* 18, 126.

Naeher, S., Gilli, A., North, R.P., Hamann, Y., Schubert, C.J., 2013. Tracing bottom water oxygenation with sedimentary Mn/Fe ratios in Lake Zurich, Switzerland. *Chem. Geol.* 352, 125–133. <https://doi.org/10.1016/j.chemgeo.2013.06.006>

Schott, J., Berner, R.A., Sjöberg, E.L., 1981. Mechanism of pyroxene and amphibole weathering—I. Experimental studies of iron-free minerals. *Geochim. Cosmochim. Acta* 45, 2123–2135. [https://doi.org/10.1016/0016-7037\(81\)90065-X](https://doi.org/10.1016/0016-7037(81)90065-X)

Søndergaard, A.S., Larsen, N.K., Olsen, J., Strunk, A., Woodroffe, S., 2019. Glacial history of the Greenland Ice Sheet and a local ice cap in Qaanaaq, northwest Greenland. *J. Quat. Sci.* 34, 536–547. <https://doi.org/10.1002/jqs.3139>

Vyse, S.A., Herzschuh, U., Andreev, A.A., Pestryakova, L.A., Diekmann, B., Armitage, S.J., Biskaborn, B.K., 2020. Geochemical and sedimentological responses of arctic glacial Lake Ilirney, chukotka (far east Russia) to palaeoenvironmental change since ~ 51.8 ka BP. *Quat. Sci. Rev.* 247, 106607. <https://doi.org/10.1016/j.quascirev.2020.106607>

3.3 LINKING CLIMATE VARIABILITY AND GLACIAL OSCILLATIONS

Once all the results of this PhD thesis were available, the integration of findings related to glacial oscillations and climate variability at both local and regional levels was undertaken. This section aims to provide a concise summary of the main insights derived from the analysis of both sources (Figure 7):

- To compare the glacial evolution inferred from CRE samples surpassing ~11 ka (particularly those derived from the Zackenberg Valley), we rely on other continuous proxy records (e.g. ice core data) as lake sediments only encompass the Holocene.
- The number of moraine and erratic boulder samples from the valley bottom at the entrance of the fjord (Zackenberg Valley) increases through the B-A to a maximum at the very end of the YD cold period. This fact reflects different glacier stabilization phases at the end of T-1 but a general ice thinning between ~13.7 and 11.2 ka.
- After the formation of moraine systems in response to the cold YD period, glaciers retreated in response to a warming and drier climate, as revealed by PC1 axis of ZAC1906 Lake record. With the long and progressive decrease in precipitation after ~10.5 cal. ka BP indicated by the same lacustrine record, glaciers retreated upvalleys. From the onset of the Holocene and until the HTM, glaciers retreated in response to prevailing warm climate as revealed by widespread polished surfaces and erratic boulders dated between 10.5 to 8 cal. ka BP in the lowest valley bottoms of several valleys (Olsen, Dolomit and Tyroler).
- The destabilization of the glacier masses is shown by the accumulation of different types of samples (mainly from polished surfaces, but also from moraine boulders) from 10.5 to 8 cal. ka BP. During this period, the influence of the local climate on glacial fluctuations is evident. The retreat is accompanied by a continuous decrease in precipitation although with abrupt changes and large variability with mild warm temperatures. The greater activity of glacial oscillations in the area (largest number of samples of different types accumulated in the entire dataset) can be related to these changes in precipitation. Furthermore, if we take into account the interpretation of each of the axes of ZAC1906, could lead to infer that changes in precipitation may exert a more pronounced influence on glacial oscillations compared to variations in temperature. During this period, when the main trend was destabilization and retreat of large ice masses, small advances were recorded in some of the valleys (Dolomit, Olsen and Tyroler) during short cooling periods, such as the 9.2 ka and 8.2 ka events. These events are well correlated with temperature decreases in the Greenland ice cores and coincide with a period of increased precipitation recorded in Lake ZAC1906.
- During the middle Holocene (8.2- 4.2 ka), no robust information on glacial oscillations was found in any of the four valleys. This would lead to the interpretation that the documentation of glacial oscillations ceased because the ice fronts were behind the present limits or in a stillstand state. Throughout this period, the ZAC1906 records show a high variability in precipitation and a general trend of slightly increasing temperatures. Only two CRE samples dated at ~7 ka (moraine boulder) and ~6 ka (polished surface) were found in Tyroler and Dolomit valleys, but more samples are needed for that period. These glacial movements could be related to the progressive trend in precipitation that marks ZAC1906

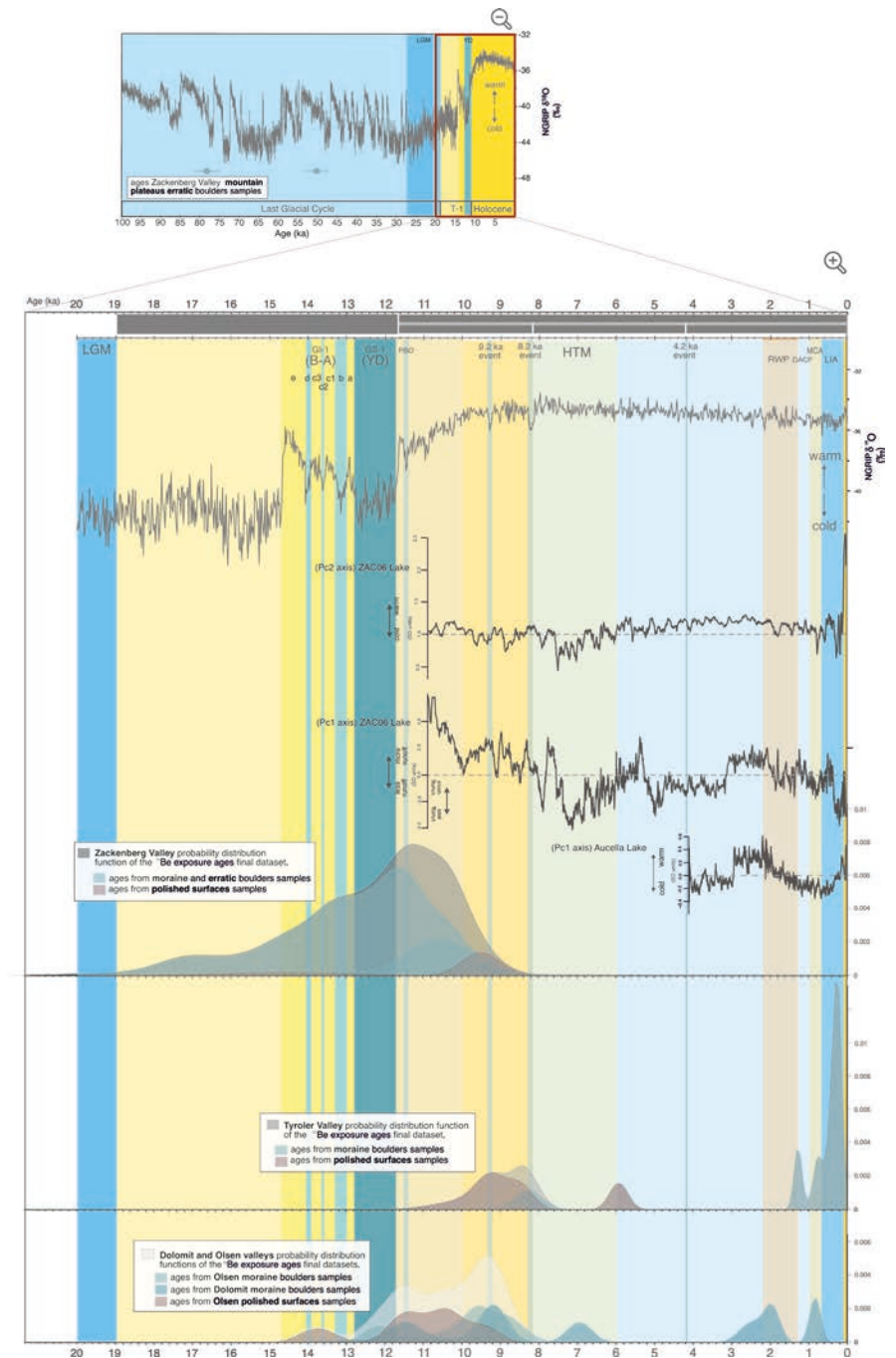


Figure 7. Summary figure with all the data obtained in this PhD thesis. Probability distribution functions of the 10Be CRE ages from each one of the valleys studied vs. temperature evolution since the last glacial cycle in the interior of Greenland based on the δ18O record of the NGRIP ice core (GICC05modelext), 5-point running mean (Rasmussen et al. 2014) and the interpreted temperature and precipitation curves obtained from the sediment cores studied.

record from the lowest point of the record at ~ 7.2 ka to ~ 5.2 ka where the peak of the increase is shown.

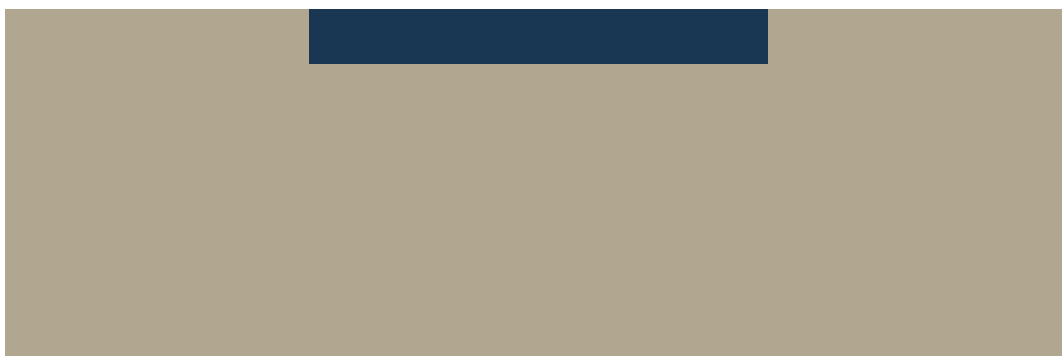
- After ~ 5.2 cal. ka BP, ZAC1906 Lake record suggest an abrupt shift to lower precipitation until ~ 3 ka cal BP, when another abrupt change to wetter and warmer conditions occurred, which is also recorded at this time in the Aucella Lake record. This shift after ~ 3 ka cal BP that brought continued high precipitation and a slight decrease in temperature, may have led to new glacial advances with the appearance of moraine samples in the middle and inner fjord valleys (Tyroler Olsen and Dolomit valleys). The probability distribution of these glacial advances is centered between ~ 2.5 and 0.3 ka.

- A glacial advance is recorded to have occurred before the MWP as revealed by external moraine ridges of the Coperland Glacier in Tyoler Valley. However, no clear signal is detected in lake records for that time that could have explained the main factor driving this glacier advance.

- The LIA is characterized by glacial advances between 1300-1850 CE, favored by high precipitation and low temperatures observed in the lake records. Conditions changed abruptly at the end of the LIA, when precipitation decreases and temperature begins to rise (marked by ZAC1906 Lake and Lake Aucella Lake), and the glacial oscillations recorded by CRE dating end. Since then, glacial fronts remained relatively close to the LIA positions.

- No clear correlation is detected between ZAC1906 PC2 axis and the glacial oscillations dated during the ~ 11 cal ka BP record. The reason may be associated with the different time response between the two systems (glaciers vs lakes). These two systems can respond reflecting changes in both temperature and precipitation, but it is well known that the Arctic freshwater systems reflect shifting climate rapidly, providing early warning signals of change (Saros et al. 2023). This could also explain that during the last 50 years record, this temperature curve (ZAC1906 PC2 axis) breaks out of its 'natural' variability and shows a very abrupt rise in temperatures. This increase is also recorded (although with less severity) at the Aucella Lake record but not on the ZAC1906 Lake PC1 axis that would mark the precipitation. Temperature would therefore be taking the system out of its natural variability at this point.

4 CONCLUDING REMARKS AND FUTURE PERSPECTIVES



The main objective of this PhD thesis was to improve the knowledge of the glacial history and climate variability of NE Greenland through a multidisciplinary approach based on different natural archives using different complementary techniques. As a result, the main findings of this thesis are the following:

1. New relevant contributions to the geomorphological setting and geochronological patterns of the deglaciation sequence since the last glacial cycle through the T-1 and Holocene to the present have been obtained for this area, although we must consider the limitations of using CRE dating in areas where paraglacial dynamics are very active.

2. New quantitative, high-resolution and multi-proxy data on past climate variability, especially temperature and precipitation regimes, have been obtained from lake sediment records. These high-resolution records have greatly improved the temporal resolution of existing climate reconstructions and filled knowledge gaps and to disentangle the natural and other environmental signals preserved in lake records.

The final results obtained during the PhD thesis development have fulfilled the initial objectives to address a series of research questions (RQ) that have been answered through the publication of four scientific articles led by the PhD candidate with the collaboration of national and international co-authors.

New findings focusing on glacial oscillations in the Zackenberg region are reported in Papers I, II, and III. They include a spatio-temporal reconstruction of patterns of glacial advance and retreat since T-1 and throughout the Holocene (RQ1) that have been identified in various valleys in the area, including the valley floor at the entrance to the fjord, further away from the ice fronts (Paper I), and those closer to the present glacier fronts (Papers II and III). These research articles include an accurate geomorphological mapping of the region with a focus on the glacial and periglacial landforms followed by their dating them using CRE dating. These papers also discuss the applicability of CRE dating in areas where postglacial environmental dynamics are highly active (RQ2), examining the limitations of this methodology (Papers I and III). The results on glacial dynamics have been also related to past local climate variability, as inferred from lake sediment records showing continuous climate change during the Mid-Late Holocene (RQ3, Paper IV). Finally, all these results have been compared and discussed in relation to results from other regions in NE Greenland and around the Greenland Ice Sheet (RQ4).

To summarize, we highlight the following results of this PhD thesis:

- The few samples, taken from the highest summit plateaus, yielded the oldest exposure ages showing evidence that during a pre-LGM glaciation the valleys and fjords were filled with ice, with only a few nunataks protruding above the ice field.
- The major deglaciation occurred during T-1 (~19-11 ka), when the fjords formed, and the highest slopes became ice-free.
- At ~13-14 ka, a period of major glacier shrinkage was recorded, followed by accelerated glacier retreat at ~10-11 ka, when the glacier valleys were separated from the main ice tongues. Deglaciation of the fjord entrance valleys and terminal valleys took place during

Far north, hidden behind grim barriers
of pack ice, are lands that hold one
spellbound. Gigantic imaginary gates,
with hinges set in the horizon, seem to
guard these lands. Slowly the gates
swing open and one enters another
world where men are insignificant
amid the awesome immensity of lonely
mountains, fords, and glaciers. Five
times have the gates opened for me.
May they do so as many times again!

- Louise A. Boyd, 1935.

the Early Holocene at ~10-8.5 ka. In general, it could be stated that, glacier retreats (marked by polished surfaces dated) are associated with mild and drier periods.

- This long-term deglaciation trend was not continuous, and it included intermittent glacial advances during the Preboreal Oscillation (PBO) (~11.5-11.4 ka) and the ~9.2 ka event (~9.5-9.2 ka interval).

- As in most areas of NE Greenland, glacial records from the mid-Holocene to the onset of the Late Holocene are lacking in the study areas, as glacial fronts were probably located behind their present positions and the lack of geomorphologic evidence suggests that glaciers were smaller during most of the Holocene than they are today.

- Glaciers have been rather stable during the last ~10 ka, with tundra expansion and permafrost aggradation.

- While this thesis has shown that CRE dating is a very useful method for reconstructing glacial history in NE Greenland, special care must be taken when interpreting CRE ages and landscape evolution, as very active postglacial processes can influence them. It may not reveal the true age of deglaciation (i.e. polished surfaces) or landform stabilization (i.e. moraines and erratic boulders). The paleolimnological reconstructions presented in this thesis cover the last ~11 ka, allowing us to establish the climatic framework for the Late Holocene glacial oscillations. The results highlight the relatively warmer conditions of the mid-Holocene and the abrupt decrease in precipitation during the Neoglacial.

- Our records on the Tyroler Valley showed a glacial advance during the Dark Ages Cold Period, coinciding with trends of low temperatures and high precipitation as shown by our lake's records.

- The LIA (~0.6 and ~0.3 cal. ka BP) is the last phase in which larger glacier systems occurred and advanced in synchrony with global climate anomalies driven by solar minima. Paleolimnological reconstructions show that the beginning of the LIA was characterized by a marked decrease in air temperature, followed by a decrease in precipitation, which reached a minimum at the end of the period.

- Since this last major advance, the glacier fronts have experienced minor oscillations, as shown by historical images, but have remained relatively close to the LIA moraines. The last 50 years of the Aucella Lake and ZAC1906 Lake records are characterized by abrupt temperature increases, the highest peaks in the last ~11 cal. ka BP, reflecting the current anthropogenic global warming.

- In general, during several periods of the record, precipitation has been observed to play a more critical role in glacial activity than temperature. However, in the most recent part of the record, it is observed that temperature is leaving the natural climate variability of the system.

These results have filled a gap in the understanding of climate variability and glacial response in NE Greenland from the last glacial cycle to the present. However, they have also raised new questions and uncertainties that need to be investigated in the future, such

as the impact of LGM glacial advance on coastal regions or the improvement of spatio-temporal patterns of Holocene glacial fluctuations.

- More samples for CRE dating will be beneficial to improve the precision of our results and provide new data on the evolution of the landscape of this area. They will help to clarify whether the chronology of Neoglacial peaks and retreats over the Mid-Late Holocene represents a local response to prevailing climatic conditions or is part of a more general pattern that occurred across the High Arctic region.

- The refinement of the chronological framework in the study area should combine multiple nuclides (e.g. ²⁶Al, in-situ ¹⁴C) to explore complex exposure histories and shed light on processes such as exhumation and prior exposures. In addition, combination with other dating methods (e.g. OSL) has proven to be very useful and should be further explored in the future.

- Despite the empirical reconstruction of the glacial chronology combining geomorphological and geochronological evidence and the reconstruction of the climate variability in the region presented in this thesis, a calibrating numerical ice model over the entire timescale is lacking. Modelling against the empirical data will serve, among other things, to better quantify retreat rates or surface extent changes.

- Although it has not been included in this PhD thesis, further palaeolimnological records have been obtained from other lakes around the area as this thesis is part of a large project. These records are still being analyzed and their results will add to the knowledge already gained.



